Problem and Research Objectives:

The Norman City Landfill is a closed municipal landfill located on the floodplain of the Canadian River in Norman, Oklahoma. The landfill accepted solid waste from the city between 1922 and 1985, at which time it was closed with a vegetated clay cap. The landfill was never lined, so at least one leachate plume has developed and now extends southward into the floodplain alluvium toward the Canadian River. The alluvium is 10 to 15 meters thick and composed of unconsolidated sediments ranging from clay to gravel. The water table is found at a depth of about 1 meter. The alluvial aquifer is underlain by the Hennessey Shale, which acts as a confining unit.

The geomorphic and sedimentologic characteristics of the floodplain and active channel have yet to be documented. These characteristics will control the permeability of the floodplain, and therefore, the migration potential of leachate plumes, known and unknown. Inspection of historical aerial photographs reveals that the Canadian River has experienced significant horizontal migration over the past few decades in the region of the Norman Landfill, initiating episodes of erosion and deposition. Lateral channel instability is expected for a sand-bed, meandering river, but bank protection has truncated meander migration. Understanding channel stability would enable more informed judgments about the likelihood that stream erosion could mobilize contaminants from the landfill in particulate form. We might anticipate a correspondence between spatial and temporal patterns of channel stability and the vertical and horizontal connectivity of alluvial units.

Objectives

The objectives of our proposed research were to describe and explain:

1) the vertical and horizontal heterogeneity in texture of floodplain alluvium to facilitate understanding of permeability pathways; and
2) the geomorphic stability of the Canadian River upstream, adjacent, and downstream of the Norman Landfill in a manner that can be used to assess past and future mobility of contaminants in particulate form.

Study Area

The Canadian River begins in the Sangre de Cristo Mountains of southeastern Colorado and flows 1460 km to its confluence with the Arkansas River in eastern Oklahoma. In the vicinity of the Norman Landfill, the Canadian River is a low-sinuosity, sand-bed river that alternates between braiding and meandering in pattern. In central Oklahoma, the Canadian River Valley ranges in width from 2.5 to 6.5 km, and is composed of two geomorphic surfaces: a late Holocene valley fill and the modern floodplain. The Norman City Landfill is situated on the north side of the Canadian River, south of the City of Norman, between Chautauqua and Jenkins avenues (Fig. 1). The base of the landfill is 3.5 meters above the thalweg of the river. The valley fill is approximately 10-15 meters deep and composed of unconsolidated sediments ranging from clay to gravel. The aquifer is underlain by the Hennessey Shale, which acts as a confining unit.

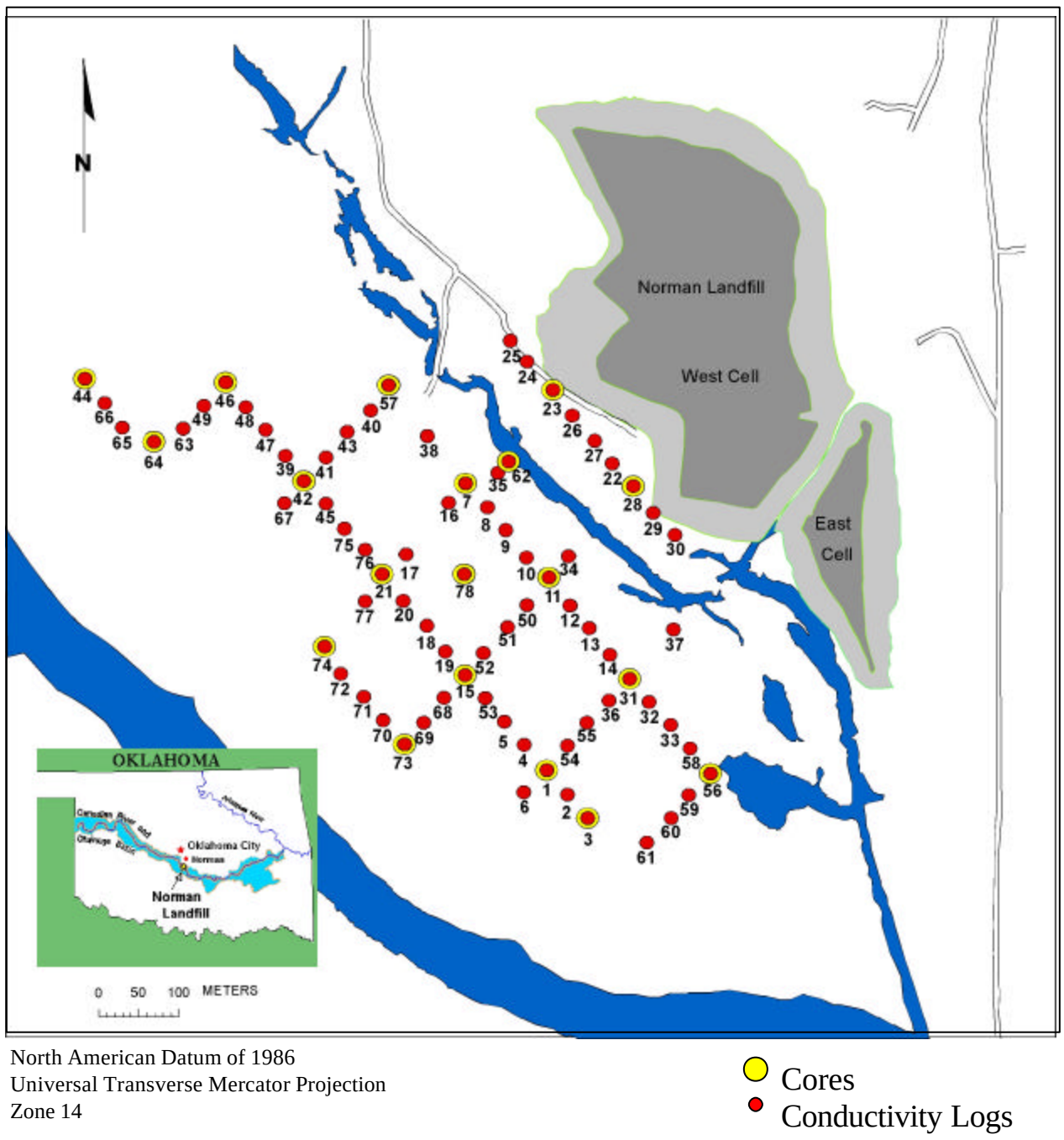

Fig. 1- Location of Data Collection Sites at Norman Landfill.
Map based on data by U. S. Geological Survey.

Methodology:

Sedimentology

The first project objective, concerning sedimentologic controls on permeability pathways, was accomplished by completing five tasks:

1) collect cores and conductivity logs from the floodplain alluvium;
2) describe and photograph the cores;
3) perform textural analysis on each core based on lithofacies;
4) determine the relationship between texture and permeability using established equations; and
5) interpret the conductivity logs for texture based on the cores and creation of a 3-D model of permeability based on log interpretation and textural analysis.

Obtaining Conductivity Logs and Cores

A sampling grid was designed to obtain uniform coverage of the floodplain alluvium. The grid was composed of cross-lines, which ran parallel and perpendicular to the Canadian River (Fig. 1). Geoprobe® conductivity logs were taken along these cross-lines to a depth of 10 to 12 meters (35 to 40 feet), and the average distance between the sample locations was about 37 meters (110 ft). A total of 78 conductivity logs were taken, and continuous cores were taken in 19 of these wells. A hand-held GPS system and map were used to locate each of the sampling locations. This GPS system could locate the latitude and longitude of each site to within 1 m (3 feet). After the samples were collected from each site, the site of each well on the floodplain was marked. A second GPS system was used by Scott Christenson from the USGS office in Oklahoma City to obtain more accurate readings. Christenson was able to measure the latitude (X), longitude (Y), and surface elevation (Z) of each well to within 2 cm. The set of readings taken by Christenson provided the X, Y, and Z data for each well in the project.

Conductivity Logs

Seventy-eight conductivity logs (Fig. 2) were collected using a Geoprobe®. A Geoprobe® is a hydraulically powered, percussion soil probing instrument. The Geoprobe® uses static weight and the percussion force of a soil probing hammer to advance a direct-push electrical-logging probe through the subsurface. The Geoprobe® is attached to a vehicle, which provides the static weight for the instrument. The direct-push e-logging probe is attached to the leading end of a tool string and advanced into the subsurface (Figs. 2, 3). The probe used is a Wenner array design that is 38 cm (15 inches) long with a maximum diameter of 3.8 cm (1.5 inches). The electrical conductivity data is transmitted to a field computer, which is attached to the Geoprobe® via a cable. The conductivity is measured in millisiemens/ft. Conductivity readings are taken every 1.5 cm (0.05 feet) and the computer displays a real-time log on its screen as the log is taken. In addition to conductivity, the system also records the rate of penetration. We discuss our data in both feet and meters because the Geoprobe measurements are taken in feet.

Once the conductivity log data was collected, it was imported to an Excel spreadsheet. In Excel, the log data was plotted as a curve with depth and printed out on oversize paper. The logs were pieced together to form the cross-sections of the study area (Fig. 4). These cross-sections were then correlated based on the following criteria:

1) vertical position of sands relative to mud layers
2) vertical variations in texture based on sieve analysis

Geoprobe Details

OSU
School of Geology

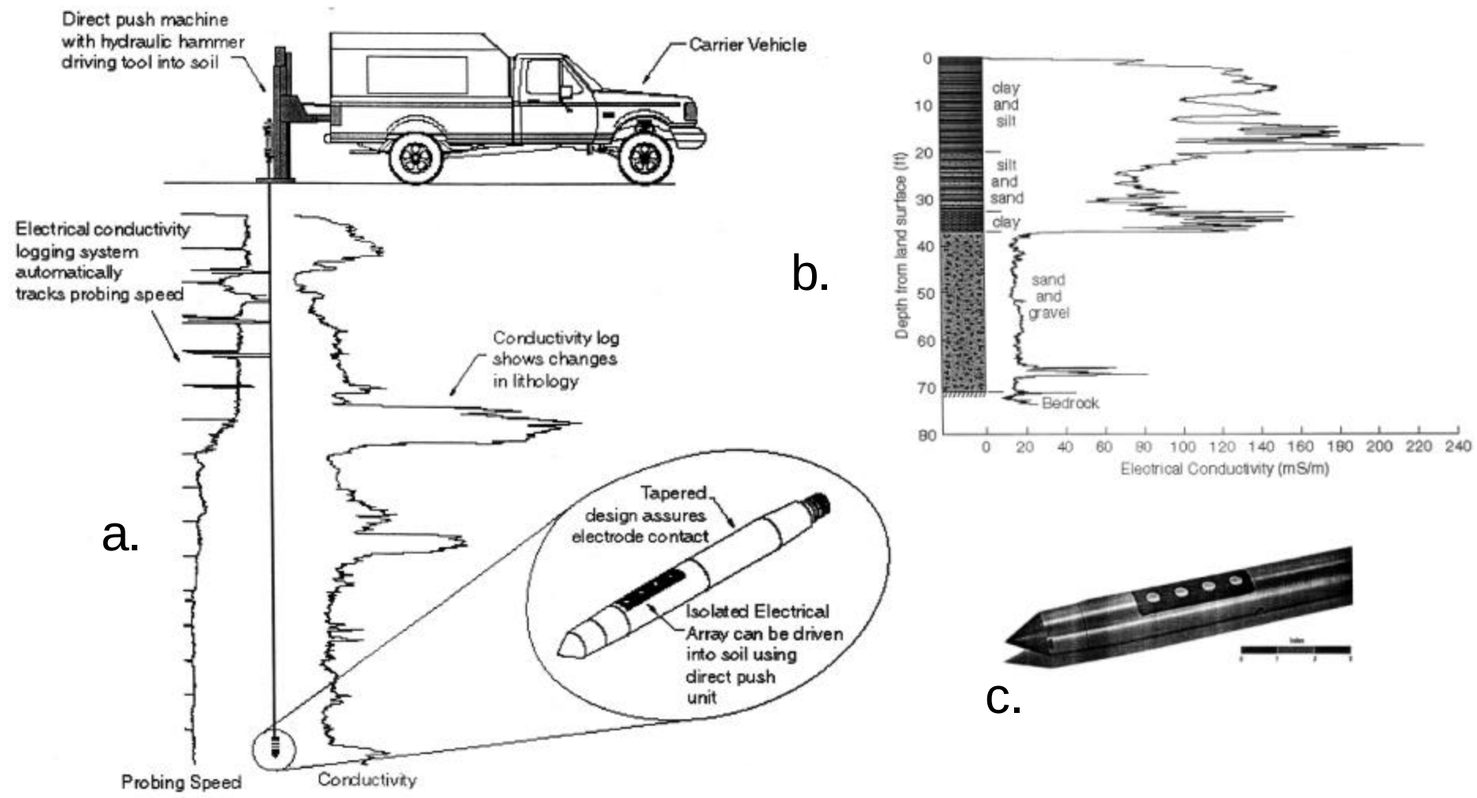

Fig. 2 – (a) Schematic showing truck with tool, (b) example log, (c) direct push (DP) e-logging probe (Illustrations courtesy of Geoprobe®).

The USGS Geoprobe in Action

Fig. 3 – Kelli Collins and Tom Kropatsch collect conductivity data in the Canadian River floodplain.

OSU
School of Geology

Cross-Sections of Study Area

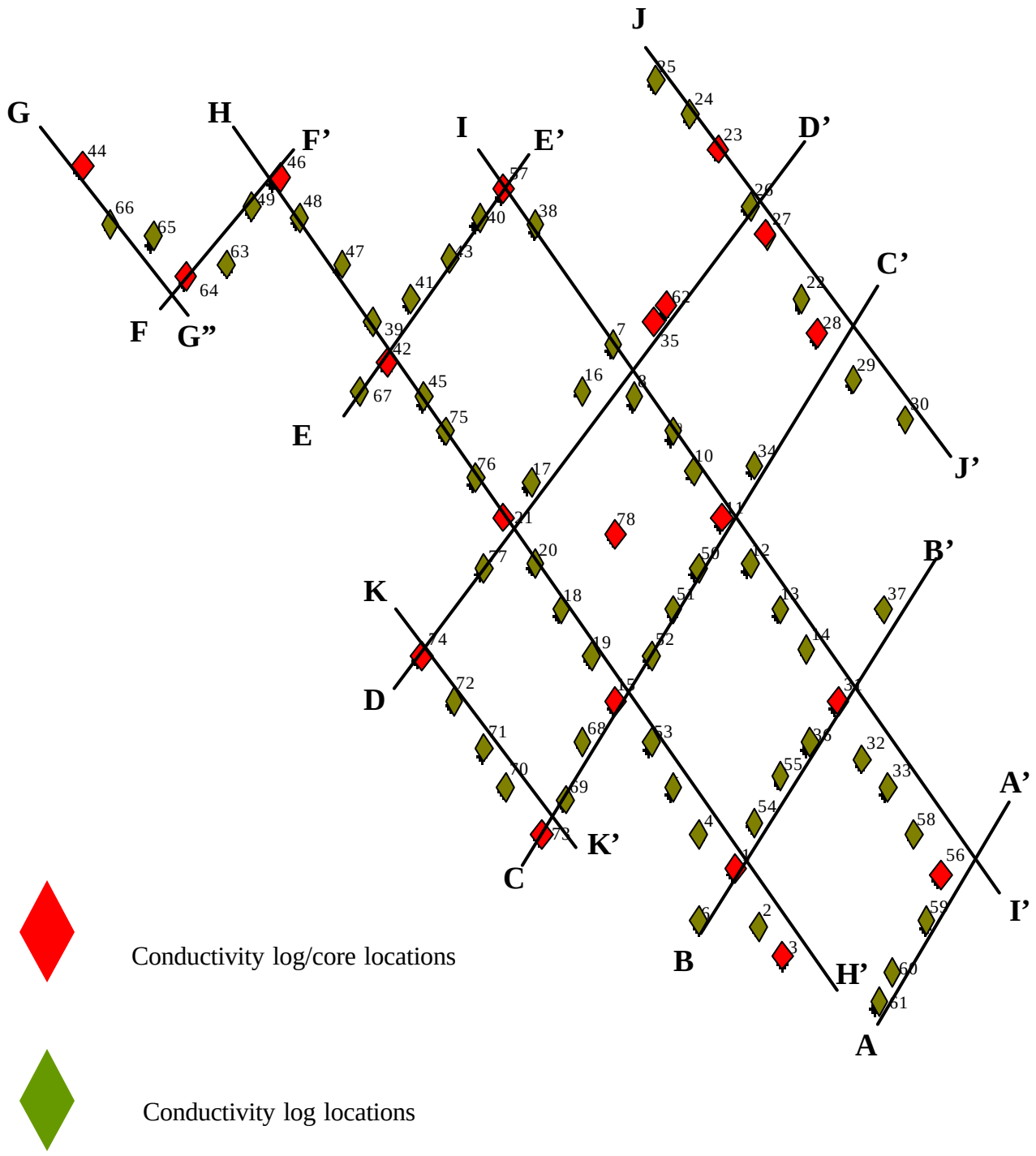

Fig. 4 - Cross-Section Lines of Conductivity Logs

3) depositional subenvironments.

The macro-cores provided a check between the conductivity logs and the actual lithology. However, there was no age control available for the cores that were collected. Therefore the strata of the conductivity logs were matched based on similar lithologic characteristics observed in the cores. The sieve data was also used to match similar strata based on the premise that similar lithologies will exhibit similar texture. Missing sections in the cores due to compaction and poor recovery provided problems for correlation. It was impossible to check the conductivity log data against known lithology for the sections that were missing.

Nineteen continuous cores were collected using the Geoprobe®. The Geoprobe® yielded cores of alluvium in 1.2-meter (4-foot) depth intervals. The total depth of each cored well ranged from 11 to 12.2 meters (6 to 40 feet) encompassing the entire thickness of the floodplain alluvium. The Geoprobe® uses a macro-core piston rod soil sampler. The macro-core sampling tube is 122 cm (48 inches) long and 5 cm (2 inches) in diameter. The sampling tube contains a removable polycarbonate core liner that is 3.8 cm (1.5 inch) in diameter (Fig. 5). The sampling tube also contains a piston rod, which keeps the sampler sealed until the desired depth is reached for each sample interval. The piston rod sampler is designed to enhance the recovery of unconsolidated materials. However, complete sample recovery proved a problem in the floodplain alluvium. When samples contained clay the recovery was around 75%, but when samples were primarily sand the recovery was as low as 25%.

The Geoprobe® can only penetrate unconsolidated materials. Underlying the alluvium is the Permian Hennessey shale bedrock. Once the Geoprobe® reached the shale, the penetration slowed or stopped completely ensuring complete coverage of the alluvium.

Core Description

Cores were described in the laboratory. They were stored upright to prevent mixing of the sediments. The core liner was split open when the cores were described, but they were kept sealed until then to prevent desiccation. The cores were described using a standard strip-log form. Core was described at a scale of 2.5 cm (1 inch) of strip log to 0.3 meter (1 foot) of core. The core descriptions included details about lamina and bed thicknesses, lithology, sedimentary structures, color, and estimates of texture (grain size, sorting). Color was determined using a visual comparator (Exxon-Mobil). Sediment texture was estimated using a binocular microscope and a grain size/sorting visual comparator. Grain size/sorting estimates were taken about every 0.46 meters (1.5 feet), and each sediment sample averaged about 1 to 2 grams. A range was recorded for the grain size of each sample. This range included the smallest to largest grain viewed in the sample. Then an average grain size was assigned to the sample based on the most frequent grain size seen in the sample. The core descriptions with grain size/sorting estimates are included in Appendix A.

After the core description was complete for each well, the core was photographed with Kodak 100 film. Each photograph of the core covered about 6.1 meters (20 feet) of the alluvial section, so a set of two photos was required to cover each well. In addition, photographs were taken of key features (texture, structures, bounding surfaces, lithoclasts) within the cores. The negatives from each core were scanned to create digital image files. The images were then inserted to Powerpoint, pieced together, and described (Appendix B).

Texture Analysis of Core Samples

Once the cores were described and photographed, they were broken up into samples for mechanical sieving. About 15 samples were taken from each of the 78 cores, and the average weight of each sample was about 150 grams. Samples were taken whenever there was an abrupt contact or change in grain size within the core. The grain size estimates performed on the cores during the description process helped to identify any key changes in grain size.

The core samples were placed into labeled sample bags. Each sample was sieved through a set of thirty wire mesh sieves using a Ro-Tap machine. The sieves ranged in size from 1 to 230 according to the U. S. Standard Sieve number (see Appendix C for list). This range is equivalent to –4.64 to 4.00 phi grain size (25.0 to 0.0625 mm). Each core sample was sieved for about 12 minutes. The amount of sediment collected in each mesh was weighed and recorded in grams using a digital scale.

The results from the sieve data were input to an Excel spreadsheet. The spreadsheet was designed to automatically calculate the weight percentages of the individual grain size fractions present in each core sample. These weight percentages were summed to form a cumulative weight percentage curve that was then plotted against phi grain size to form a standard grain size cumulative curve (Fig. 6). A cumulative curve was generated for each sample (Appendix C). Each curve was then used to determine a graphic mean and inclusive graphic standard deviation for that sample. The graphic mean is equivalent to a mean grain size and the standard deviation is equivalent to sorting. The equation used to calculate the graphic mean is:

$$Mz = (\phi_{16} + \phi_{50} + \phi_{84}) /3 \qquad \text{(eq. 1)}$$

The phi grain size was read from the cumulative curves at the 16%, 50%, and 84% marks. By reading the data from these intervals the central two thirds of the grain size data was encompassed. These three values were then averaged to provide a mean grain size for the sample. The equation used to calculate the standard deviation is:

$$\sigma_I = (\phi_{84} - \phi_{16})/4 + (\phi_{95} - \phi_5)/6.6 \qquad \text{(eq. 2)}$$

For this equation the phi grain size was read at 5%, 16%, 84%, and 95% from each of the curves and input into the equation. The inclusive standard deviation is an average of the standard deviation calculated from ϕ_{16} and ϕ_{84}, and the standard deviation calculated from ϕ_5 and ϕ_{95}. This is the best overall measure of sorting because it includes 90% of the distribution (Folk, 1980). The mean grain size and sorting were then used to calculate the permeability.

The equations used to calculate the graphic mean and inclusive graphic standard deviation followed the recommendations of Folk (1980). These equations were used for this analysis because of their inherent sensitivity to the "tails" of the grain size distribution. This sensitivity is important to determinations of sediment grain sorting, a major control on the porosity and permeability of sands.

Texture-Permeability Equation

The raw data (ϕ, K, grain size, sorting) from the classic Beard and Weyl (1973) paper was used to generate a permeability equation (Table 1, Fig. 7). These raw data were input to an Excel spreadsheet that was imported to SAS (v.8.01). SAS was used for analyzing the relationships among the variables. A step-wise multivariate statistical technique was used to evaluate the

Geoprobe Details

OSU
School of Geology

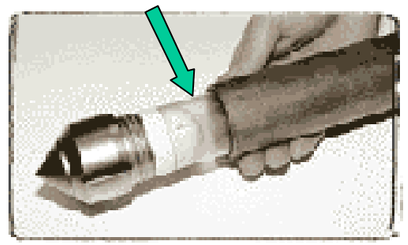

a.

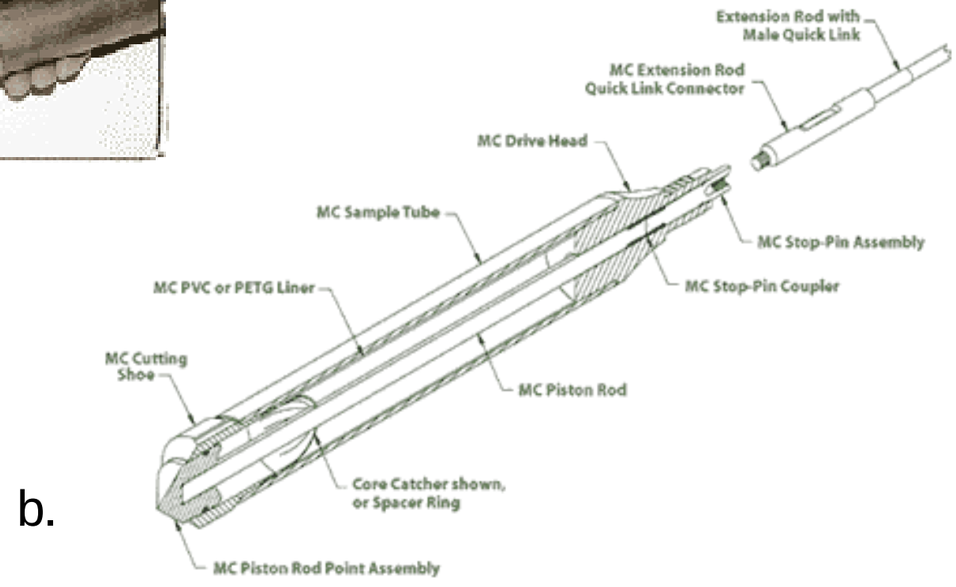

b.

Fig. 5 – (a) Schematic showing MC core catcher with liner (arrow) and (b) macrocore piston rod sampler. (Illustrations courtesy of Geoprobe® web site, www.geoprobesystems.com).

Cumulative Curves for Samples in Well #1

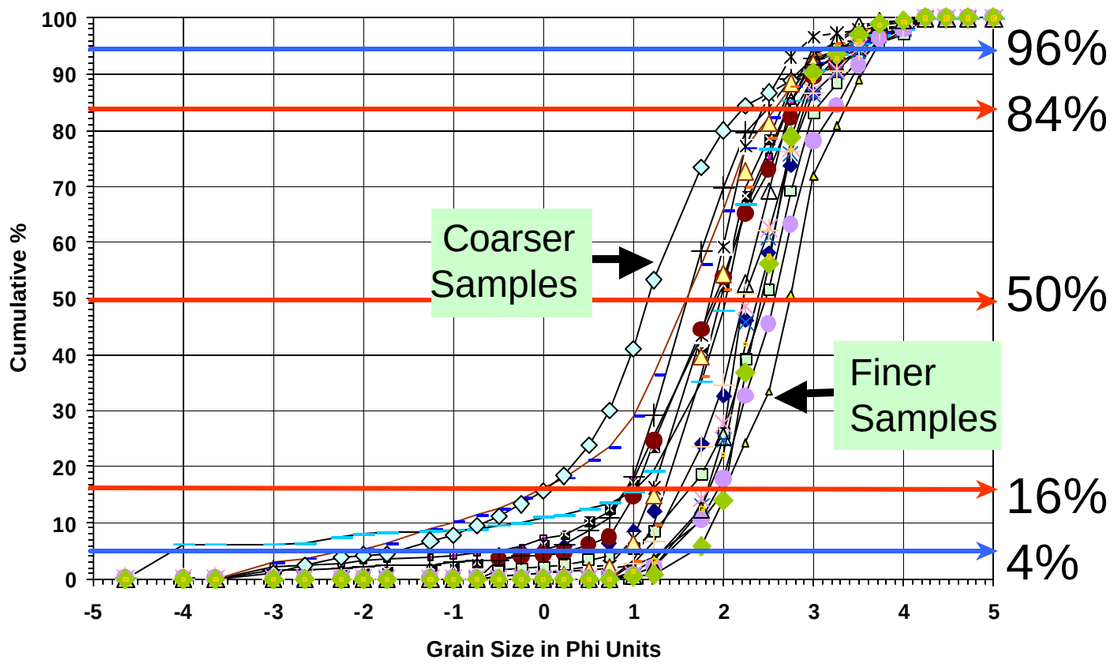

OSU
School of Geology

Fig. 6 – Example of cumulative curves used for estimating graphic mean and standard deviations for use in the permeability prediction equation.

Raw Data

Table 1- Grain size and sorting controls on pre-burial porosity & permeability. These raw data were used for generating the permeability equation discussed in the text.

Data from Beard and Weyl (1973)

Sample	Sorting	Size	phiGS	Porosity	Permeability	Darcies	LogPerm
Sample 1	1.0500	0.8550	0.2260	43.10	475000	475	5.6767
Sample 2	1.0500	0.6050	0.7250	42.80	238000	238	5.3766
Sample 3	1.0500	0.4250	1.2345	41.70	119000	119	5.0755
Sample 4	1.0500	0.3000	1.7370	41.30	59000	59	4.7709
Sample 5	1.0500	0.2135	2.2277	41.30	30000	30	4.4771
Sample 6	1.0500	0.1510	2.7274	43.50	15000	15	4.1761
Sample 7	1.0500	0.1065	3.2311	42.30	7400	7.4	3.8692
Sample 8	1.0500	0.0660	3.9214	43.00	3700	3.7	3.5682
Sample 9	1.1500	0.8550	0.2260	40.80	458000	458	5.6609
Sample 10	1.1500	0.6050	0.7250	41.50	239000	239	5.3784
Sample 11	1.1500	0.4250	1.2345	40.20	115000	115	5.0607
Sample 12	1.1500	0.3000	1.7370	40.20	57000	57	4.7559
Sample 13	1.1500	0.2135	2.2277	39.80	29000	29	4.4624
Sample 14	1.1500	0.1510	2.7274	40.80	14000	14	4.1461
Sample 15	1.1500	0.1065	3.2311	41.20	7200	7.2	3.8573
Sample 16	1.1500	0.0660	3.9214	41.80	3600	3.6	3.5563
Sample 17	1.3000	0.8550	0.2260	38.00	302000	302	5.4800
Sample 18	1.3000	0.6050	0.7250	38.40	151000	151	5.1790
Sample 19	1.3000	0.4250	1.2345	38.10	76000	76	4.8808
Sample 20	1.3000	0.3000	1.7370	38.80	38000	38	4.5798
Sample 21	1.3000	0.2135	2.2277	39.10	19000	19	4.2788
Sample 22	1.3000	0.1510	2.7274	39.70	9400	9.4	3.9731
Sample 23	1.3000	0.1065	3.2311	40.20	4700	4.7	3.6721
Sample 24	1.3000	0.0660	3.9214	39.80	2400	2.4	3.3802
Sample 25	1.7000	0.8550	0.2260	32.40	110000	110	5.0414
Sample 26	1.7000	0.6050	0.7250	33.30	55000	55	4.7404
Sample 27	1.7000	0.4250	1.2345	34.20	28000	28	4.4472
Sample 28	1.7000	0.3000	1.7370	34.90	14000	14	4.1461
Sample 29	1.7000	0.2135	2.2277	33.90	7000	7	3.8451
Sample 30	1.7000	0.1510	2.7274	34.30	3500	3.5	3.5441
Sample 31	1.7000	0.1065	3.2311	35.60	2100	2.1	3.3222
Sample 32	1.7000	0.0660	3.9214	33.10	1100	1.1	3.0414
Sample 33	2.3500	0.8550	0.2260	27.10	45000	45	4.6532
Sample 34	2.3500	0.6050	0.7250	29.80	23000	23	4.3617
Sample 35	2.3500	0.4250	1.2345	31.50	12000	12	4.0792
Sample 36	2.3500	0.3000	1.7370	31.30	6000	6	3.7782
Sample 37	2.3500	0.2135	2.2277	30.40	3700	3.7	3.5682
Sample 38	2.3500	0.1510	2.7274	31.00	1900	1.9	3.2788
Sample 39	2.3500	0.1065	3.2311	30.50	930	0.93	2.9685
Sample 40	2.3500	0.0660	3.9214	34.20	460	0.46	2.6628
Sample 41	4.2000	0.8550	0.2260	28.60	14000	14	4.1461
Sample 42	4.2000	0.6050	0.7250	25.20	7000	7	3.8451
Sample 43	4.2000	0.4250	1.2345	25.80	3500	3.5	3.5441
Sample 44	4.2000	0.3000	1.7370	23.40	1700	1.7	3.2304
Sample 45	4.2000	0.2135	2.2277	28.50	830	0.83	2.9191
Sample 46	4.2000	0.1510	2.7274	29.00	420	0.42	2.6232
Sample 47	4.2000	0.1065	3.2311	30.10	210	0.21	2.3222
Sample 48	4.2000	0.0660	3.9214	32.60	100	0.1	2.0000

OSU
School of Geology

Beard and Weyl Data (1973)

OSU
School of Geology

Grain Size & Sorting - Controls on Pre-Burial Porosity & Permeability

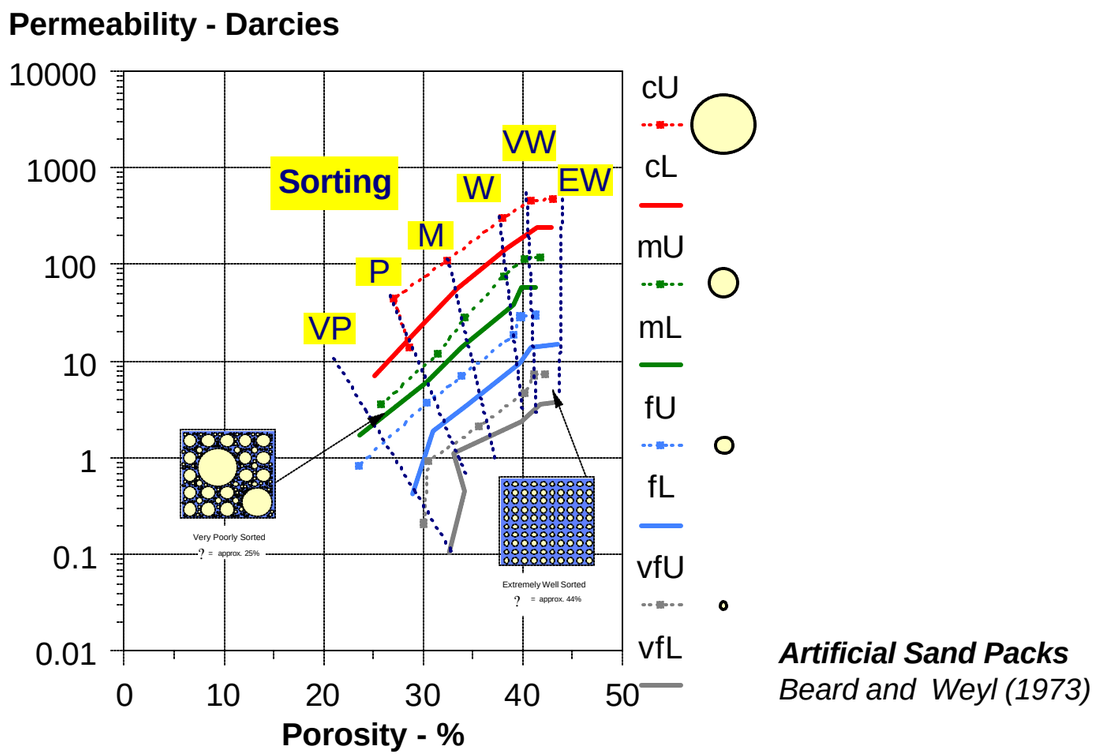

Fig. 7 – This plot of porosity vs permeability is based on the raw data of Beard and Weyl (1973). These data were used to generate the permeability equation used for calculating the permeability of the NLF point bar layers.

controls on the permeability log units. The results indicate the grain size was the most important to the permeability equation. Grain size phi explained 64% of the total variation, while sorting explained 32%. The r^2 value for the multiple regression was 0.97, significant at the $p< 0.001$ level. This value is so high that one suspects that the Beard and Weyl raw data has been adjusted by some additional factor (Shell Research internal results).
The multivariate equation that was produced to calculate the permeability is:

$$\text{Log(permeability)} = 6.190 - 0.495(S_0) - 0.572\ (\phi gs) \qquad \text{(eq. 3)}$$

or

$$\text{Permeability} = (10)^{6.19 - 0.495(So) - 0.572(\phi gs)} \qquad \text{(eq. 4)}$$

where S_0 = sorting and ϕgs = phiGS.

Interpretation of Conductivity Logs for Texture and Generation of 3-D Block Diagrams

A database was set up in Rockworks 99 that contained the latitude (X), longitude(Y), and surface elevation (Z) for each of the sample locations. The conductivity log curve files were then associated with their sample locations in the database. Once these curve files were imported into Rockworks with their corresponding X, Y, and Z locations, the software was able to plot the conductivity logs as cross-sections and 3-D block diagrams. Digital strip logs for display were also created for each of the 19 cores based on the log form descriptions (Appendix A).

Geomorphology

The second project objective, concerning geomorphology, was accomplished by completing three tasks:

1) map and analyze surface sediments,
2) evaluate the stability of the landfill clay-vegetation cap, and
3) analyze the horizontal stability of the Canadian River.

Surface Sediment Analysis

A map of surface sediment texture was compiled to better understand spatial patterns of deposition on the floodplain. Approximately 350 samples were extracted from the uppermost 30 cm (1 foot) of the surface using a hand-held auger. The position of each sample was determined using a portable Global Positioning System; samples were acquired with a 37-meter (121 feet) spacing. The texture of each sample was estimated using the "texture-by-feel" method of Northcote (1979). Sediment texture classes were determined using a standard sand-silt-clay ternary diagram. These data were used to derive a polygon map of surface sediment texture using ArcInfo and ArcEdit.

Evaluation of Landfill Cap Stability

The stability of the landfill cap was evaluated to determine its resistance to fluvial erosion during floods. This cap, composed of clay and heavily vegetated, was emplaced in 1985 in an effort to protect the landfill from erosion. The landfill contains two cells, designated east cell and west cell, and measurements were taken on the south slope of each cell, at 15-meter intervals, for a total of 47 sample sites. Measurements were acquired one meter above the base of the landfill, since this would be the area initially affected by either flooding or natural stream migration. The position of each sample was determined using the same portable GPS.

At each sample point, a hand-held penetrometer was used to measure the compressive strength of the cap in units of kg/cm^2. The penetrometer was pressed into the sediment to a designated depth, and the value was read on the scale within the device. Two different sets of measurements were taken with the penetrometer. First, we took a reading on the surface, since this would be the first to be eroded in the case of stream inundation. Then, we took a reading on the sediment pulled out with the auger. There was a very large difference between the two sets of values, mostly due to the presence of an incoherent organic soil layer above the cohesive clay cap. Instead of averaging the two sets of measurements, each was taken independent of the other. This assured that equal weight was given to both sets of values, since the organic upper layer and the clay lower layer would both be affected, although at different times, during a flood event.

The percent vegetation cover was estimated within a one meter square area around each sample point using visual charts prepared by Hodgson (1974). Vegetation, as used here, is defined as all above-ground living biomass that has a root system and therefore offers stability to the landfill cap, rather than simple ground litter which would wash away immediately upon contact with stream flow.

The final measurement taken was the slope gradient of the landfill at each site. From the top of the landfill, a clinometer was sighted down the face of the landfill to determine the slope angle. The lower the slope angle, the higher the degree of stability of the landfill at that site.

All values were entered into a Microsoft Excel spreadsheet. For each variable (penetrometer reading for the soil and the clay cap, vegetation percentage and slope angle), a mean and a standard deviation were calculated. With this information, a Z score was determined using the following equation:

$$Z = \frac{\text{numerical value} - \text{arithmetic mean}}{\text{standard deviation}} \qquad \text{(eq. 5)}$$

Once this value had been determined, a composite Z score was calculated according to the following formula:

$$Z_{composite} = Z_{soil\ permeability} + Z_{clay\ permeability} + Z_{vegetation} - Z_{slope} \qquad \text{(eq. 6)}$$

In doing this statistical transformation, the values are all normalized and can be compared to one another. Once all z-scores were calculated, a percentile rank was established at the 33% and 67% values. All z-scores below the 33% value were assigned a rank of one, meaning that those areas were the least stable when all variables were taken into account. Z-scores between the 33% and 67% values were assigned a rank of two (moderately stable), and those above the 67% value were assigned a rank of three (most stable). These values were plotted, using ArcInfo and ArcEdit, on the same map as the surface sediments and were color coded according to the designated rankings.

Stream Stability Analysis

The lateral migration of the Canadian River was assessed to determine the likelihood that the landfill could be impacted by channel erosion. This analysis utilized 13 aerial photographs spanning from 1937 to 1997. Curtis and Whitney (2000) had digitized these photos to show the landfill, bankfull stage of the channel, and low-flow active channel. The aerial photos were

registered to one another and a grid was created as an overlay, with each grid cell have dimensions of 53 meters by 53 meters. Each aerial photo was inspected in turn to determine whether or not the low-flow active channel occupied each grid cell. The number of times the low-flow channel occupied each cell was tabulated from which the probability of channel occupation for each cell could be calculated. The horizontal and vertical distance from each cell to the low-flow channel was also measured.

Principal Findings and Significance:

Figures 8, 9, 10 and 11 provide some of the best examples of the sedimentary features noted in the 19-cored wells. The depth units are expressed in English units rather than metric units as the Geoprobe probe rods are manufactured in increments of 4' lengths.

Fig. 8 - *Well #1 Core* has a thin, incipient soil (b), mud rip-up clasts (b), and a sharp contact of sands with the underlying mud layer (b). No cross bedding is obvious in the sand beds.

Fig. 9 - *Well #3 Core* shows an excellent example of an accumulation of silt and clay that has been carried past the piston by flowing water (due to sudden pressure drop in the core barrel (b). This well also has mud clasts and a solid contact with the underlying Hennessey Fm.

Fig. 10 - *Well #7 Core* shows an excellent recovery of gravel near the base of the valley fill and a very sharp contact with the underlying Hennessey red bed (b). Mud in this core is both red and black (organic-rich).

Fig. 11 - *Well #46 Core* has some of the best-preserved cross bedding in any of the 19 cored wells. We noted that sedimentary structures were always absent or disturbed below the water table due to rapid movement of water into the well bore during penetration of the probe. The preserved tough cross bedding in this well occurred above the water table (b). Disruption (doming) of layering due to water movement is apparent in images 11b and d. Poorly sorted gravels were recovered near the base of the well (c). Image 11e contains two fining upward cycles, each with gravel at the base.

Criteria for Correlating the Conductivity Logs

The vertical succession of the point bar from the basal contact with the underlying Permian Hennessey Fm. to the present day land surface was vertically subdivided on the basis of conductivity profiles, mud layers, and rapid changes in sediment texture (grain size, sorting). We have no strong independent age-control on the stratigraphy of the point bar. Consequently, the criteria used for correlating the conductivity logs were:

1) similarities in conductivity response patterns,
2) stratigraphic position (superposition), and
3) lithologic similarity.

Our correlation style was strongly tempered by observations about the nature and distribution of the modern Canadian River floodplain sediments.

<u>Well #1</u> – Canadian River Floodplain

a.

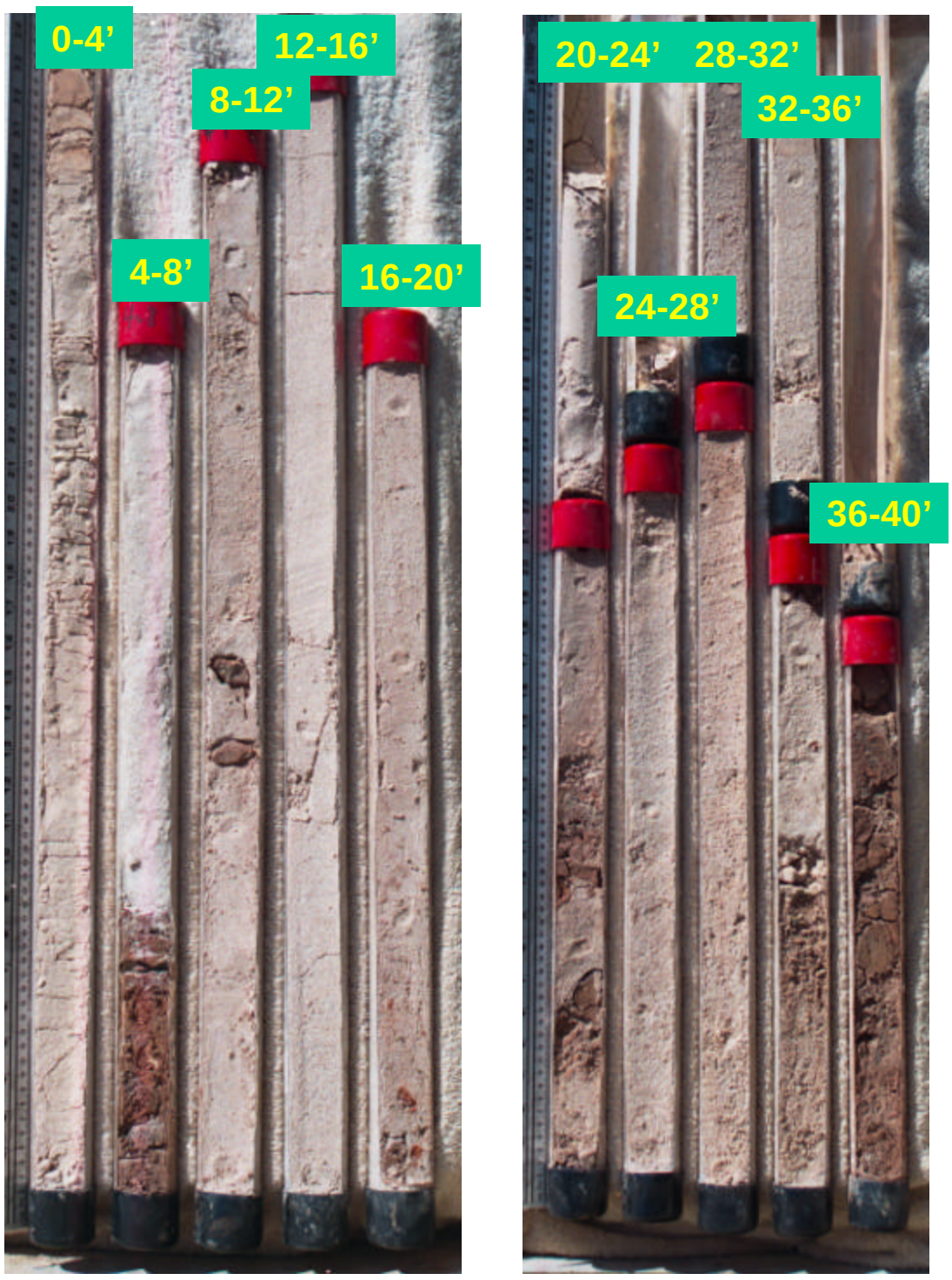

Figs. 8a, b (facing page) – Cores from Well #1 showing sand / mud layers and mud clasts. Each core segment is 4’ in length though compaction of the sediment and loss of some materials (failure of core catcher?) always results in core length segments that are <4’.

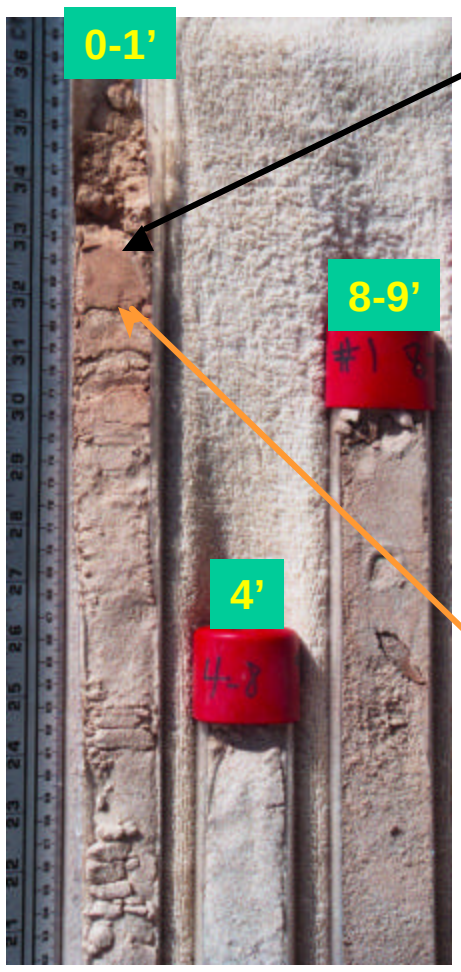

Incipient Soil Zone

Well #1
Canadian River Floodplain

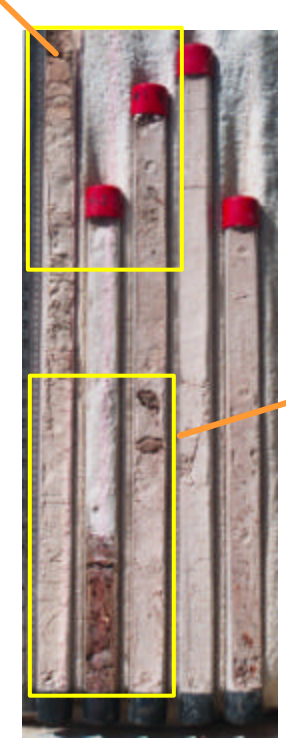

b.

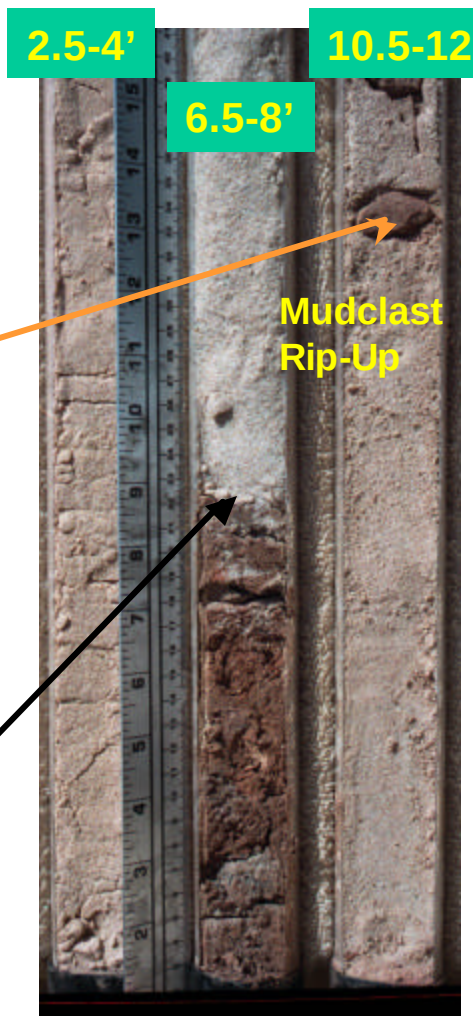

Note sharp contact of sand with underlying mud.

<u>Well #3</u> – Canadian River Floodplain

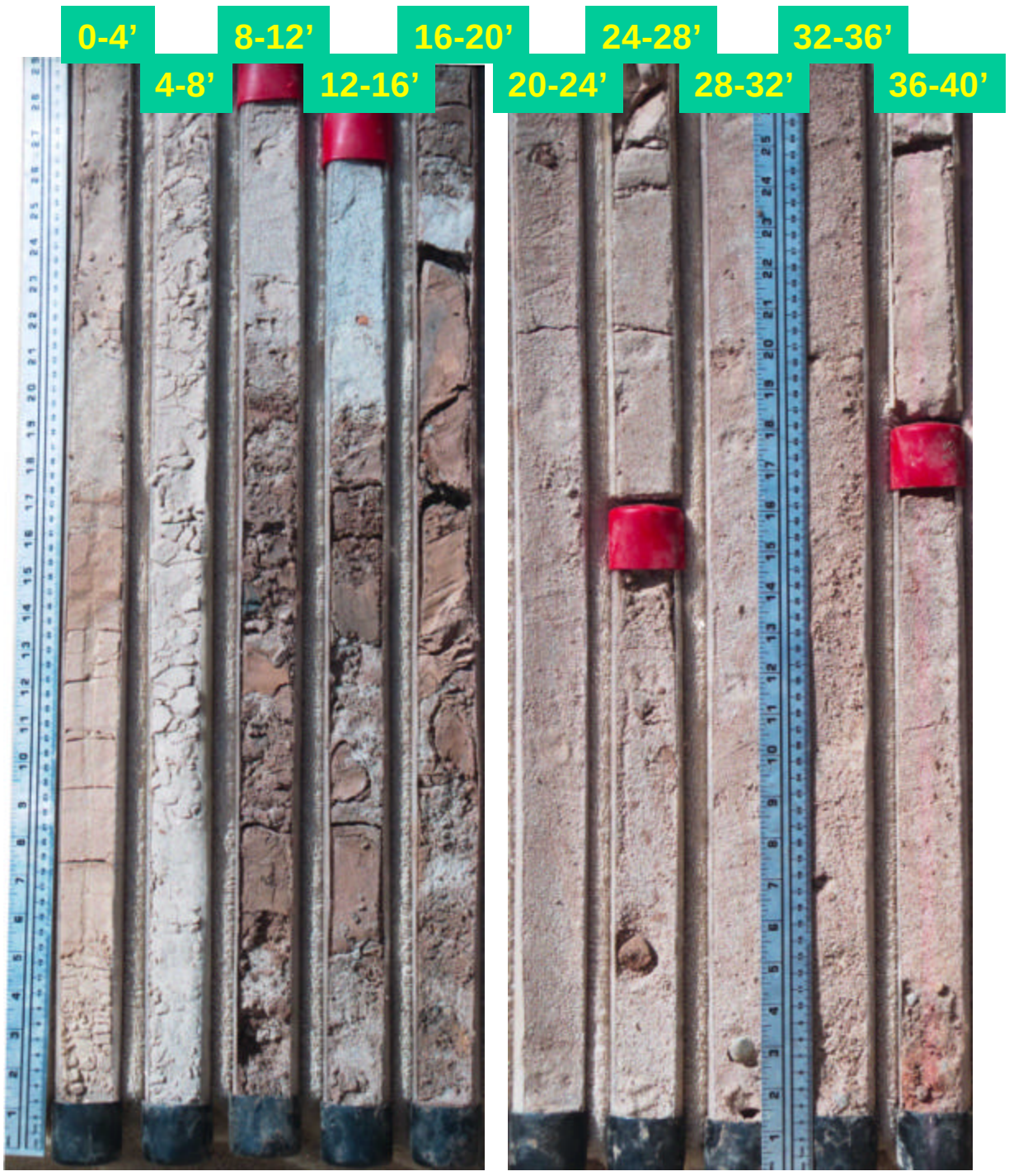

a.

Figs. 9a, b (facing page) – Cores from Well #3 showing layers, mud clasts, and the underlying Hennessey Fm. Due to movement of water into the well bore, some sediment is always transported up around the coring piston, accumulating in the upper portion of the core sleeve.

<u>Well #3</u> – Canadian River Floodplain

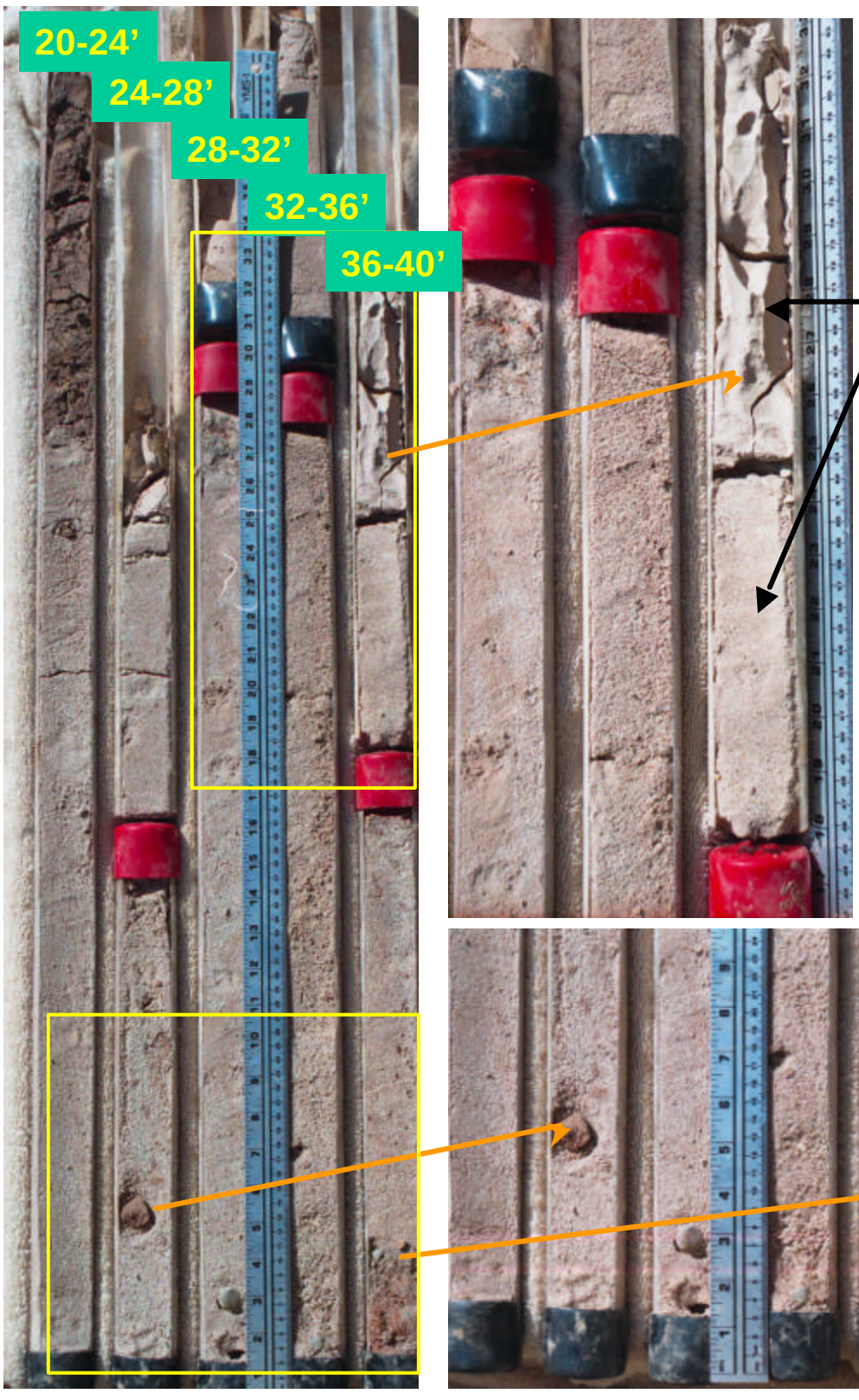

<u>Well #7</u> – Canadian River Floodplain

a.

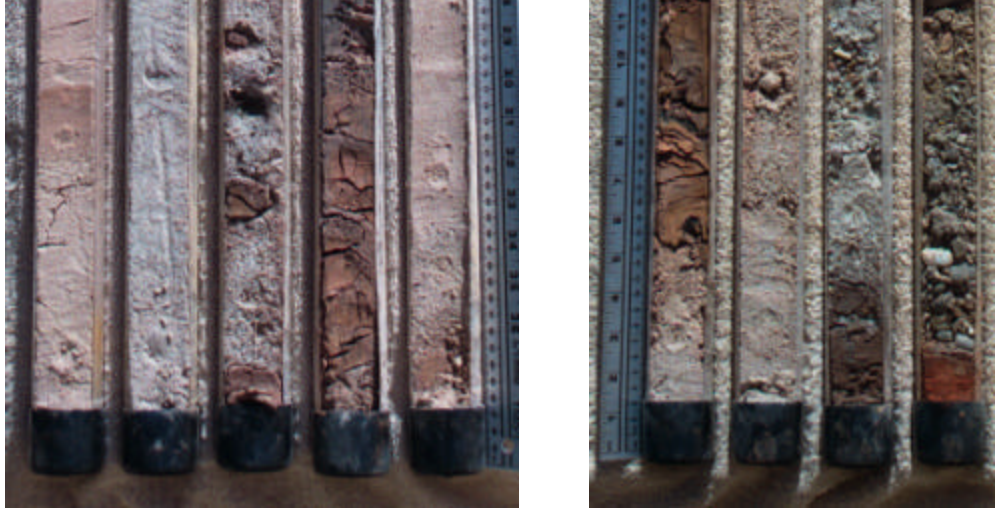

Figs. 10a, b (facing page) – Cores from Well #7 showing sand / mud layers and gravel at the basal contact with the Hennessey Fm.

Well #7

Canadian River Floodplain

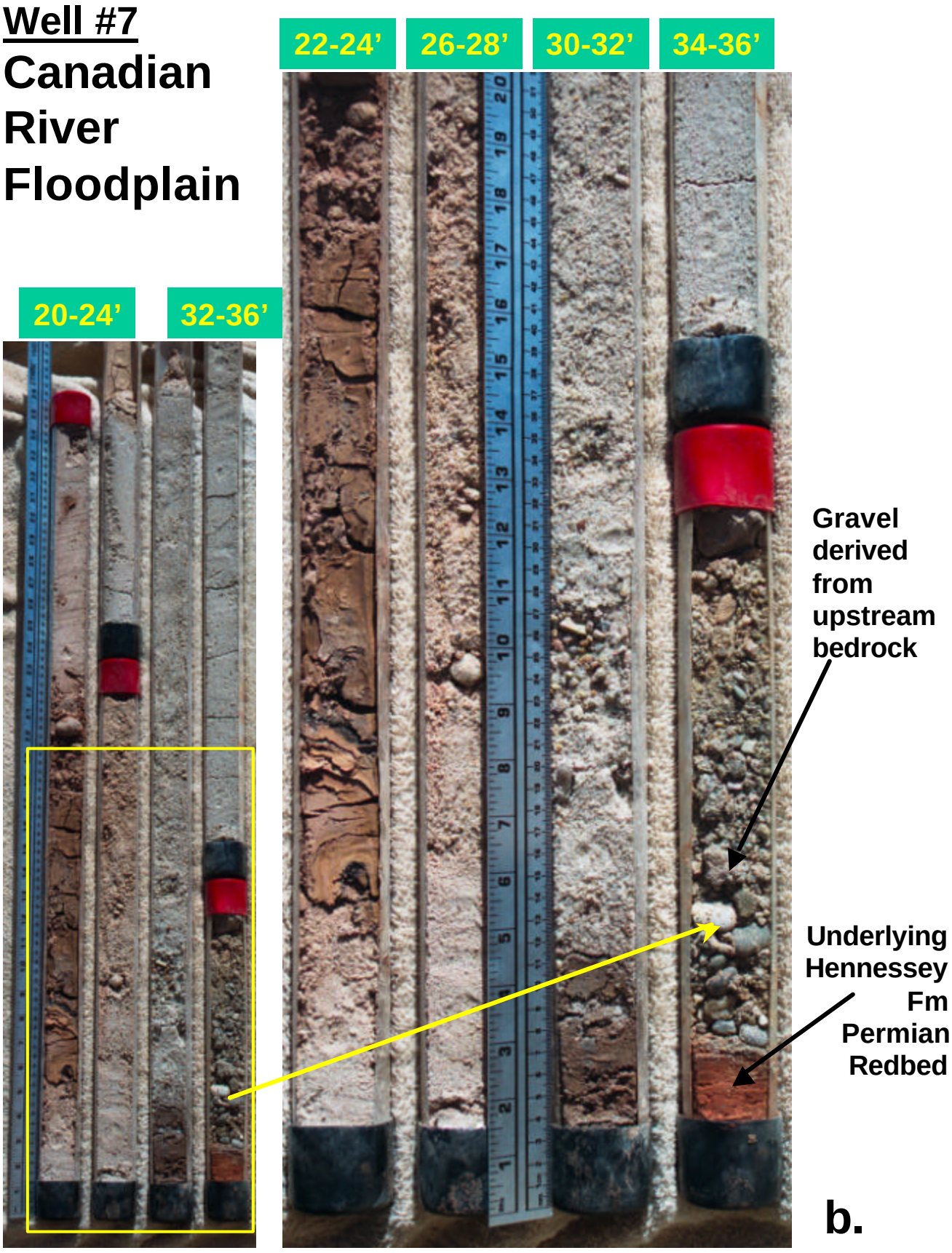

b.

Well #46 – Canadian River Floodplain

a.

Figs. 11a-e (facing pages) – Cores from Well #46 showing sand / mud layers, trough cross bedding, fining upward cycles, and gravel intervals that have high calculated permeability.

Well #46

Canadian River Floodplain

b.

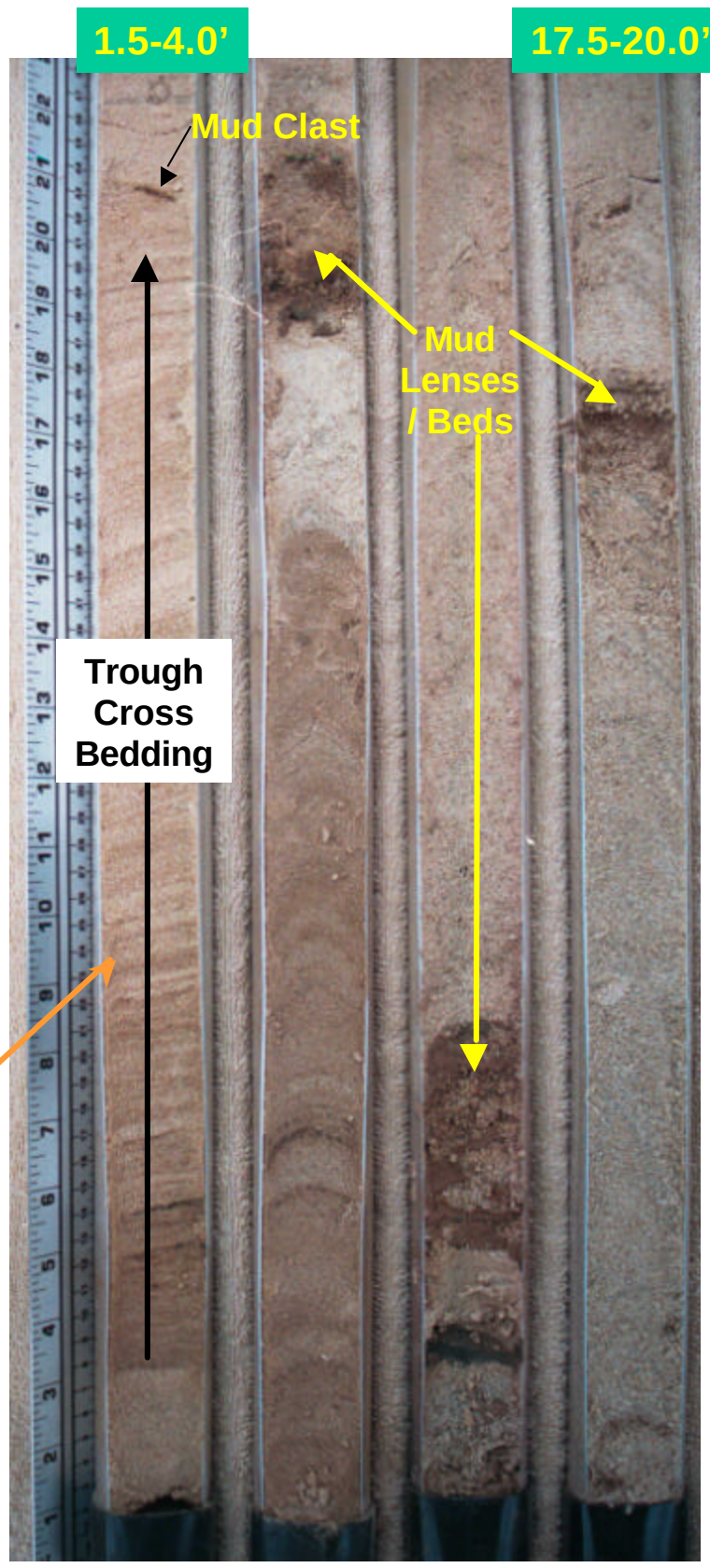

c.

Well #46

Canadian River Floodplain

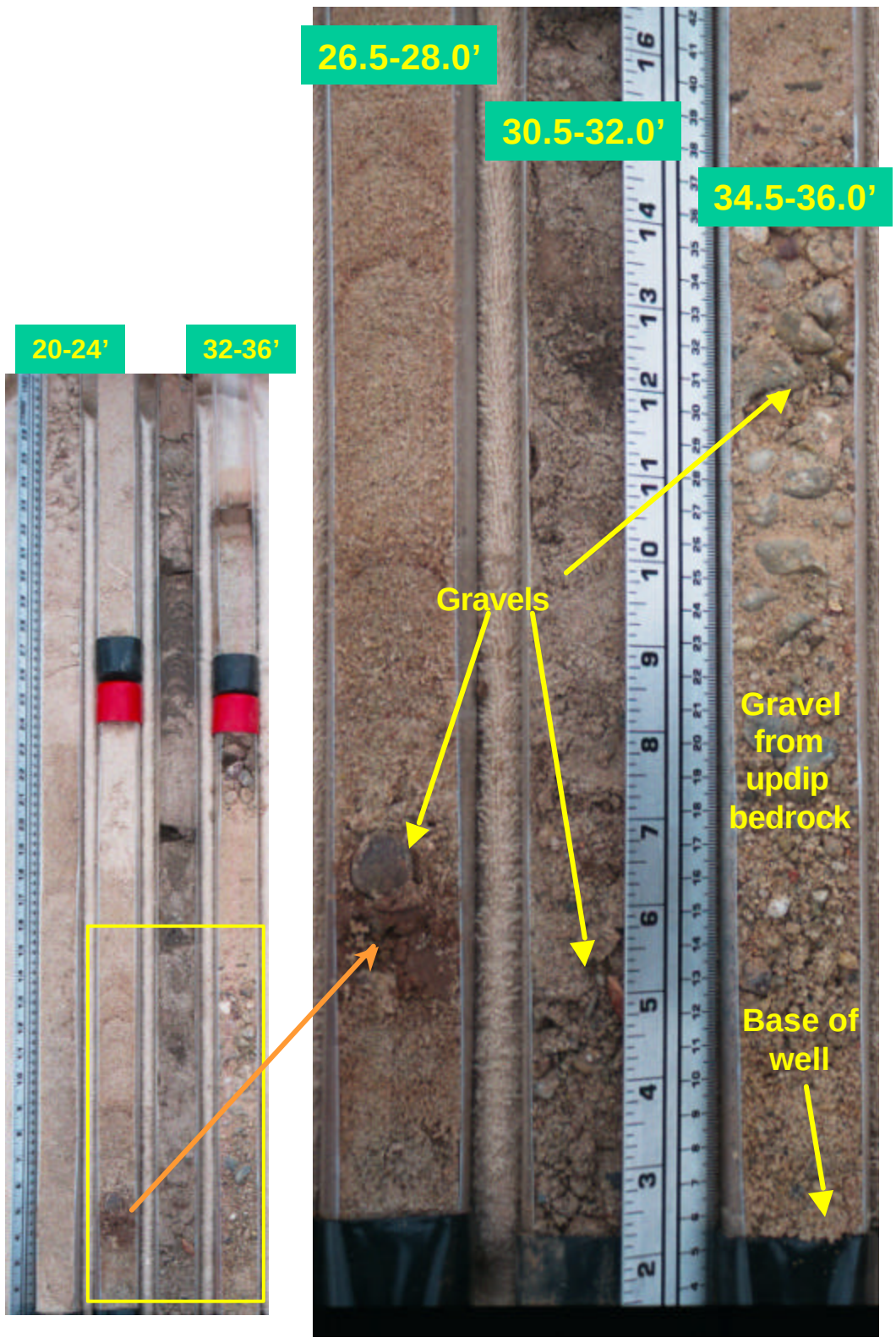

Well #46

Canadian River Floodplain

d.

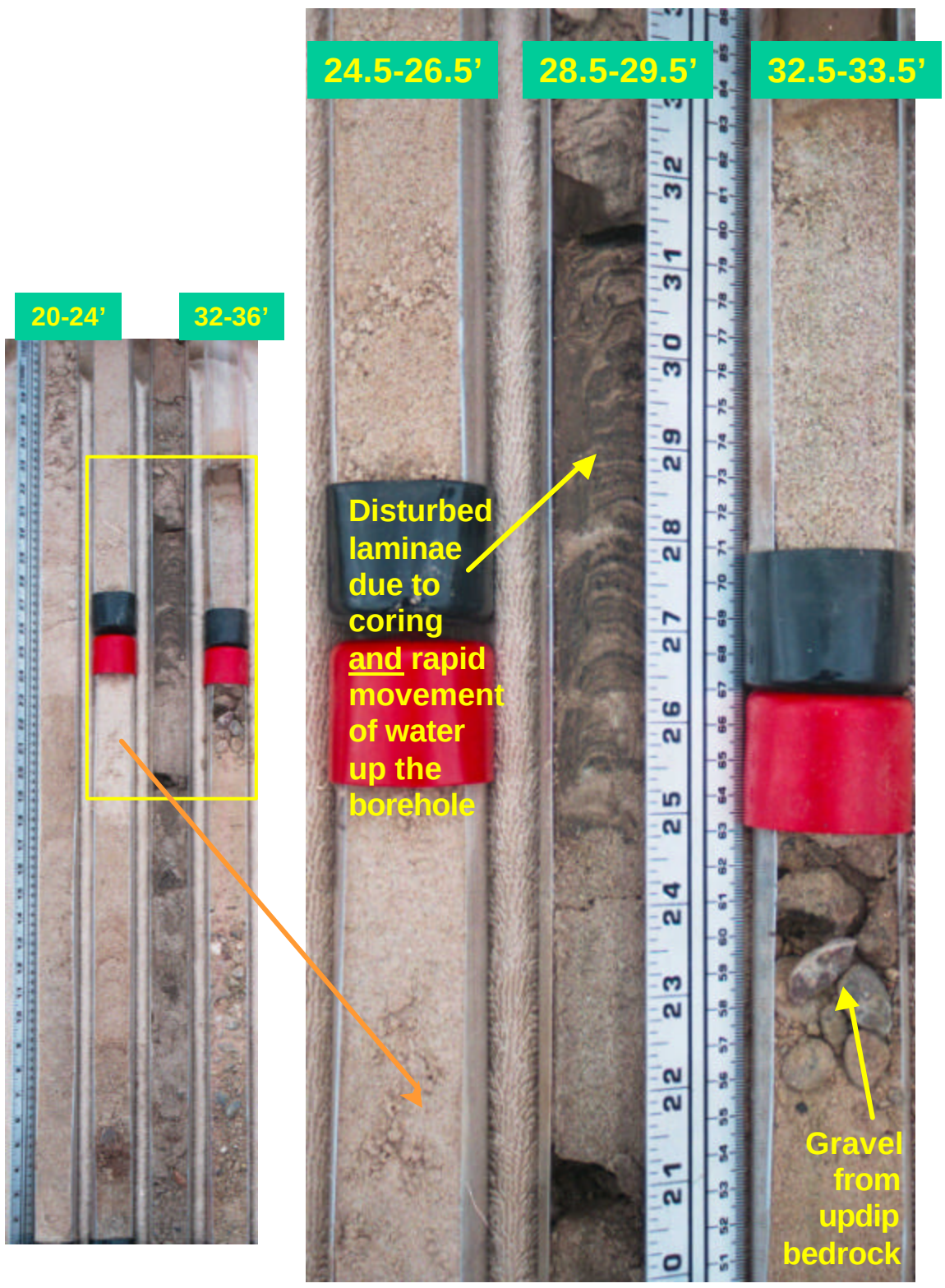

e.

Well #46

Canadian River Floodplain

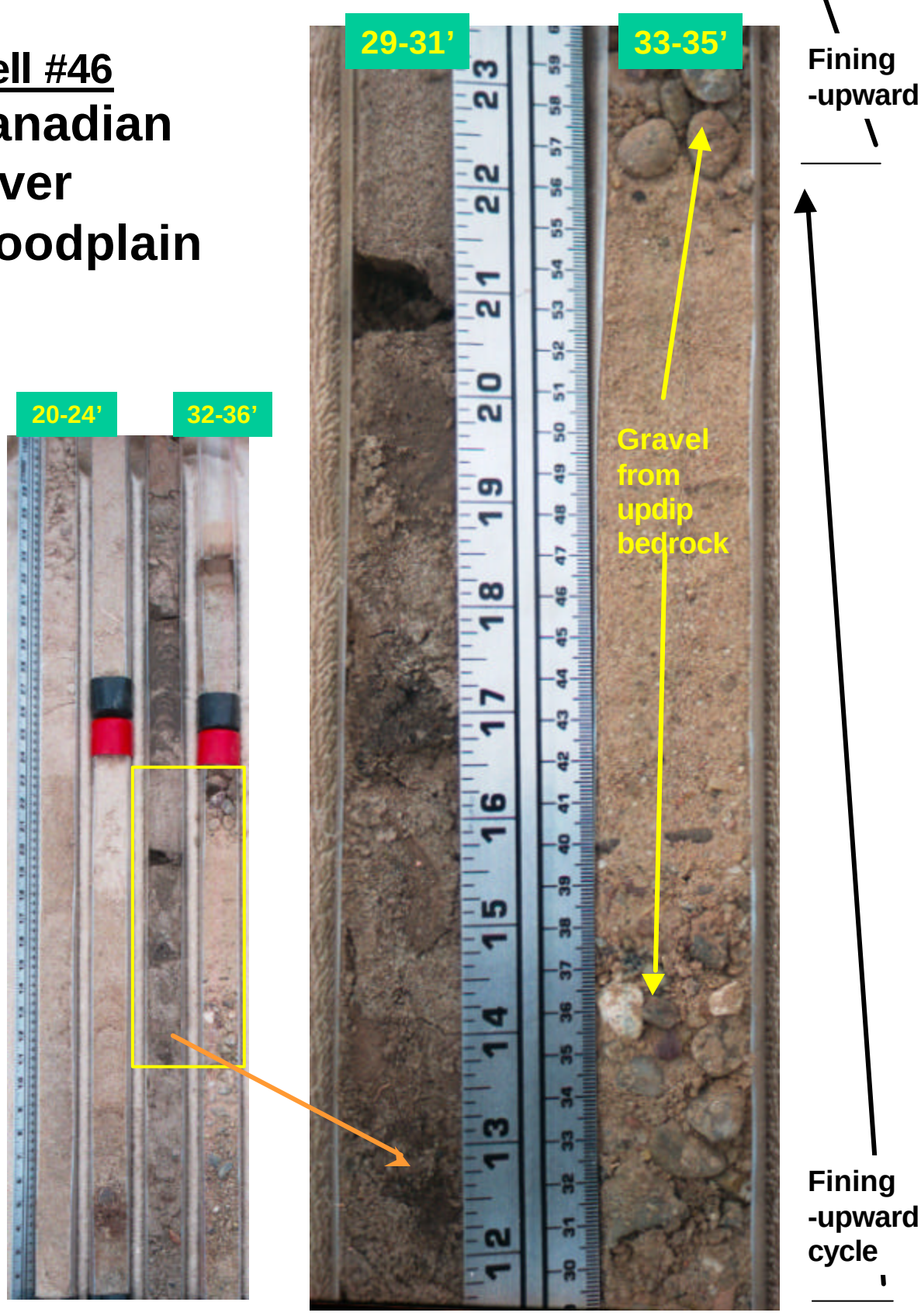

1) Floodplain: very flat with little relief (see Fig. 12)
2) Sand Bars:
    a) Initially sinuous-crested linguoid-shaped dunes that form during high discharge events (Fig. 13, 14)
    b) final morphology results from continuous dissection of the constructional bar forms by braids of channelized flow that accompany waning flow (Fig. 12)
    c) incision of the constructional bar forms continues until the occurrence of the next high discharge event
3) Mud Layers
    a) Occur adjacent to main channels; are flat-topped, may onlap an erosional surface, are discontinuous (Fig. 15)
    b) mud layers develop as silt and clay settles from suspension each time high water (which has a high suspended load in the Canadian River) inundates the topographic lows on the floodplain
    c) the topographic lows are the erosional features mentioned above and are produced subsequent to a high-discharge event

In this sense, the internal morphology of a bar-form in the Canadian River is constructional while erosional processes have shaped the external morphology. Subsurface evidence confirms these observations with respect to bar form shape and relationship to mud layers. The contacts of mud layers with underlying bar sands were observed in core to sometimes onlap erosional surfaces and vice versa (Fig. 16). In addition, mud clasts are found at the base of some of the sandbars (Fig. 17). The mud clasts were derived from the mud layers as the river reasserts itself and erodes the surface sediments during a high discharge event.

Conductivity Cross Sections

Cross-sections of the conductivity logs were correlated across the study area. Eleven cross-sections were created. Six of the cross-sections run perpendicular to the point bar and five run parallel to the point bar. Two cross-sections are included here: Cross-section D-D' (Fig.18) runs perpendicular to the point bar, and a portion of cross-section I-I' (Fig. 19) runs parallel to the point bar. The remaining cross-sections are in Appendix D.

The cross-sections indicate that the gross stratigraphy of the floodplain is essentially horizontal (layer-cake) and similar to flat floodplain topography seen today (Fig. 12). The floodplain alluvium was broken up into 5 intervals that are labeled as Unit 100 through Unit 500. These units are identified on each of the cross-sections.

Unit 100: Basal layer of the alluvium. It ranges in thickness from 1.8 to 2.4 meters (6 to 8 feet) from the base of the alluvium. This unit is characterized by coarse-grained sediments and gravels.

Unit 200: Sand overlying the basal layer. It is about 3 m (10 feet) thick.

Unit 300: Unit overlying the 200 unit. It ranges in thickness from 4.5 to 6 m (15 to 20 feet). This layer contains extensive mud layers and lenses.

Incised North Bank of the Canadian River, Norman, Oklahoma

Fig. 12 – A portion of the Canadian River floodplain that has been incised and abandoned. Note the flat, horizontal nature of the floodplain. The inset photograph shows a thin, dried mud layer that will be eroded during the next major high discharge event. This mud layer was observed near the yellow arrow in the larger photograph.

Sand Bars in Oklahoma Rivers

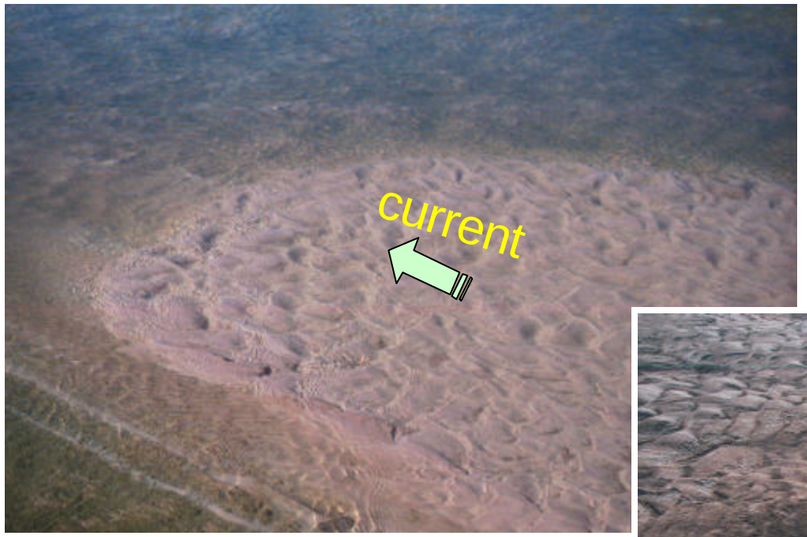

Fig. 13b - Migration of a thin unit bar down the Canadian River channel at low flow – linguoid ripples are advancing up the back of the bar form.

OSU
School of Geology

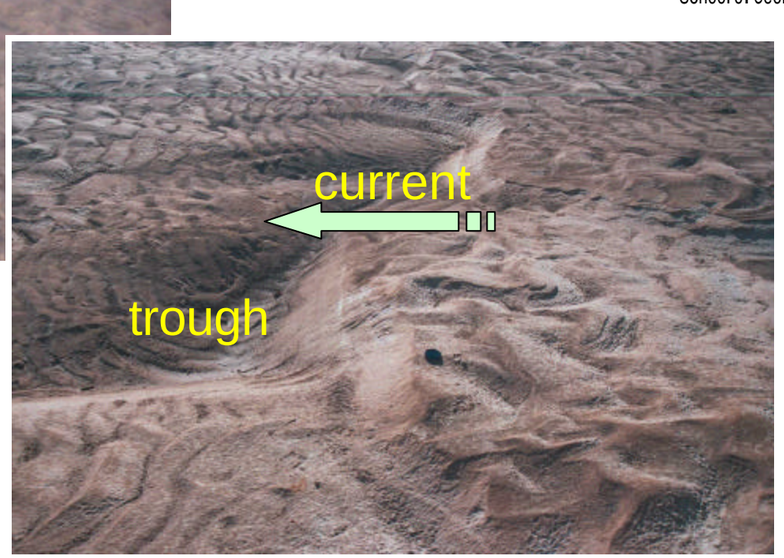

Fig. 13a – Ripples on the surface of a series of large advancing dunes in the Cimarron River of Oklahoma - note the trough in front of the bar form - these dunes and troughs formed during a high a rate of discharge

Foresets in an Exhumed Subaqueous Dune, South Bank of Canadian River

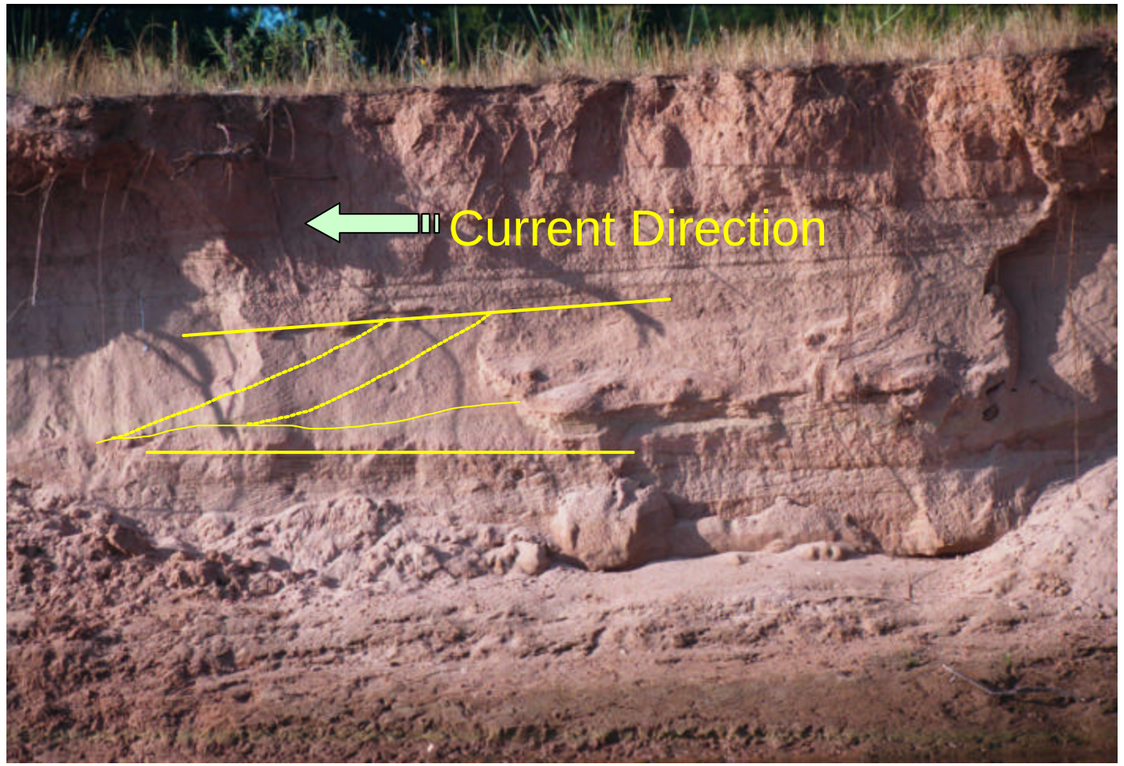

Fig. 14 - Cross Bedding in a stacked unit bar that migrated from right (west) to left (east) in the Canadian River near Norman, Oklahoma

Development of Mud Layers in the Canadian River, Norman, Oklahoma

Fig. 15 - Subtle topographic lows on the margin of the main channel accumulate muds (and some algae) that form the discontinuous mud layers seen in the subsurface cores and as depicted the cross sections.

Evidence for Deposition on Erosional Surfaces Internal to the Point Bar

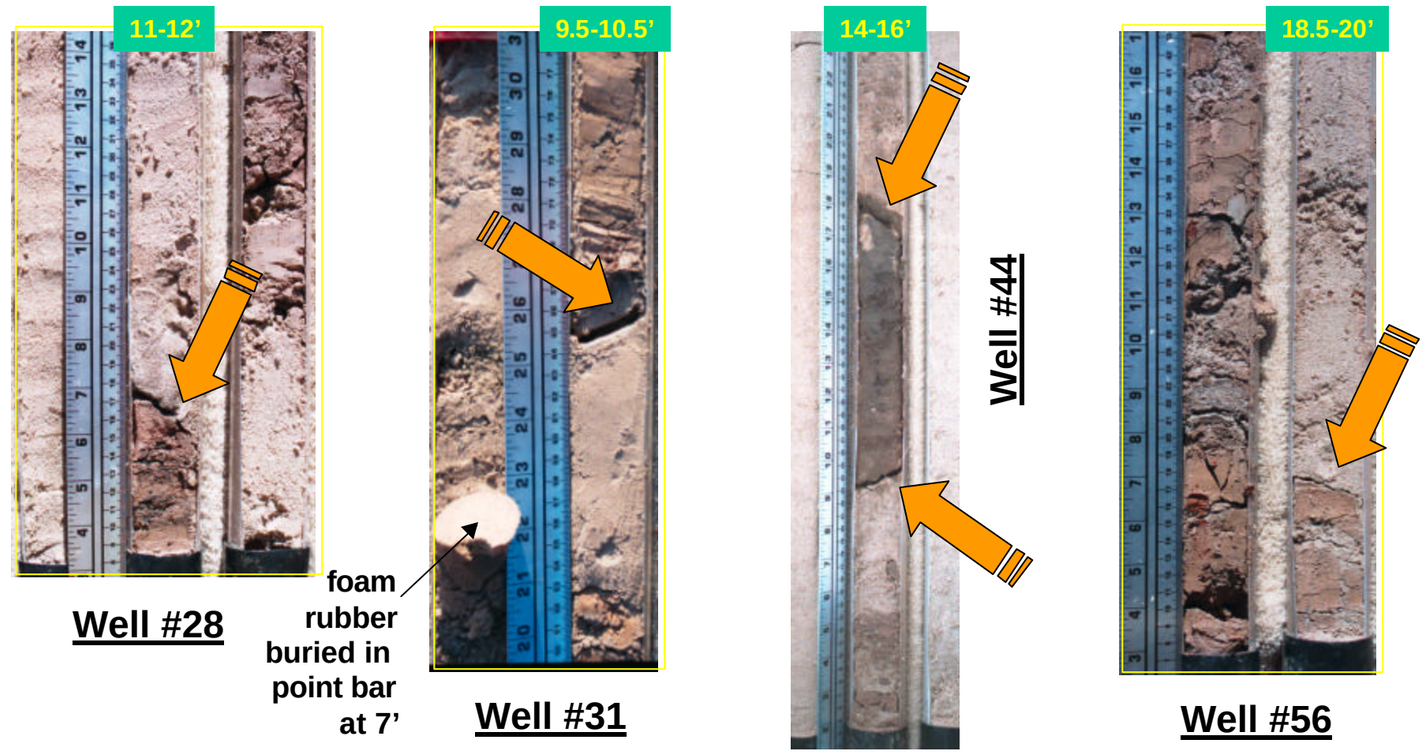

Fig. 16 – The onlap of sand or mud layers onto stratal surfaces that exhibit relief suggests the basal contact of each correlation unit in the point bar (**Intervals 200-500**) is erosional (in part or entirely?). The basal contact of the **100 Interval** with the underlying Hennessey is clearly erosional. This contact is highlighted in other core photos.

Well #11

Canadian River Floodplain

28-32’

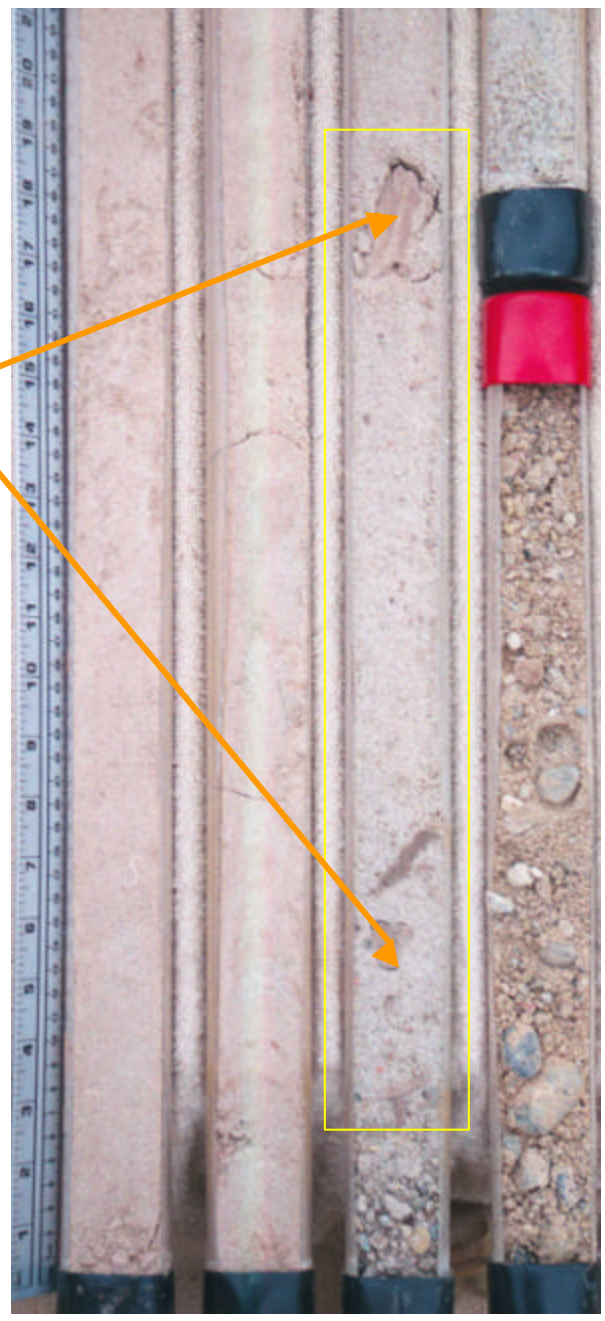

Fig. 17 – Mudclasts or “rip-ups” commonly occur at or near the base of many of the major sand beds in the Norman Landfill point bar.

Norman Landfill
Cross-Section D-D’

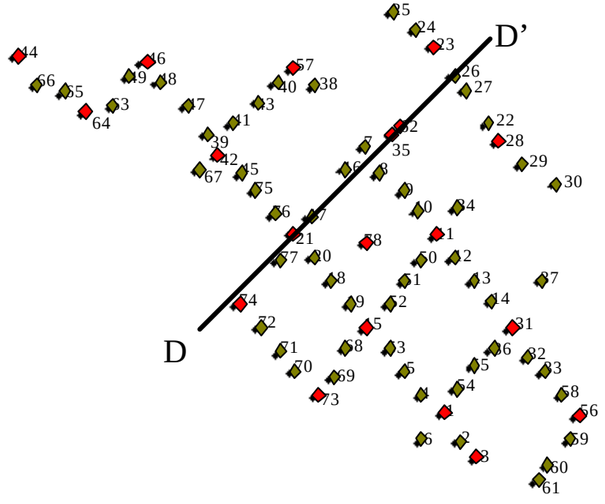

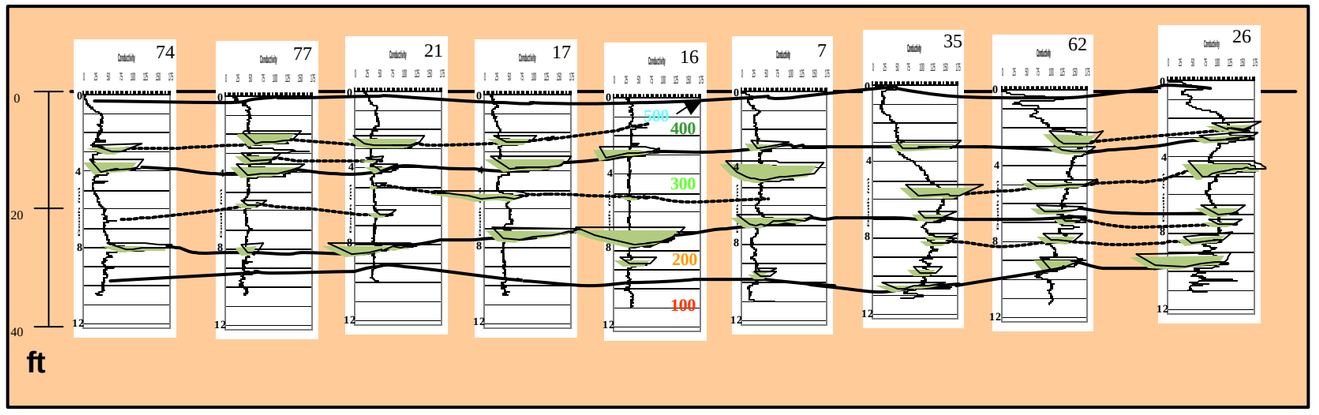

Fig. 18 – Example cross section running perpedicular to the point bar

Norman Landfill
Cross-Section I-I’

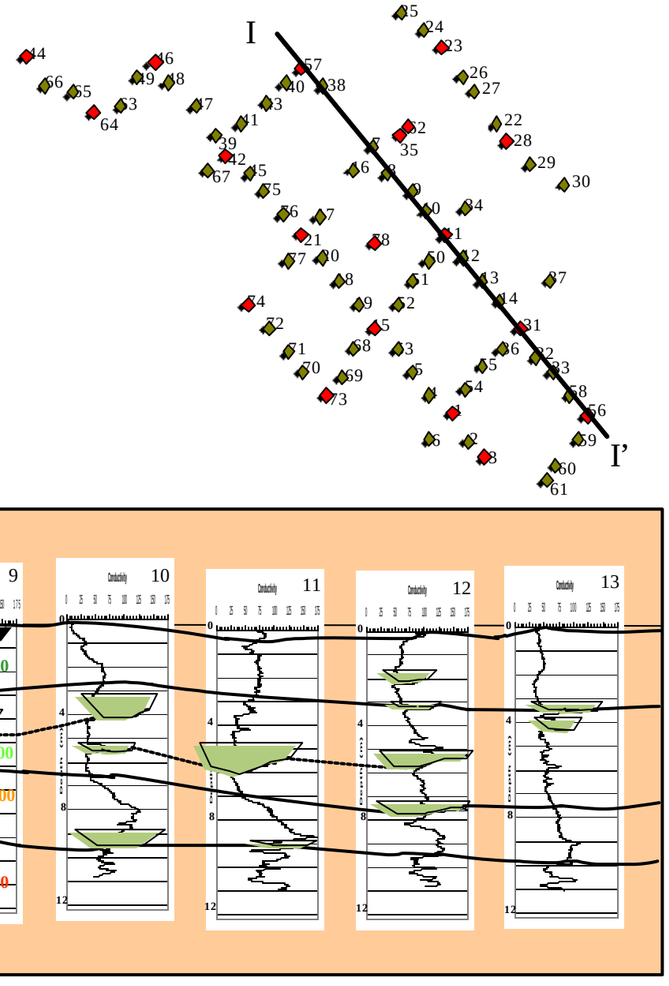

Fig. 19 – Example cross section running parallel to the point bar (complete cross-section is shown in Appendix D)

Unit 400: Sand unit overlying the 300 unit. It is about 2.4 to 2.7 m thick (8 to 9 feet).

Unit 500: Unit extending from the surface down to about 1 m (3 feet). This unit is composed of very fine-grained sands.

These intervals each have distinct texture (grain size/sorting) and are bounded by mud layers. Mud layers were drawn on the cross-sections to illustrate the number and thickness of the muds in the floodplain alluvium. The cross-sections indicate that the number and thickness of muds increases toward the slough. The lateral extent of the mud layers throughout the alluvium is as follows:

1) Mud layers perpendicular to the bar complex range in length from <37 meters (<120 feet) to about 148 meters (485 feet)
2) Mud layers parallel to the bar complex range in length from <37 meters (<120 feet) to about 222 meters (728 feet)

Vertical Profiles and Interval Units for Correlation

A Type Conductivity Log (Well #1, Fig. 20) shows the standard vertical succession of sand and mud encountered in the 19 cores taken from the point bar. The lower 6-8' of the fill yields a characteristic 'choppy' conductivity response that is related to the basal layer (our *100 Interval*) deposited on top of the underlying Permian Hennessey Formation. The frequency distributions of grain size (Fig. 21) and sorting (Fig. 22) for the basal layer are negatively skewed and bimodal. One mode is medium grained (0.25-0.5mm) and moderately sorted. The other mode is very coarse grained (0.5-1mm) and poor- to very poorly sorted. Some wells contain granule- (2-4mm) and pebble-size materials (>4mm).

At this point, we are unable to see any geographic significance to the bimodality. The bimodality may reflect inadequate sample size for such a heterogeneous population (n=55). The texture (grain size / sorting) of the basal layer is distinctly different from the texture of all the overlying layers on the basis of a Satterthwaite* t-test ($p < 0.0001$) performed in SAS, v. 8.01, 1999-2000 (Tables 2, 3). The null hypothesis (H_o) for this test assumes that the means for the two populations are equal (or not different). In this exercise, we assumed a real difference to exist between populations means if $p < 0.1$.

A well developed but discontinuous mud layer (1-3' thick) is commonly present above the basal gravel. The overlying sand layer (*Interval 200*) is about 3 meters (10 feet) thick. This interval is fine to medium grained and moderately to moderately-well sorted. A few of the wells in this interval contain coarse grained, poorly sorted sand.

Another discontinuous interval of mud lenses (1-3’ in thickness) lies above *Interval 200*. The *300 Interval* is fine to medium grained and moderately to moderately-well sorted. This interval is the thickest (about 15-20’) and most heterogeneous of the layers with respect to the occurrence of mud layers and lenses. A t-test suggests that *the 300 Interval* mean grain sorting is significantly different from the underlying *200 Interval* ($p < 0.0001$). The grain sizes between the two layers are slightly different ($p < 0.08$) (Tables 2, 3). Another 1-3’ thick mud lenses occurs throughout the point bar at a depth interval between 5 and 10’.

The *400 Interval* is 2.4-2.7 meters (8-9 feet) thick and contains fine-grained, moderately-well to well sorted sand. T-tests again indicate that the 400 Interval sand is finer grained ($p < 0.04$) and better sorted ($p < 0.01$) than the underlying *300 Interval*.

* Satterthwaite assumes unequal variances

Norman Landfill – Well #7

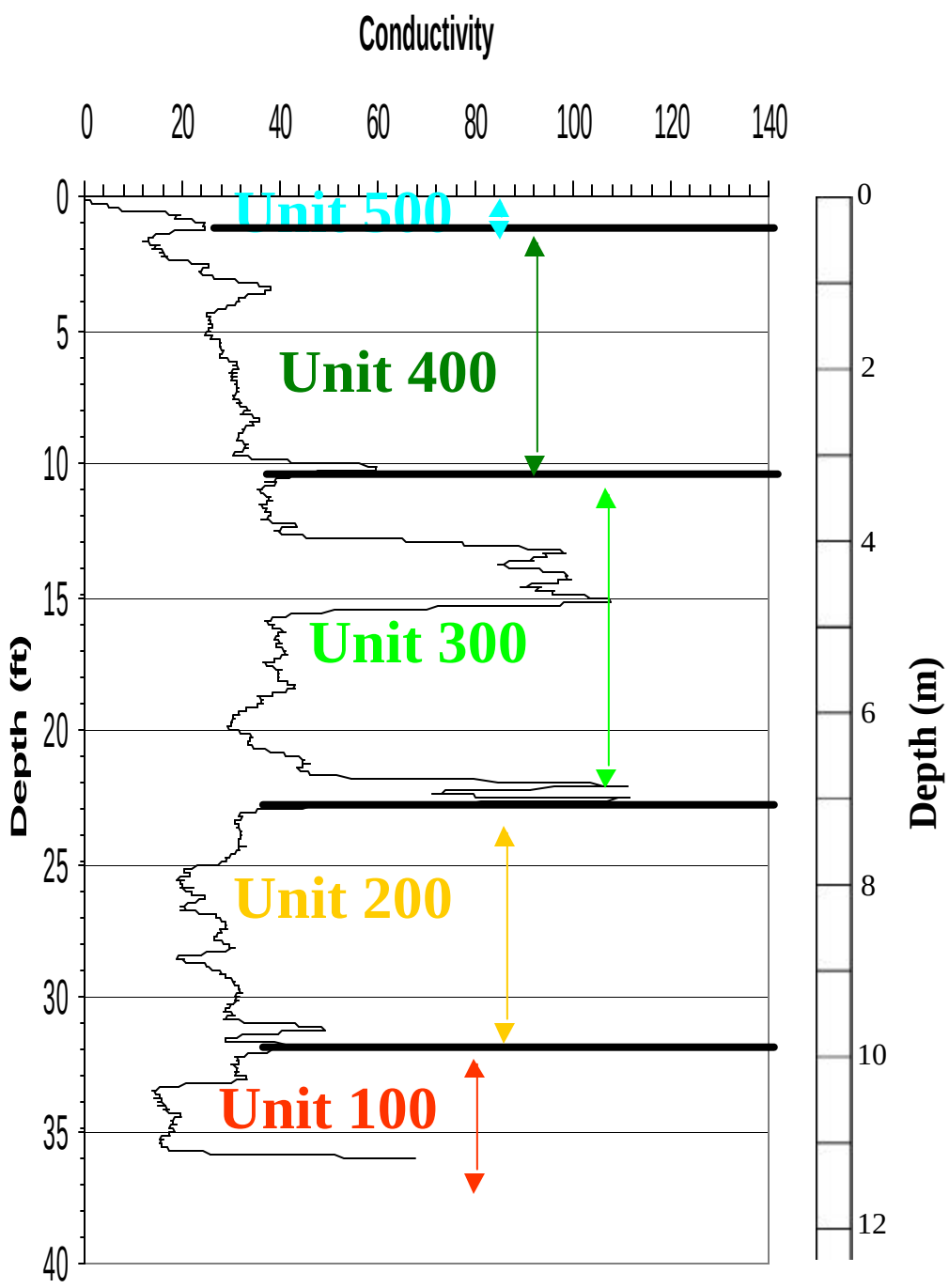

Fig 20. This is a type conductivity log from the Norman Landfill.

The *500 Interval* extends from the surface down to about 1 meter (3 feet). This unit is fine to very-fine grained and moderately-well to well sorted. The *500 Interval* is significantly different from the underlying *400 Interval* with respect to grain size ($p < 0.0001$). Sorting does not vary between the *500 and 400 Intervals* ($p < 0.85$). The textural character of this upper layer is shaped by both soil forming processes and aeolian sedimentation.

Calculated Permeabilities Relative to Stratigraphic Intervals

A SAS (v. 8.01) step-wise multivariate analysis of the grain size, sorting, and permeability data taken from the experiments of Beard and Weyl was performed. The intent of this analysis was to estimate the relative importance of grain size and sorting in controlling the permeability of the grain packs used in their experiments. This analysis indicates that phi grain size explains 60% of the variation in permeability. This is followed in importance by grain sorting, which accounted for another 37% (60 + 37 = 97% total variation in permeability accounted for by these two variables). This analysis and inspection of the permeability equation (eq.4) suggests that point bar permeability will increase strongly with increasing grain size and vice versa. Likewise, better-sorted sands will have higher permeability, but this tendency can be offset quickly if the grain size grows small, resulting in lower permeability.

Accordingly, the vertical permeability profile for all the sieve data* (Fig. 23a) suggests that permeability varies more strongly with grain size than with sorting. Consequently, the permeability profile appears more similar in shape to the grain size profile (Fig. 23b) than to the sorting profile (Fig. 23c). The basal *100 Interval* (in red) exhibits the highest calculated permeabilities in the profile due to a population of large grains. This high permeability population has not been offset by the potential reduction in permeability due to poor sorting. Clearly, calculated permeabilities would be much higher if the coarsest grained Norman Landfill point bar sediments were better sorted. Likewise, the rapid fall in permeability in the *500 Interval* at the surface is due to a strong grain size shift to very fine-grained sand in these moderately-well sorted sands.

T-tests were performed on the permeability populations (Fig. 24) to determine if real permeability differences exist between the layers of the point bar. The basal *100 Interval* permeability is significantly different from the overlying *200 Interval* ($p < 0.0001$). The *200 and 300 Interval* permeabilities are not significantly different from one another ($p < 0.47$). Likewise, the *300 and 400 Intervals* are essentially the same with respect to permeability ($p < 0.19$). The mean permeability of the *500 Interval* population is significantly different from the underlying *400 Interval* ($p < 0.002$). These tests are summarized in Table 4.

Permeability and Fining Upward Profile of Fluvial Sediments

Vertical profiles of the sieve data (Fig. 23) indicate that the 'classic fining-upward' profile for fluvial systems is punctuated at both the channel base and at the top by rapid changes in grain size and / or sorting (at least for the Canadian River). The *100 Interval* displays a very rapid yet progressive grain size decrease and improvement in size sorting from the channel base to about 8' up from the base. Likewise, the grain size of the upper few feet (*500 Interval)* of the point bar is much finer grained. As mentioned above, this rapid shift to finer grain size is due primarily to aeolian reworking of the floodplain sediments.

Excluding these deepest and shallowest intervals, the grain-size sorting improves progressively from 30' to a depth of about 3'. Grain size does not change very much through the

* calculated from an equation generated from data published by Beard and Weyl, 1973

Testing for Differences Between Layers in the NLF Point Bar

Table 2 - Grain Size (phi units)

Interval	Variable	Method	Variances	DF	t Value	Pr > |t|
500 vs 400	**Grain Size**	Pooled	Equal	82	-3.63	0.0005*****
		Satterthwaite	Unequal	19.7	-4.71	0.0001*****
400 vs 300	**“**	Pooled	Equal	165	-2.24	0.0264*****
		Satterthwaite	Unequal	114	-2.12	0.0365*****
300 vs 200	**“**	Pooled	Equal	161	-1.91	0.0578*****
		Satterthwaite	Unequal	96.2	-1.75	0.0836*****
200 vs 100	**“**	Pooled	Equal	121	-6.78	<.0001*****
		Satterthwaite	Unequal	79.5	-6.40	<.0001*****

*** significant difference between population means**

OSU
School of Geology

Testing for Differences Between Layers in the NLF Point Bar

Table 3 - Sorting (phi units standard deviation)

Variable	Method	Variances	DF	t Value	Pr > |t|
Interval					
500 vs 400	**Sorting**	Pooled	Equal	82	-0.11	0.9158**ns**
		Satterthwaite	Unequal	38.7	-0.19	0.8519**ns**
400 vs 300	**“**	Pooled	Equal	165	2.68	0.0081*****
		Satterthwaite	Unequal	107	2.50	0.0138*****
300 vs 200	**“**	Pooled	Equal	161	4.99	<.0001*****
		Satterthwaite	Unequal	83.9	4.44	<.0001*****
200 vs 100	**“**	Pooled	Equal	121	4.89	<.0001*****
		Satterthwaite	Unequal	83.2	4.64	<.0001*****

*** significant difference between population means**
ns – not significant, means between two populations are the same

OSU
School of Geology

Testing for Differences Between Layers in the NLF Point Bar

Table 4 – Permeability (log units, mDarcies)

Variable	Method	Variances	DF	t Value	Pr > |t|
Interval					
500 vs 400	**Log Perm**	Pooled	Equal	82	4.98	<.0001*****
		Satterthwaite	Unequal	14.6	4.85	0.0002*****
400 vs 300	**“**	Pooled	Equal	165	1.35	0.1775**ns**
		Satterthwaite	Unequal	140	1.33	0.1867**ns**
300 vs 200	**“**	Pooled	Equal	161	-0.75	0.4537**ns**
		Satterthwaite	Unequal	122	-0.72	0.4715**ns**
200 vs 100	**“**	Pooled	Equal	121	6.68	<.0001*****
		Satterthwaite	Unequal	81.2	6.32	<.0001*****

*** significant difference between population means**
ns – not significant, means between two populations are the same

OSU
School of Geology

Grain Size - NLF

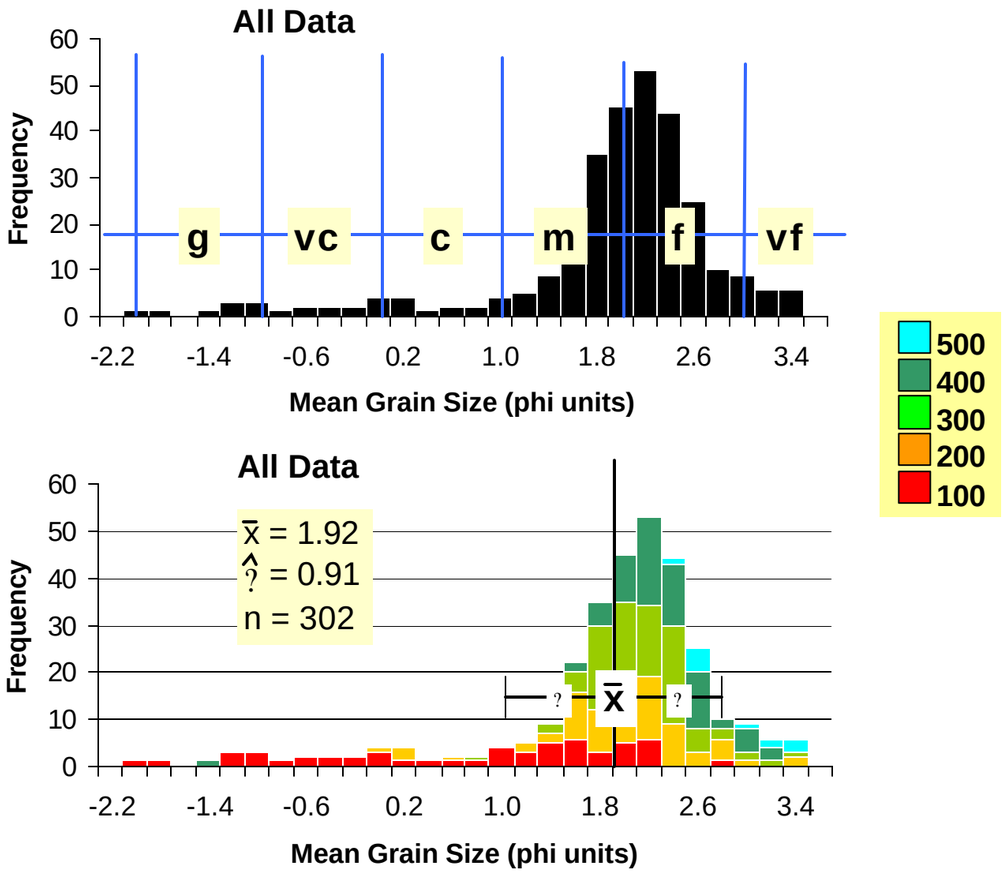

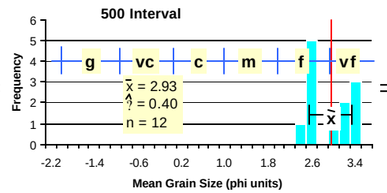

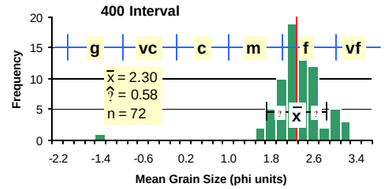

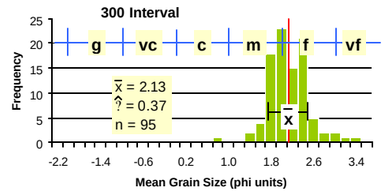

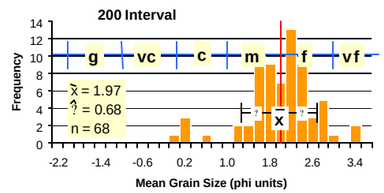

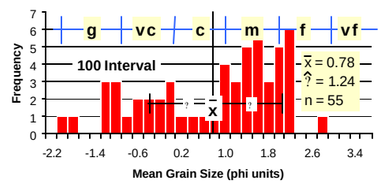

Fig. 21 – Frequency distributions of mean grain size from sieve data. The intervals or unit designations (100, 200, etc.) used for correlation purposes are shown to the right.

Grain-Size Sorting - NLF

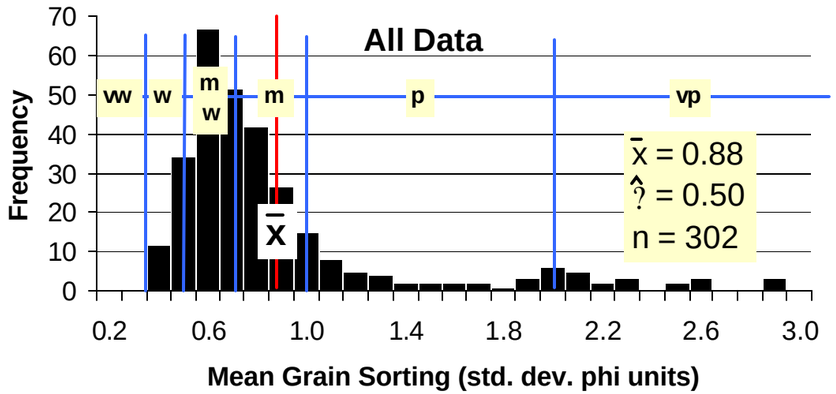

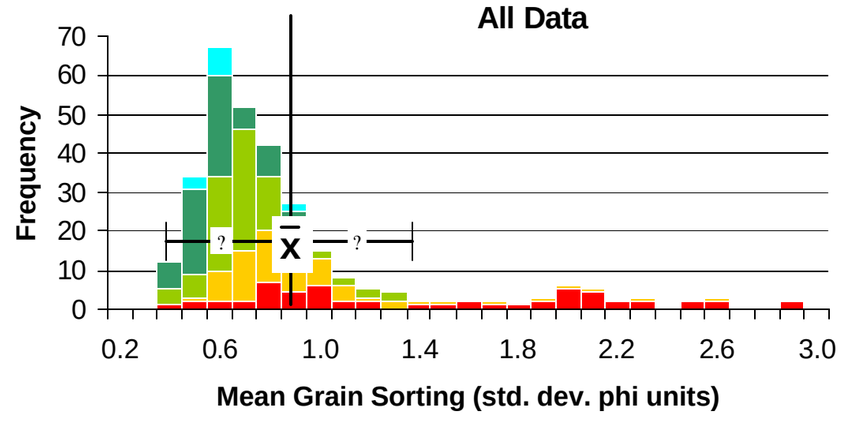

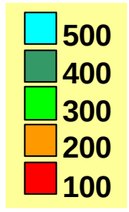

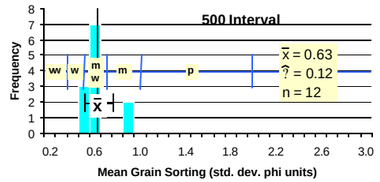

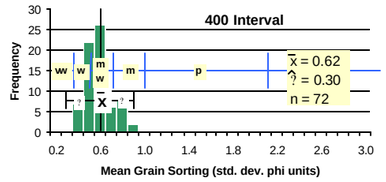

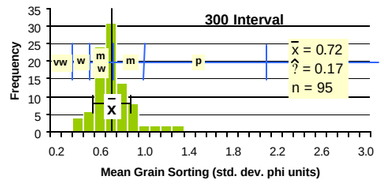

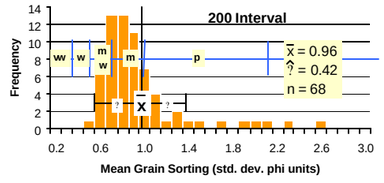

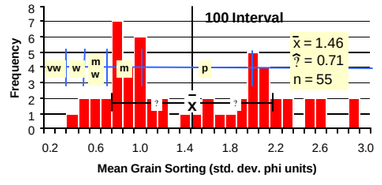

Fig. 22 – Frequency distributions of mean grain sorting from sieve data. The intervals or unit designations (100, 200, etc.) used for correlation purposes are shown to the right.

Vertical Profiles in NLF Point Bar Deposit

Canadian River, Oklahoma

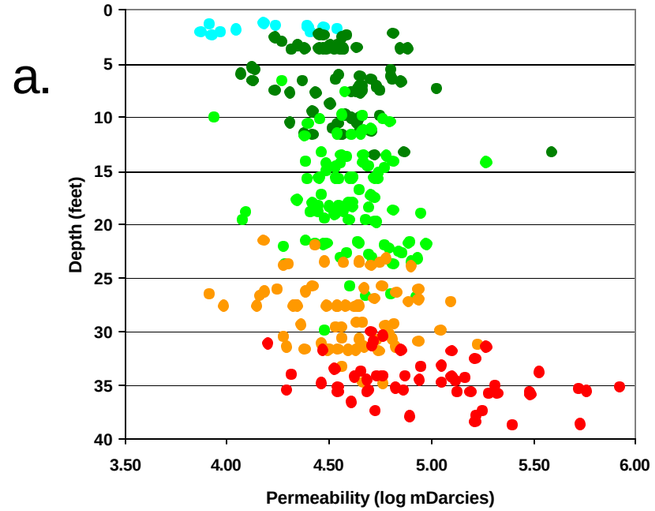

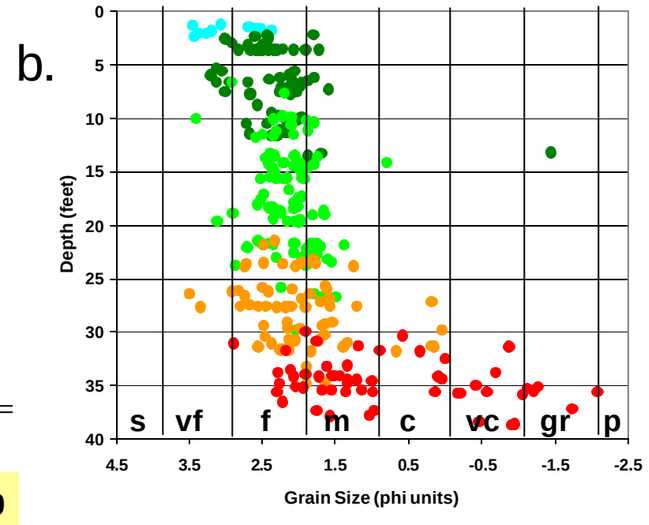

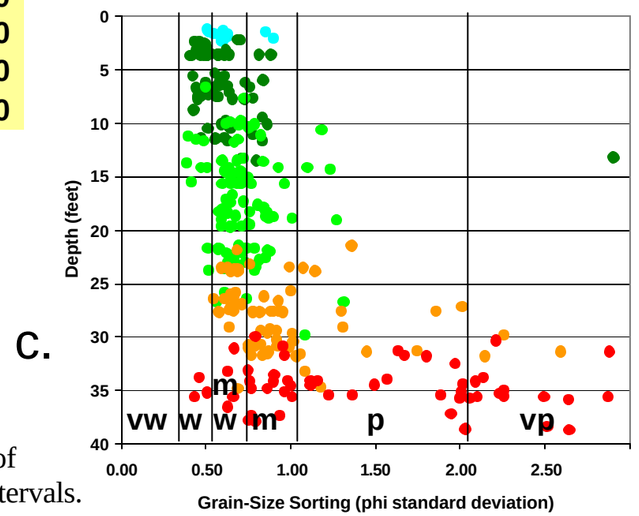

Fig. 23 – Profiles of calculated permeability from measurements of grain size / sorting in the Norman Landfill point bar subsurface intervals.

Permeability - NLF

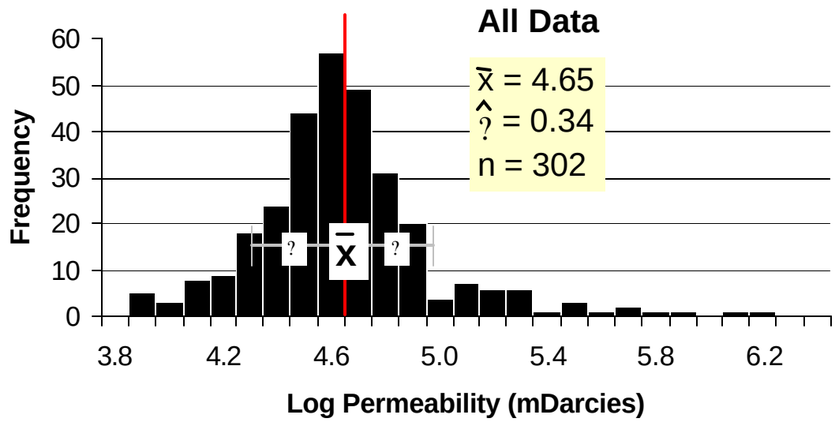

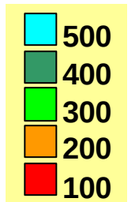

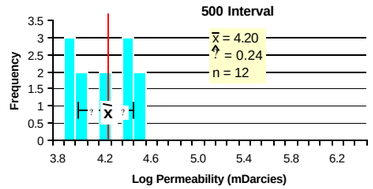

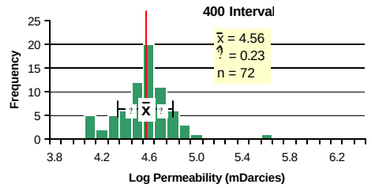

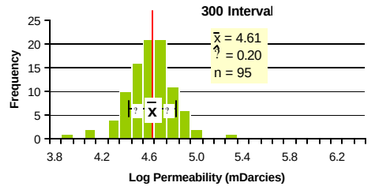

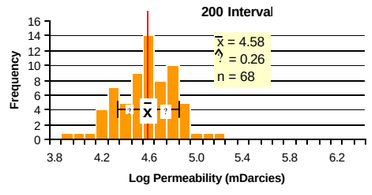

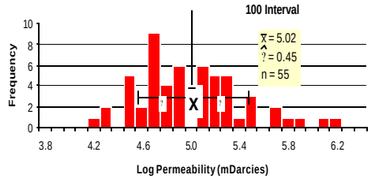

Fig. 24 – Frequency distributions of mean permeability calculated from sieve data. The intervals or unit designations (100, 200, etc.) used for correlation purposes are shown to the right.

Hydraulic Conductivity

a.

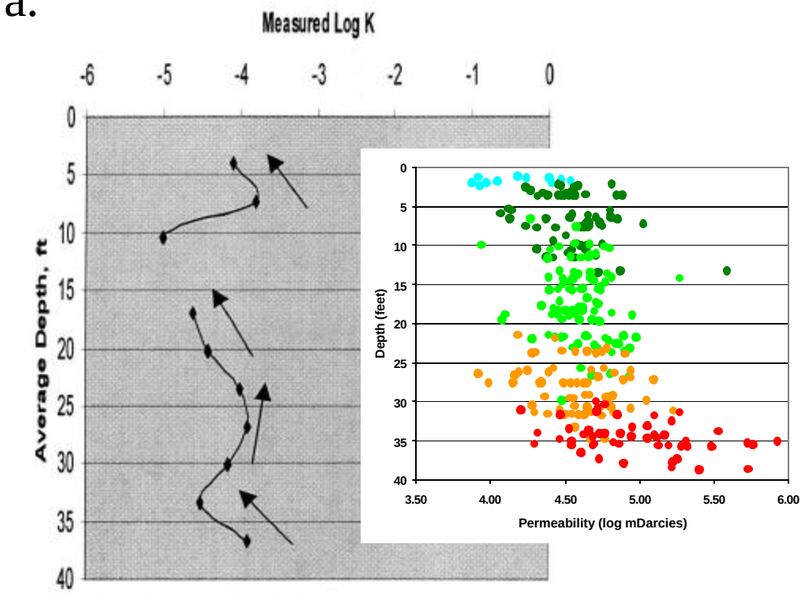

b.

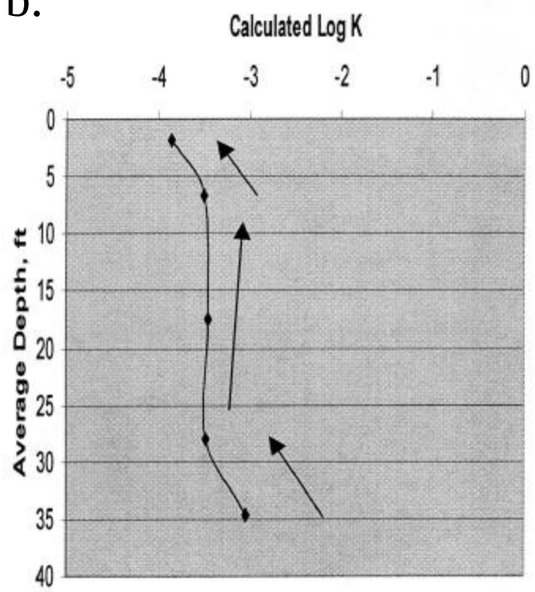

Fig. 25 – Calculated hydraulic conductivity (right, this study) compared to measured hydraulic conductivity (left) reported by Scholl and Christenson (1998) at Norman Landfill well 37SL1. The hydraulic conductivity units are in m / s. The color inset shows the vertical profile of permeability that is color coded by the interval layers.

Norman Landfill
Calculated Rate of Plume Movement

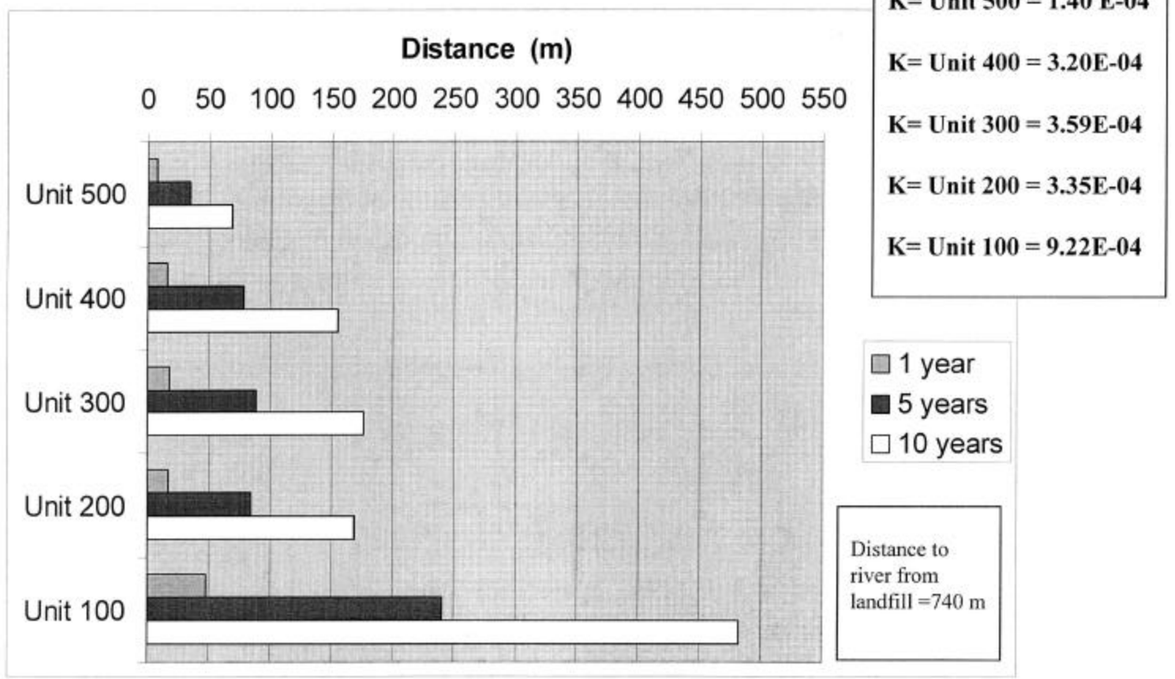

K= Hydraulic Conductivity (m/s)

K= Unit 500 = 1.40 E-04

K= Unit 400 = 3.20E-04

K= Unit 300 = 3.59E-04

K= Unit 200 = 3.35E-04

K= Unit 100 = 9.22E-04

Fig. 26 – Rate of plume movement based upon calculated hydraulic conductivity of each of the sand intervals. The velocity of the plume was calculated using the equation V = (K * I) / effective porosity. The effective porosity for each unit was calculated from the mean grain size / sorting data obtained from the cores. A gradient (I) of 0.006 was used for the calculation. This gradient is characteristic of the floodplain between the slough and the river. The gradient becomes steeper near the slough and landfill.

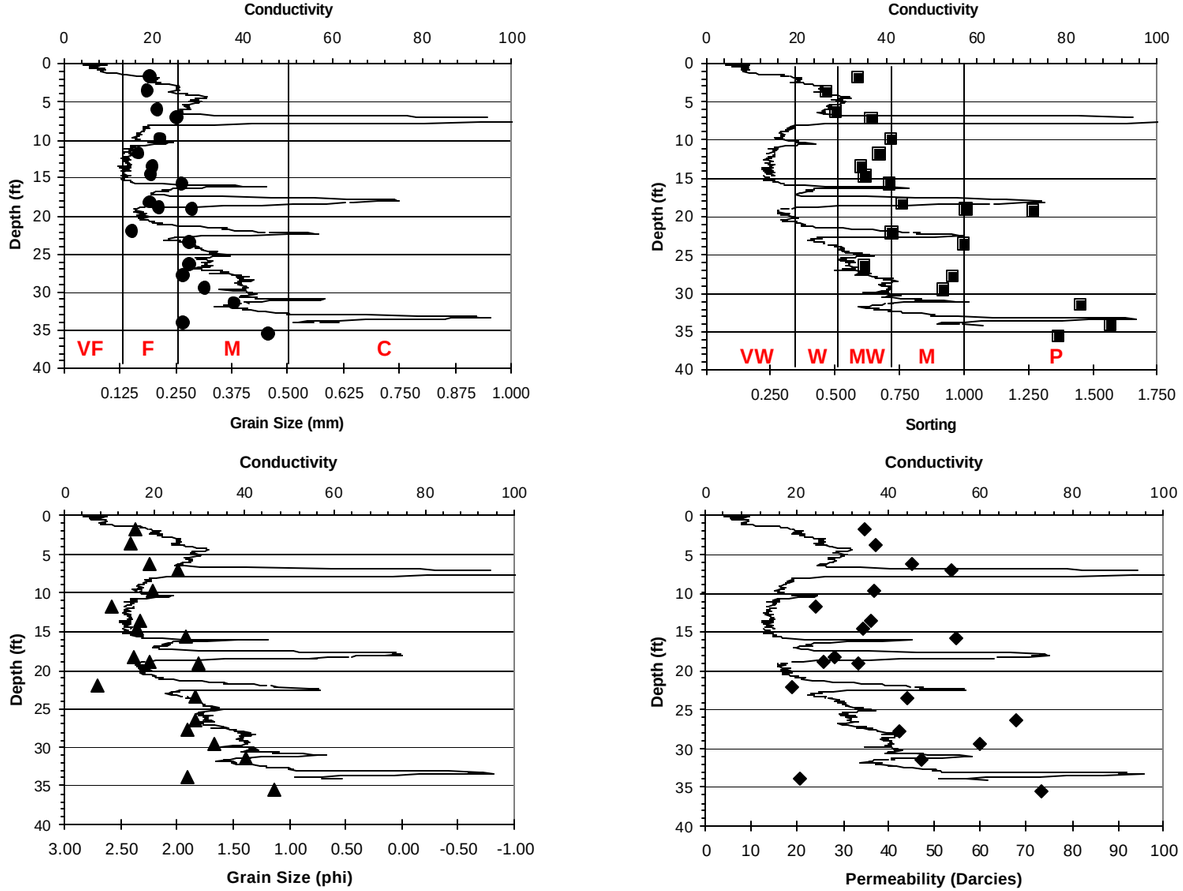

Fig. 27 – Vertical profiles of grain size, sorting and calculated permeability in Norman Landfill well #1. Note the correspondence between conductivity and the sediment grain size and sorting.

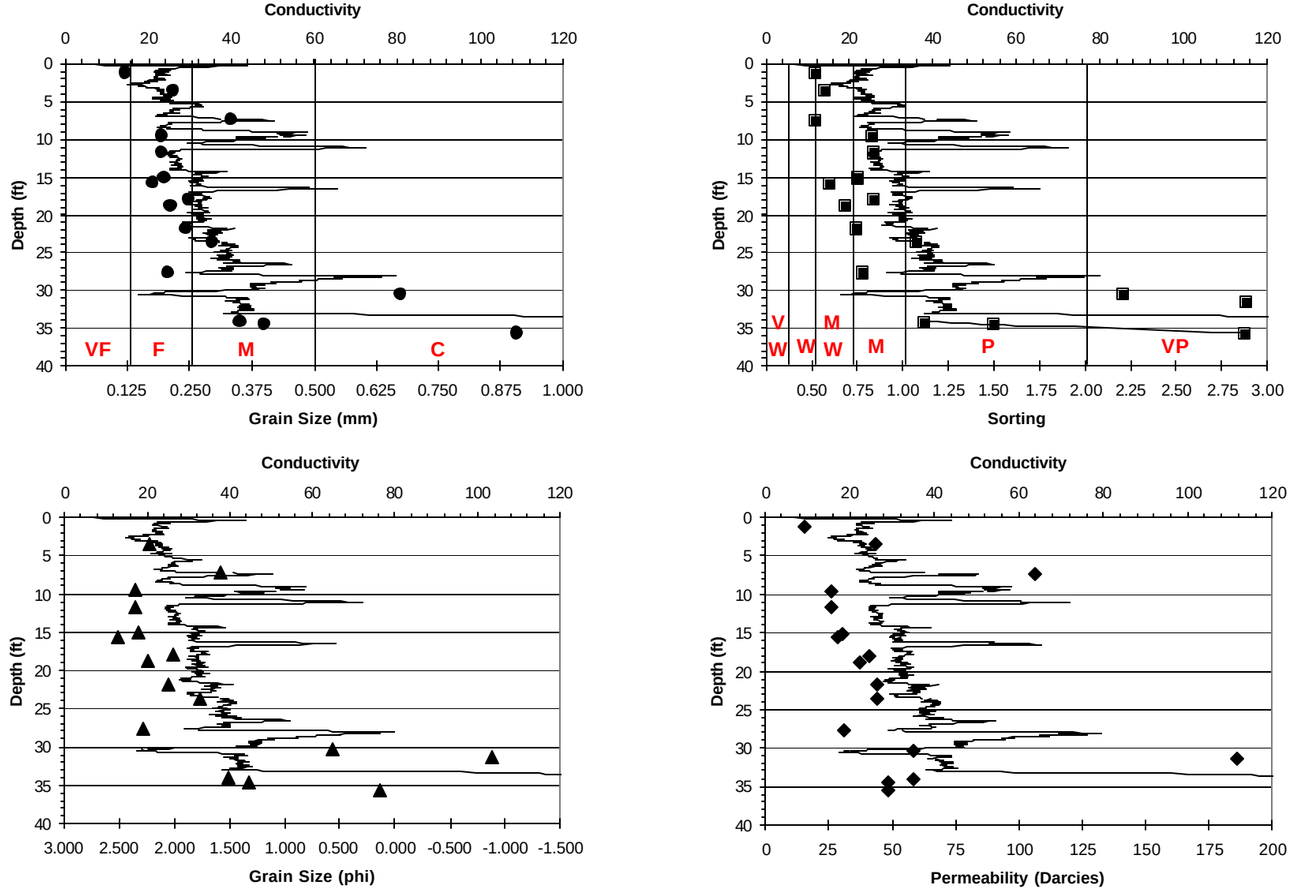

Fig. 28 – Vertical profiles of grain size, sorting and calculated permeability in Norman Landfill well #15. Note the correspondence between Geoprobe conductivity and the sediment grain size and sorting. Permeability also tracks the conductivity.

base of the *200 Interval* to the top of the *400 Interval* (Fig. 23). Visual inspection of the grain size trends in the thick *300 Interval* shows no vertical variation in grain size. The statistically significant differences in grain size noted earlier for the *200 to 400 Intervals* (upward fining) appears to not be translated to an upward decrease in permeability. This finding appears compatible with the following observations: (1) the vertical grain size differences are quite subtle and (2) there is a concomitant improvement (statistically significant) in grain sorting. The improved grain sorting has resulted in higher porosity that compensates for the progressively decreasing grain size upward.

The work of Christensen et al. (1998) used slug tests and calculations of hydraulic conductivity to conclude that the highest permeability in the alluvium adjacent to the NLF is located at the base of the sediment package. The vertical permeability profile in Fig. 23a is similar in appearance to the data of Christensen et al. (1998) (Fig. 25a).

Conversion of the NLF permeabilities calculated from sieve data to hydraulic conductivity values (Fig. 25b) yields a profile that is also similar in appearance to the Christensen et al (1998) data. The present study concurs with the findings of the Christensen et al. (1998) and finds significant evidence for a preferred permeability pathway at the base of the alluvial fill. However, the sand intervals above the base (with exception of the 500 Interval near the surface) all have comparable permeability.

The calculated hydraulic conductivity resulted in a range from 1.4E-04 m/s to 9.22E-04 m/s. The higher hydraulic conductivity was seen in the basal segment of the alluvium. It was estimated that the plume is moving at rate of at least 48 meters per year in the basal unit (Fig. 26). This estimate was calculated using a gradient of .0006 that is characteristic between the floodplain and the slough. However, the gradient becomes steeper as you approach the slough so the rate of plume movement may increase. This rate of movement also decreases shallower in the section as hydraulic conductivity of the sediments declines.

Texture and permeability profiles for Wells #1 and 15 are provided in Figs. 27 and 28, respectively. In some of the wells, the correspondence between grain sizes, sorting, and conductivity is quite striking (Fig. 27, 28). The correspondence suggests that lower conductivity sand intervals are finer grained and better sorted than higher conductivity sand intervals. We do not understand this relationship. The data would suggest that deeper, coarser grained and more poorly sorted sand intervals contain more disseminated silt and clay than the shallow sand intervals. We see no evidence for this in our cores.

Block Diagrams

Block diagrams were created of the floodplain alluvium. They provide a 3-D perspective of the geometry and thickness of the 5 distinct sand intervals in the point bar. There are 6 block diagrams. Three view the study area from the southwest corner (Fig. 29), and three view it from the southeast corner (Fig. 30). Both the southwest and southeast view are illustrated with 25%, 50%, and 75% of the model cutaway. These diagrams provide a 3-D view of the gross stratigraphy of the floodplain. As determined by the cross-sections it is essentially horizontal (layer-cake) and similar to the flat floodplain topography seen today.

Block diagrams of the conductivity data were also created. These diagrams provide visuals of changes in conductivity throughout the floodplain. Two diagrams were made of the entire study site. One is viewing the site from the southeast corner (Fig 31), and the other is viewing the site from the southwest corner (Fig. 32). In Figure 31 the higher conductivity values near the slough are apparent between 1055 and 1075 feet. These higher conductivity zones are

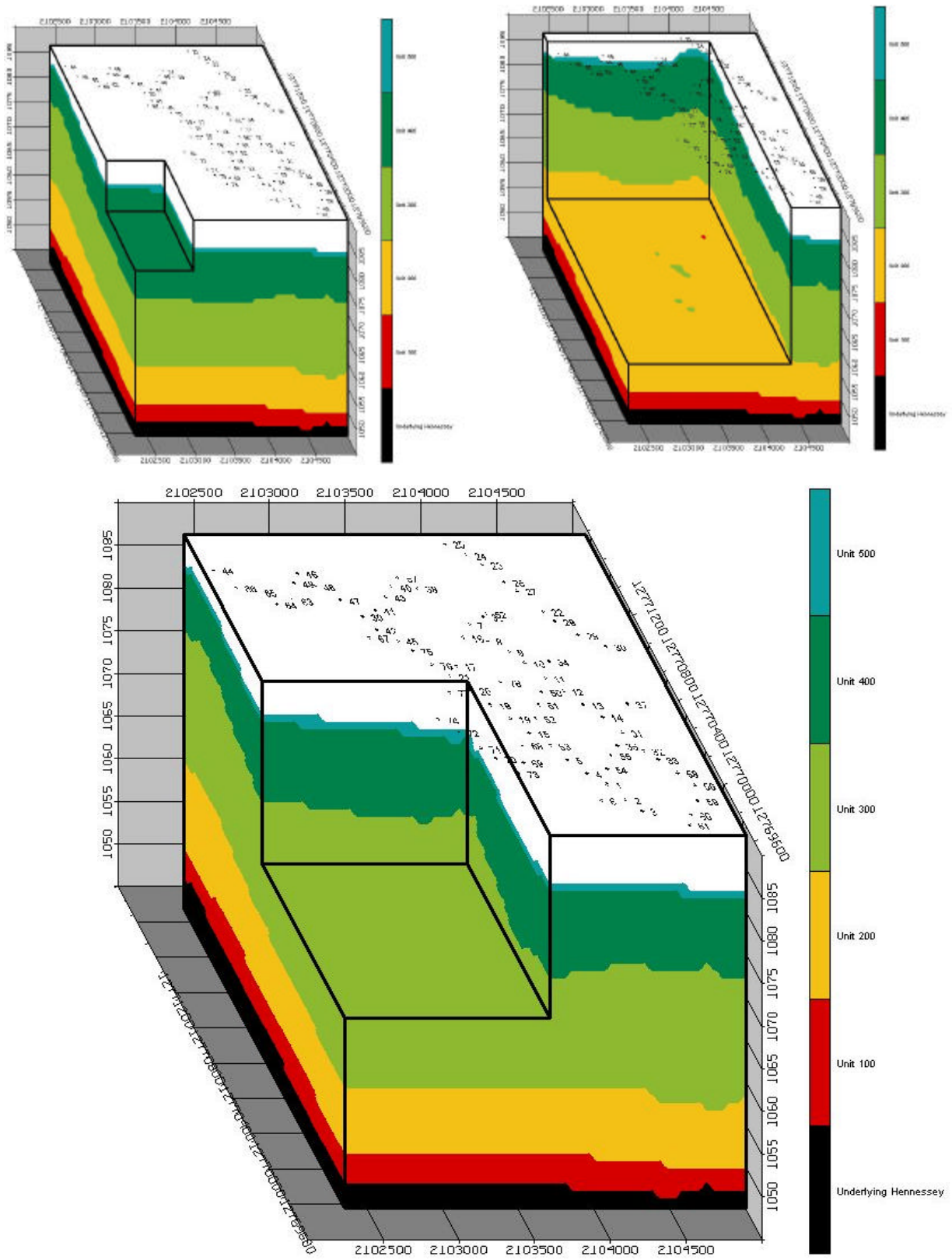

Fig. 29 - Block diagrams of the alluvium intervals. View is from southwest corner of study area. Easting and Northing are based on UTM-Zone 14 in feet. Mean sea level elevation is in feet.

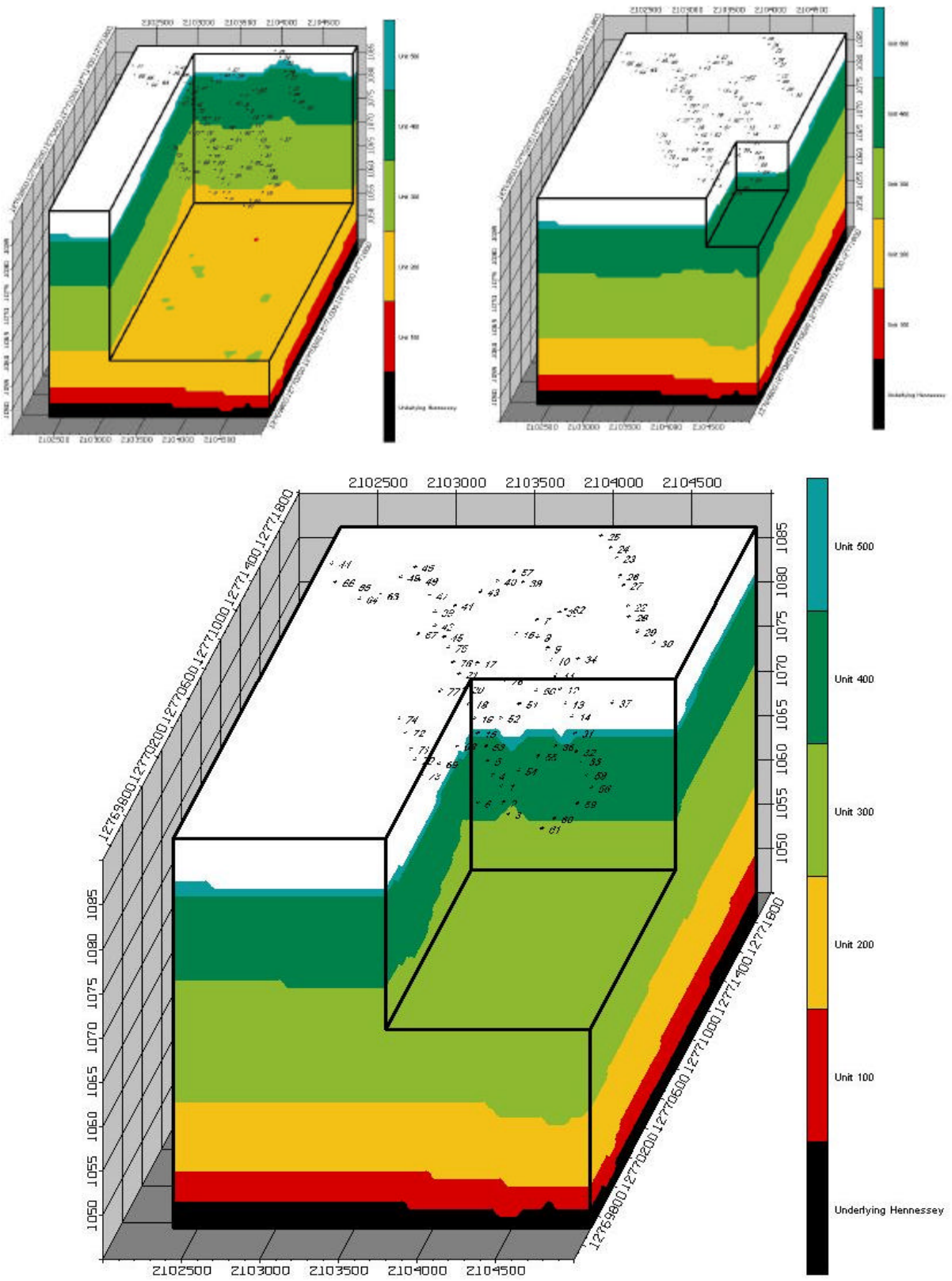

Fig. 30 - Block diagrams of the alluvium intervals. View is from southeast corner of study area. Easting and Northing are based on UTM-Zone 14 in feet. Mean sea level elevation is in feet.

View from Southeast

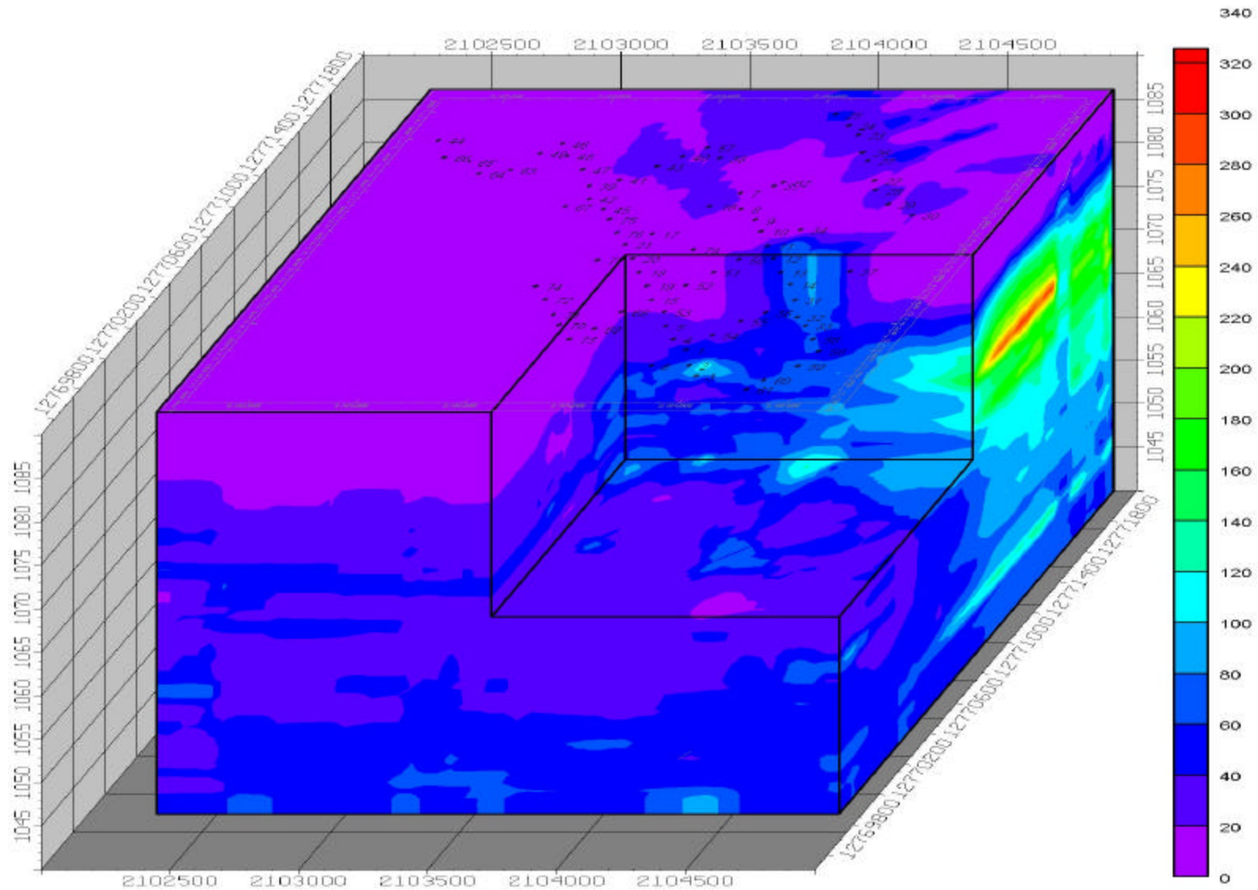

Fig. 31- Block diagram of conductivity values. View is from southeast corner of the study area. Easting and Northing are based on UTM Zone 14 in feet. Elevation above mean sea level is in feet.

View from Southwest

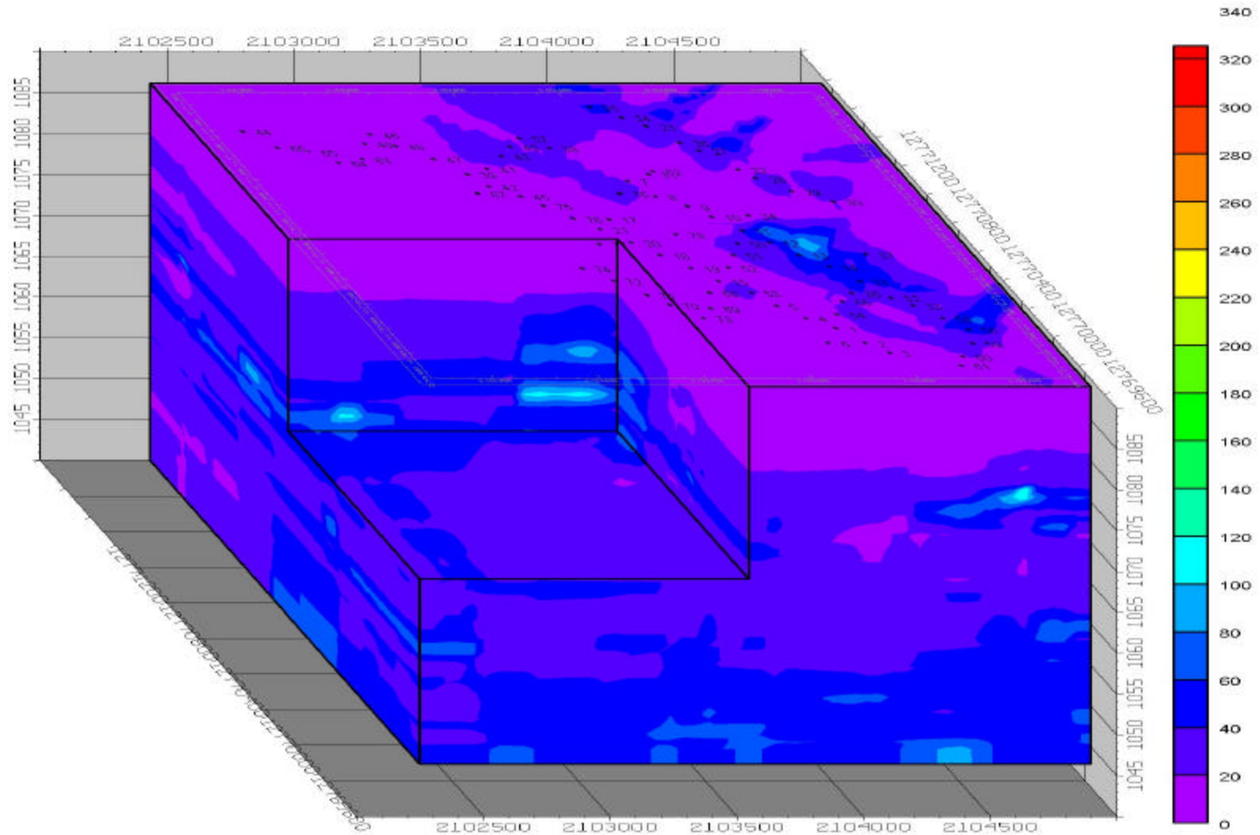

Fig. 32- Block diagram of conductivity values. View is from southwest corner of the study area. Easting and Northing are based on UTM Zone 14 in feet. Elevation above mean sea level is in feet.

Unit 100

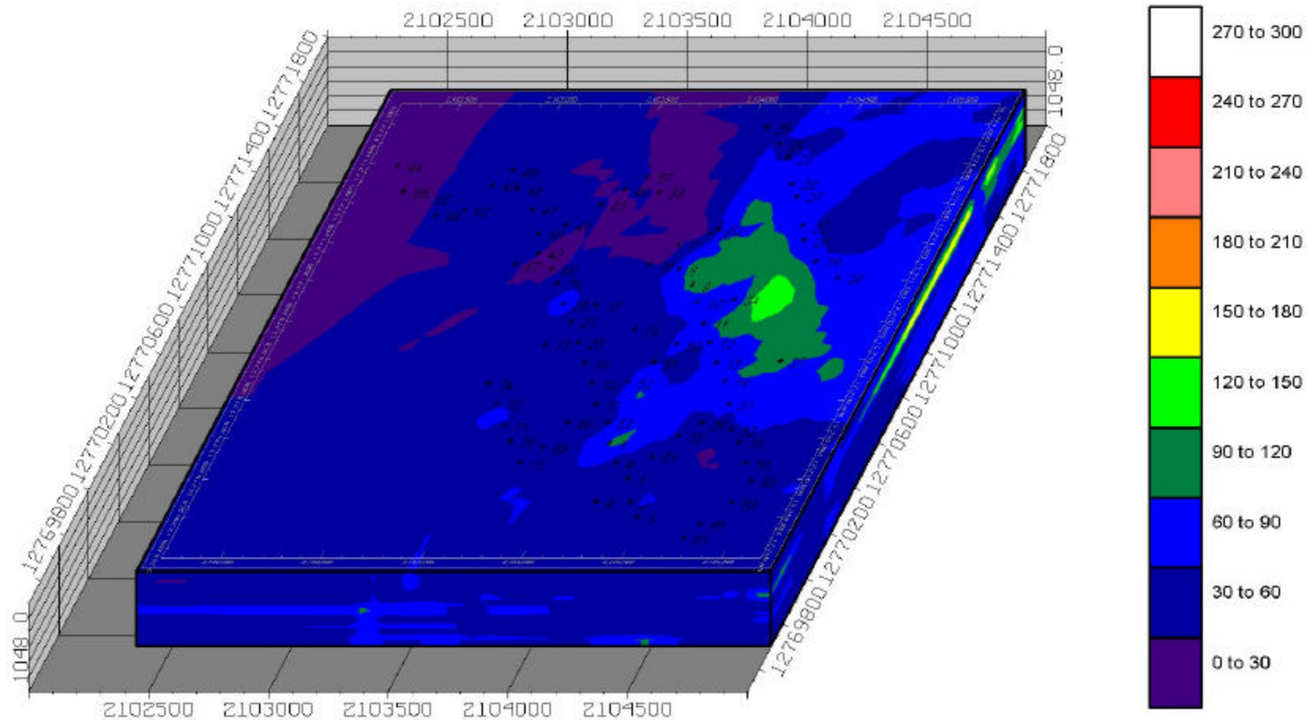

Fig. 33- Conductivity map of the 100 Unit slice. View is from southeast corner of the study area. Easting and Northing are based on UTM Zone 14 in feet. Elevation above mean sea level is in feet.

Unit 200

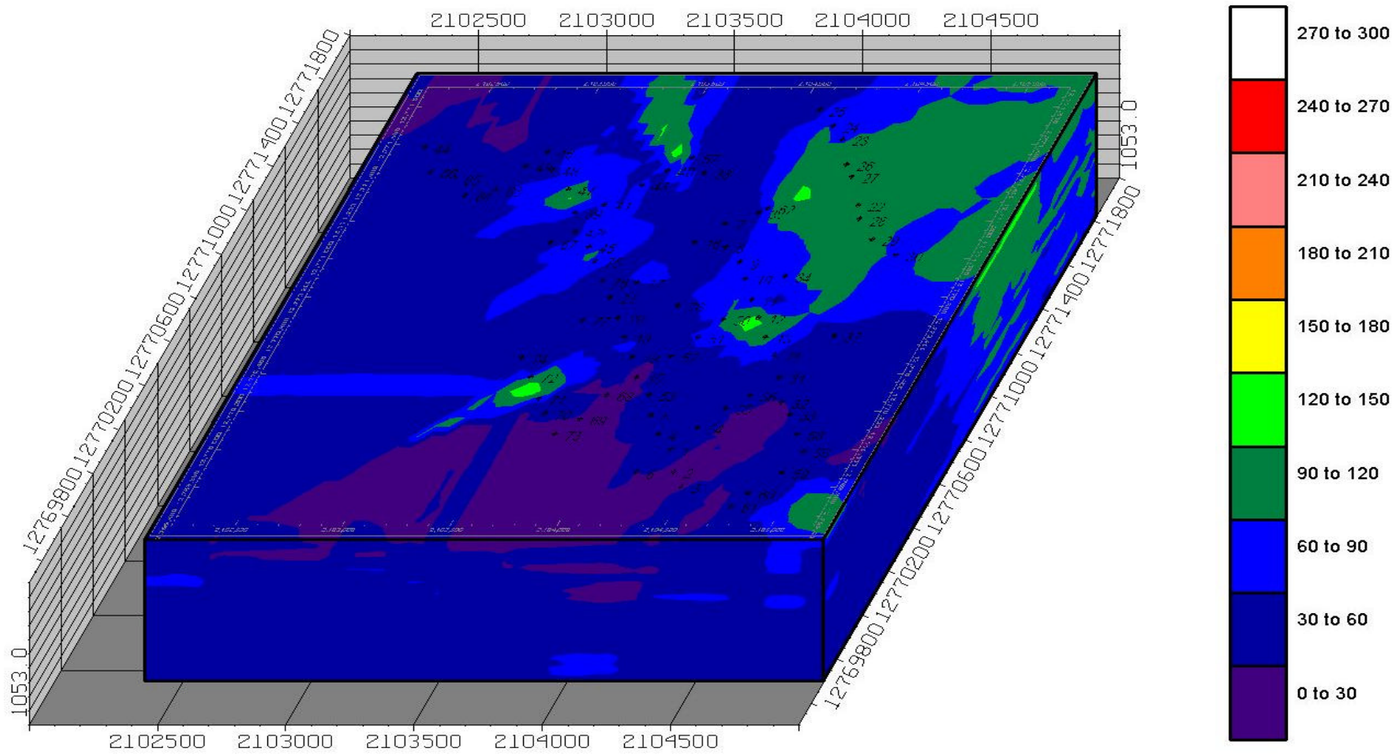

Fig. 34- Conductivity map of the 200 Unit slice. Easting and Northing are based on UTM Zone 14 in feet. Elevation above mean sea level is in feet.

Unit 300

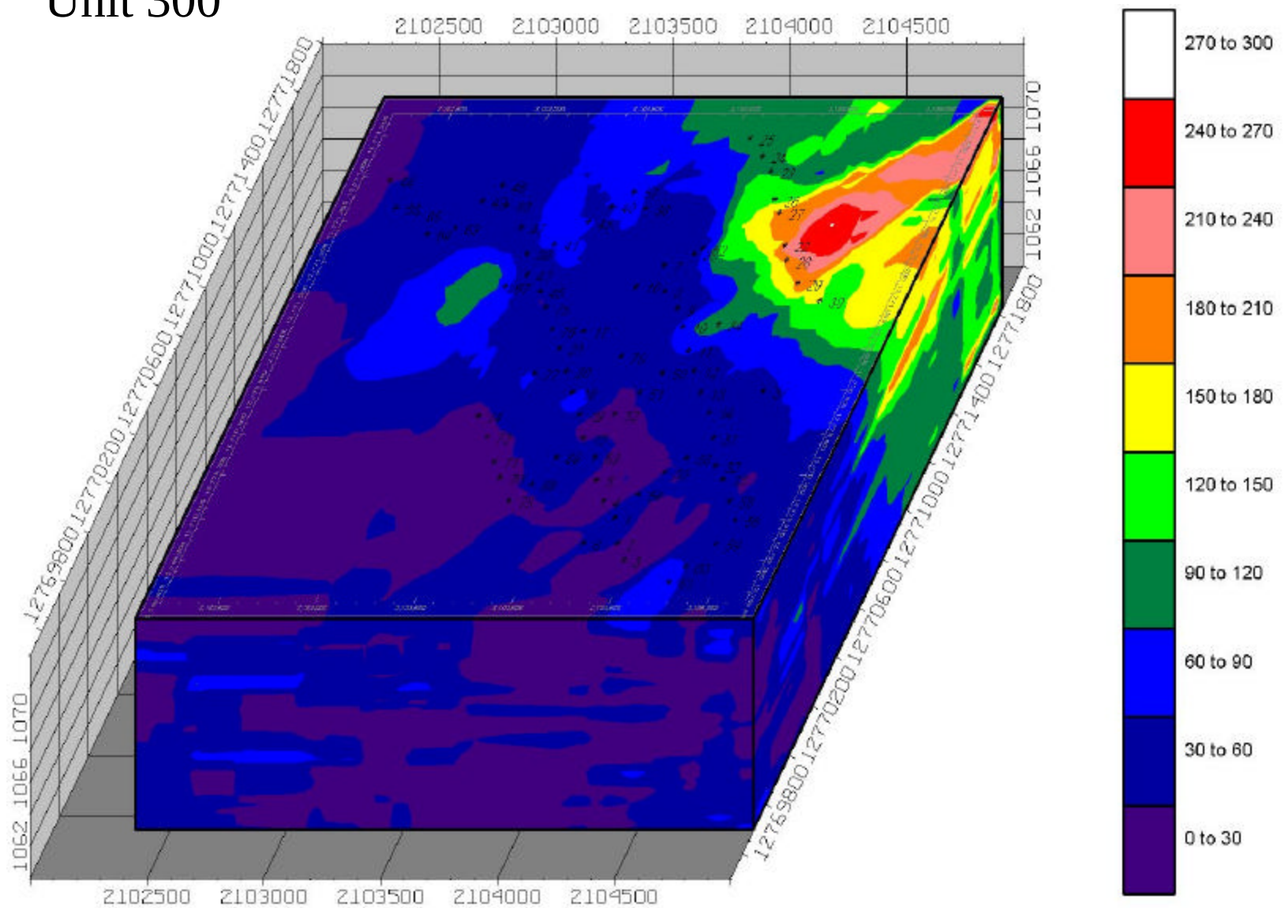

Fig. 35 - Conductivity map of the 300 Unit slice. Easting and Northing are based on UTM Zone 14 in feet. Elevation above mean sea level is in feet.

Unit 400

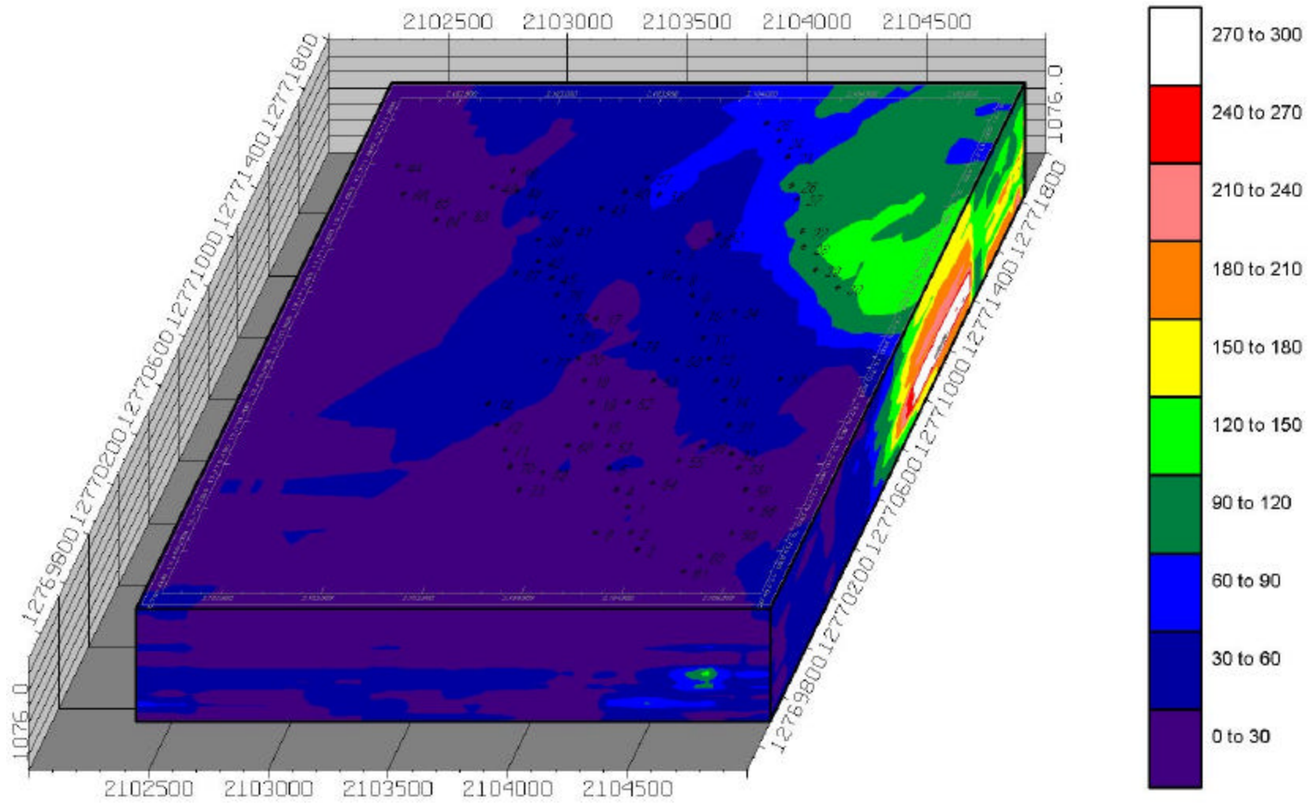

Fig. 36- Conductivity map of the 400 Unit slice. Easting and Northing are based on UTM Zone 14 in feet. Elevation above mean sea level is in feet.

Unit 500

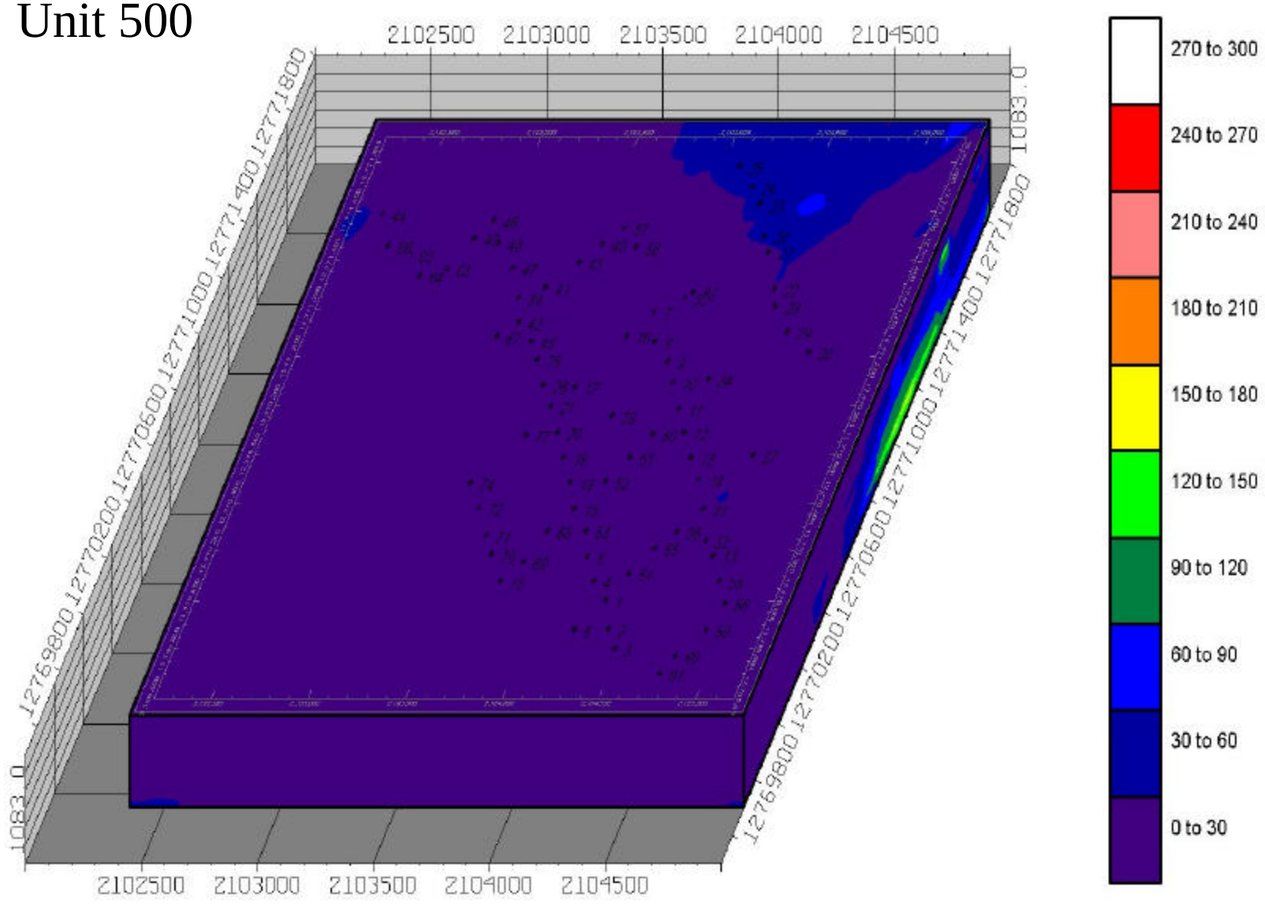

Fig. 37- Conductivity map of the 500 Unit slice. Easting and Northing are based on UTM Zone 14 in feet. Elevation above mean sea level is in feet.

near Wells #23 and #28, which are between the slough and the landfill. Thick, dense clay layers were found in these cores about 1070 feet, which is 15 feet below the surface.

Conductivity slices were also created for each of the five sediment intervals (Figs. 33-37). The slices provide visualization of conductivity changes with depth. By comparing each of the slices it is seen that there is not much differentiation in conductivity in the west side of the study area. The highest conductivity zones are limited to the area adjacent to the landfill. In the east side of the study area there is very high conductivity seen in the base of the 200 Unit (Fig. 34). This high conductivity zone is associated with the thick, dense clay as seen in cores 23 and 28. The conductivity in this zone remains high near the landfill and decreases as you move further west. Conductivity near the landfill is higher than expected for clay rich sediment, and may suggest interaction of the clay with the leachate.

The high conductivity zone seen adjacent to the landfill appears to extend vertically through units 400, 300, 200 and 100. The conductivity values then begin to decline as you move away from the landfill towards the floodplain. These elevated conductivity values could be due to the increase in number of muds in the east side of the study site. However in our observations we did not see a significant enough increase in muds as to result in a distinction between east and west sides of the study area. Therefore, it could be possible that the leachate contamination is reflected in the higher conductivity areas. However, there is not enough information to distinguish between what may be the plume or may be clays.

Surface Sediment Analysis

The map created with the surface sediment data shows some patterns distinctive of meandering to braided stream systems (Fig. 38). There are obvious ripple and dune complexes with interdune areas composed of much finer material, which is indicative of gradual channel migration. Topographically low areas contain a substantially larger proportion of fine-size sediment than the surrounding higher areas. In addition, the sand observed in this particular environment behaves as quicksand when located close to the water table.

Grain size on the surface of the floodplain is rarely larger than medium to coarse sand, and the dune areas exhibit distinct longitudinal patterns running parallel to the channel. These units are similar to the longitudinal bars found in braided streams, although the grain size is smaller than usually found in common braided systems. The reason for this is most likely its distance from source, which may be found in southeastern Colorado.

In most natural river systems like the Canadian River, this pattern of dune highs with muddy interdune lows can be followed down the floodplain. In our study area, it may be noticed that there is an obvious discontinuity of sediment patterns from the northwest portion of the map area toward the southeast. An asphalt company extracts sand from the floodplain and active channel. One entire section of the frontal dunes that lie immediately adjacent to the river has been removed, as well as most of the inland dunes toward the asphalt plant. This activity has disrupted the expected patterns of sediment texture on the floodplain. Sediment in this area is so fine that the threshold for erosion and entrainment is very low. In addition, the mean elevation of the southeast portion of the floodplain is noticeably lower than the northwest. Any inundation of the stream, either by natural migration or by flood activity, will pass over the southeast portion of the floodplain without barrier until it reaches the landfill.

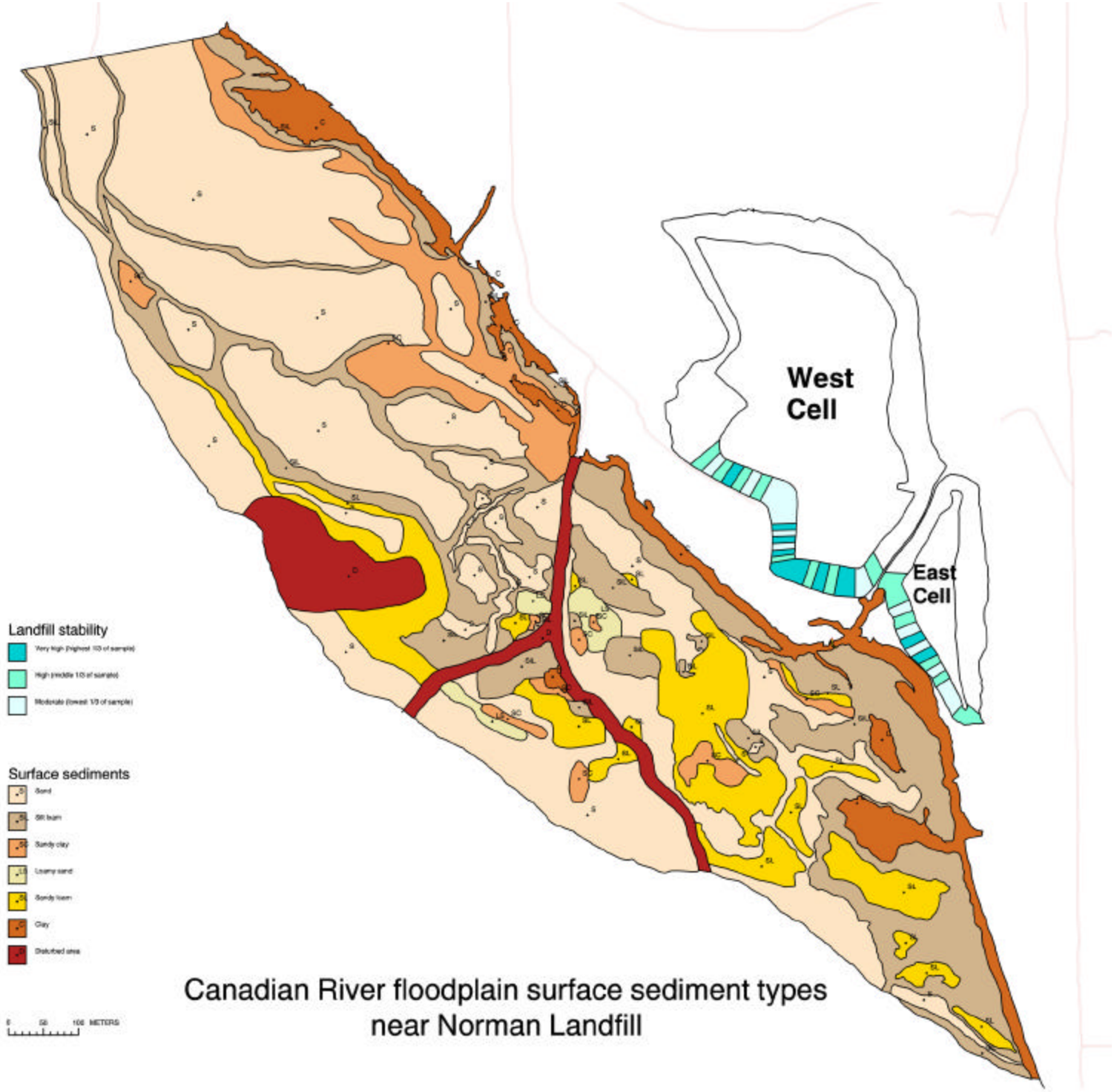

Canadian River floodplain surface sediment types
near Norman Landfill

Landfill Stability Analysis

Patterns created by the landfill stability data yielded some interesting yet relatively inconclusive results (Fig. 38). Results attained from this study do not necessarily show that there is a preferred region of either instability or stability within the landfill itself. The clay cap is generally homogeneous and becomes very hard upon exposure to the sun. In the event of a flood or natural stream migration to the base of the landfill, though, the clay would again become saturated and would lose any inherent stability it would otherwise have if it were "baked." The clay that composes the landfill cap is tacky and highly cohesive. From external observation only, it also seems to increase in thickness toward the bottom of the landfill, simply from downslope sediment movement. Portions of the landfill that protrude furthest into the path of floodwaters are no less stable than other portions of the landfill. A 1986 peak flow of 2180 cms, a 15-year event, removed rip-rap protection for the landfill, penetrated the clay cap, and eroded 5013 m^3 of landfill contents.

Stream Stability Analysis

The probability map of channel location reveals several specific areas of the floodplain that are particularly prone to channel inundation (Fig. 39). It is interesting to notice that the area of the floodplain nearest the landfill has relatively high probability values. An overflow channel exists (the “slough”) that runs parallel to the base of the landfill. Whenever the level of the river reaches flood stage, water travels through the slough and erodes material from the base of the landfill.

The probability, horizontal distance to the channel and vertical distance to the channel were log-normally distributed. Multiple regression analysis was performed to determine the controls on probability. The r^2 value for the multiple regression was 0.30, significant at the $p < 0.001$ level.

$$\text{Log}(P) = 2.44 - (0.605)(\text{LogLD}) - (0.251)(\text{LogUD}) \quad \text{(eq. 7)}$$

or

$$P = 275(\text{LD})^{-0.605}(\text{UD})^{-0.251} \quad \text{(eq. 8)}$$

where P is the probability of stream presence, LD is the lateral distance to the low-flow channel (in meters) and UD is the upstream/downstream distance to the river channel (in meters).

CONCLUSIONS

Principle findings of the study are as follows:

1) On the basis of conductivity patterns, sediment texture, and vertical succession, five distinct layers are seen throughout the floodplain area. Of these, the basal layer will be the most significant in the transport of the plume. Earlier studies based on specific conductance of the groundwater have determined that the plume is already in this layer.
2) The flow pathways are bounded by mud layers that are discontinuous. These mud layers are found in similar stratigraphic positions and were likely formed during periods of time when the surface was exposed. Some layers do appear to be more extensive throughout the area. The dimensions of these larger mud layers are:
    a) Mud layers perpendicular to the bar complex range in length from <37 meters (<120 feet) to about 148 meters (485 feet)
    b) Mud layers parallel to the bar complex range in length from <37 meters (<120 feet) to about 222 meters (728 feet)

Fig. 39. Probability of Channel Presence

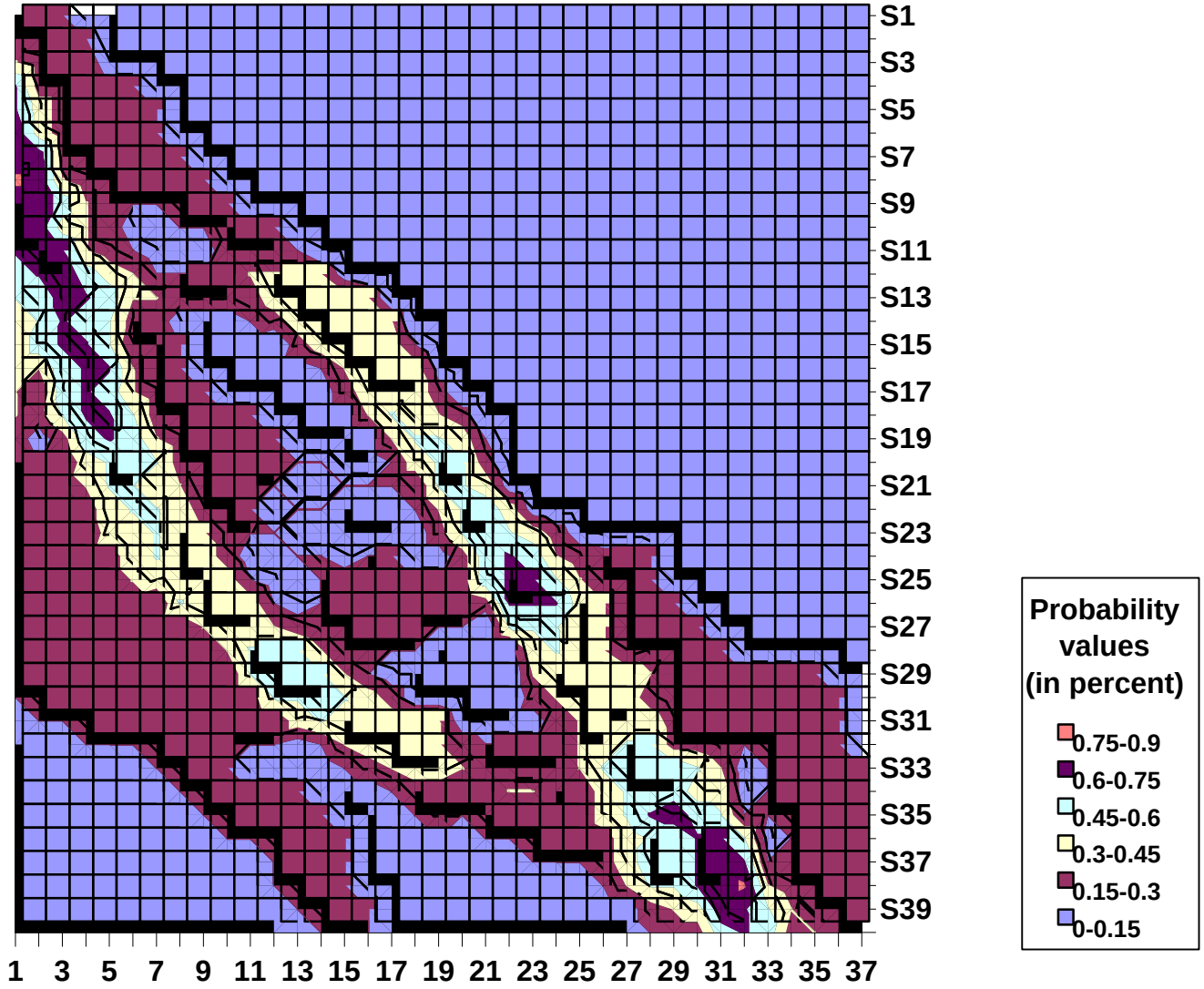

3) The number and thickness of mud layers increases toward the slough (adjacent to the landfill.
4) The maximum permeability pathway (as defined by grain size / sorting) is located in the basal segment of the valley fill. This interval encompasses the lower 1.8 to 2.4 meters (6 to 8 feet) of the alluvium and has an average permeability of 105 Darcies.
    a) The sediment overlying the basal unit has a permeability of 38 Darcies. This encompasses units 200, 300, and 400 for a total thickness of about 8.6 meters (28 feet).
    b) The sediments in the upper 0.6 meters (2 feet) of the alluvium have a permeability of 16 Darcies. These sediments are mainly aeolian.
5) Block models of the different sand units provide a 3-D view of the geometry and thickness of the 5 distinct sand intervals in the point bar.
6) Conversion of permeability data to hydraulic conductivity resulted in a range from 1.4E-04 m/s to 9.22E-04 m/s. The higher hydraulic conductivity was seen in the basal segment of the alluvium. This data compared very favorably to hydraulic conductivity measurements taken by Scholl and Christenson (1998).
7) It was estimated that the plume is moving at a rate of at least 48 meters per year in the basal unit. This estimate was calculated using a gradient of .0006 that is characteristic between the floodplain and the slough. However, the gradient becomes steeper as you approach the slough so the rate of plume movement may increase. This rate of movement also decreases shallower in the section as hydraulic conductivity of the sediments declines. Our estimate of the plume movement is higher than previously reported.
8) Block models were also created of the conductivity data. These models show higher conductivities near the landfill and slough. This supports the findings that the number and thickness of muds increases as the slough is approached. A thick, dense clay layer is located about 4 meters below the surface between the landfill and the slough (well 23 and 28). This clay is highly conductive as compared with the rest of the landfill alluvium and does not appear in cores away from the slough.
9) On balance, much higher conductivities are found in the areas near the slough and landfill. This is in part due to the number of clays in the area. Moreover, the base conductivity level for clean sands in this area is much higher than seen in most of the floodplain sands. Therefore, it is possible these higher conductivities are an indication of direct detection of the leachate plume with the Geoprobe conductivity tool.
10) The pebbles and gravels in the high permeability zones are not derived from the bedrock in the vicinity of Norman, Oklahoma.
11) The pattern of sediment deposition that one expects on a floodplain has been found only on the upstream end of the floodplain adjacent to the landfill. Asphalt plant mining operations have disrupted the pattern elsewhere. The majority of the floodplain is mantled with aeolian sediment, reworked from fluvial deposits during the low-flow season.
12) Lateral migration of the thalweg Canadian River is frequent, as expected for a low-gradient, sand-bed river. The thalweg has been positioned near the base of the landfill approximately 15 percent of the years between 1937-1997. The position of the thalweg indicates where maximum stream power is likely to be directed during flood events. The cross-section analyses completed in this study indicate that vertical scour of floodplain

alluvium during flood events may reach six meters (20 feet). Any portion of the plume within six meters of the surface can be expected to enter the Canadian River faster through erosion than it would by movement through the alluvium.

13) The landfill cap does exhibit a range in stability but no spatial pattern to the stability is evident. The base of the landfill remains subject to direct attack by flood flows, including rather peak flows of relatively high frequency and low magnitude. Additional protection of the base of the landfills on the south side may be warranted to prevent direct erosion of the landfill contents as had occurred in the past.

REFERENCES

Beard, D. C. and P. K. Weyl, 1973, Influence of texture on porosity and Permeability of Unconsolidated Sand: AAPG Bulletin, v. 57, no. 2, p. 349-369.

Boggs, Sam Jr., 1995, Principles of Sedimentology and Stratigraphy: Prentice Hall, New Jersey, p. 520.

Curtis, Jennifer and Whitney, John W. 2000. Geomorphology and flood hazards at a toxic landfill on the Canadian River floodplain, central Oklahoma. Preliminary draft of a USGS report.

Folk, Robert L., 1980, Petrology of Sedimentary Rocks (Second Edition): Hemphill Publishing Company, Austin, Texas, p. 42-43, 184.

Geoprobe Systems. www.geoprobesystems.com

Hodgson, J.M. (ed.). 1974. Soil Survey Field Handbook. Soil Survey Technical Monograph no. 5, Harpenden, Rathamsted Experiment Station.

Northcote, K.H. 1979. A Factual Key for the Recognition of Australian Soils. Adelaide, South Australia, Rellim Technical Publications.

Scholl, Martha A. and Scott Christenson, 1998, Spatial Variation in Hydraulic Conductivity Determined by Slug Tests in the Canadian River Alluvium Near the Norman Landfill, Norman, Oklahoma, USGS, Water Resources Investigations Report 97-4292, p. 1-28.

APPENDIX A

CORE DESCRIPTION

Well #1
Canadian River
Floodplain

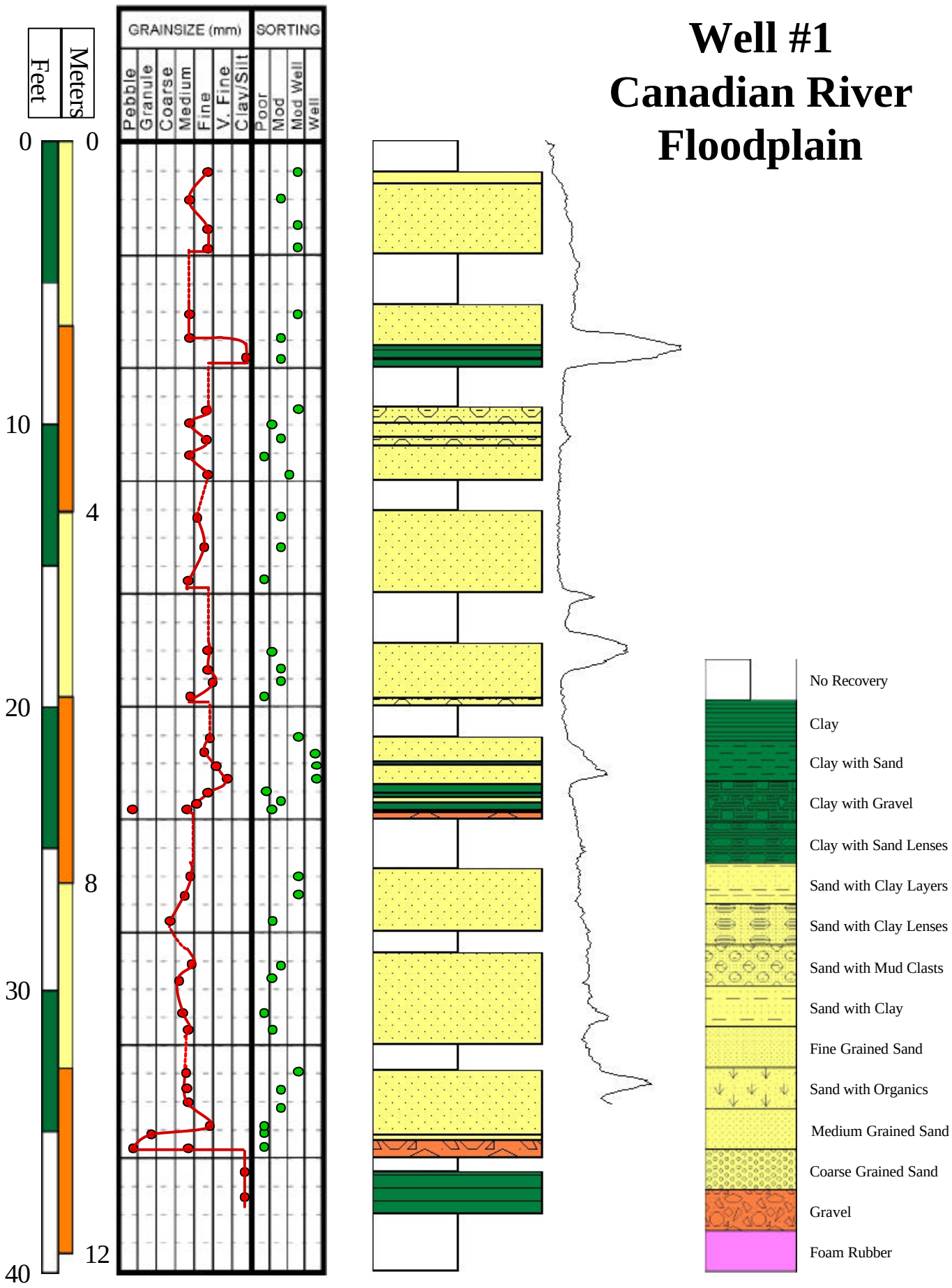

Well #3
Canadian River
Floodplain

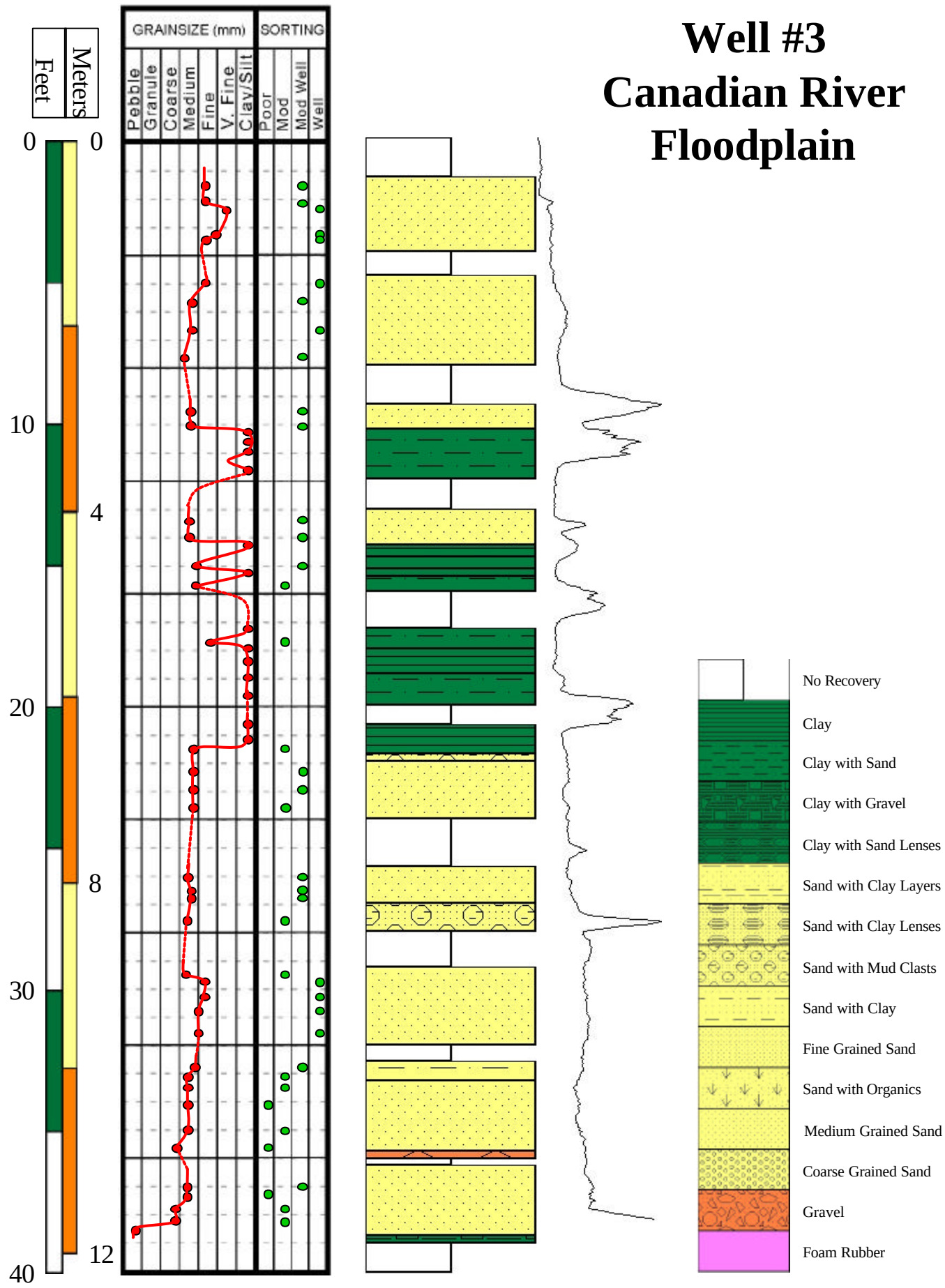

Well #7
Canadian River
Floodplain

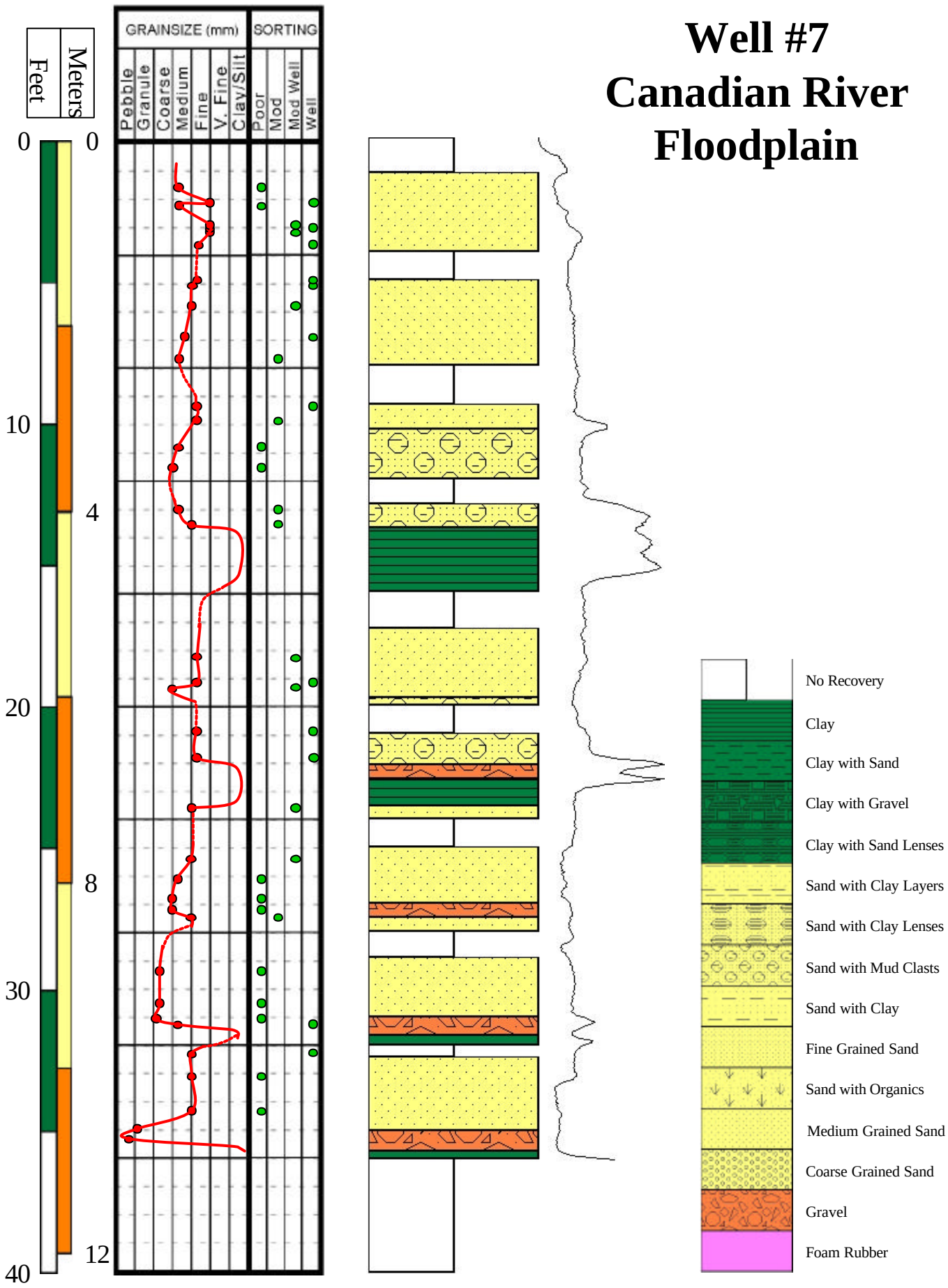

Well #11
Canadian River
Floodplain

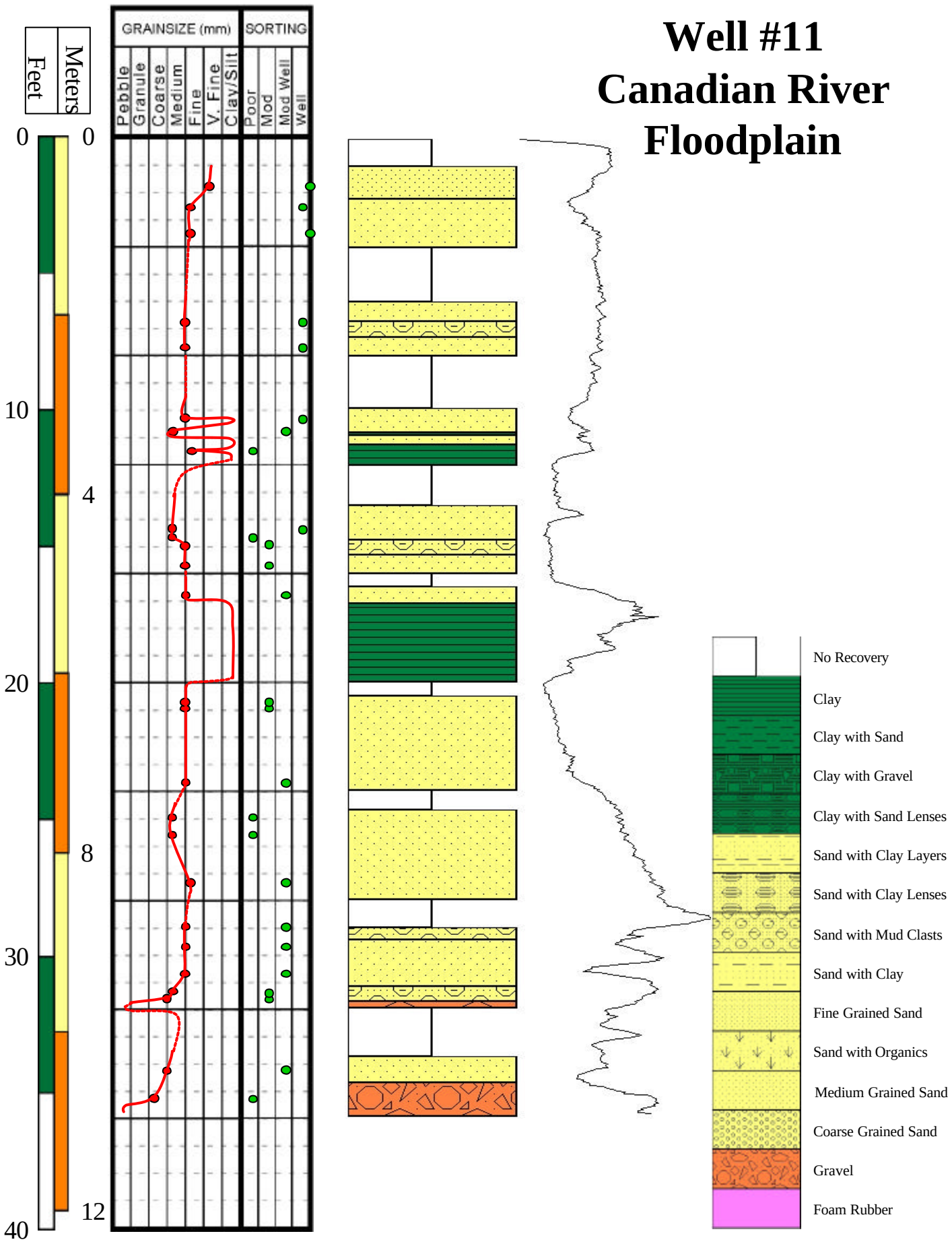

Well #15
Canadian River
Floodplain

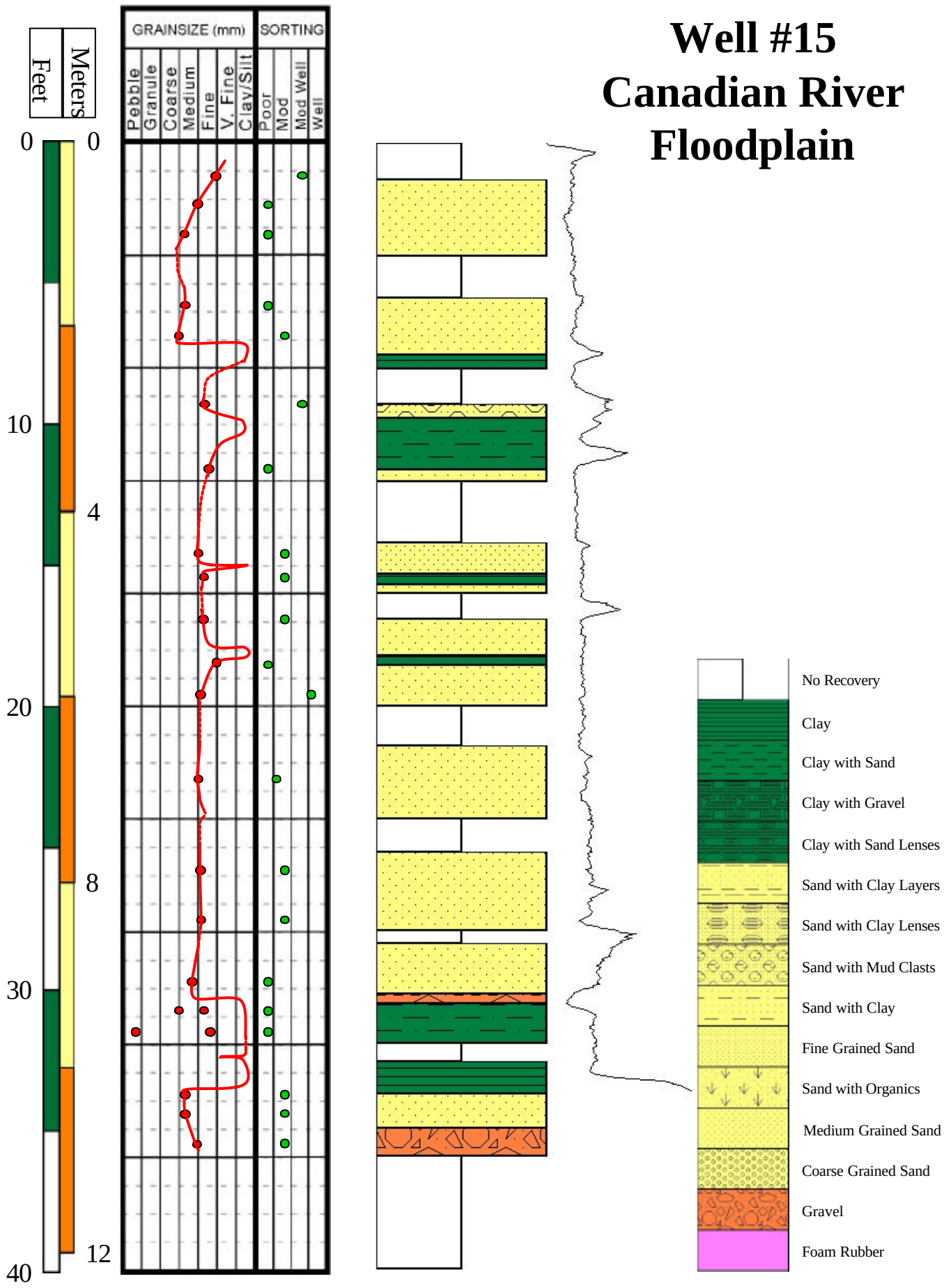

Well #21
Canadian River
Floodplain

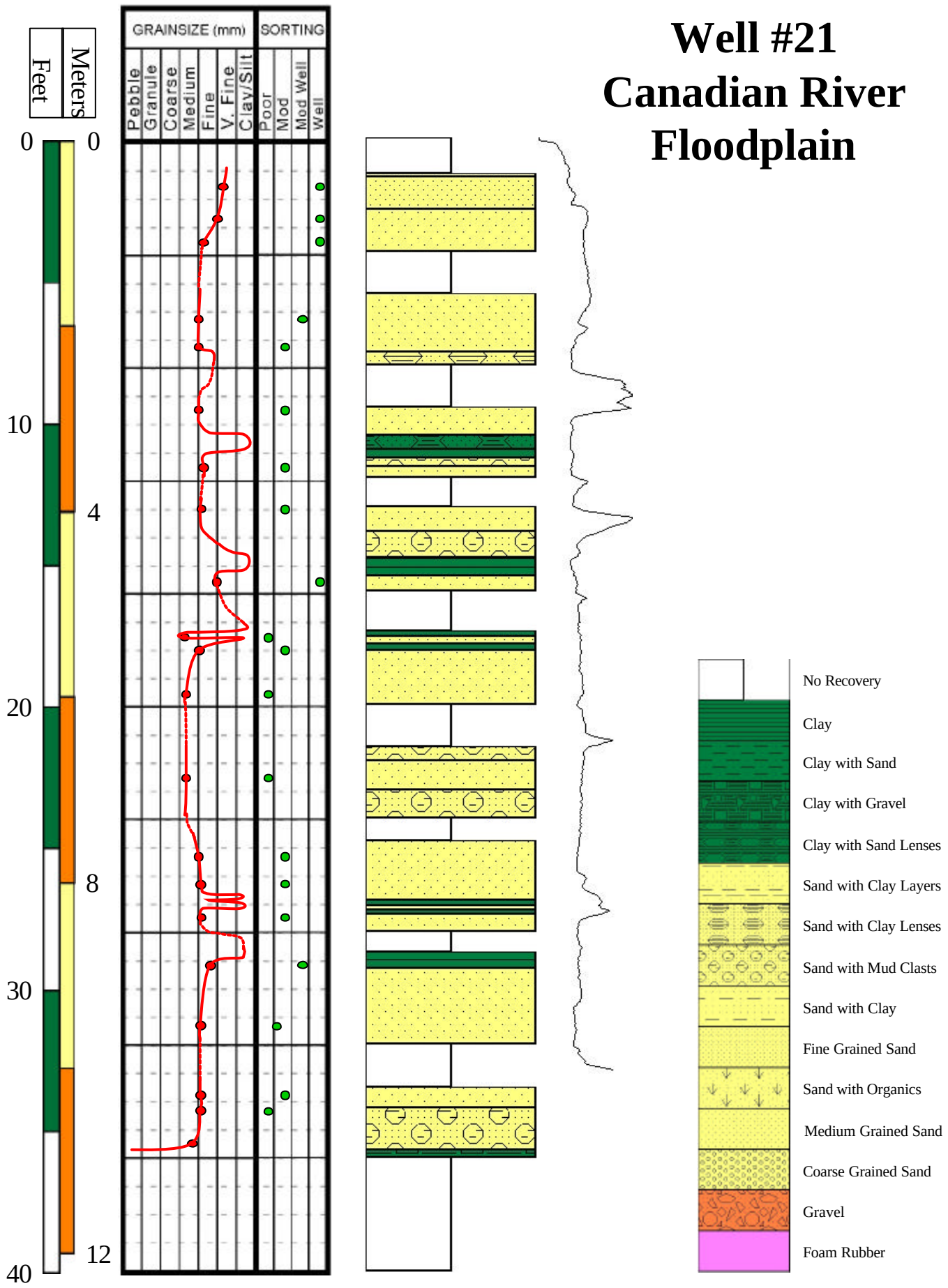

Well #23
Canadian River
Floodplain

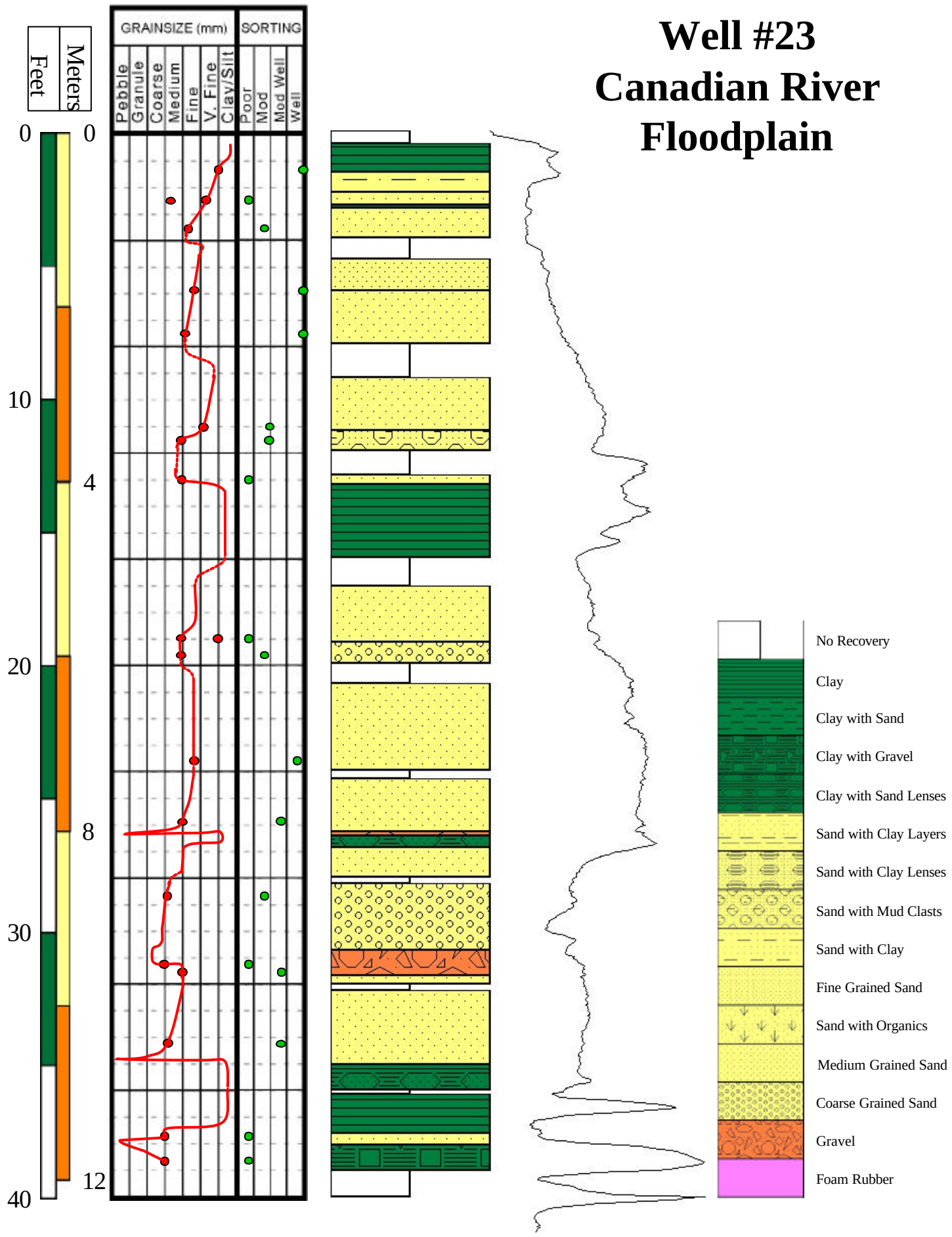

Well #28
Canadian River
Floodplain

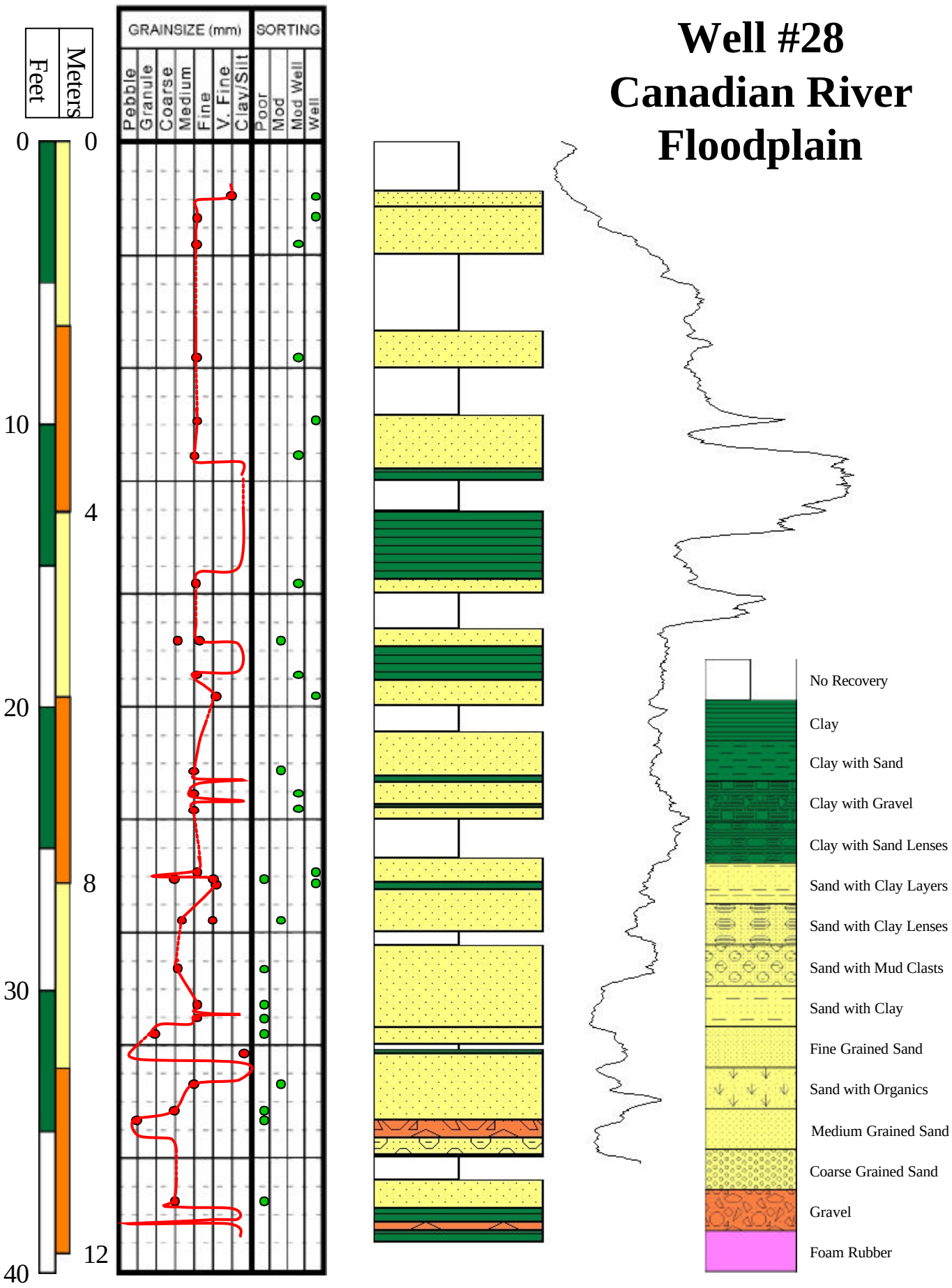

Well #31
Canadian River
Floodplain

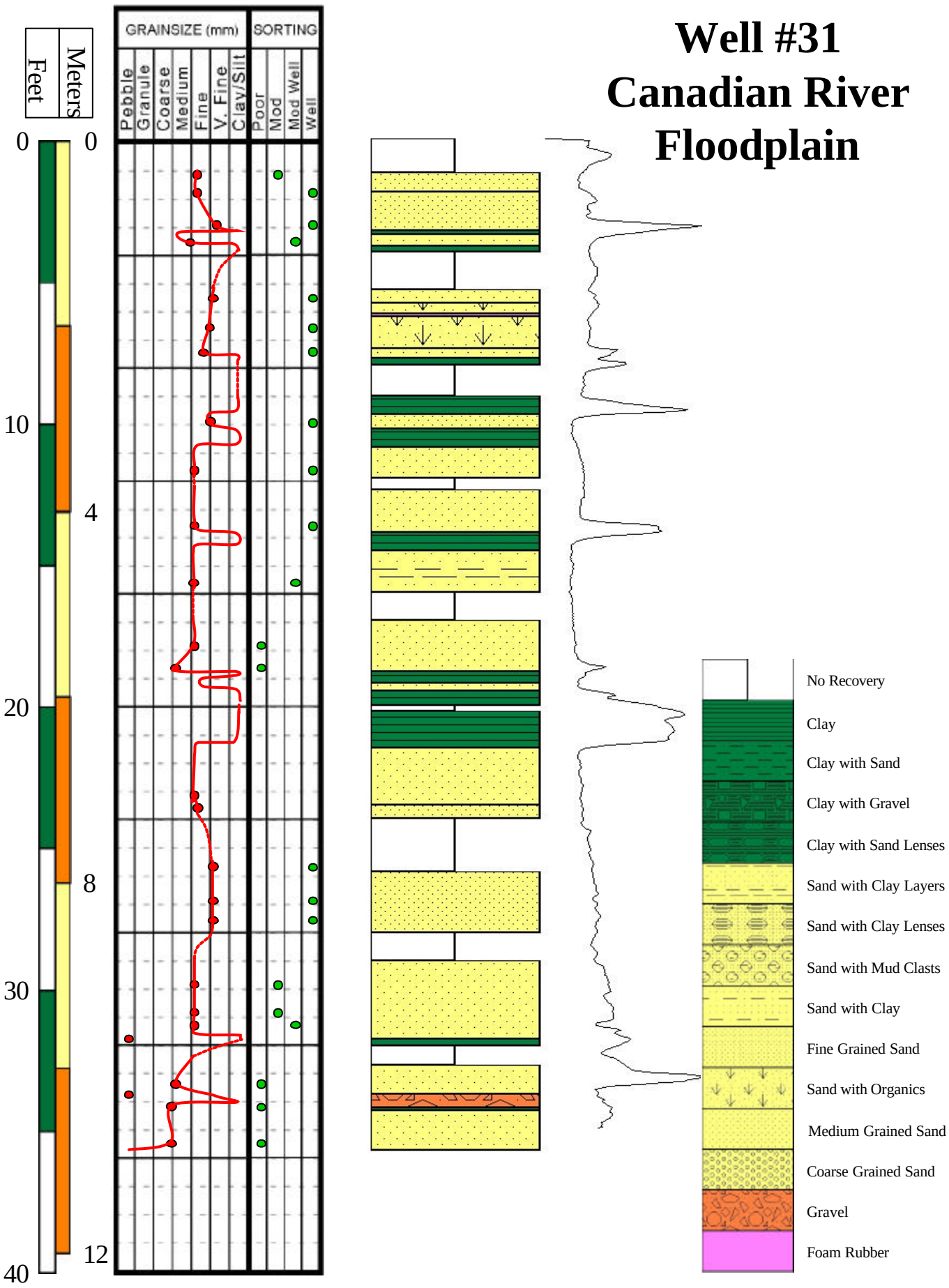

Well #42
Canadian River
Floodplain

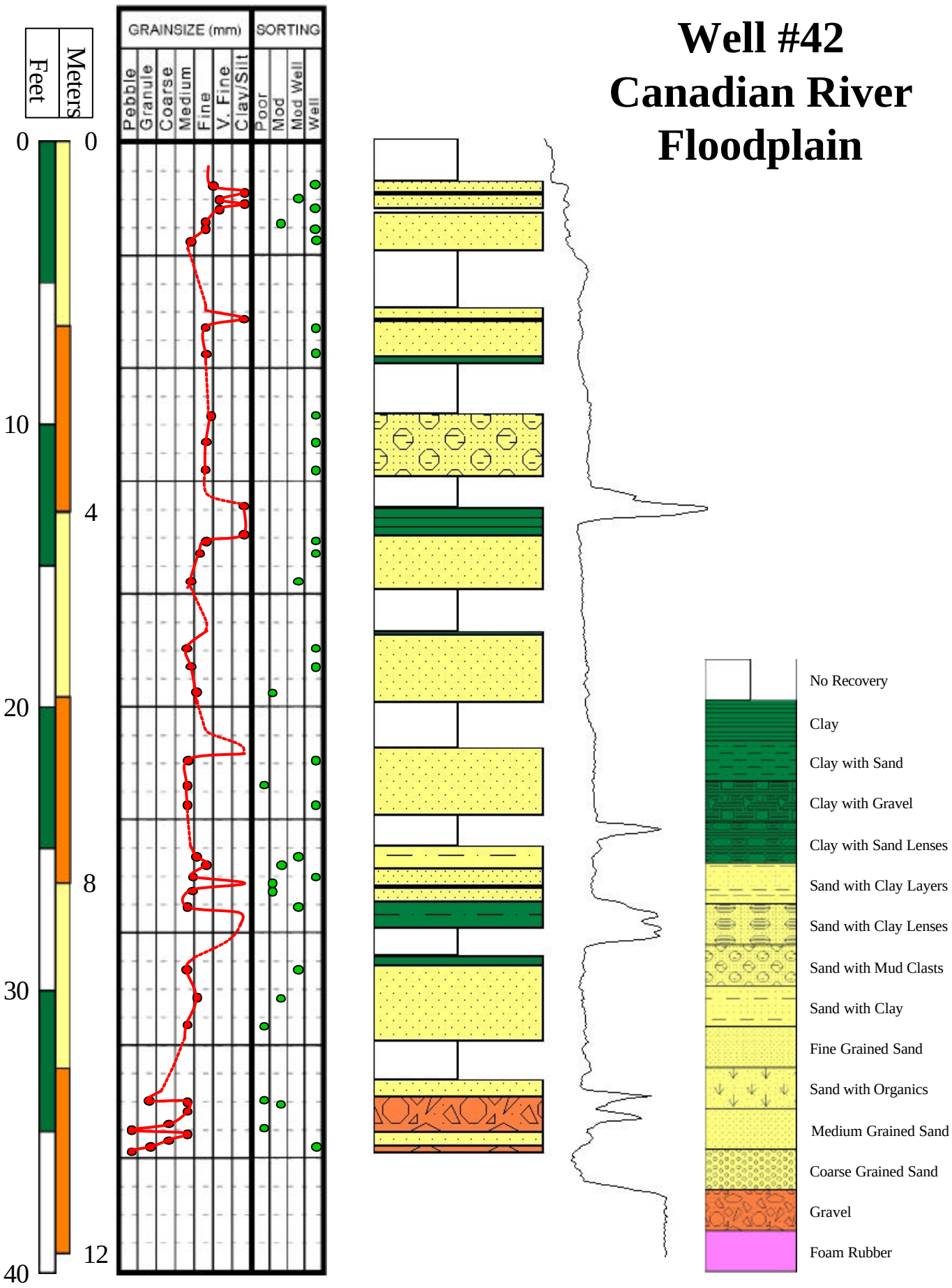

Well #44
Canadian River
Floodplain

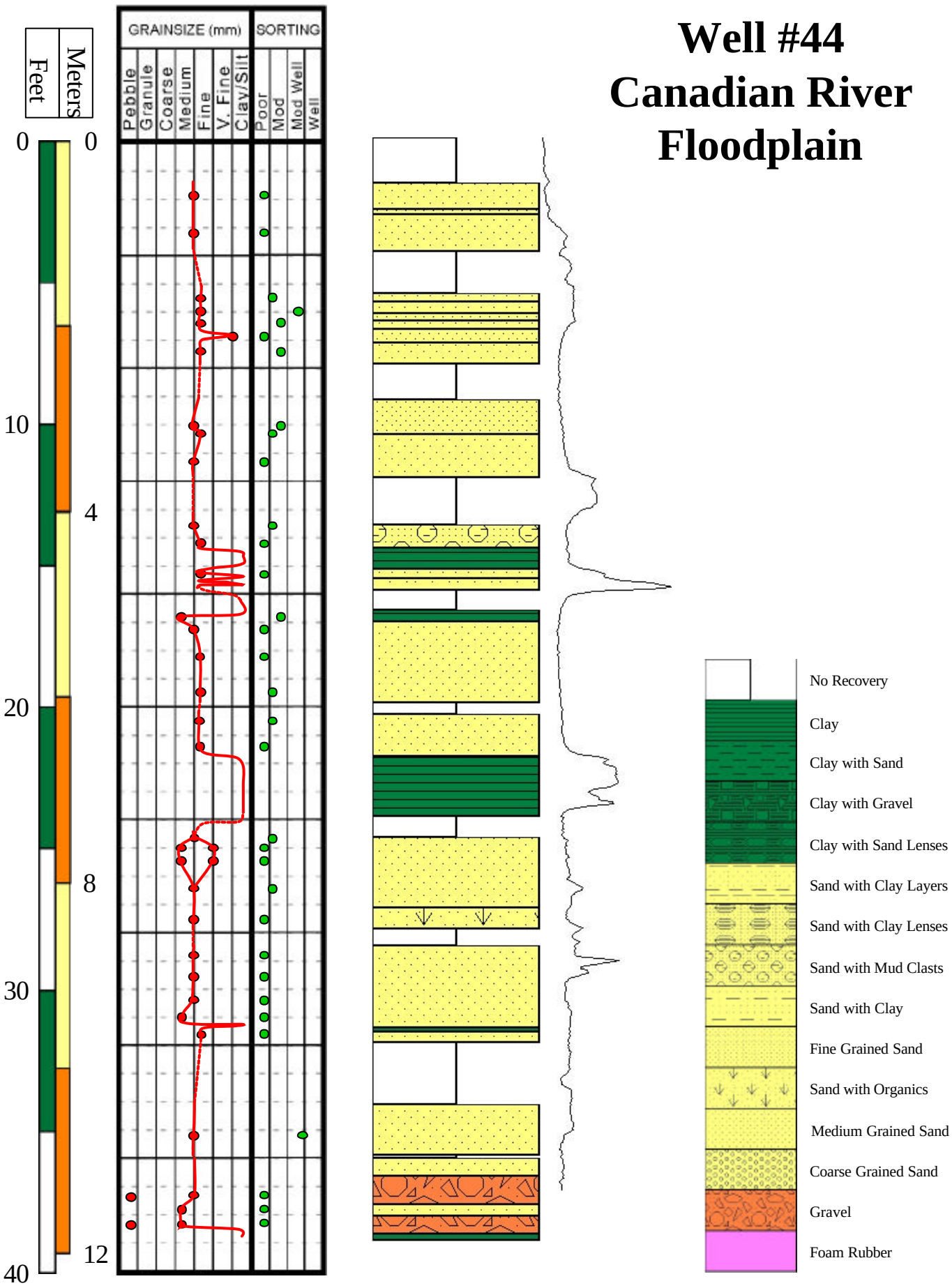

Well #46Canadian River Floodplain

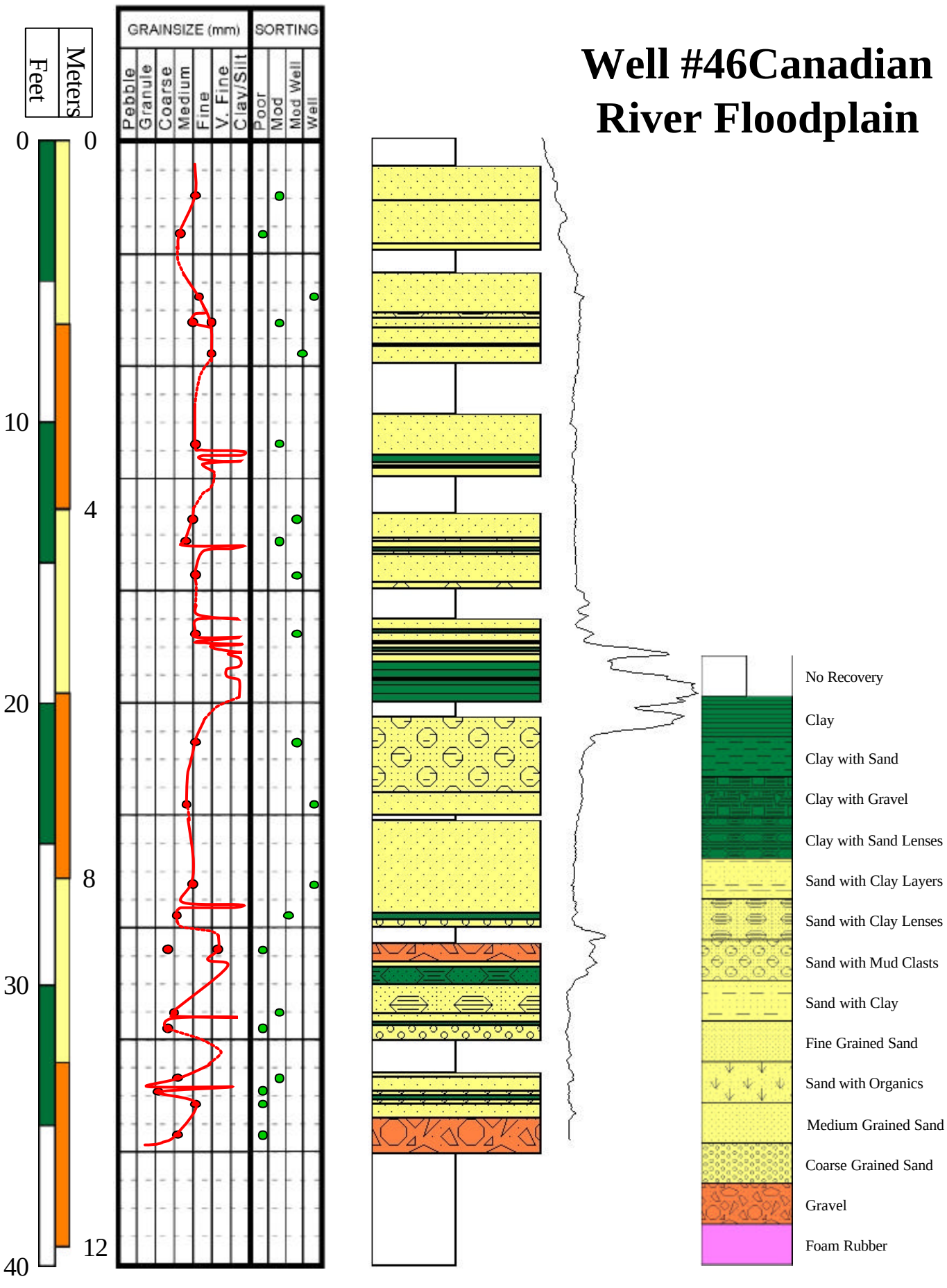

Well #56
Canadian River
Floodplain

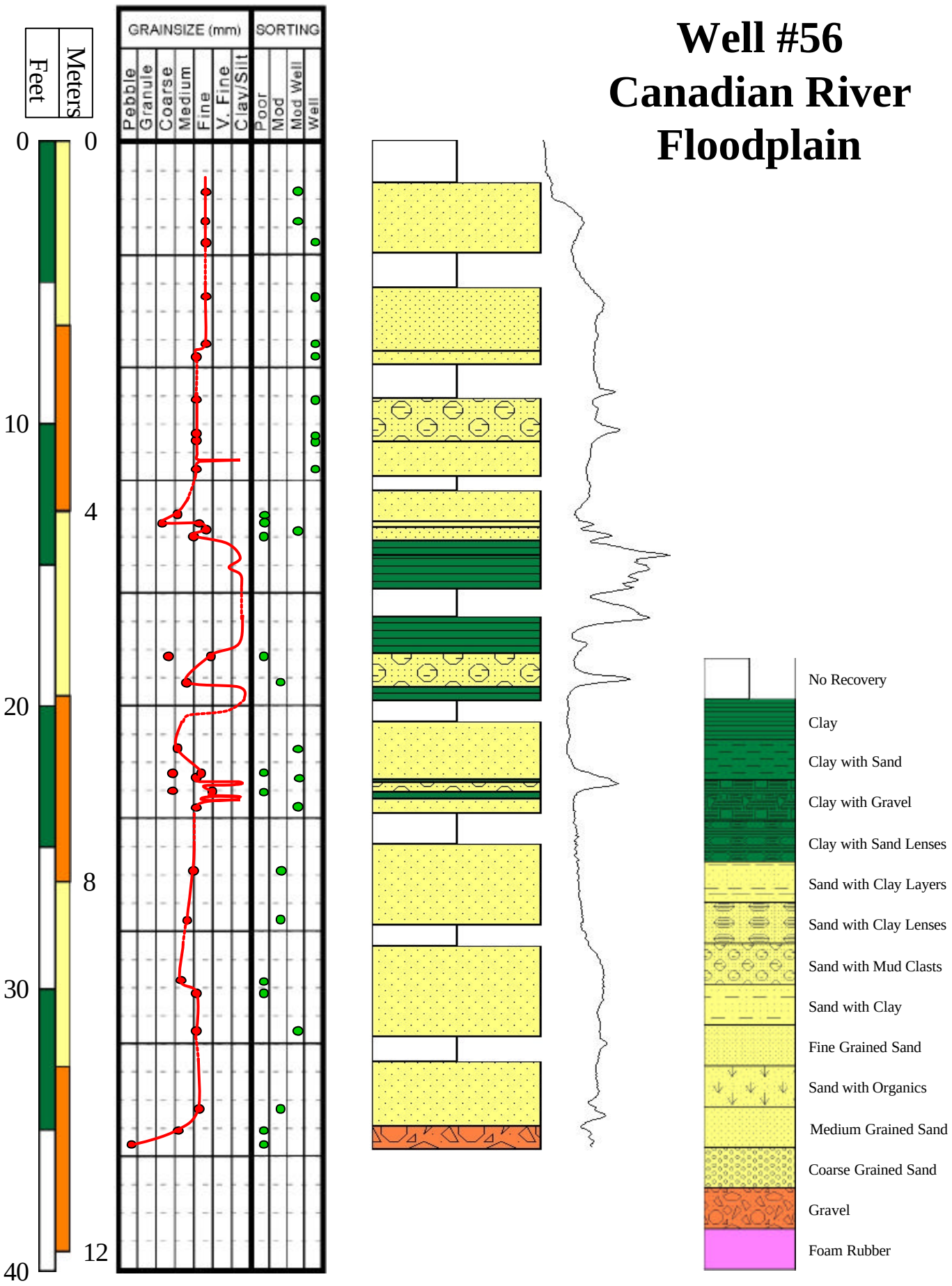

Well #57
Canadian River
Floodplain

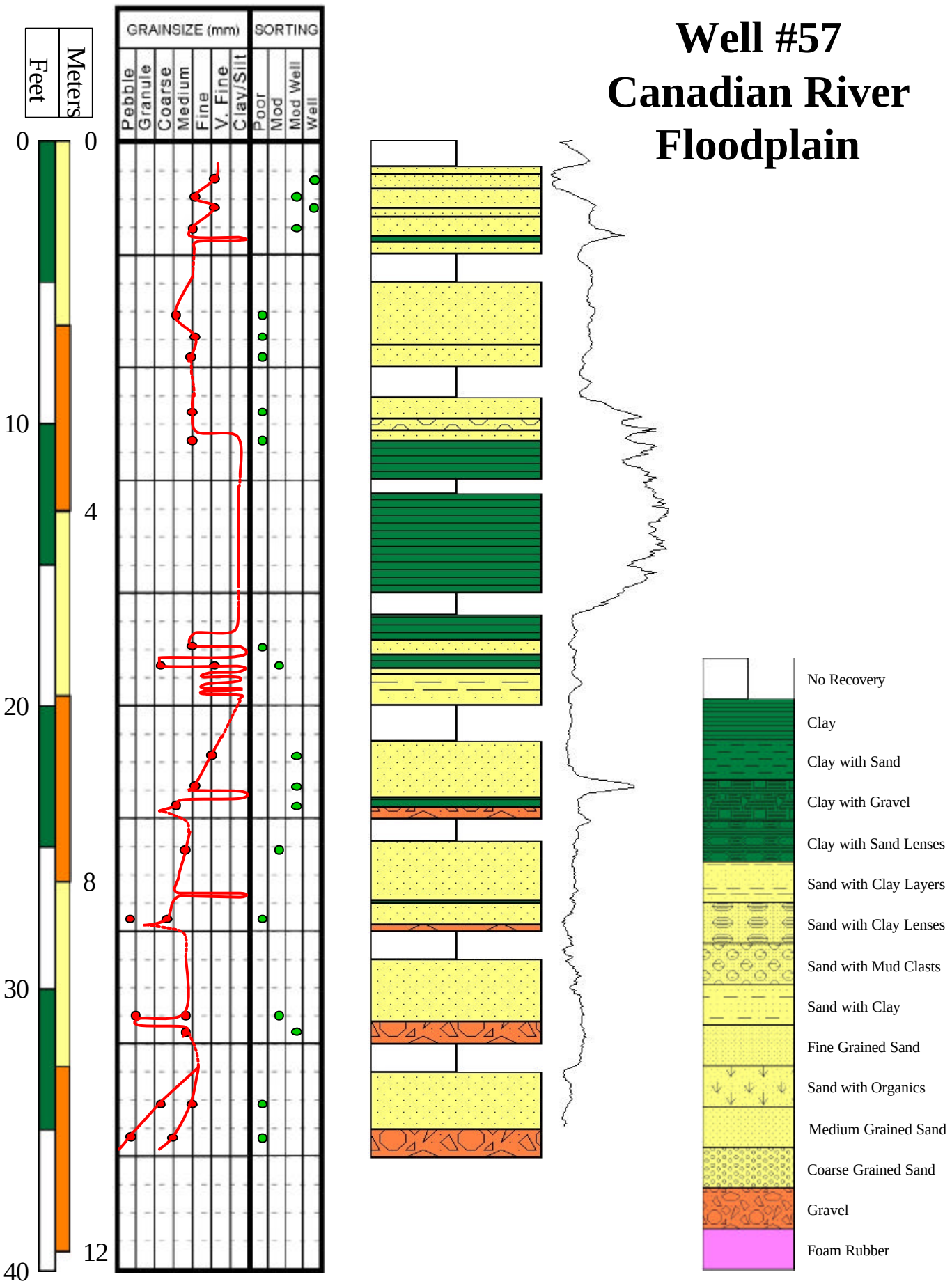

Well #62
Canadian River
Floodplain

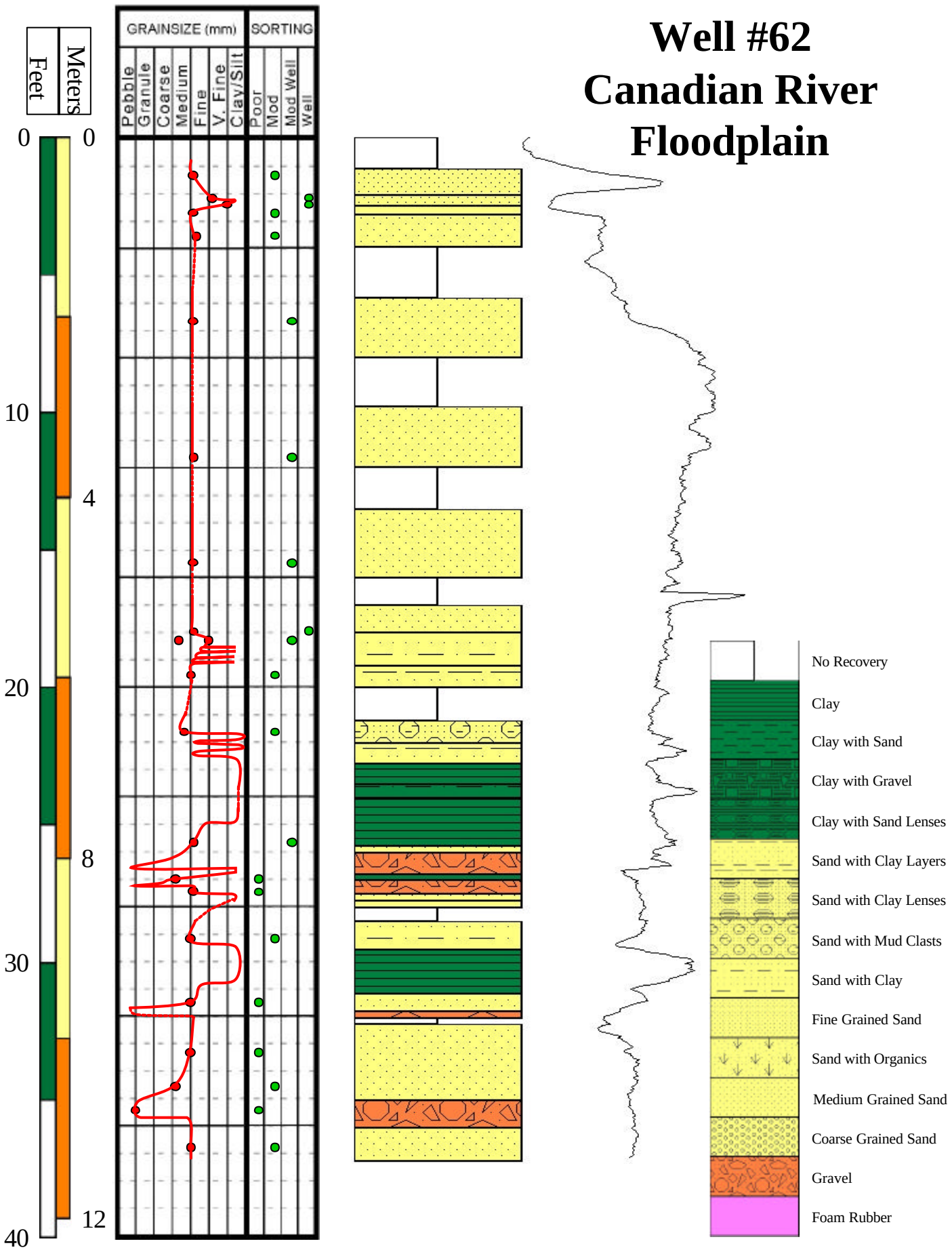

Well #64
Canadian River
Floodplain

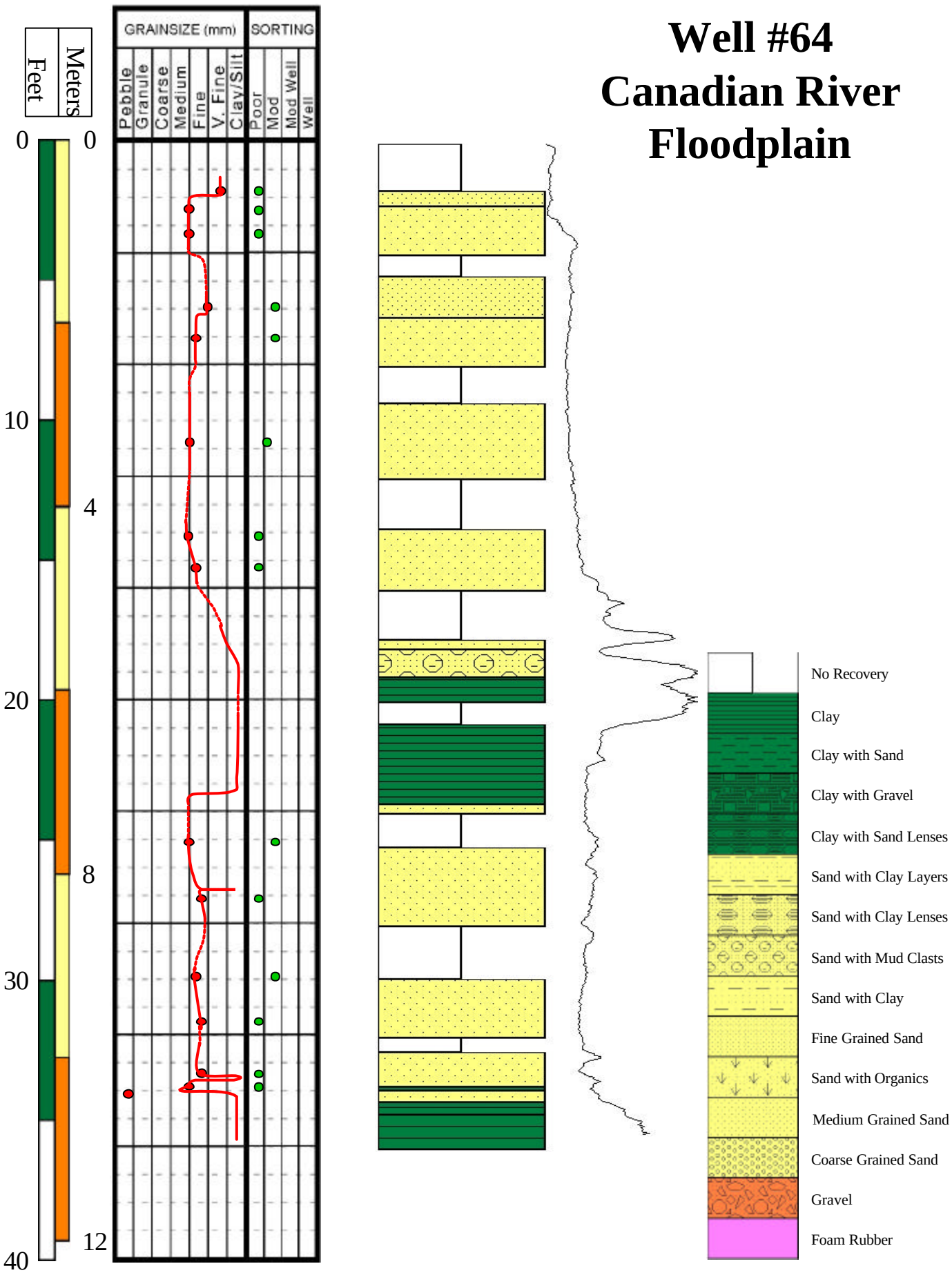

Well #73
Canadian River
Floodplain

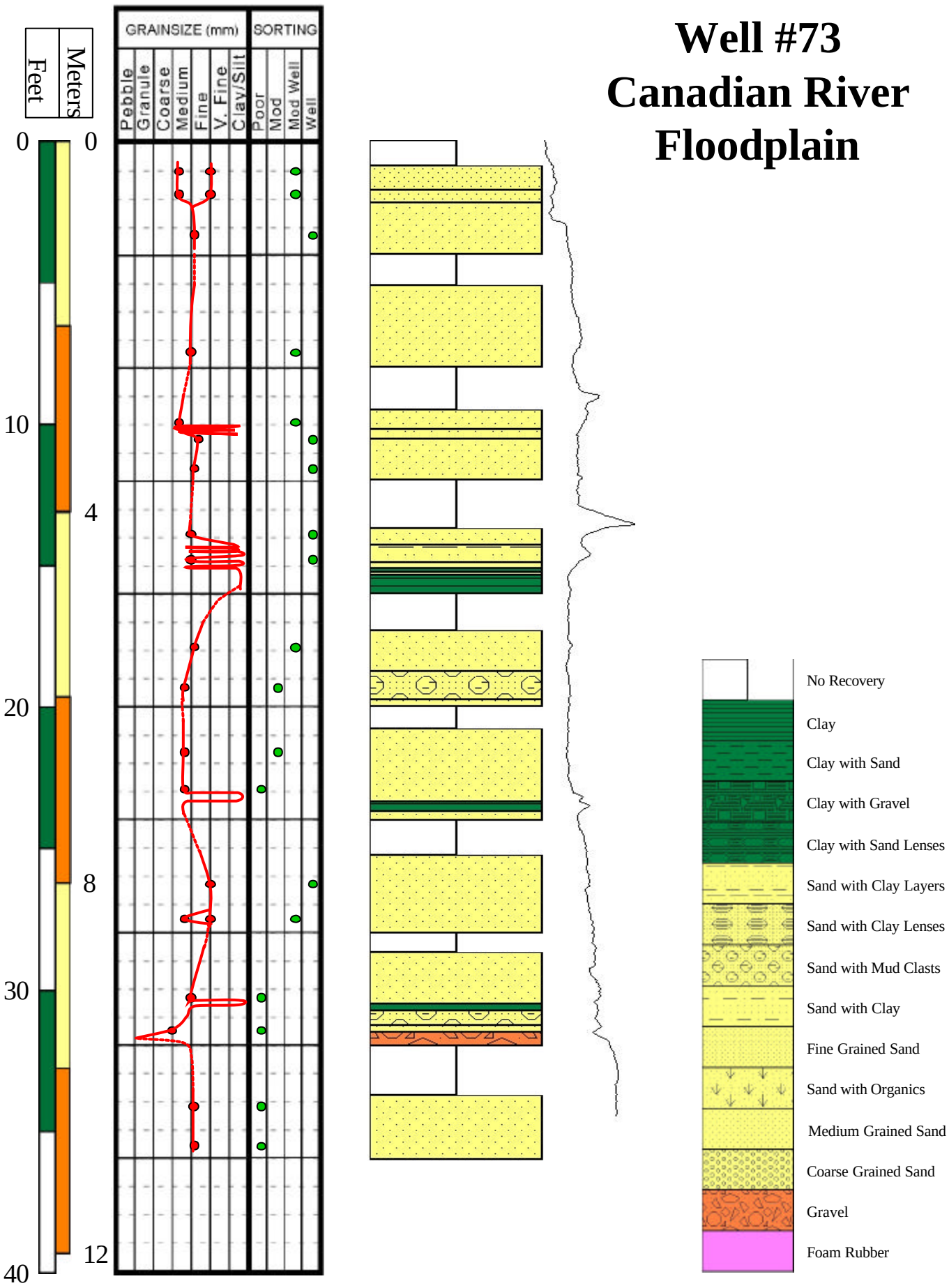

Well #74
Canadian River
Floodplain

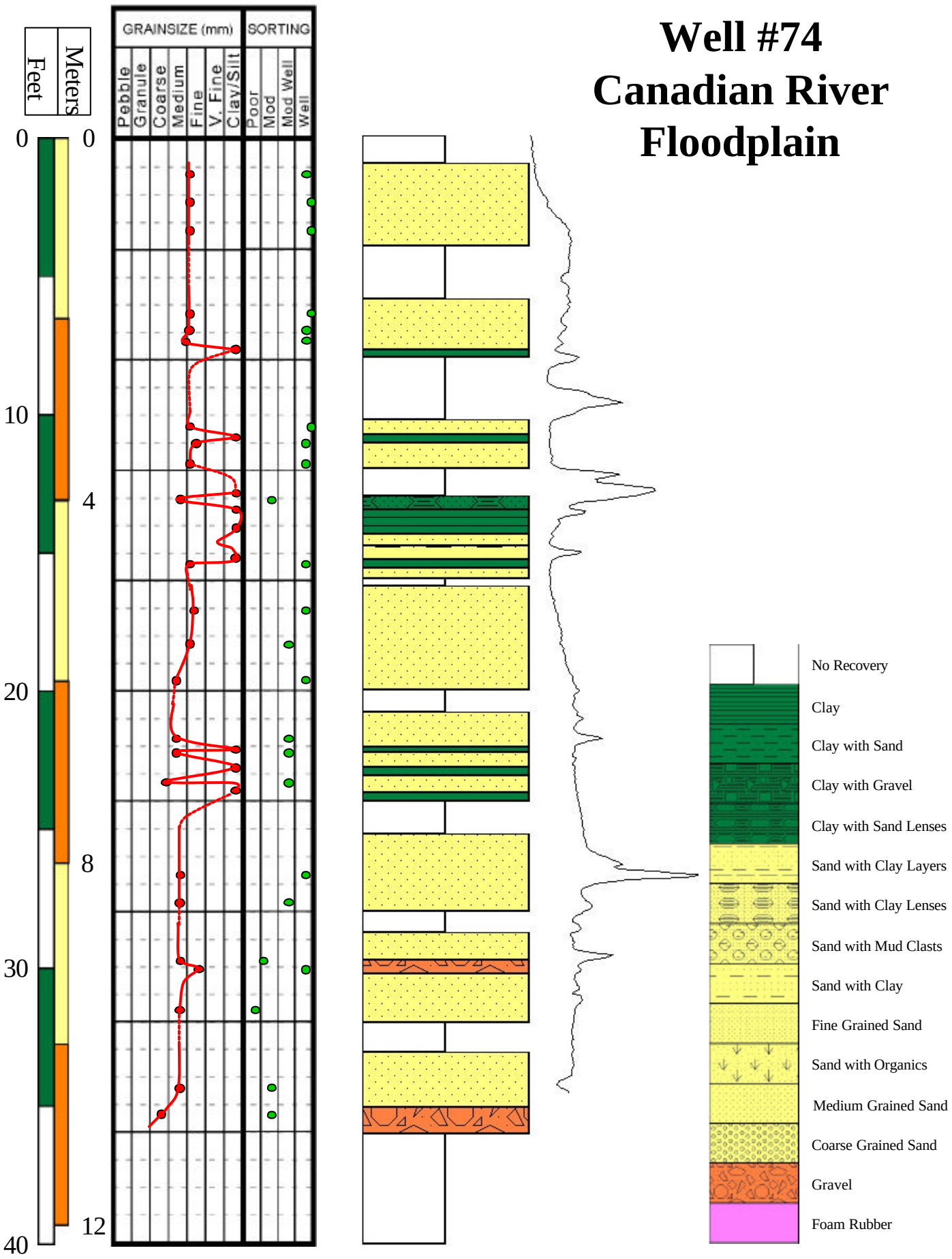

Well #78
Canadian River
Floodplain

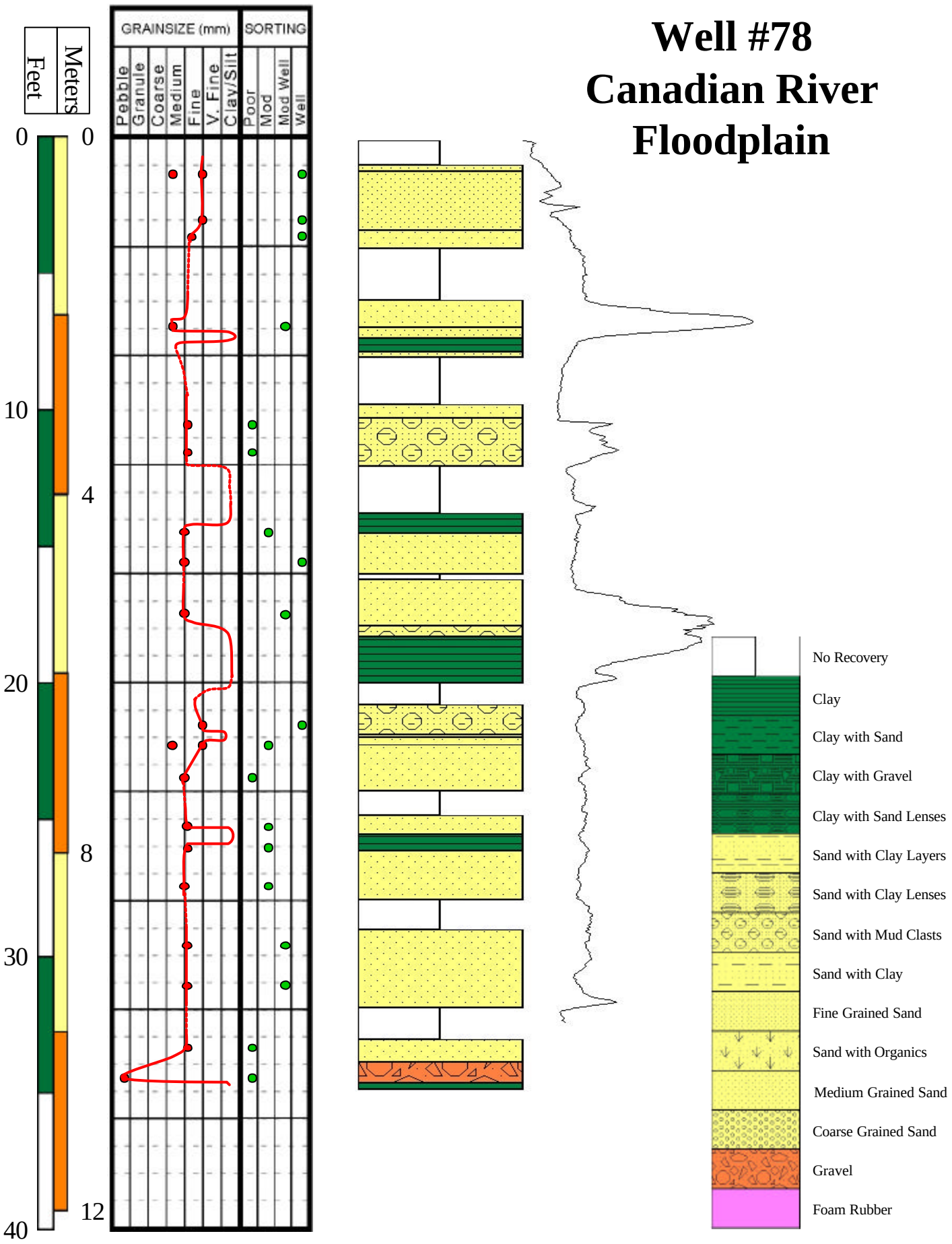

APPENDIX B

CORE PHOTOS

<u>Well #1</u> – Canadian River Floodplain

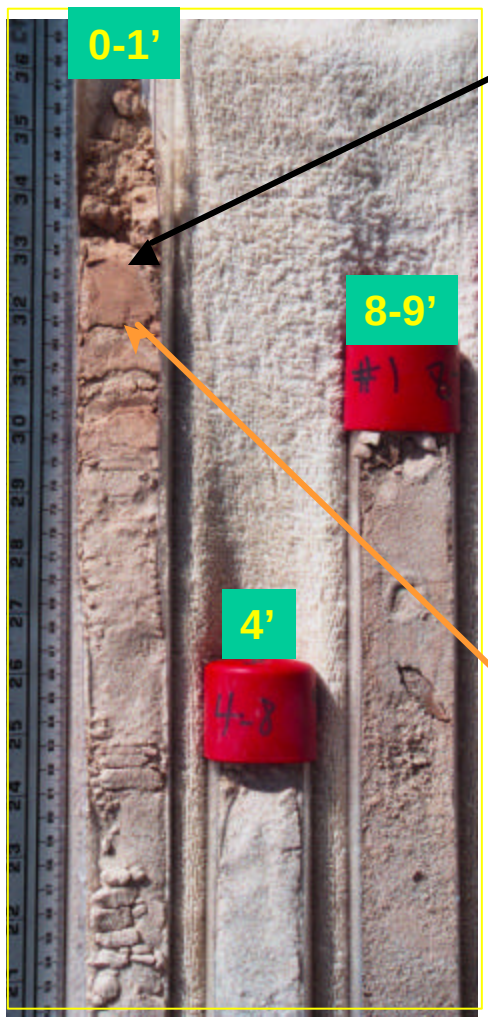

Incipient Soil Zone

Well #1

Canadian River Floodplain

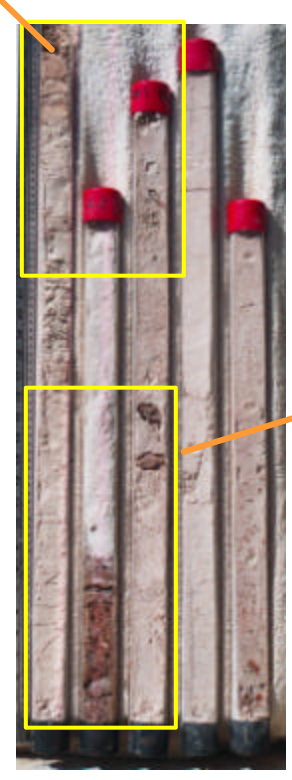

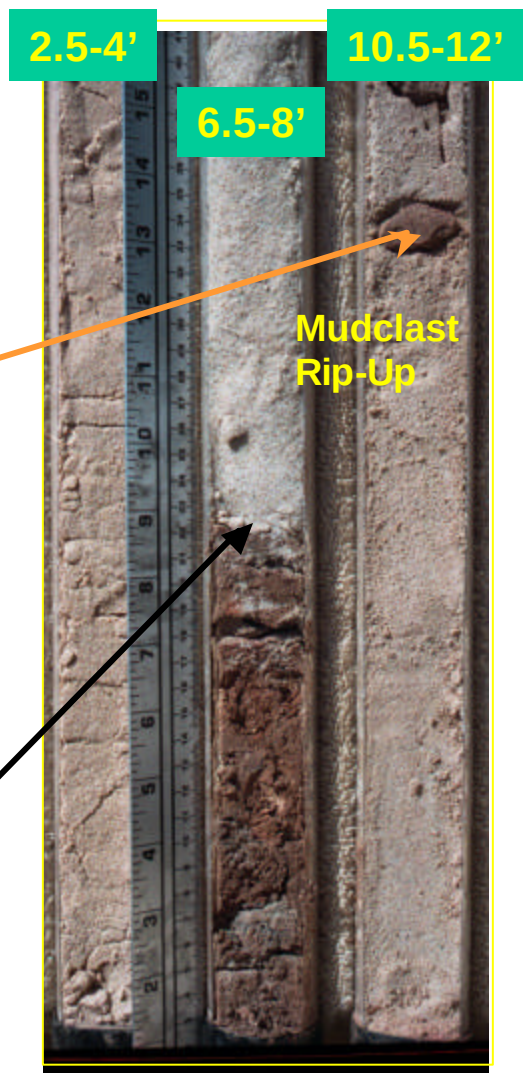

Note sharp contact of sand with underlying mud.

<u>Well #3</u> – Canadian River Floodplain

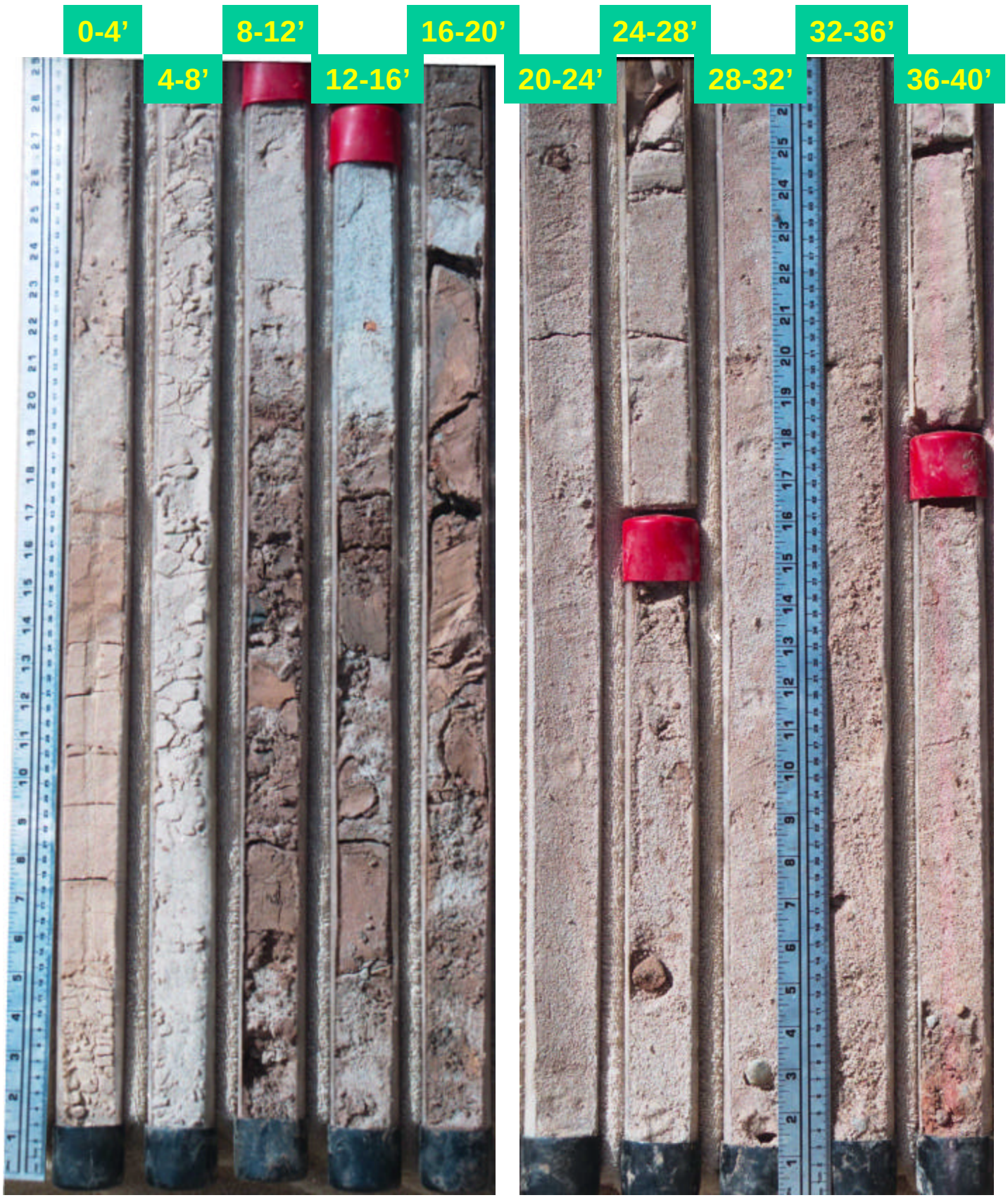

<u>Well #3</u> – Canadian River Floodplain

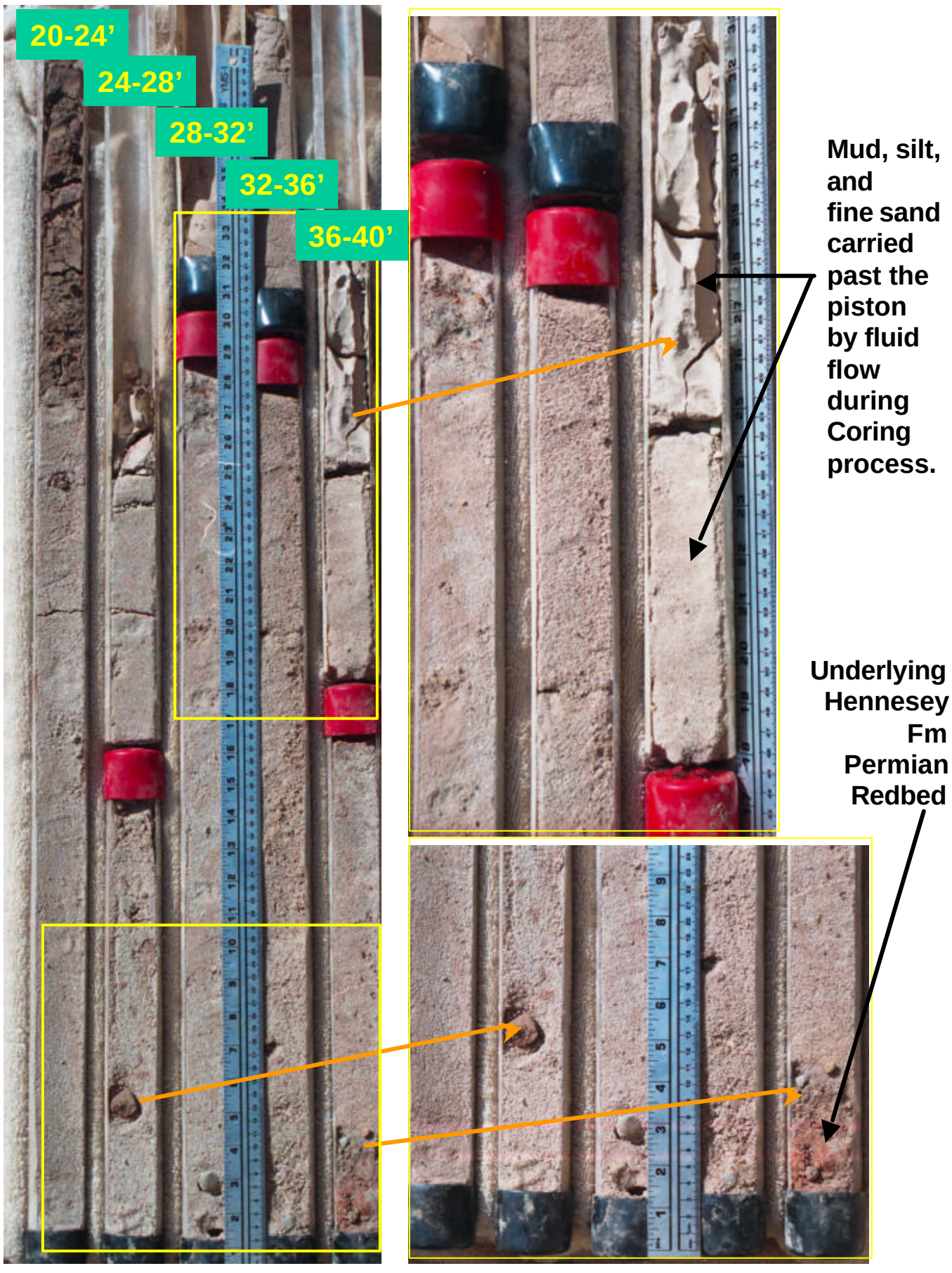

<u>Well #7</u> – Canadian River Floodplain

Well #7

Canadian River Floodplain

<u>Well #11</u> – Canadian River Floodplain

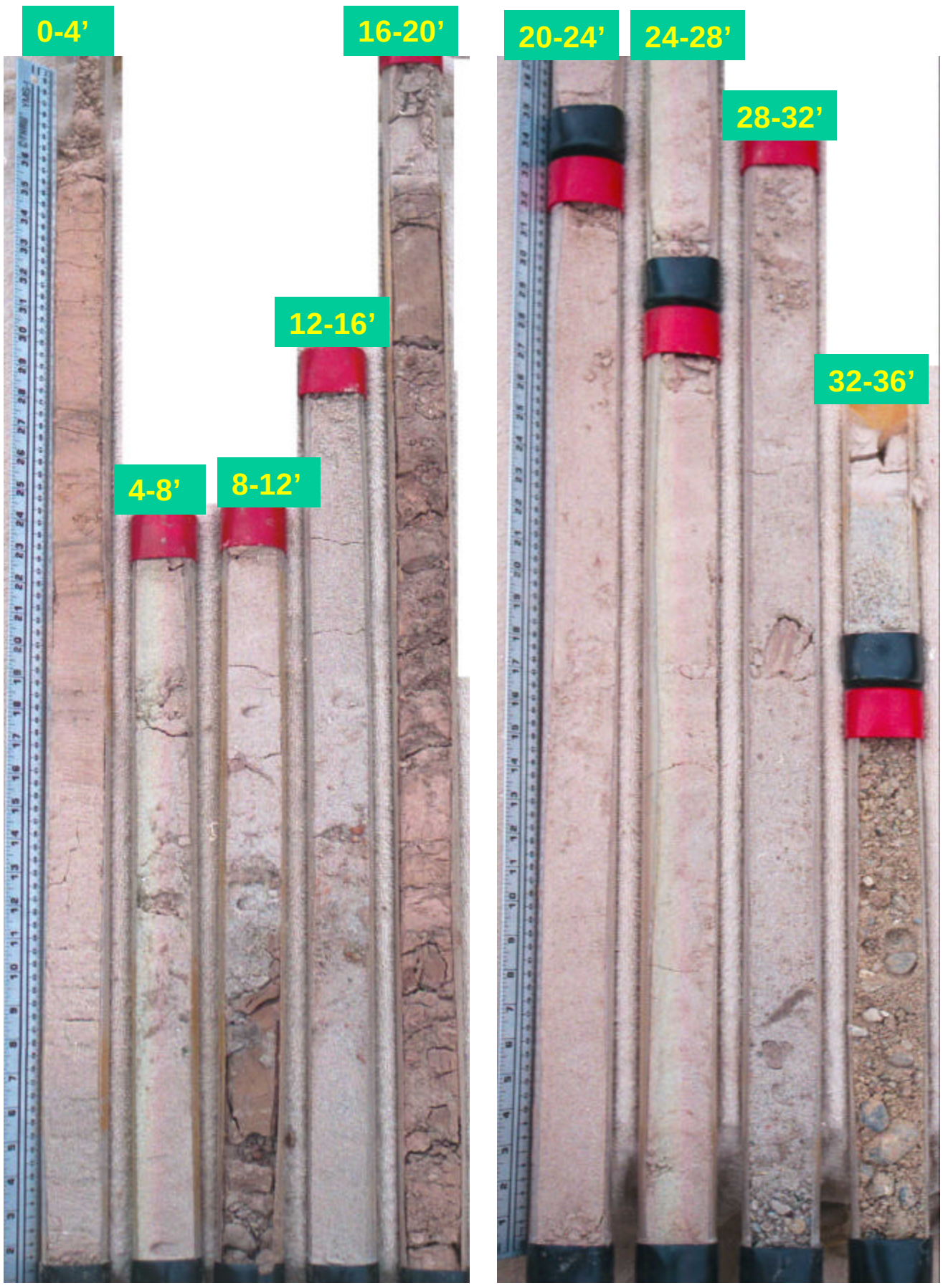

<u>Well #11</u> – Canadian River Floodplain

Sand and mud contacts

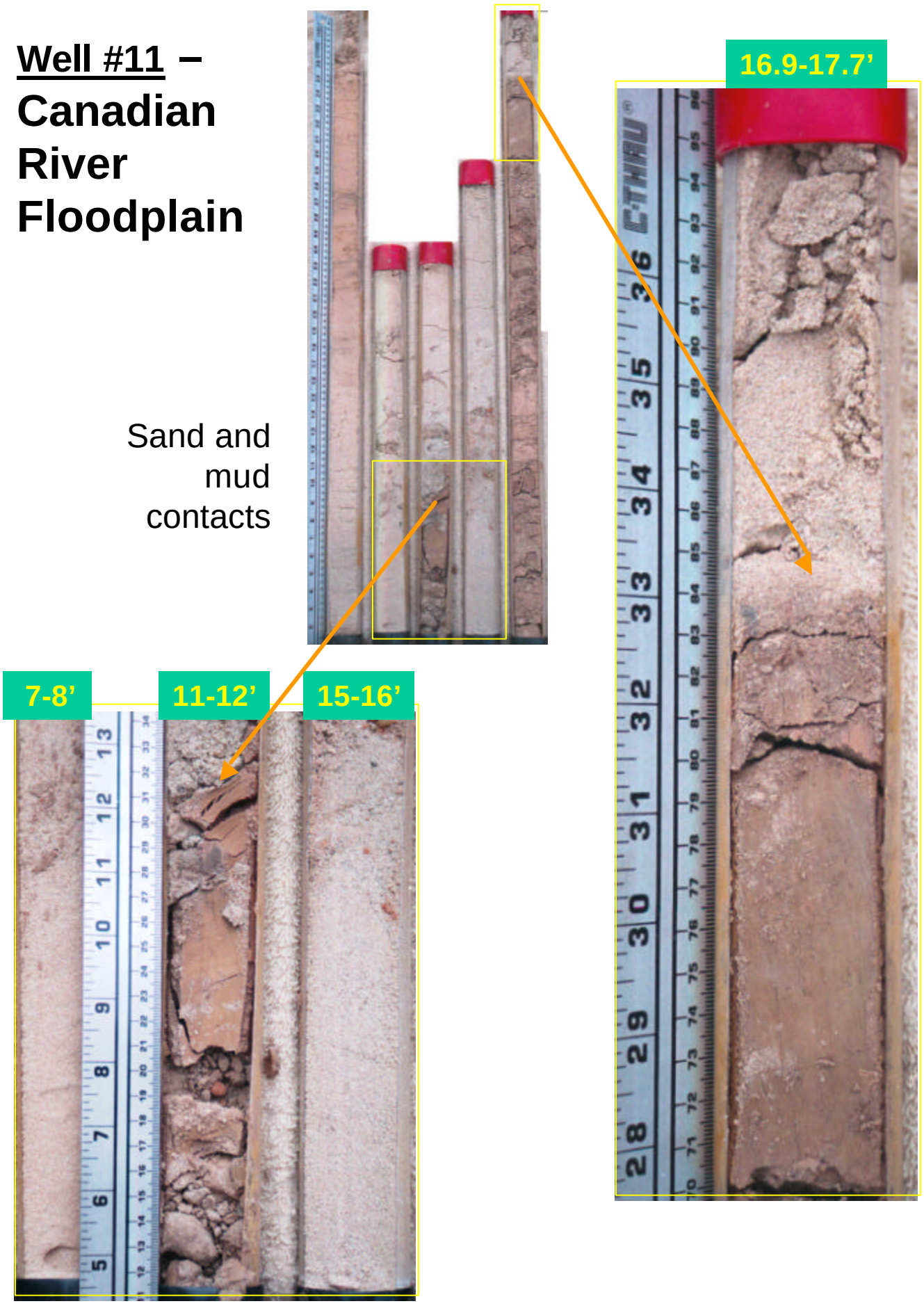

<u>Well #11</u> – Canadian River Floodplain

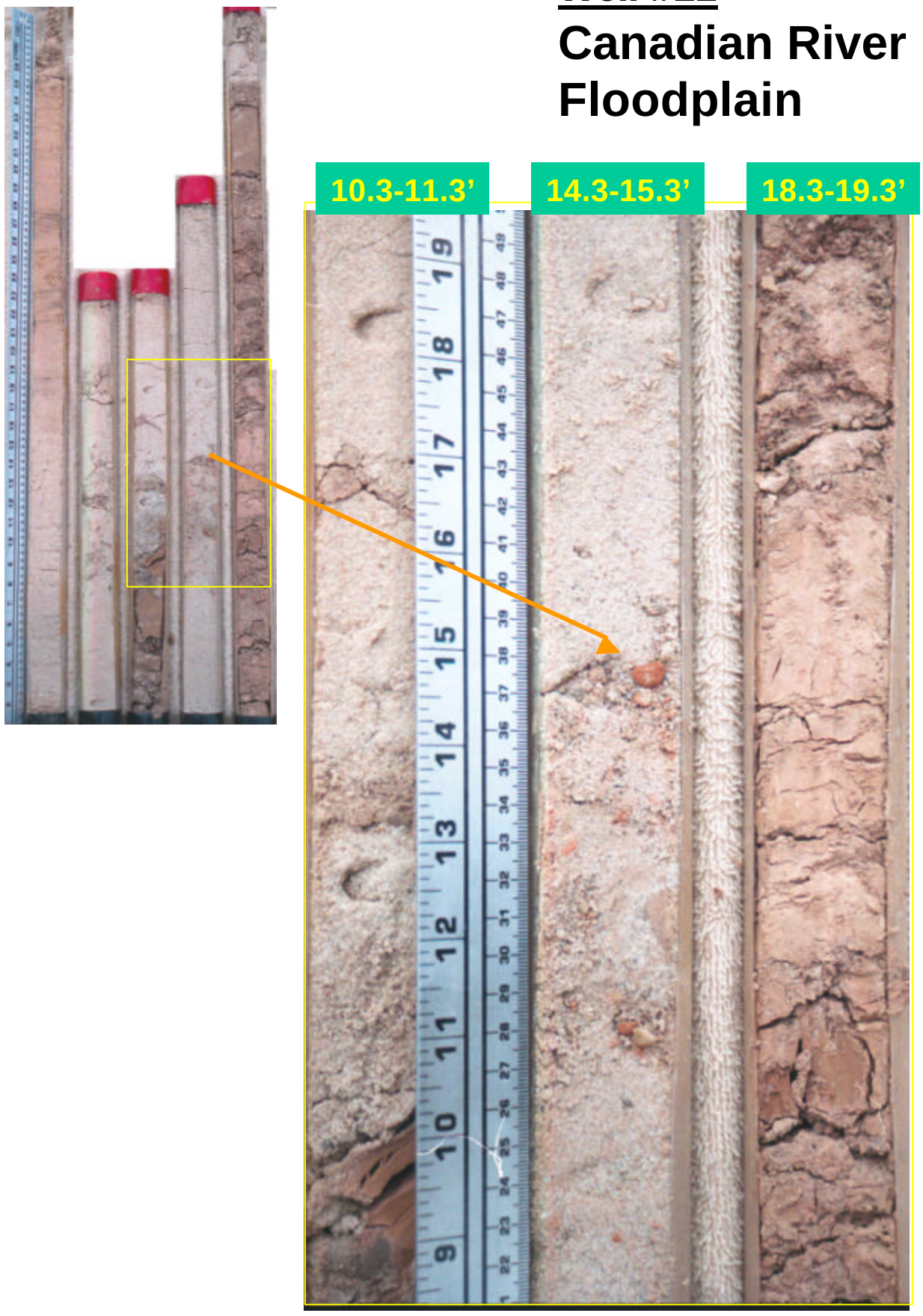

<u>Well #11</u> – Canadian River Floodplain

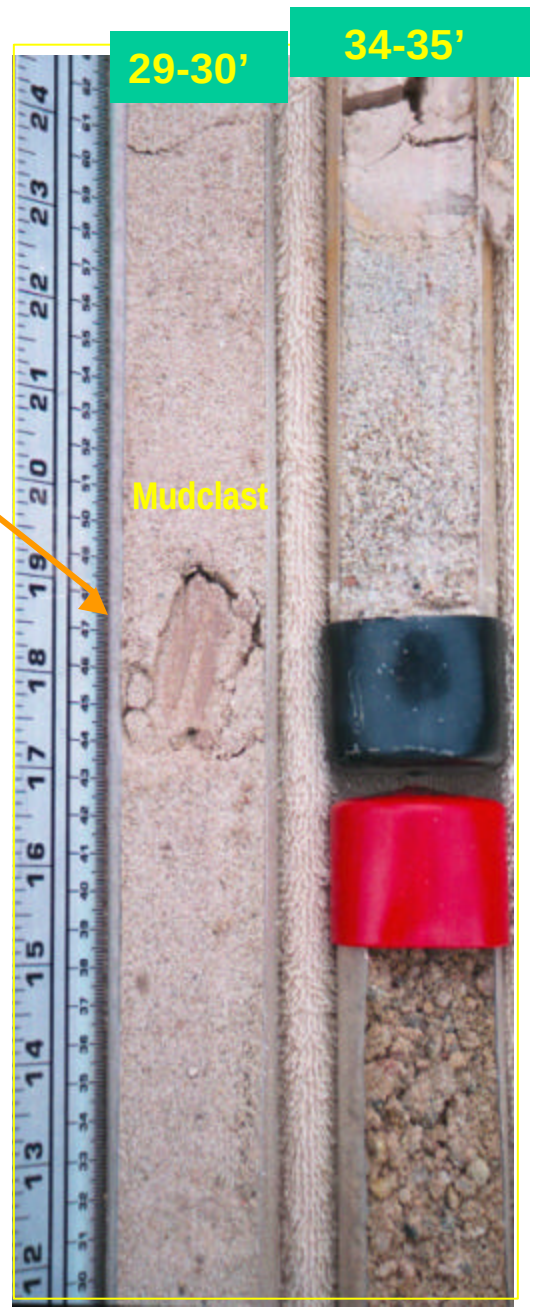

Gravel at base of alluvium

<u>Well #15</u> – Canadian River Floodplain

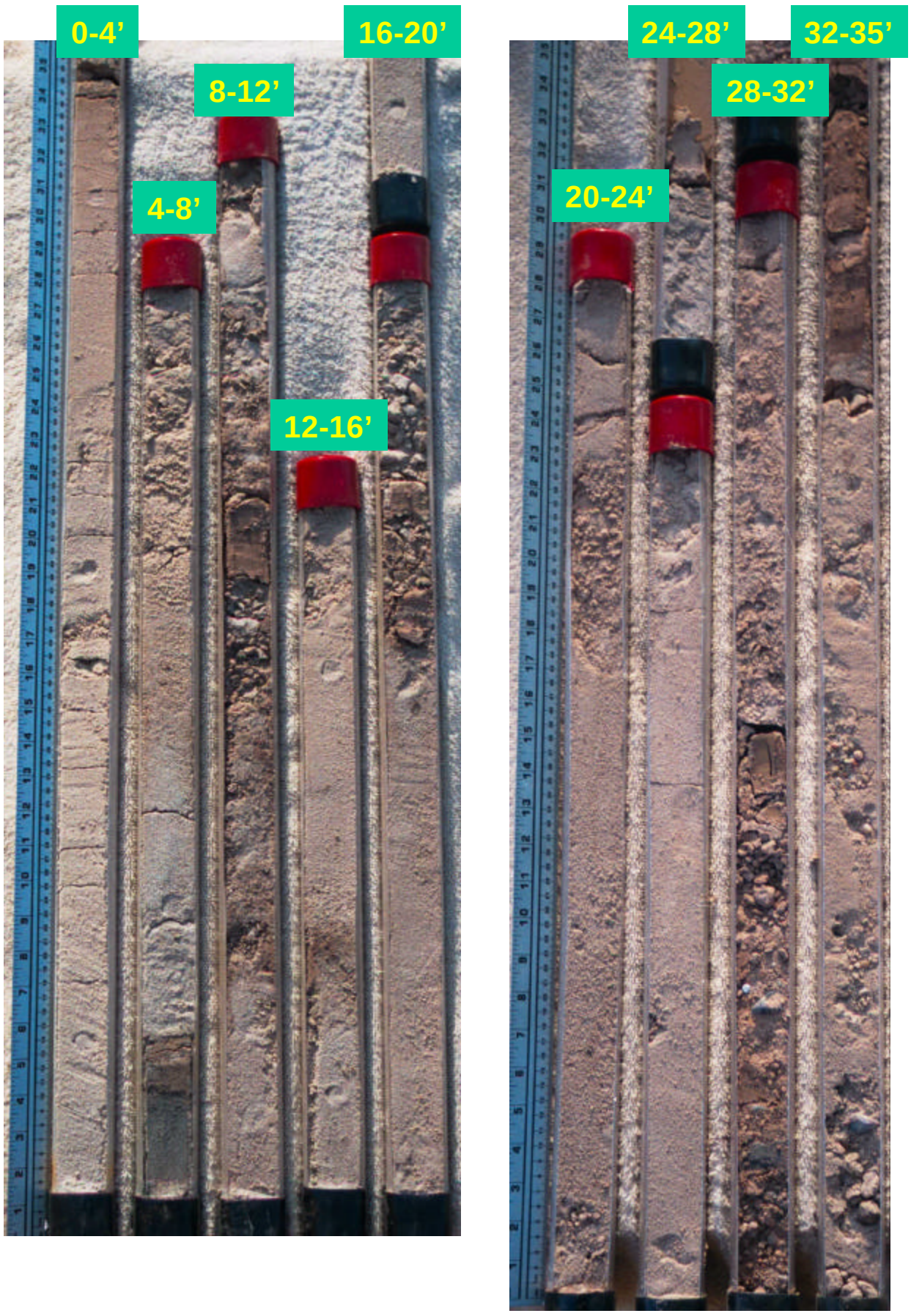

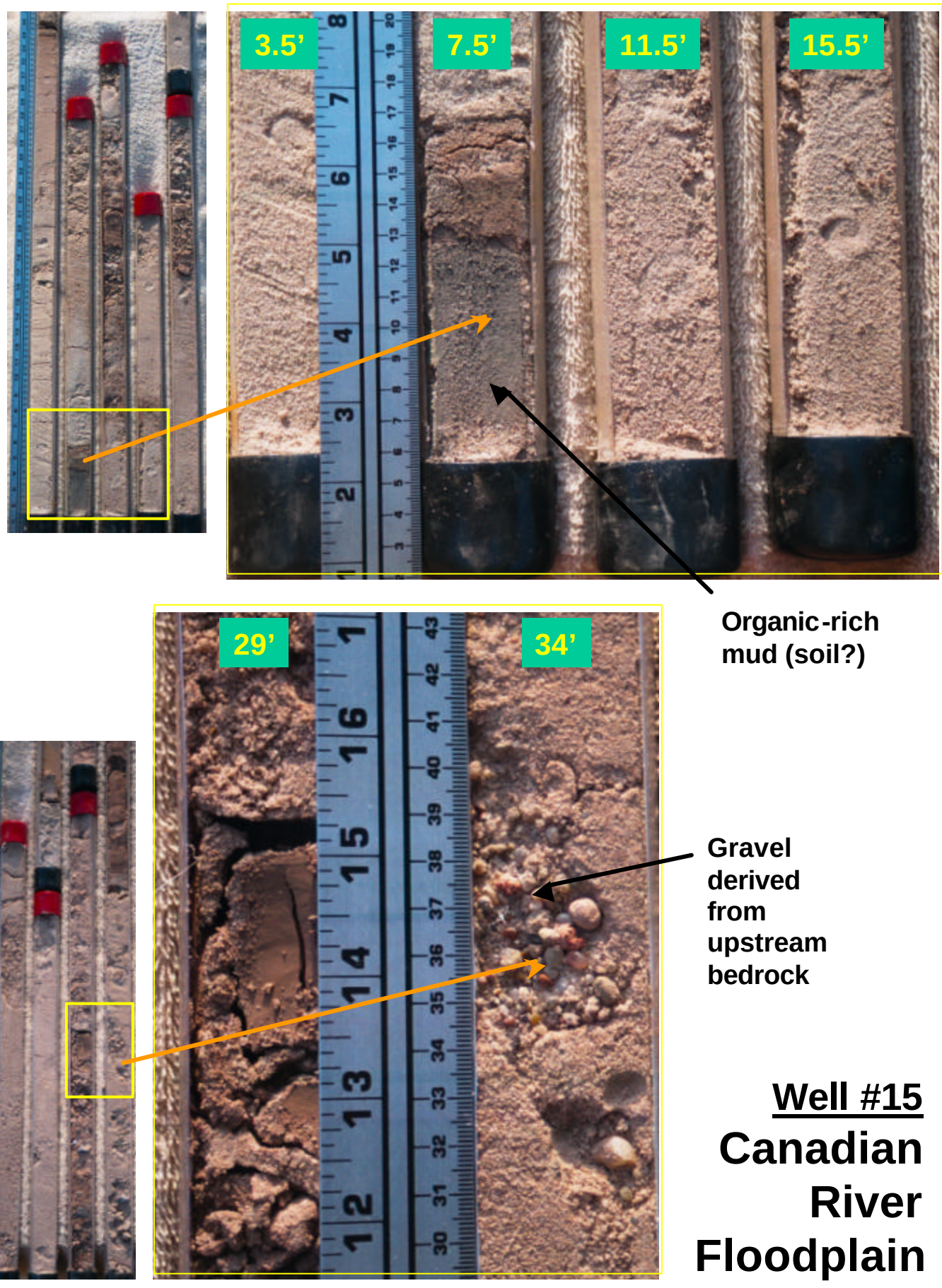

Organic-rich mud (soil?)

Gravel derived from upstream bedrock

Well #15

Canadian River Floodplain

<u>Well #21</u> – Canadian River Floodplain

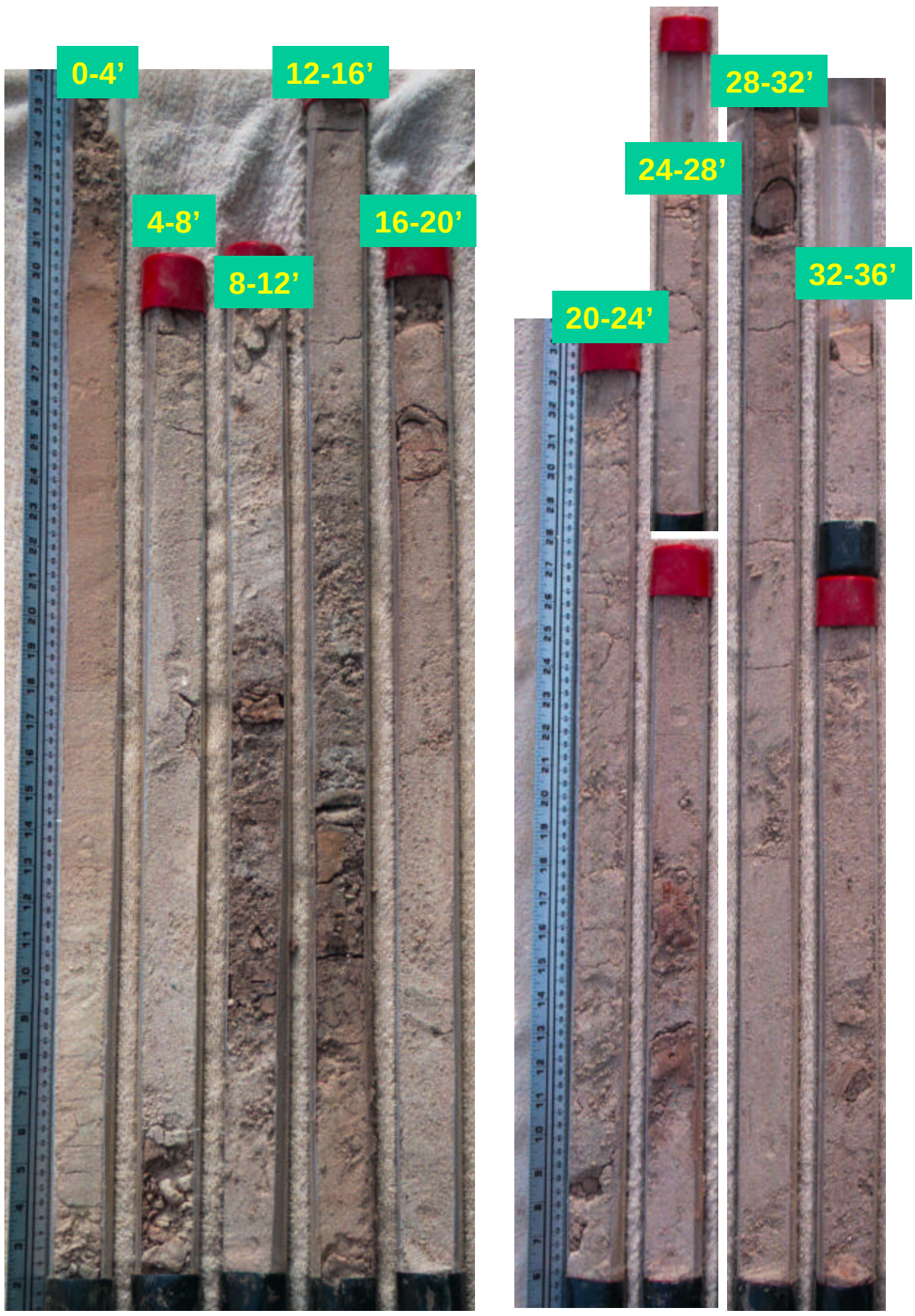

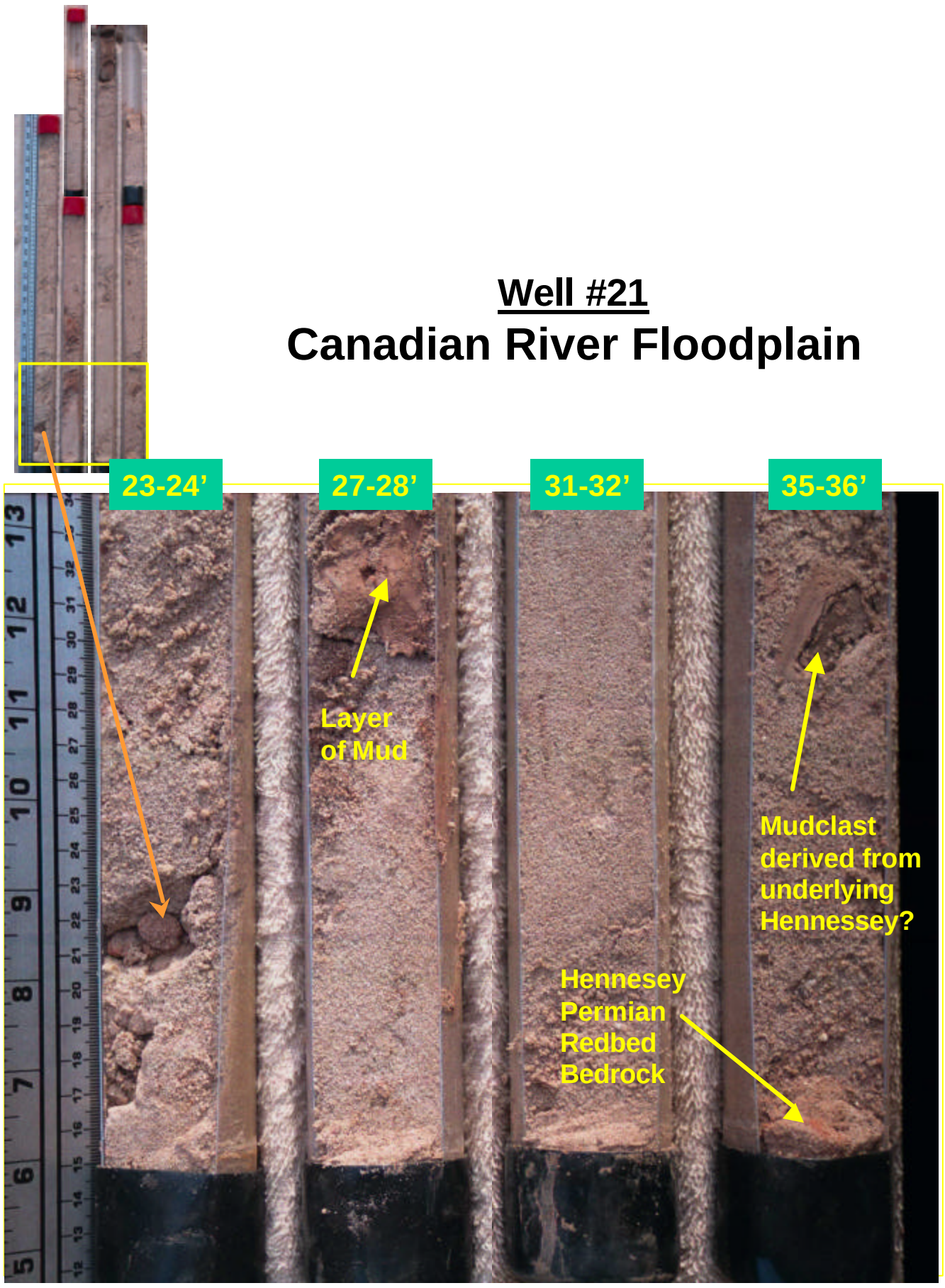
Well #21
Canadian River Floodplain
23-24’
27-28’
31-32’
35-36’
Layer
of Mud
Mudclast
derived from
underlying
Hennessey?
Hennesey
Permian
Redbed
Bedrock

<u>Well #23</u> – Canadian River Floodplain

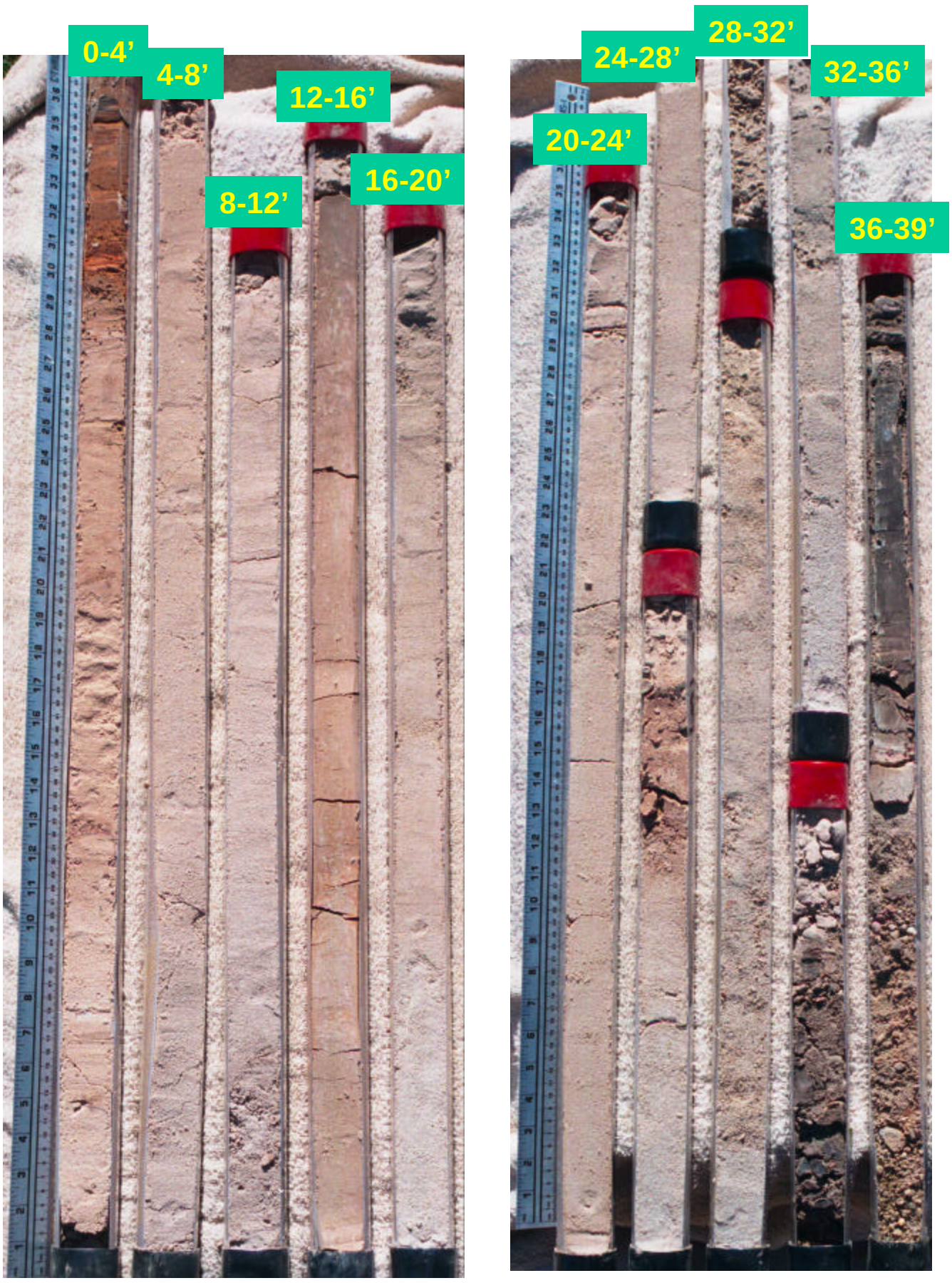

<u>Well #23</u> – Canadian River Floodplain

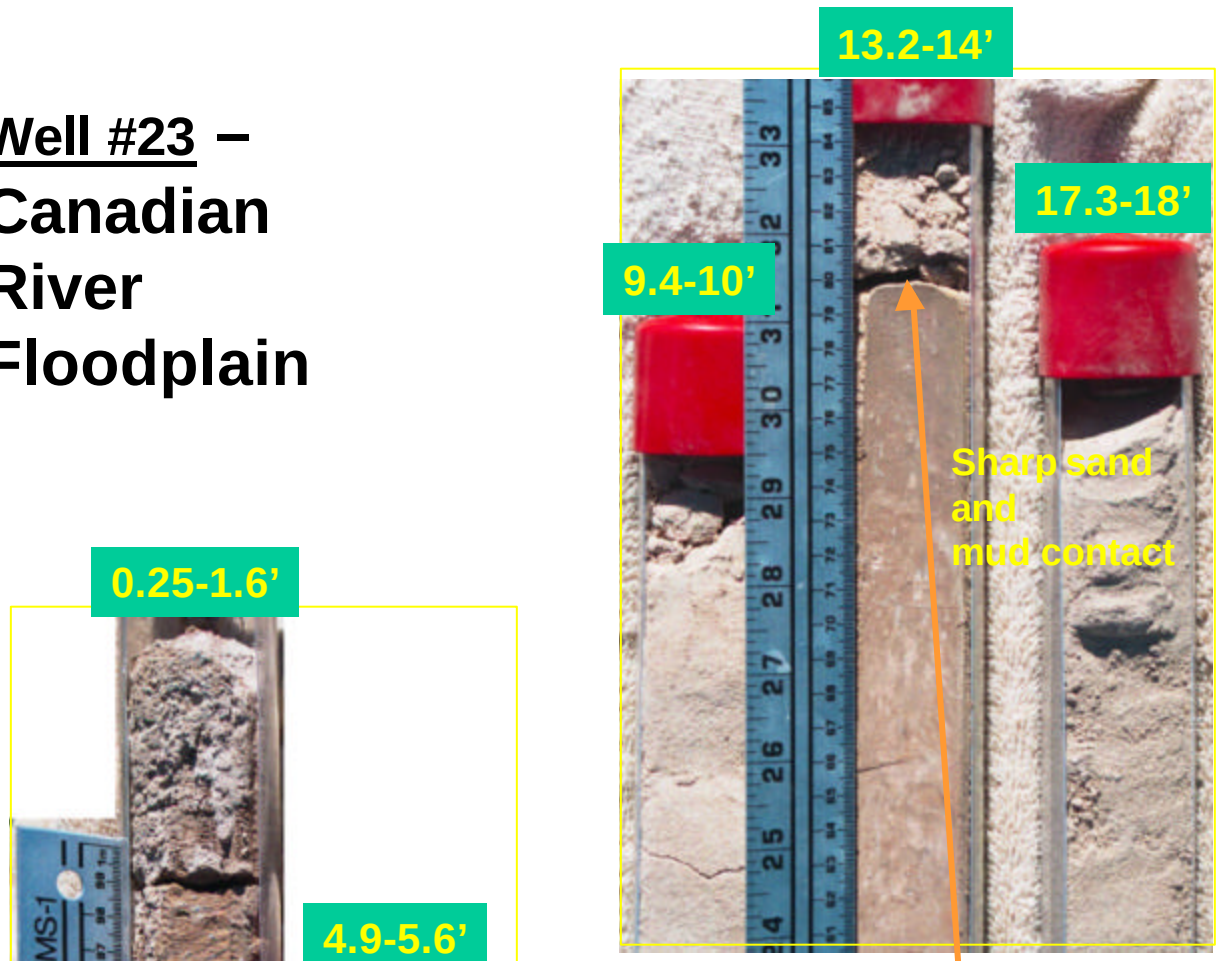

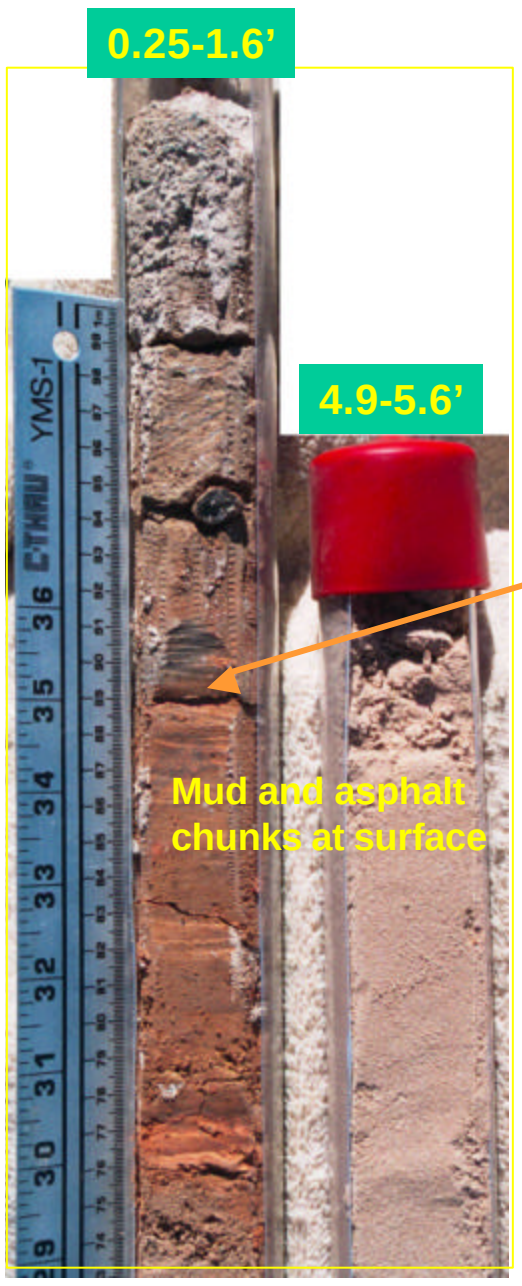

<u>Well #23</u> – Canadian River Floodplain

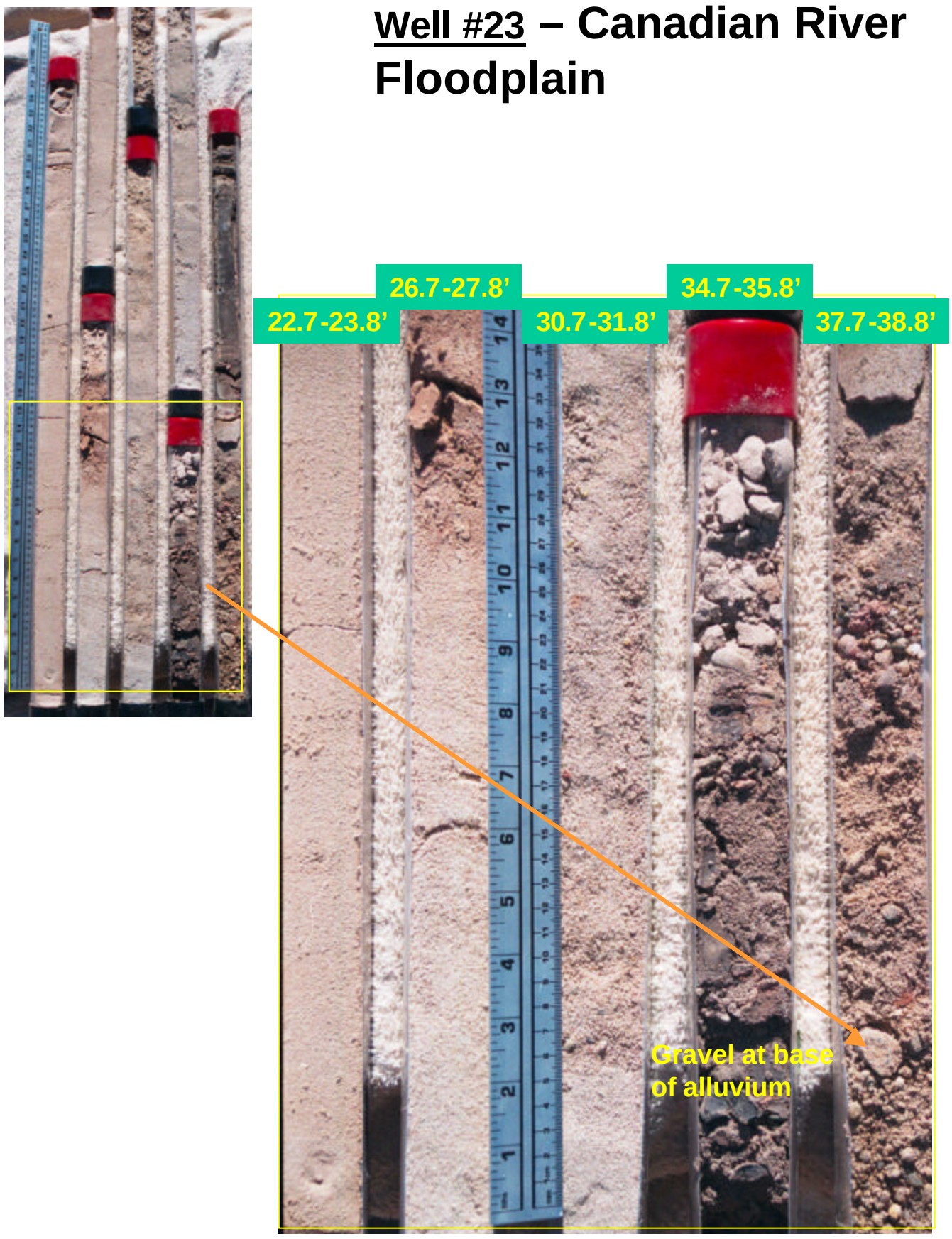

<u>Well #23</u> – Canadian River Floodplain

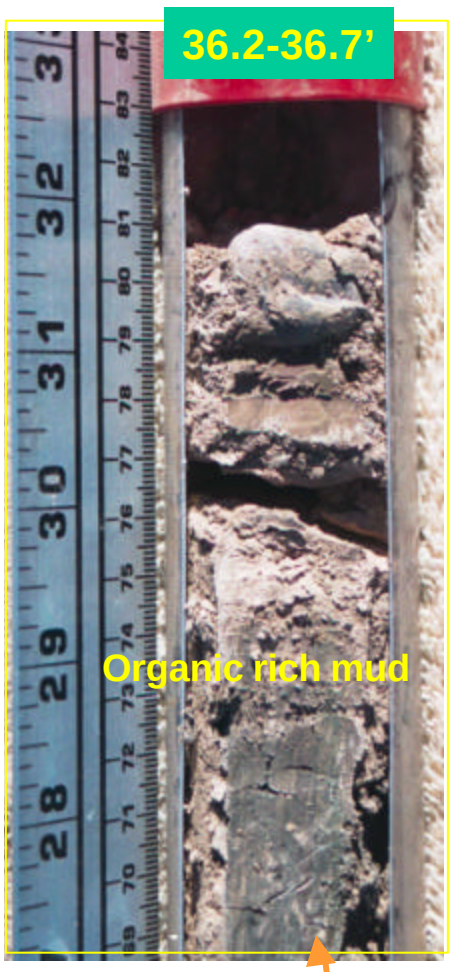

<u>Well #28</u> – Canadian River Floodplain

<u>Well #28</u> – Canadian River Floodplain

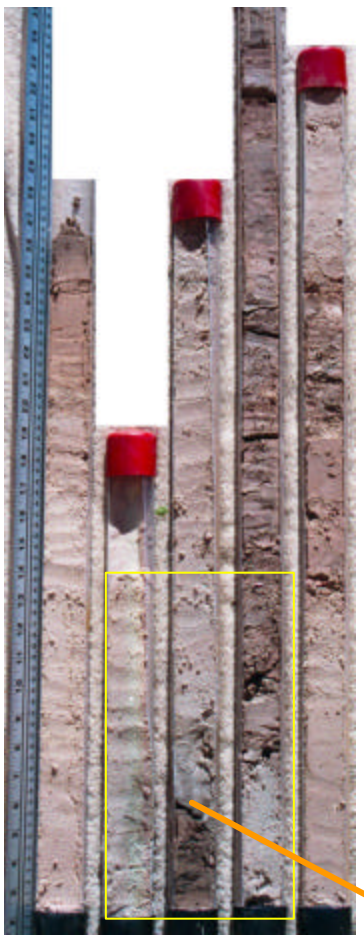

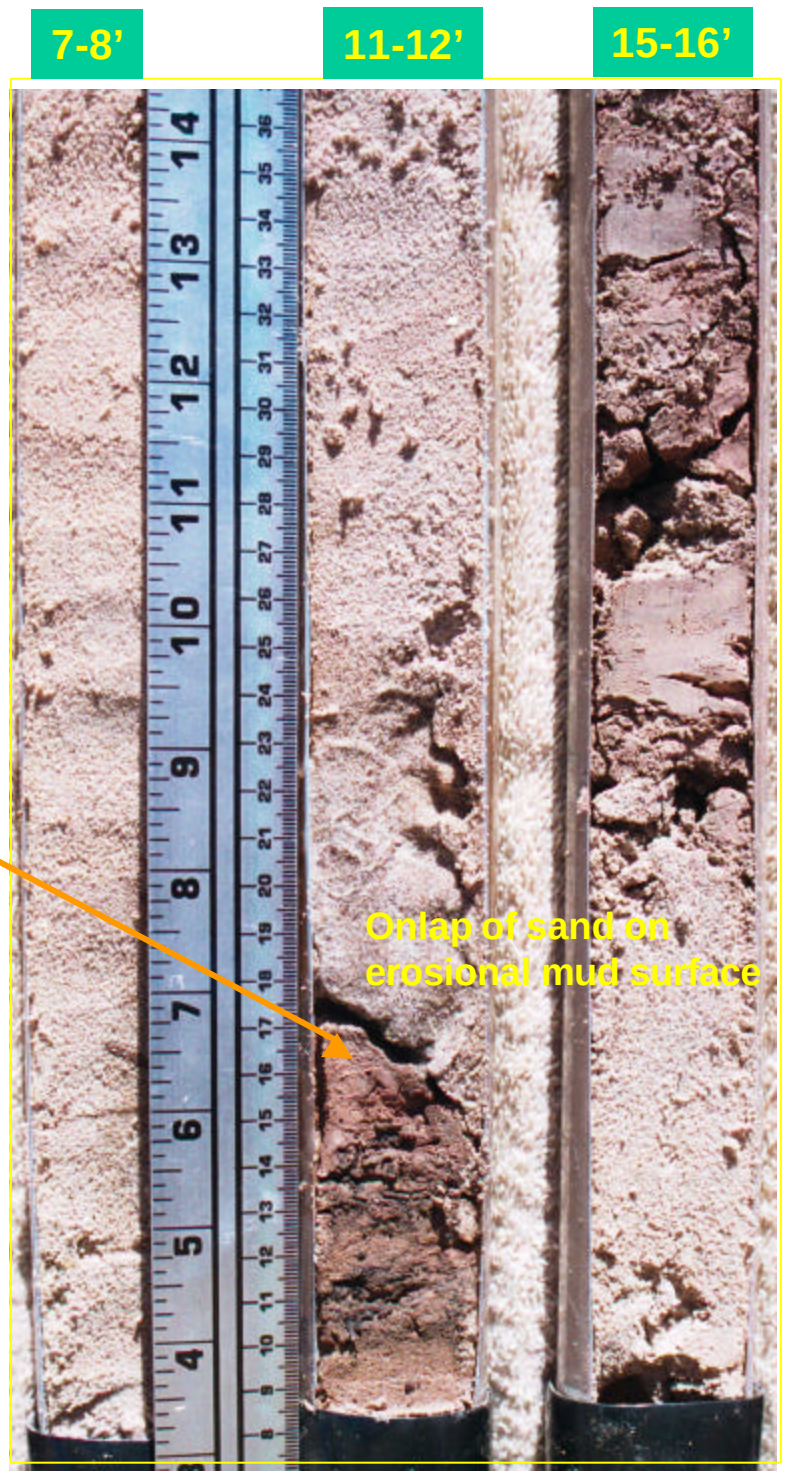

Well #28 – Canadian River Floodplain

28.5-29.8’

32.5-33.8’

Organic rich mud

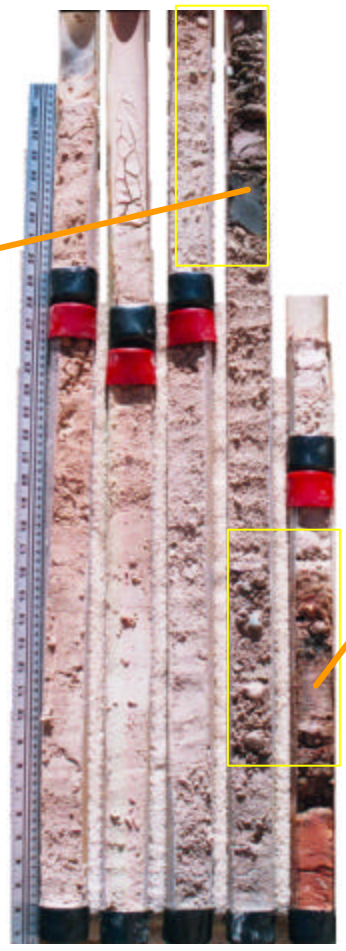

34.5-35.6’

37.5-38.6’

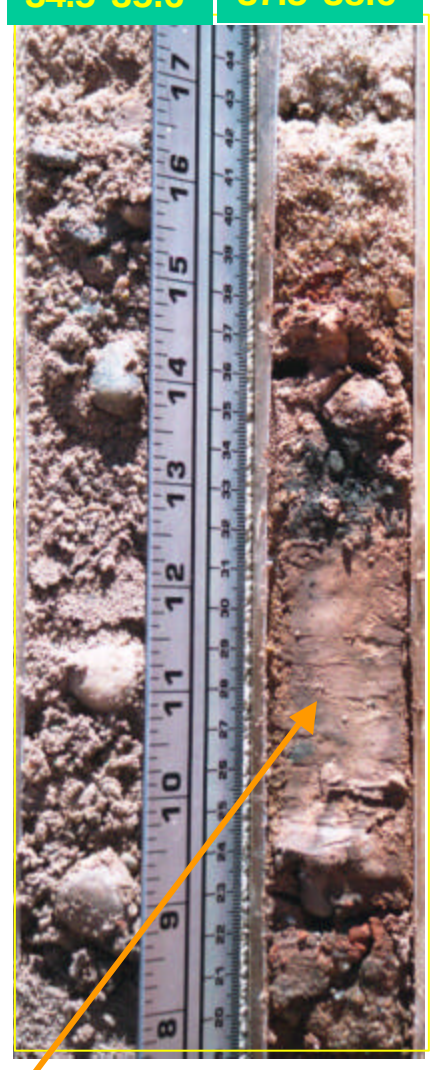

<u>Well #28</u> –
Canadian River Floodplain

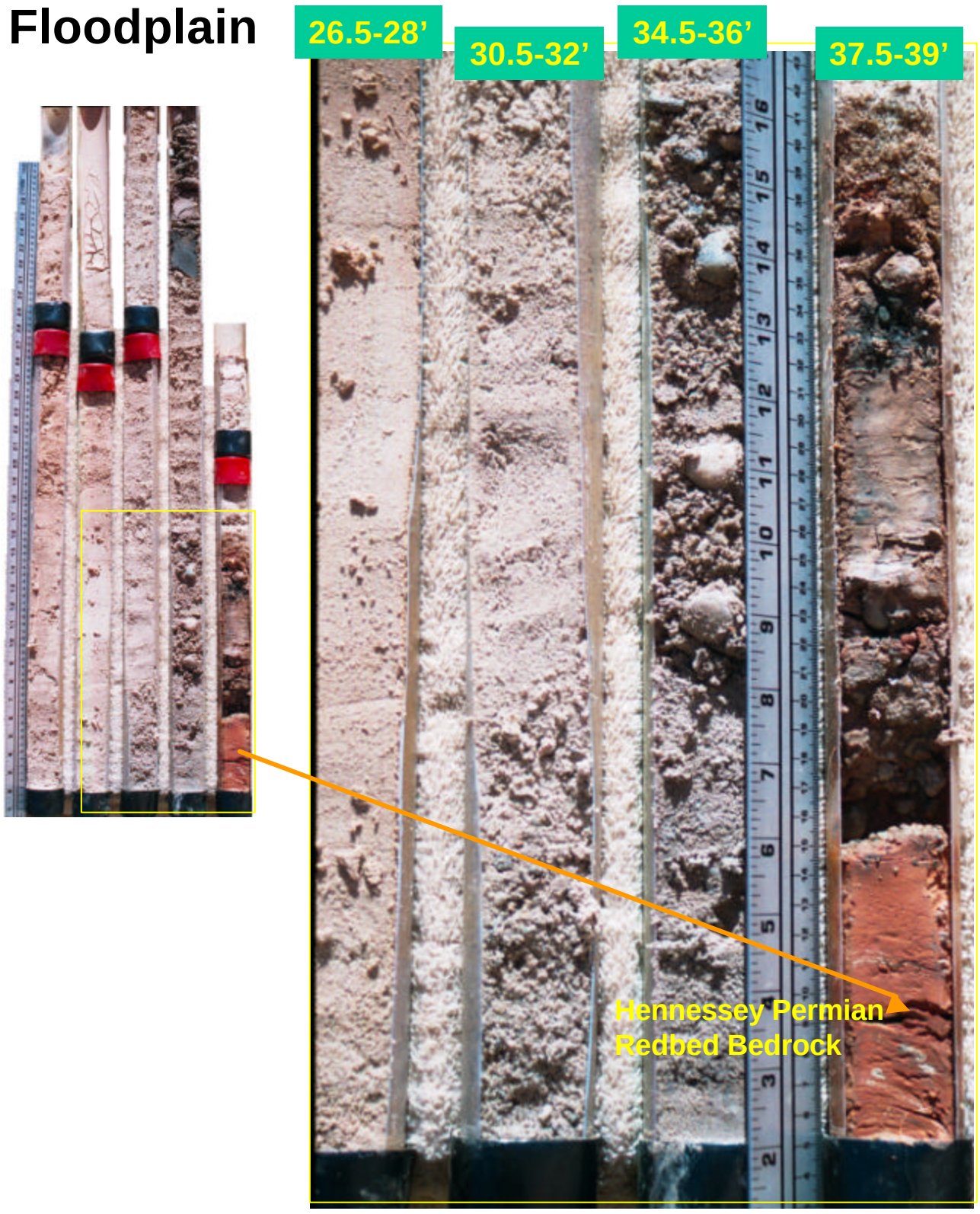

<u>Well #31</u> – Canadian River Floodplain

<u>Well #31</u> – Canadian River Floodplain

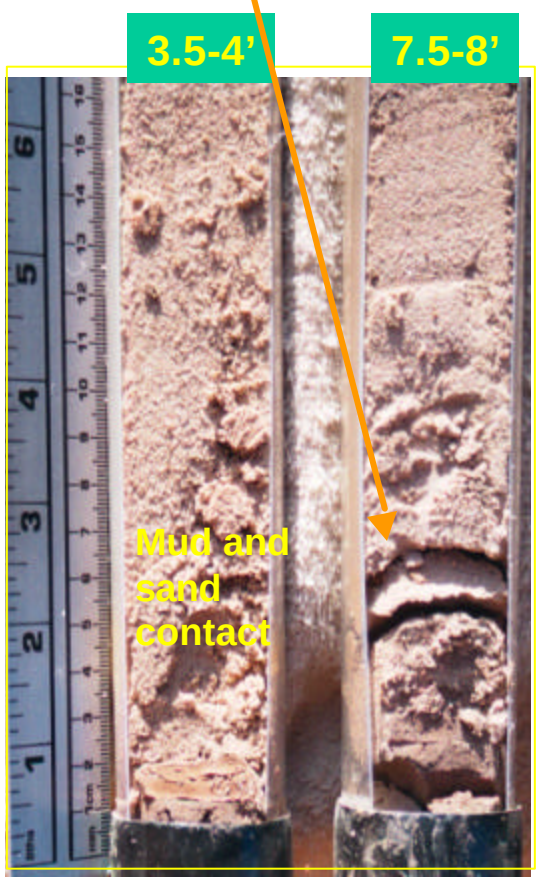

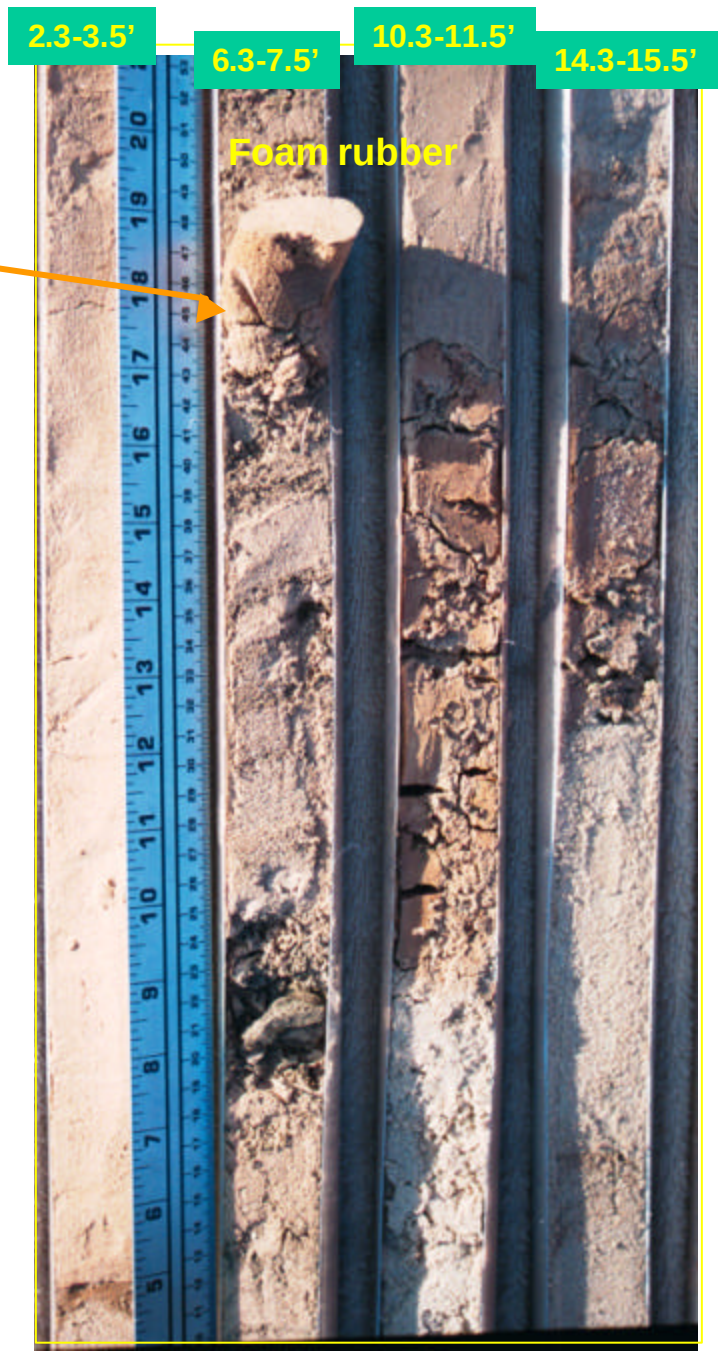

<u>Well #31</u> – Canadian River Floodplain

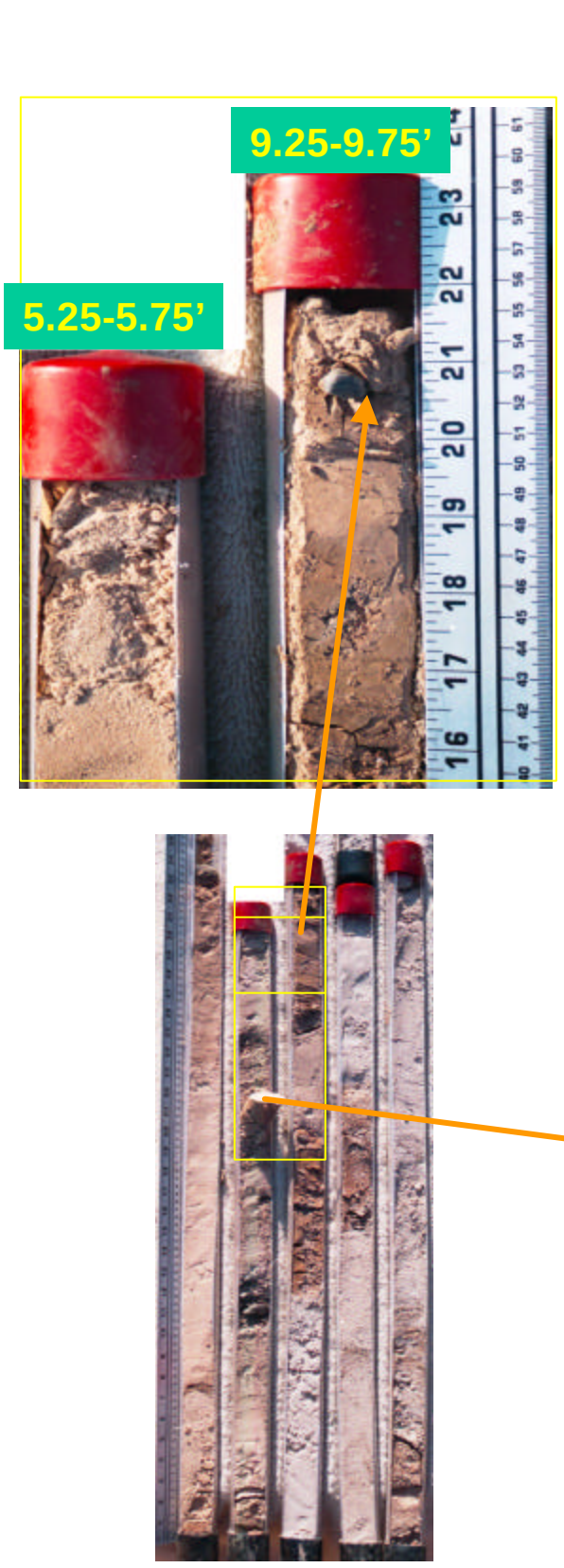

<u>Well #31</u> – Canadian River Floodplain

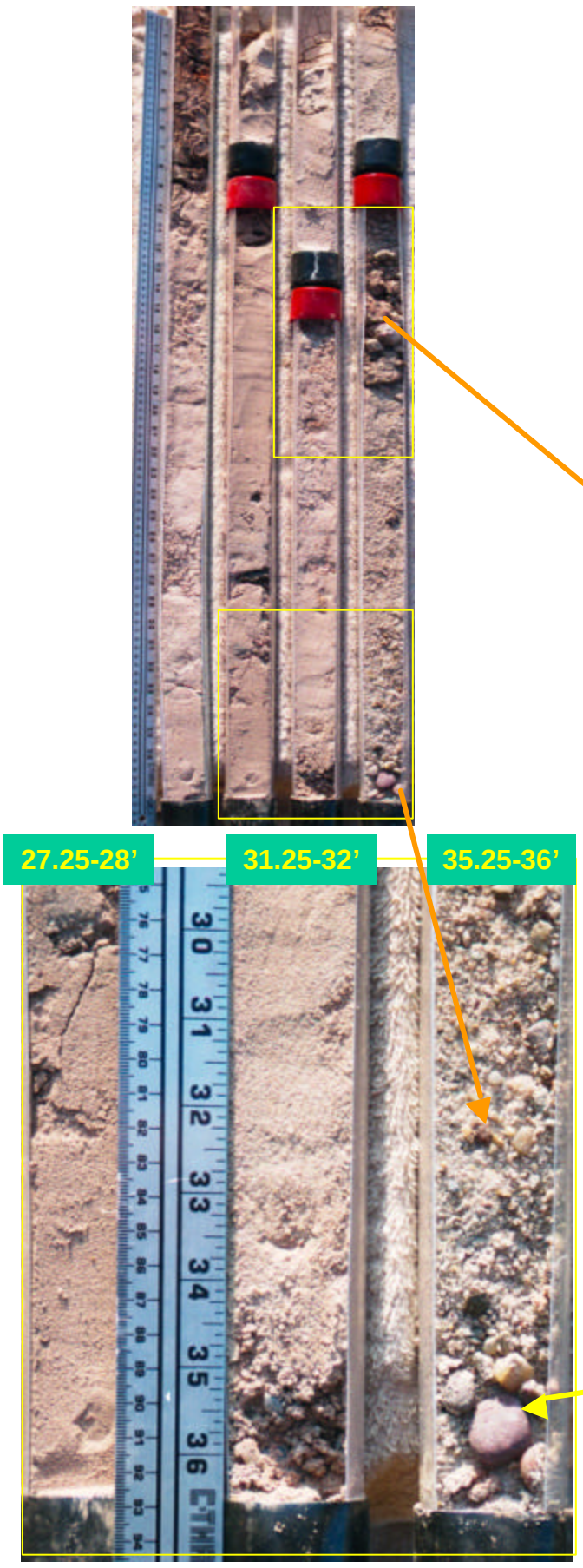

<u>Well #42</u> – Canadian River Floodplain

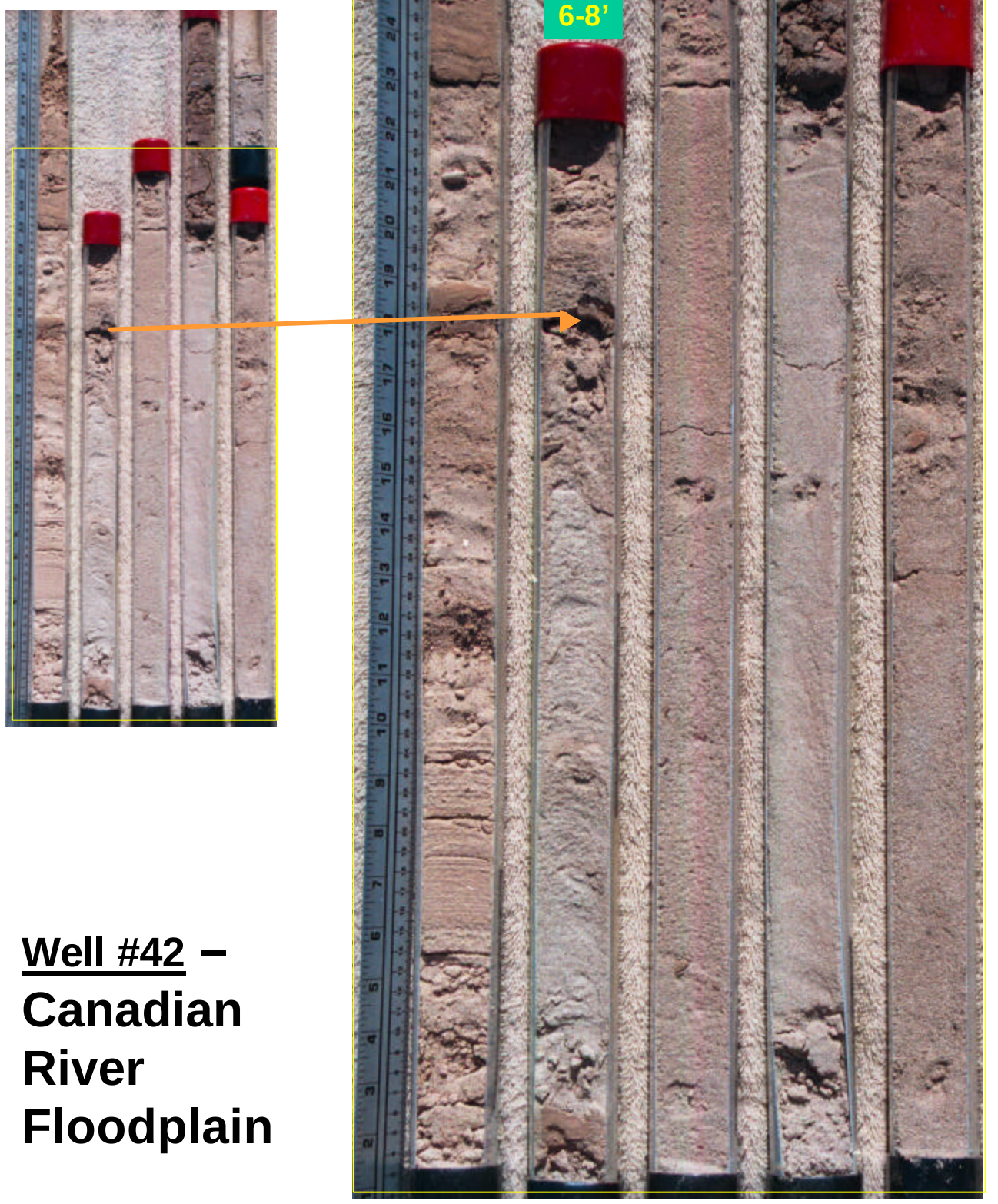

<u>Well #42</u> – Canadian River Floodplain

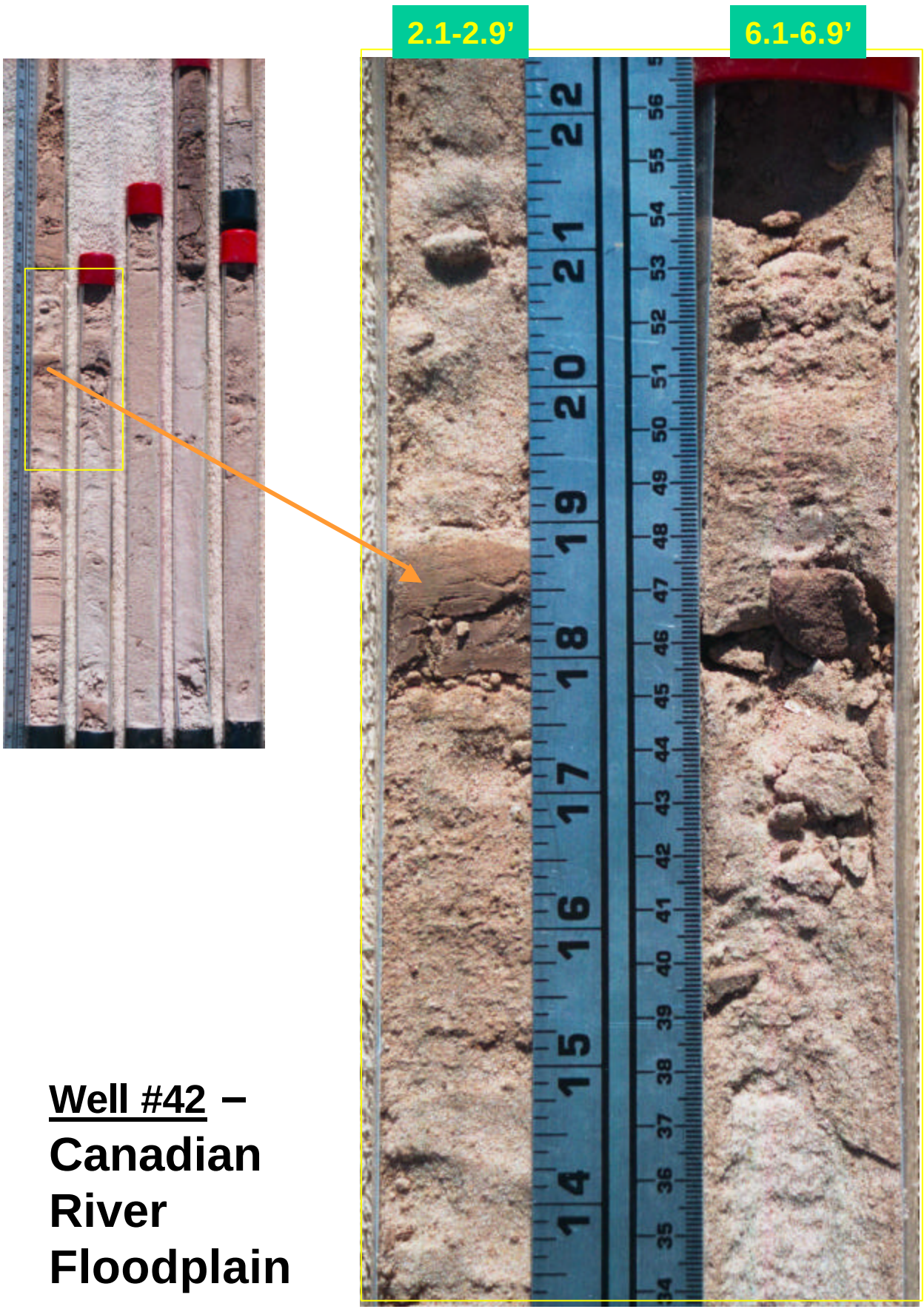

<u>Well #42</u> – Canadian River Floodplain

<u>Well #42</u> – Canadian River Floodplain

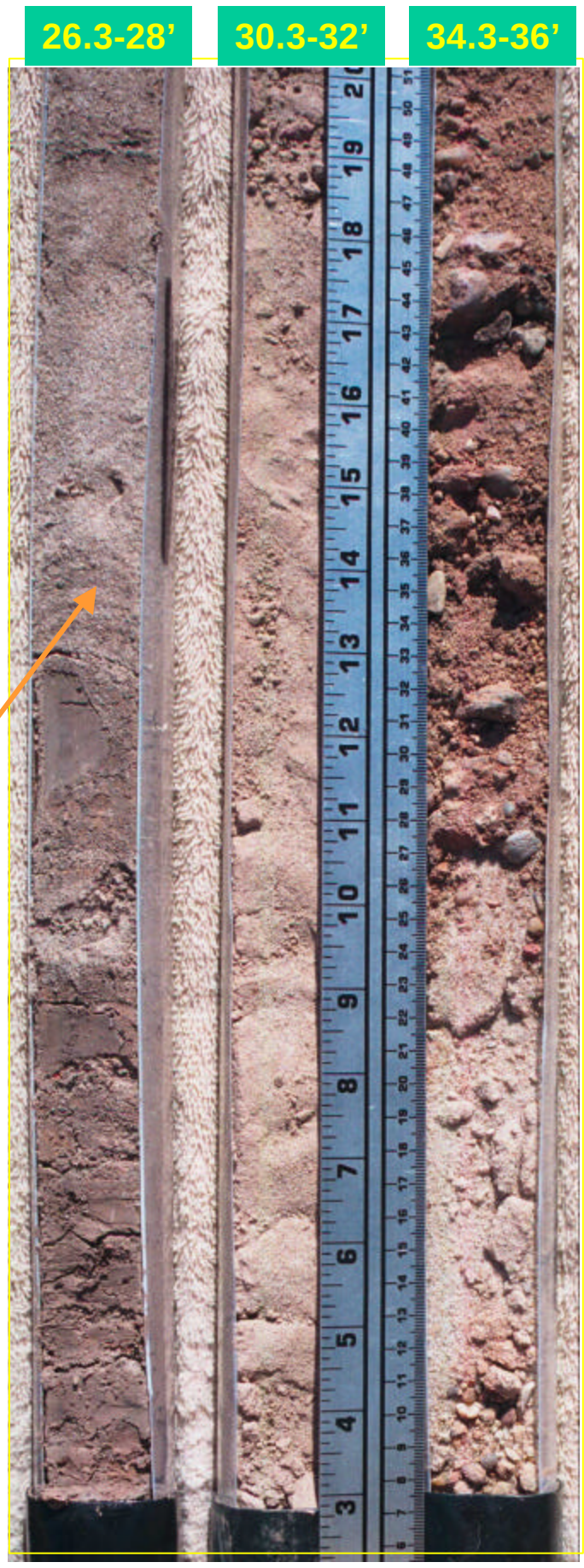

EXTRAS

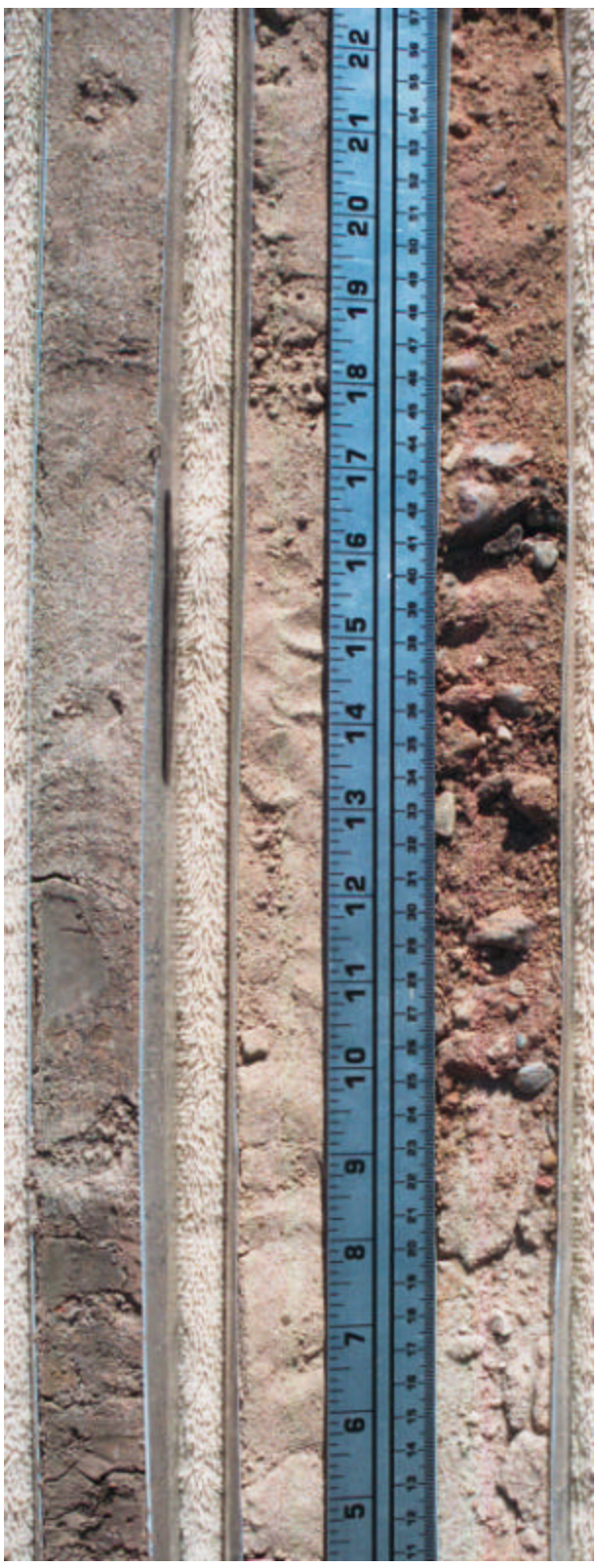

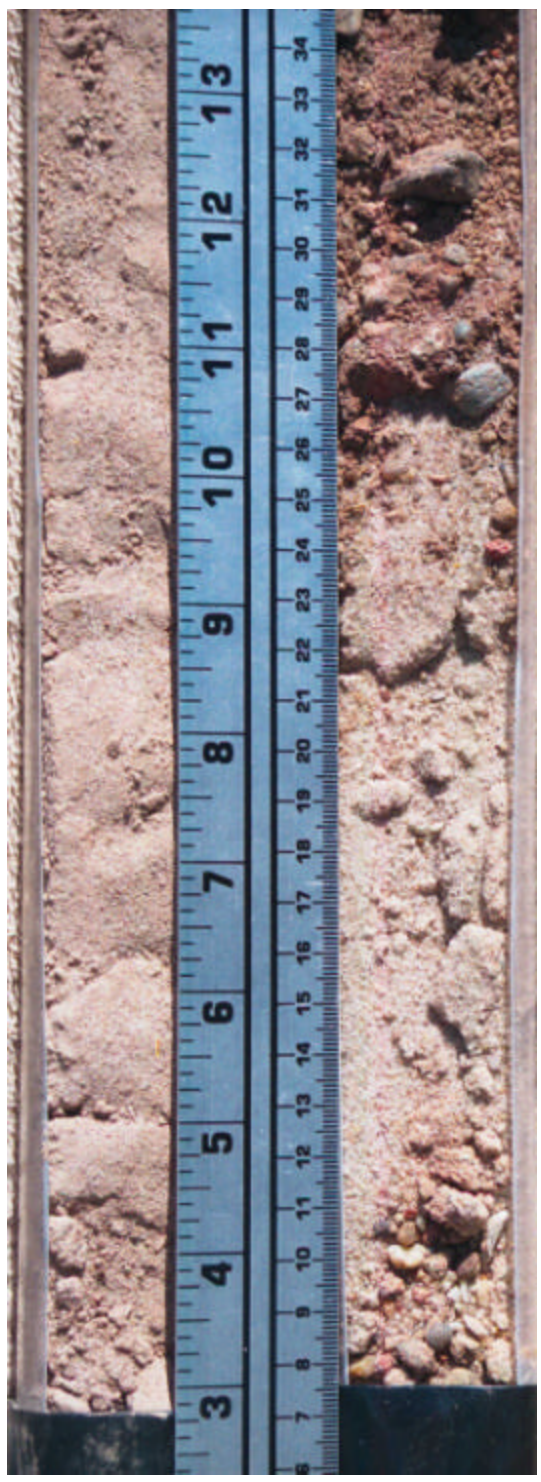

<u>Well #44</u> – Canadian River Floodplain

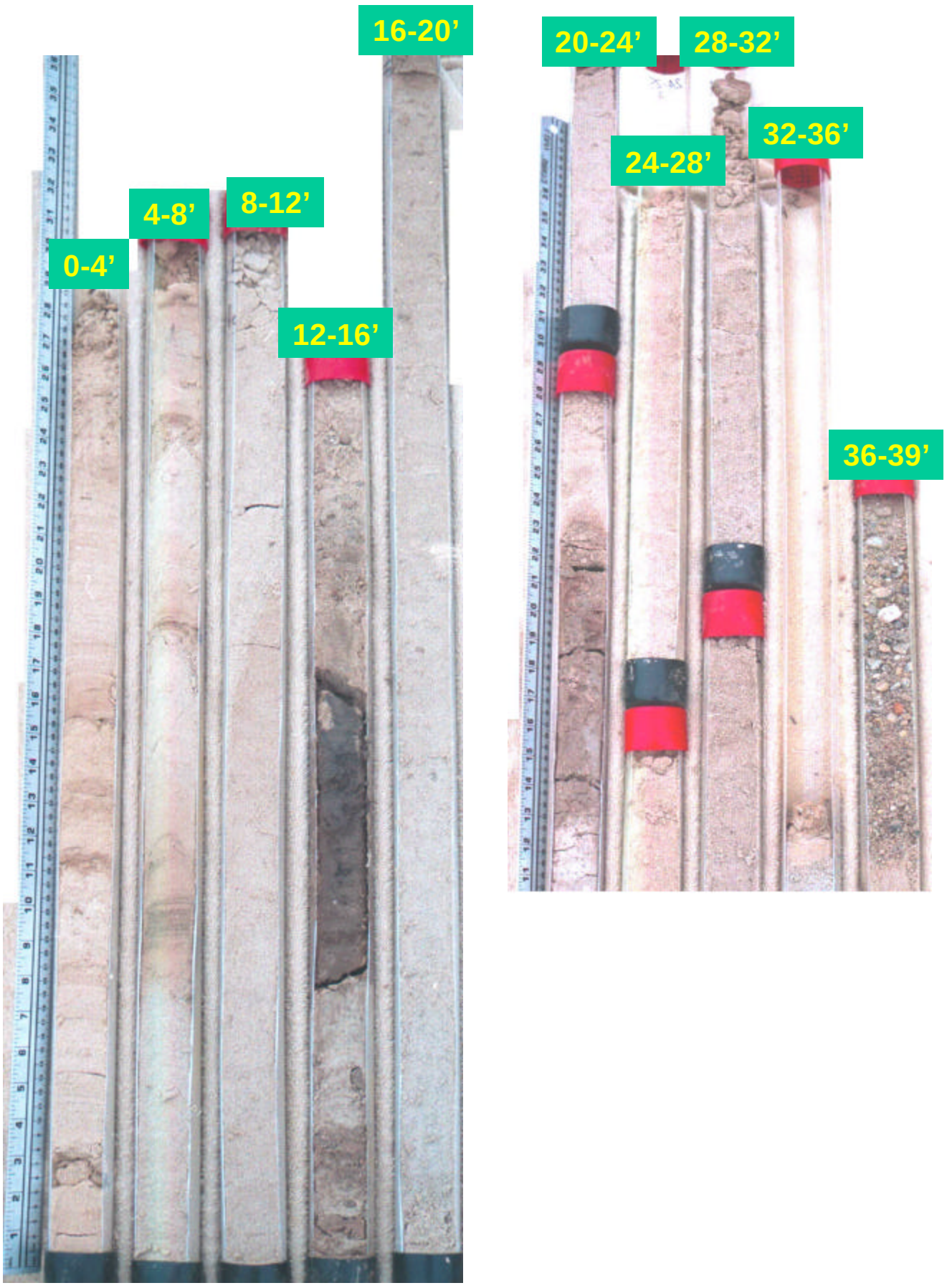

<u>Well #44</u> – Canadian River Floodplain

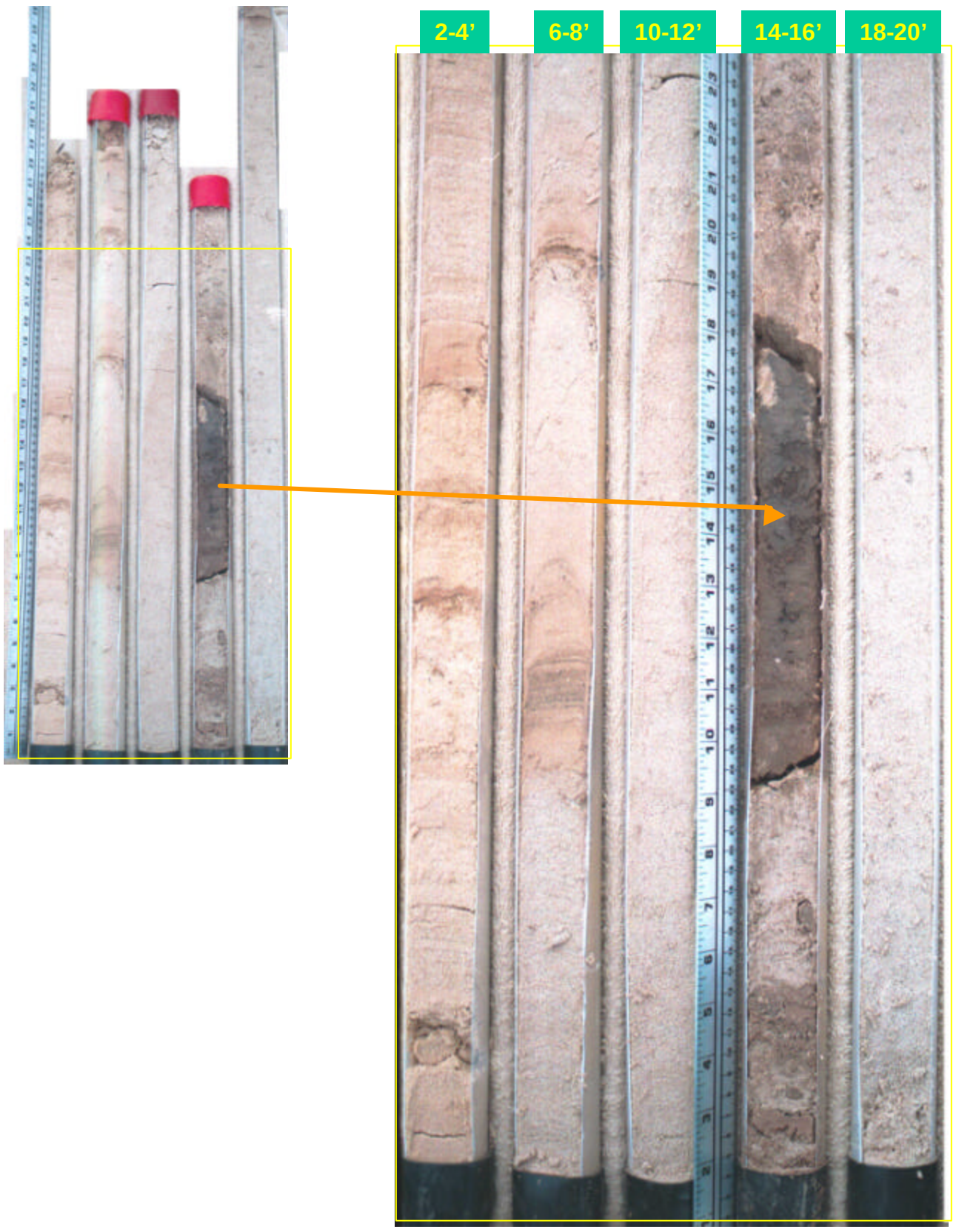

22-24’ 26-28’ 30-32’ 34-36’ 37-39’

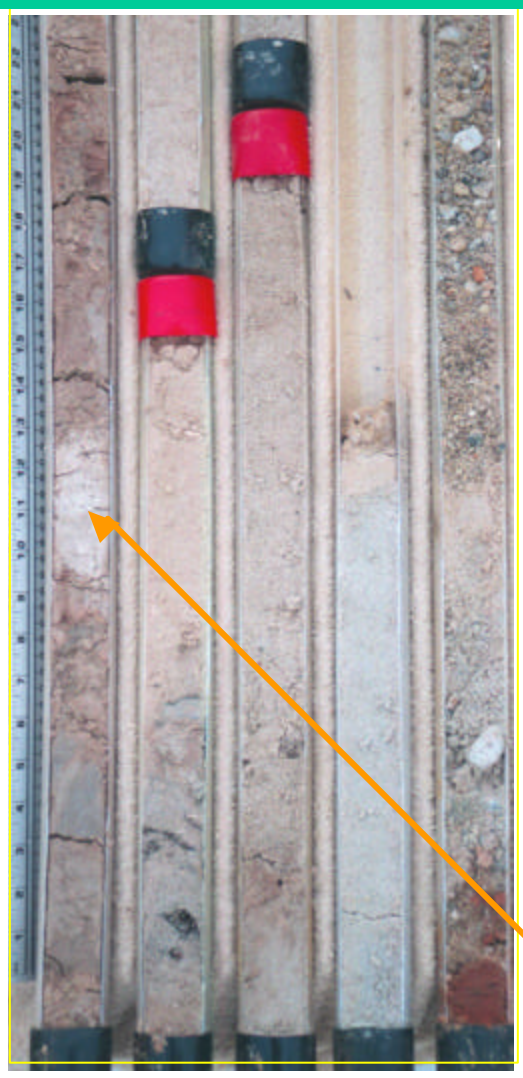

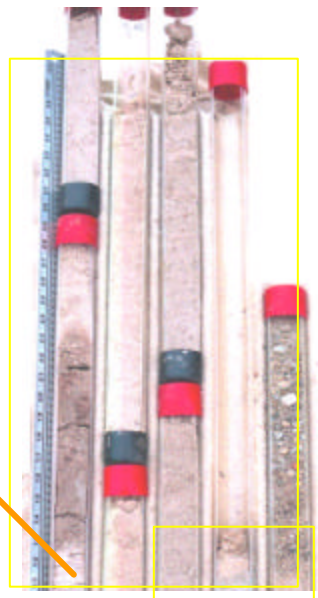

30.5-32’ 34.5-36’ 37.5-39’

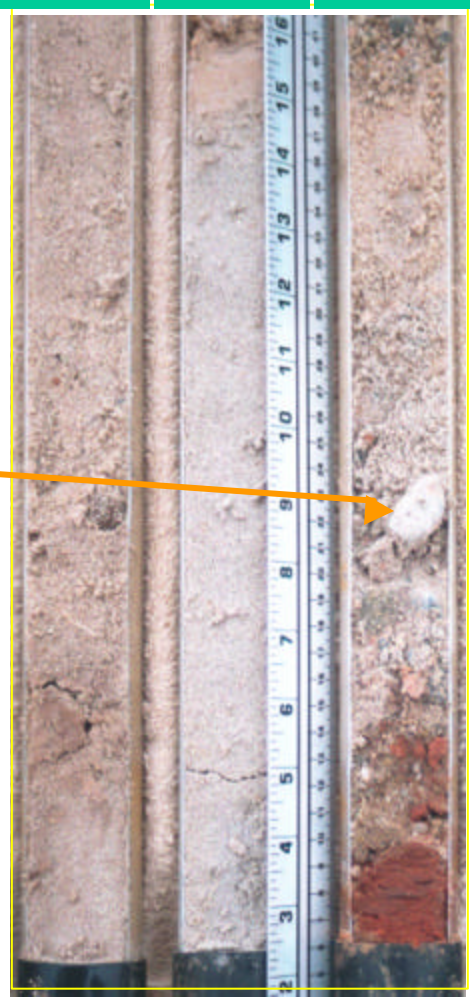

<u>Well #44</u> –
Canadian River Floodplain

<u>Well #46</u> – Canadian River Floodplain

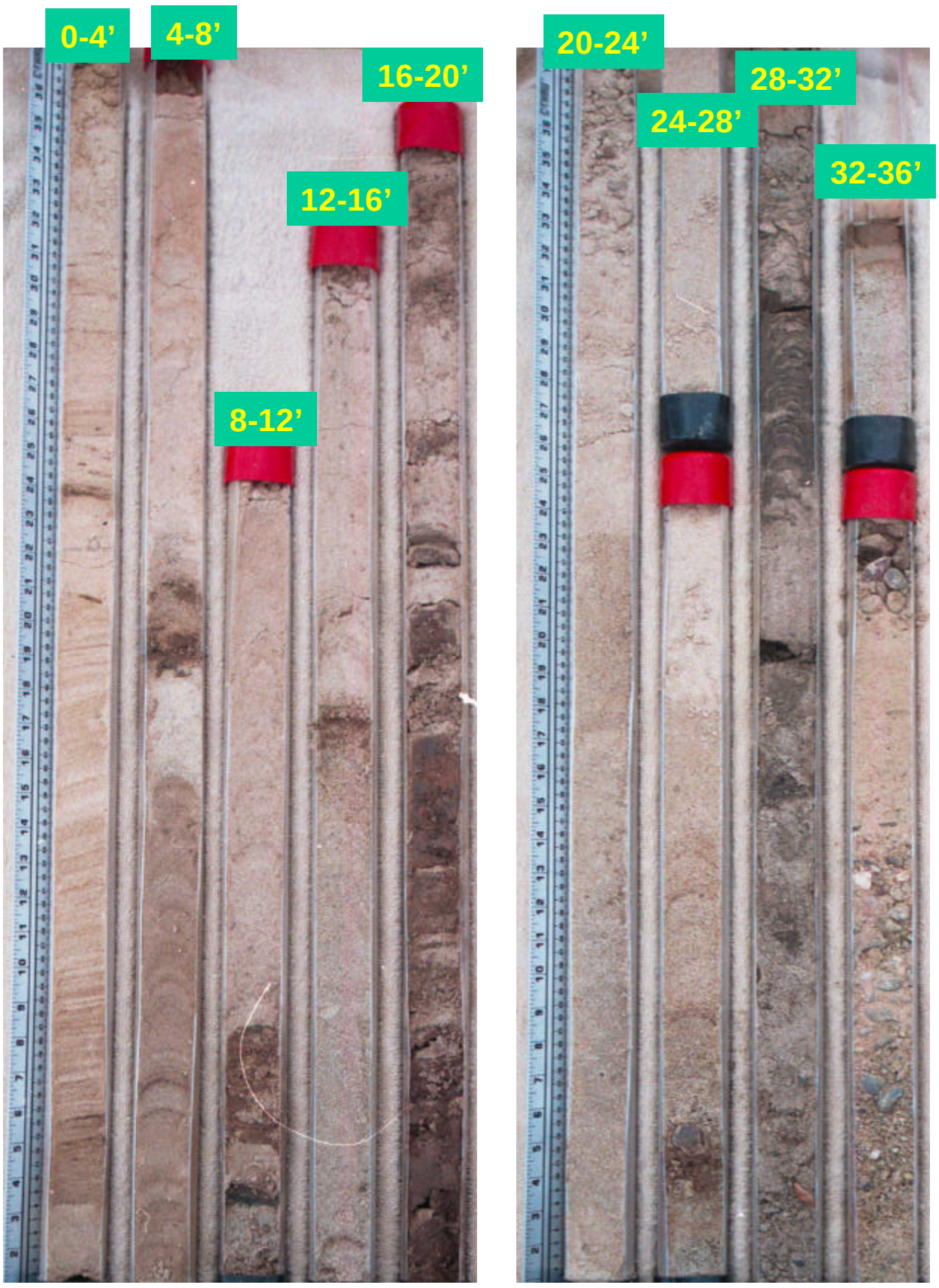

Well #46

Canadian River Floodplain

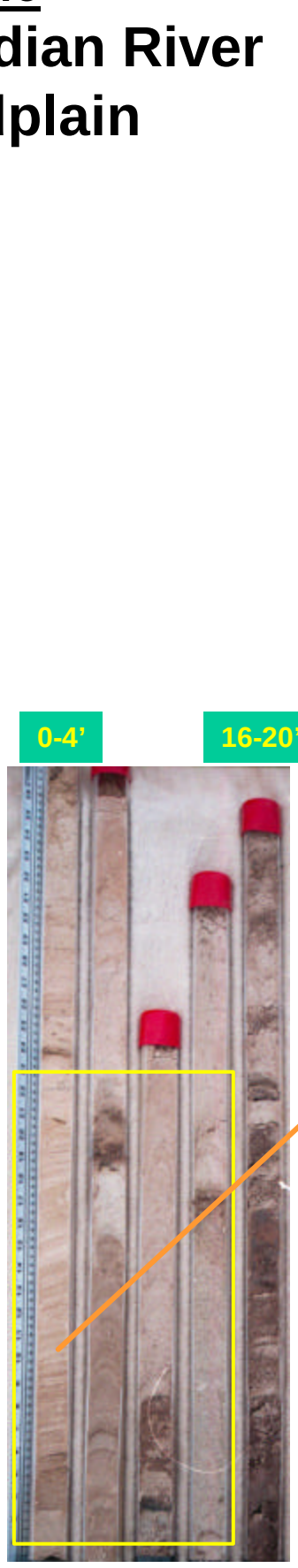

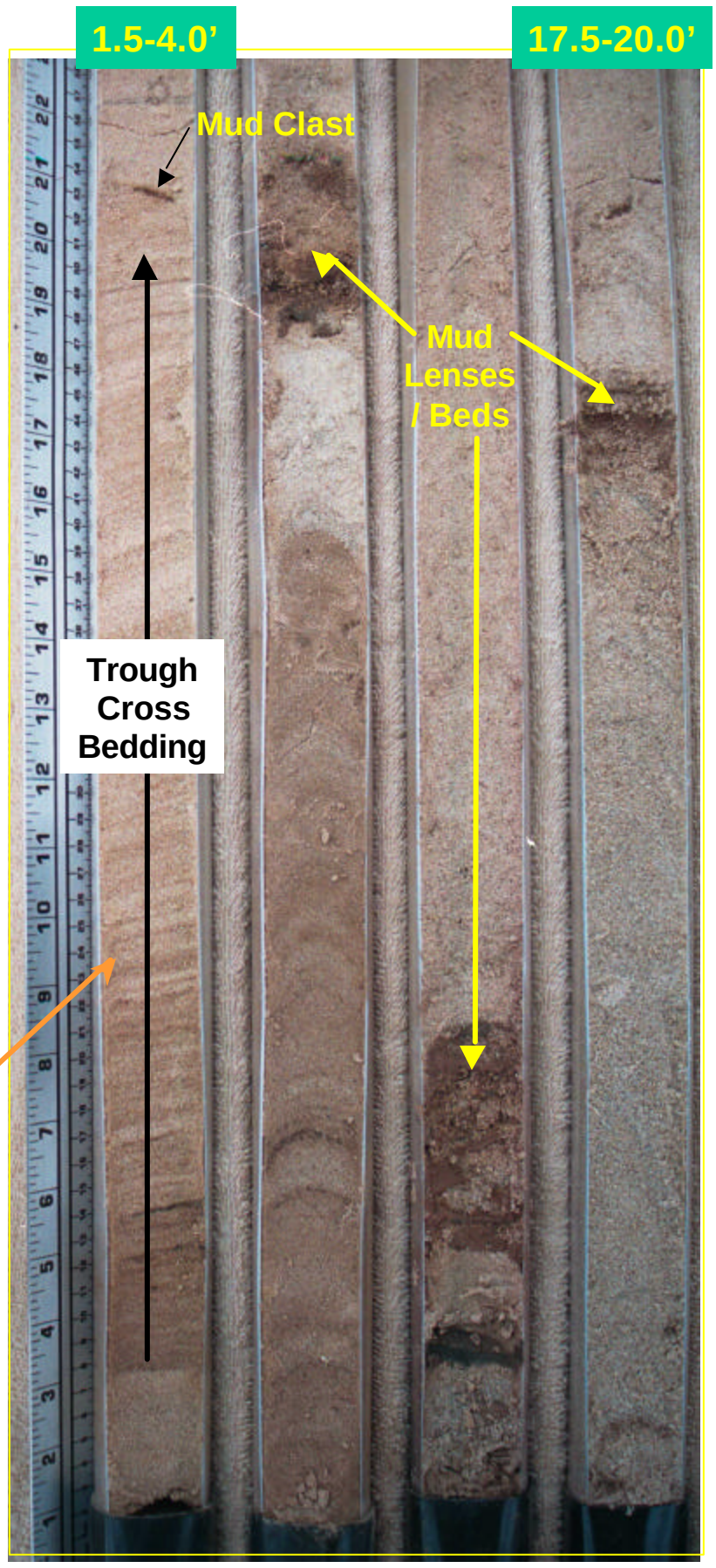

Well #46

Canadian River Floodplain

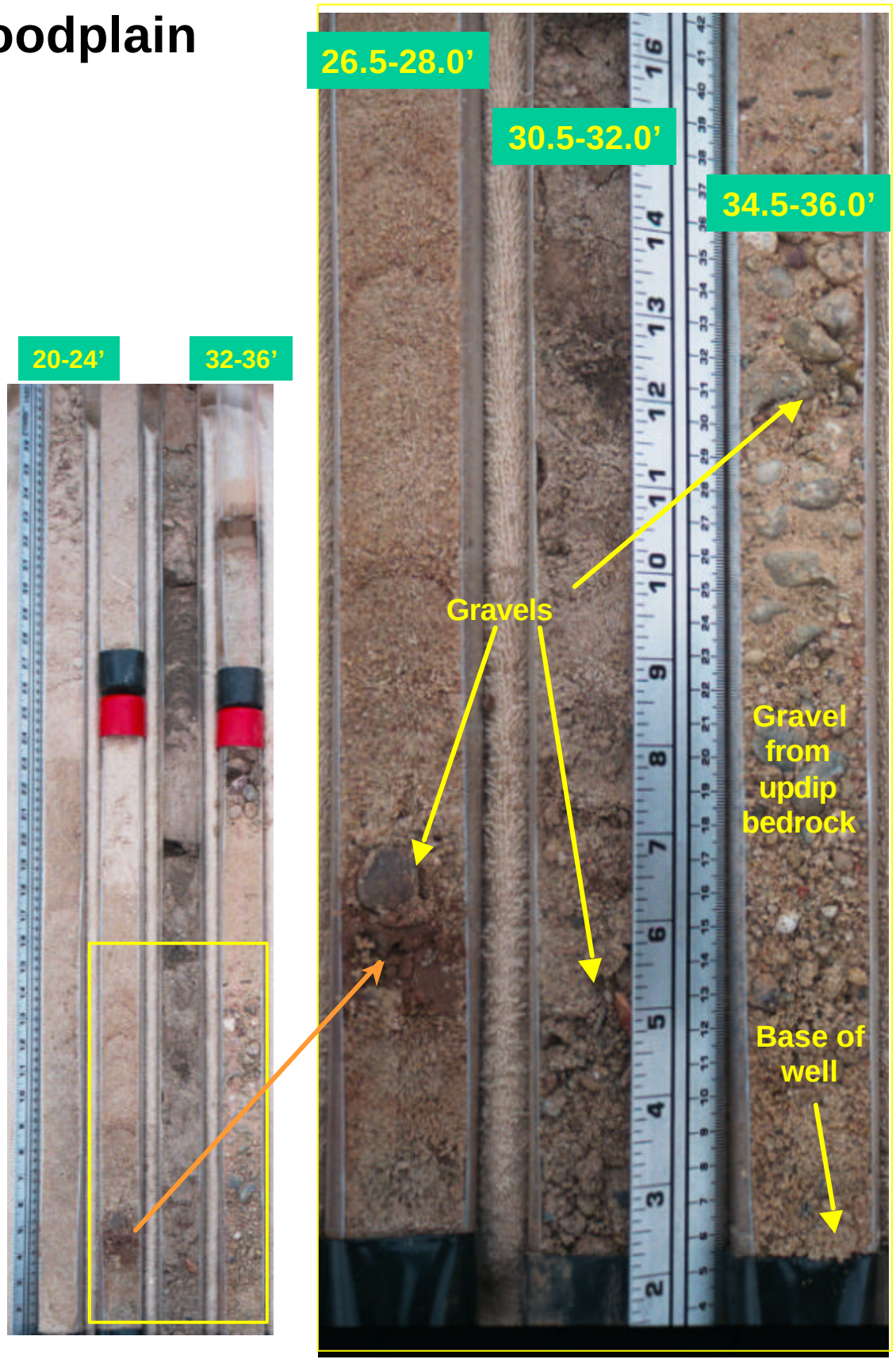

Well #46

Canadian River Floodplain

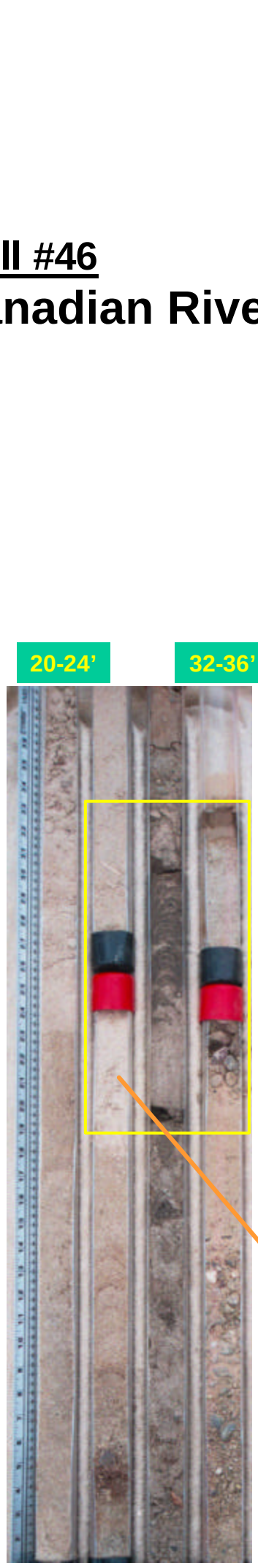

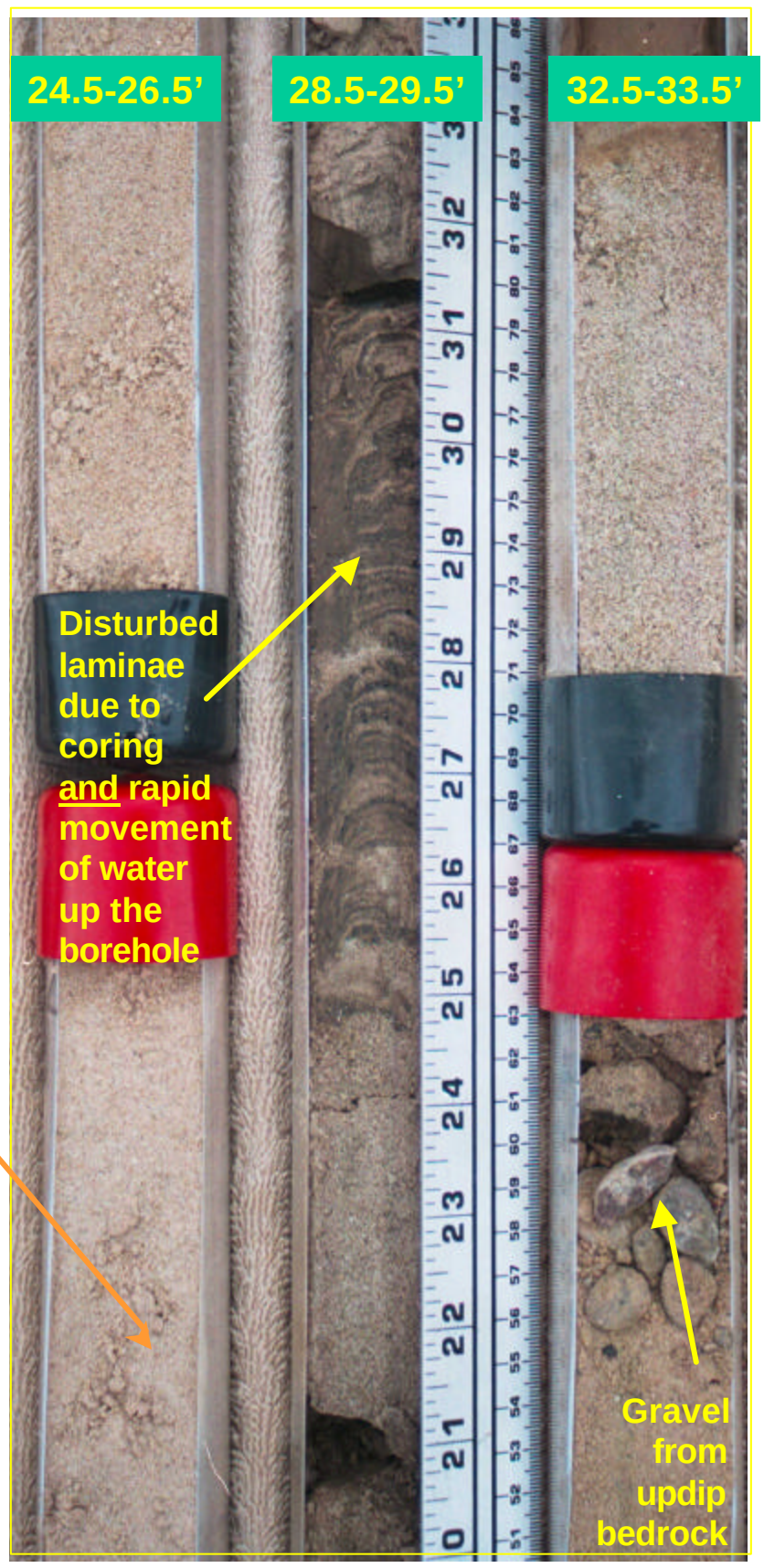

Well #46

Canadian River Floodplain

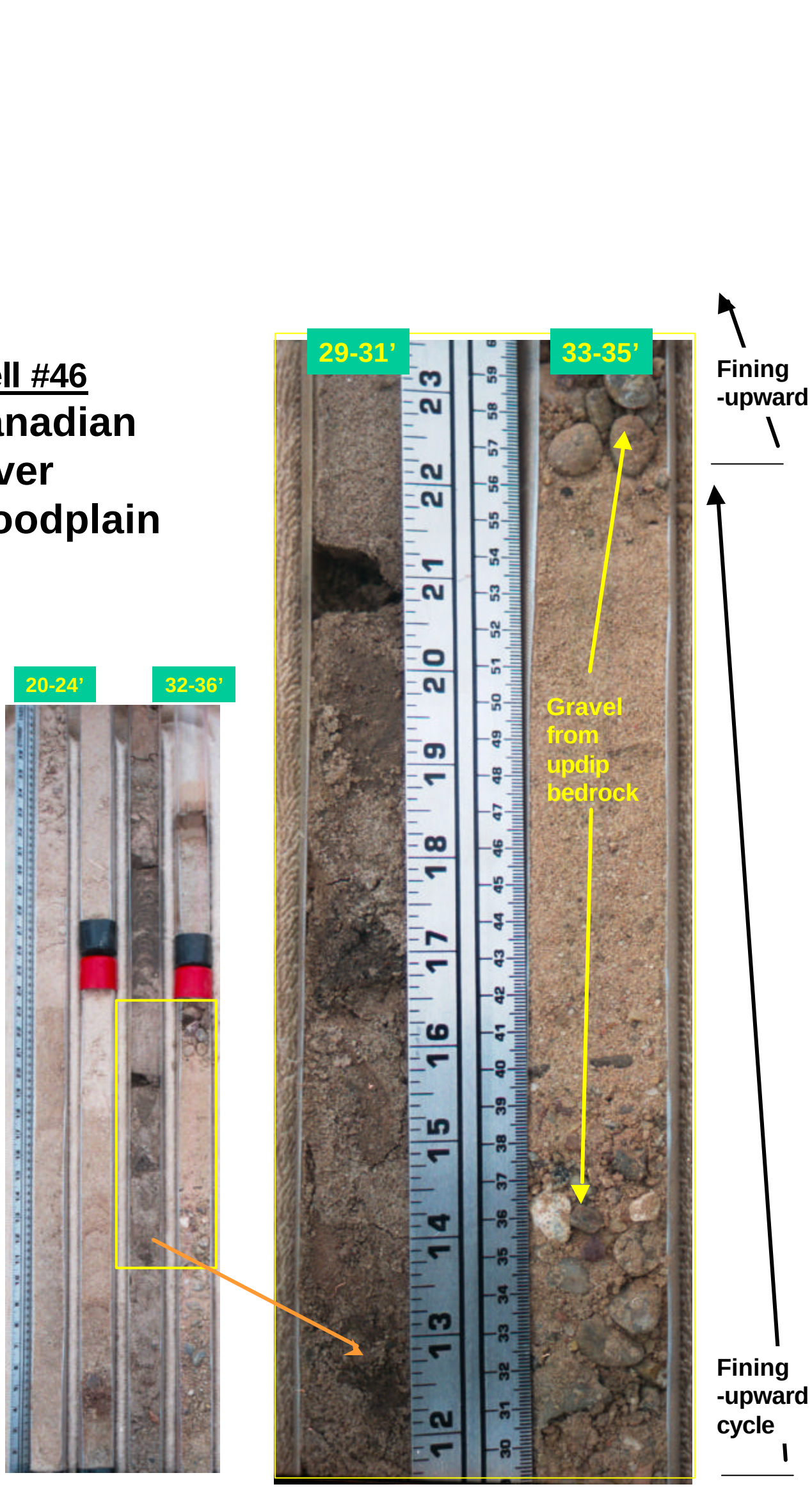

<u>Well #56</u> – Canadian River Floodplain

<u>Well #56</u> – Canadian River Floodplain

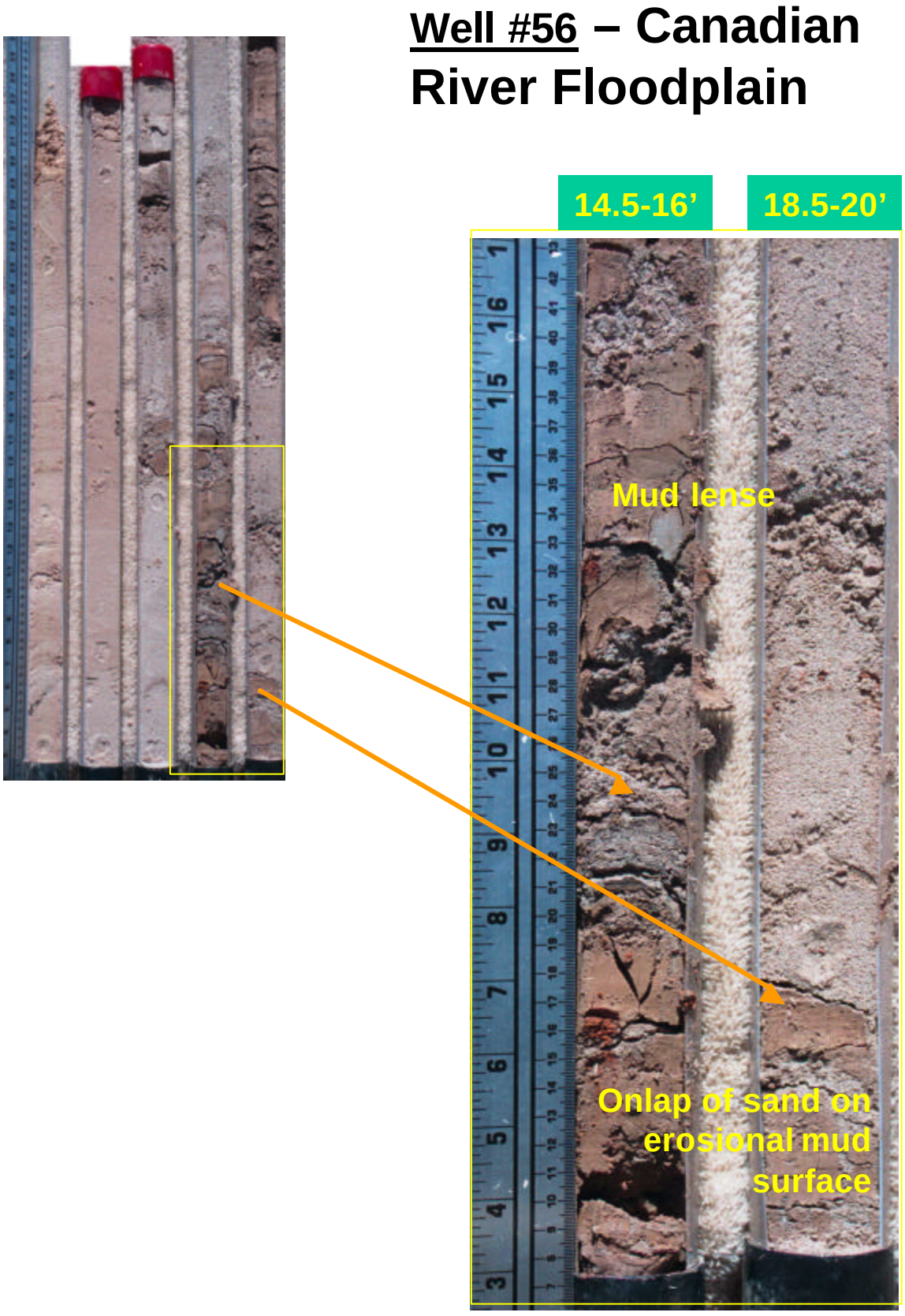

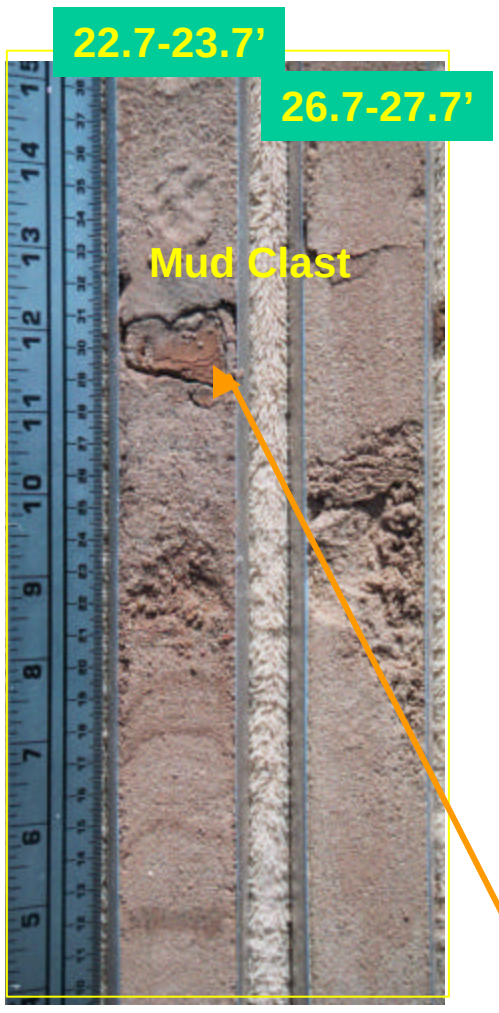

<u>Well #56</u> – Canadian River Floodplain

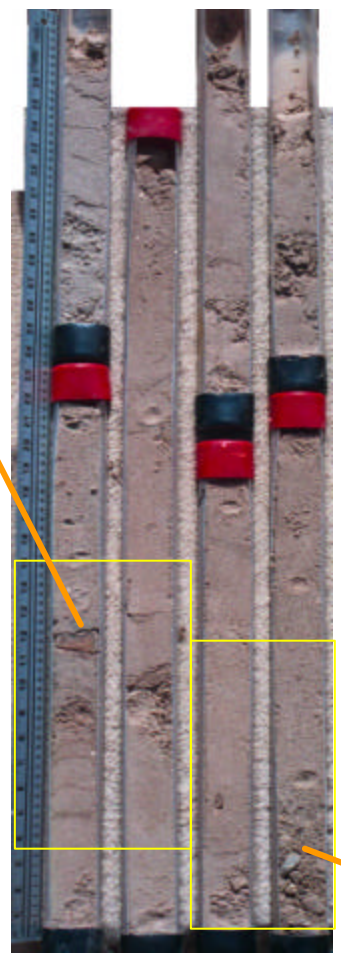

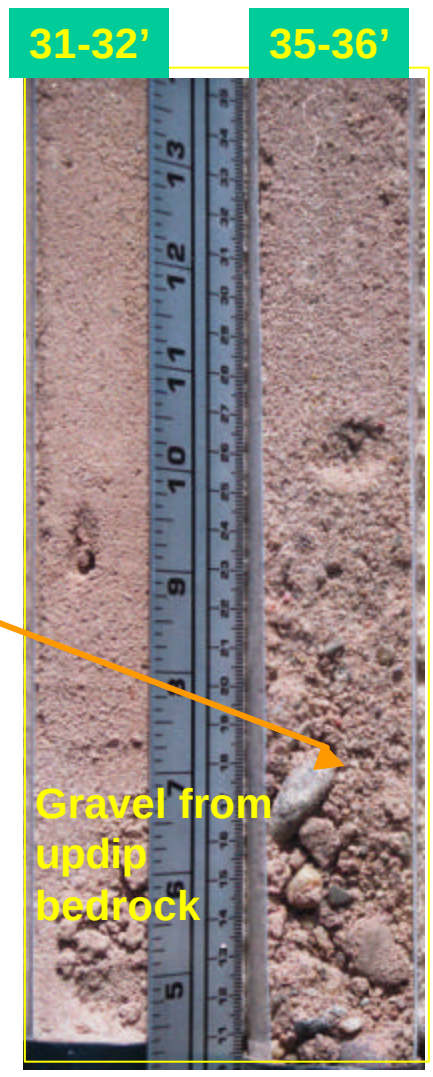

<u>Well #57</u> – Canadian River Floodplain

<u>Well #57</u> – Canadian River Floodplain

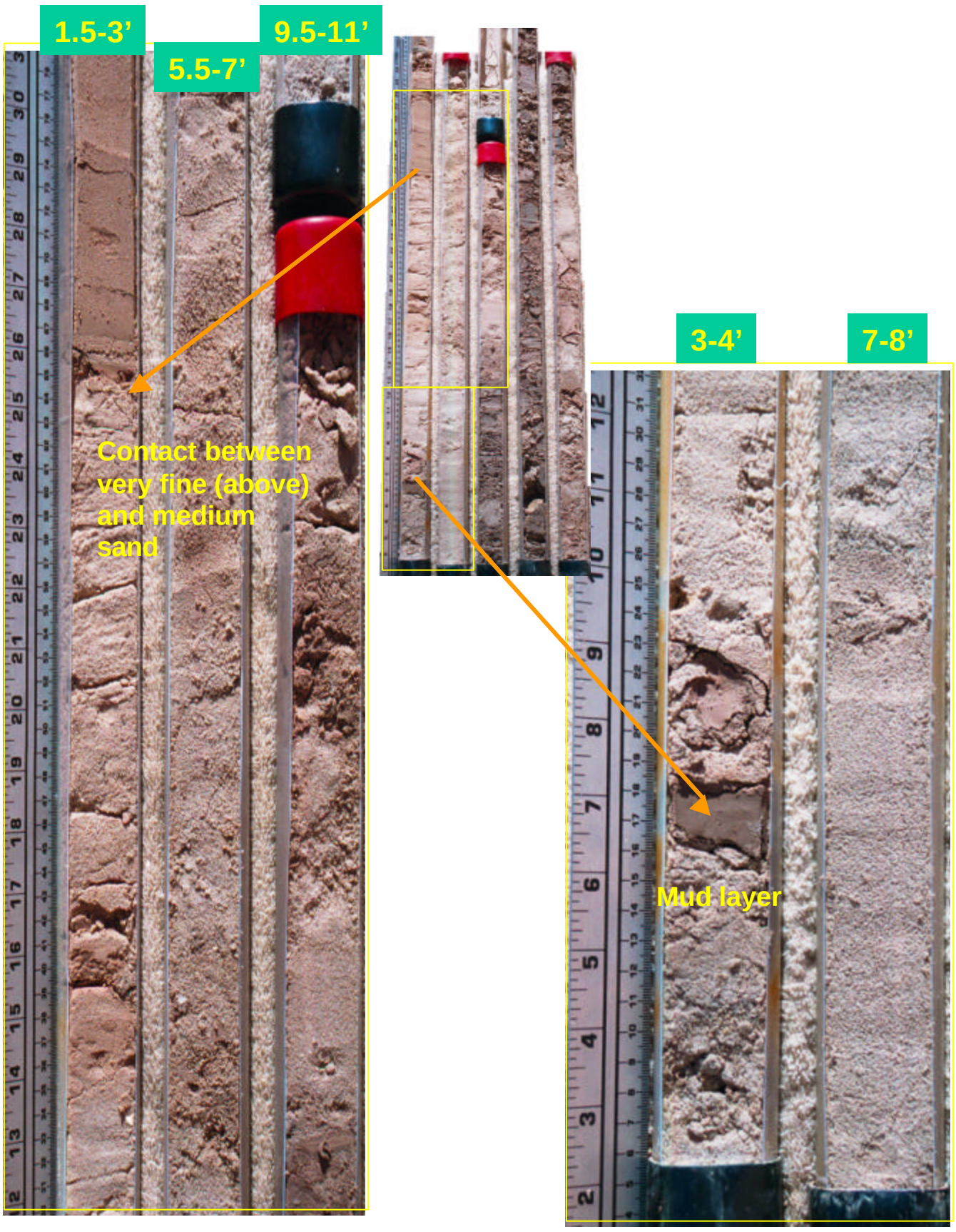

<u>Well #57</u> – Canadian River Floodplain

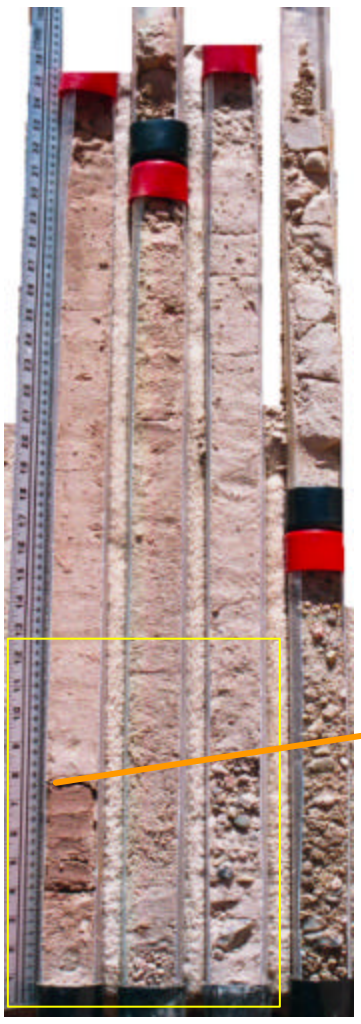

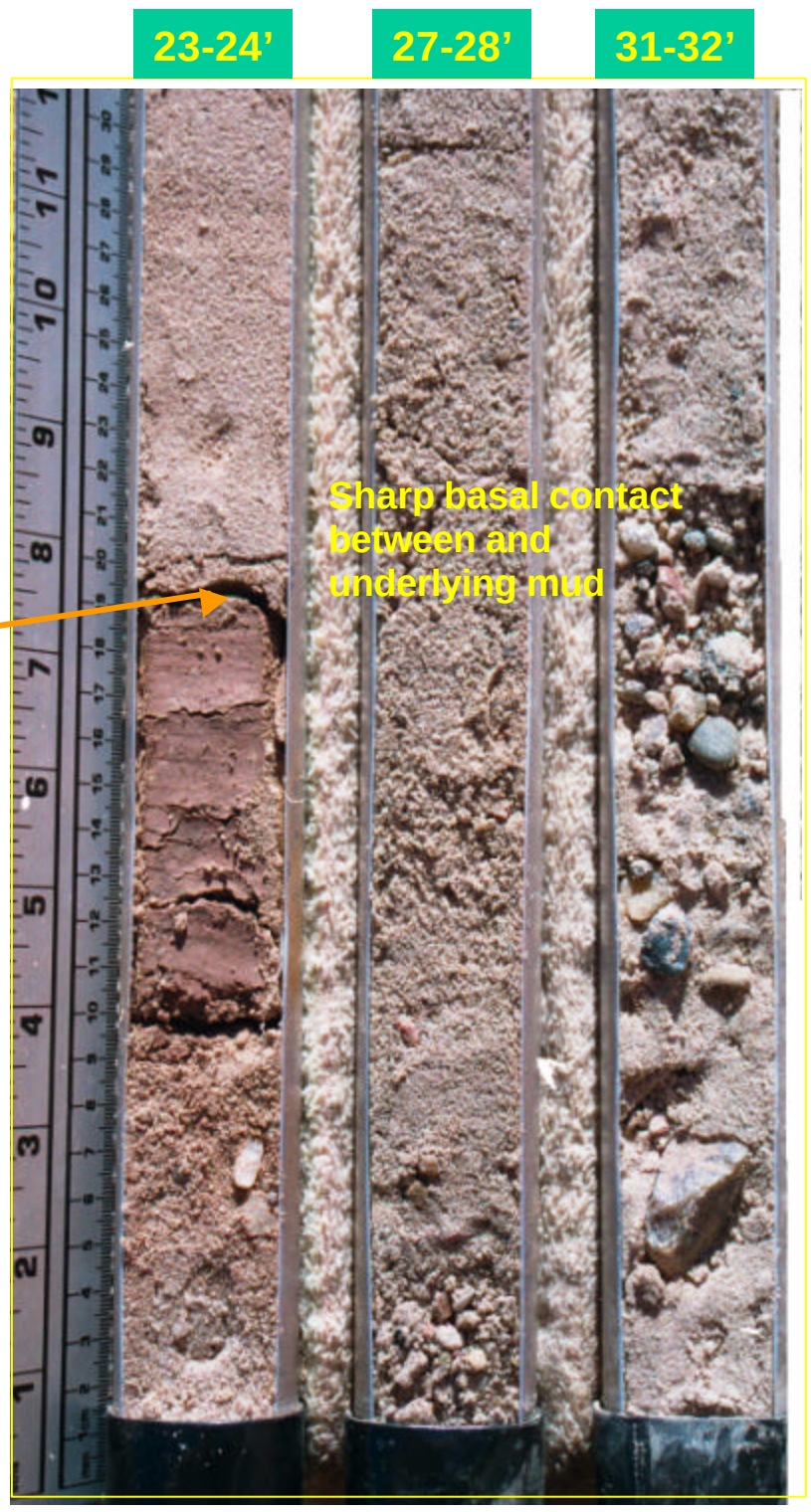

<u>Well #62</u> – Canadian River Floodplain

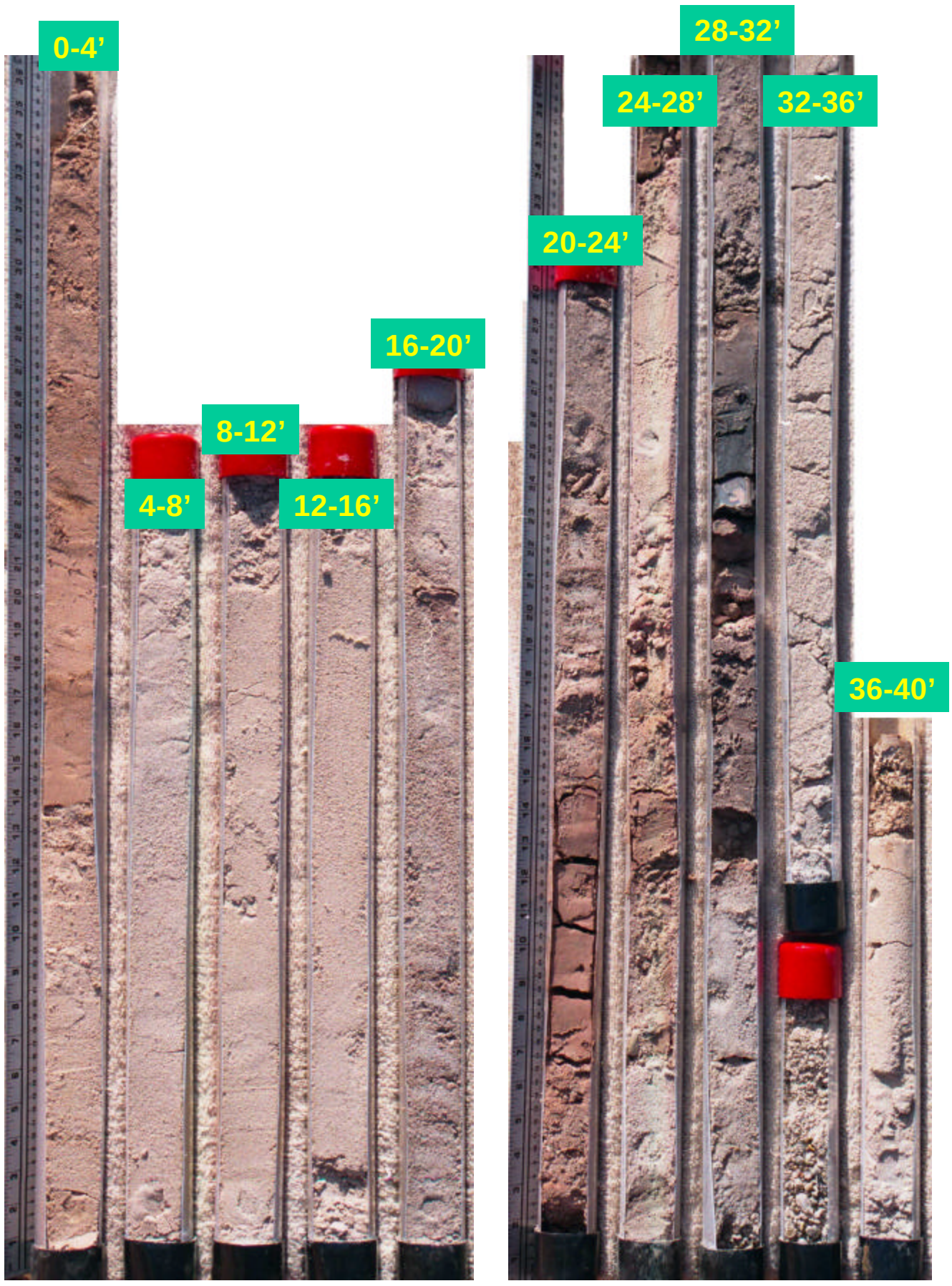

<u>Well #62</u> – Canadian River Floodplain

2.4-3.5’

6.4-7.5’

Sharp contact between very-fine sand (above) and medium sand

<u>Well #62</u> – Canadian River Floodplain

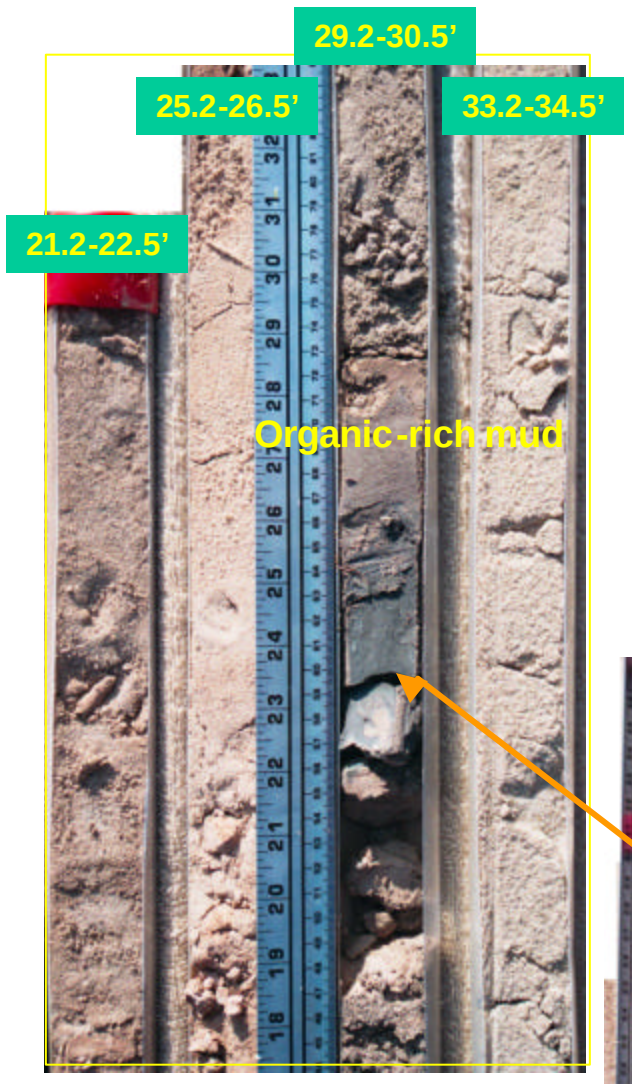

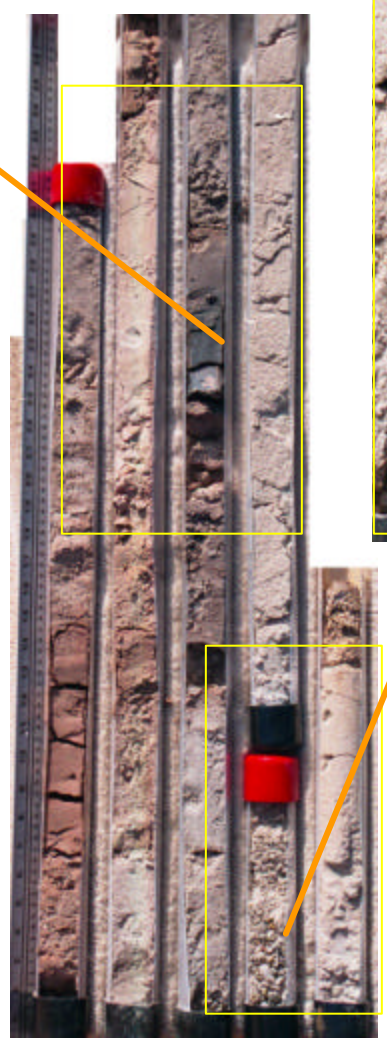

Gravel derived from updip bedrock

<u>Well #64</u> – Canadian River Floodplain

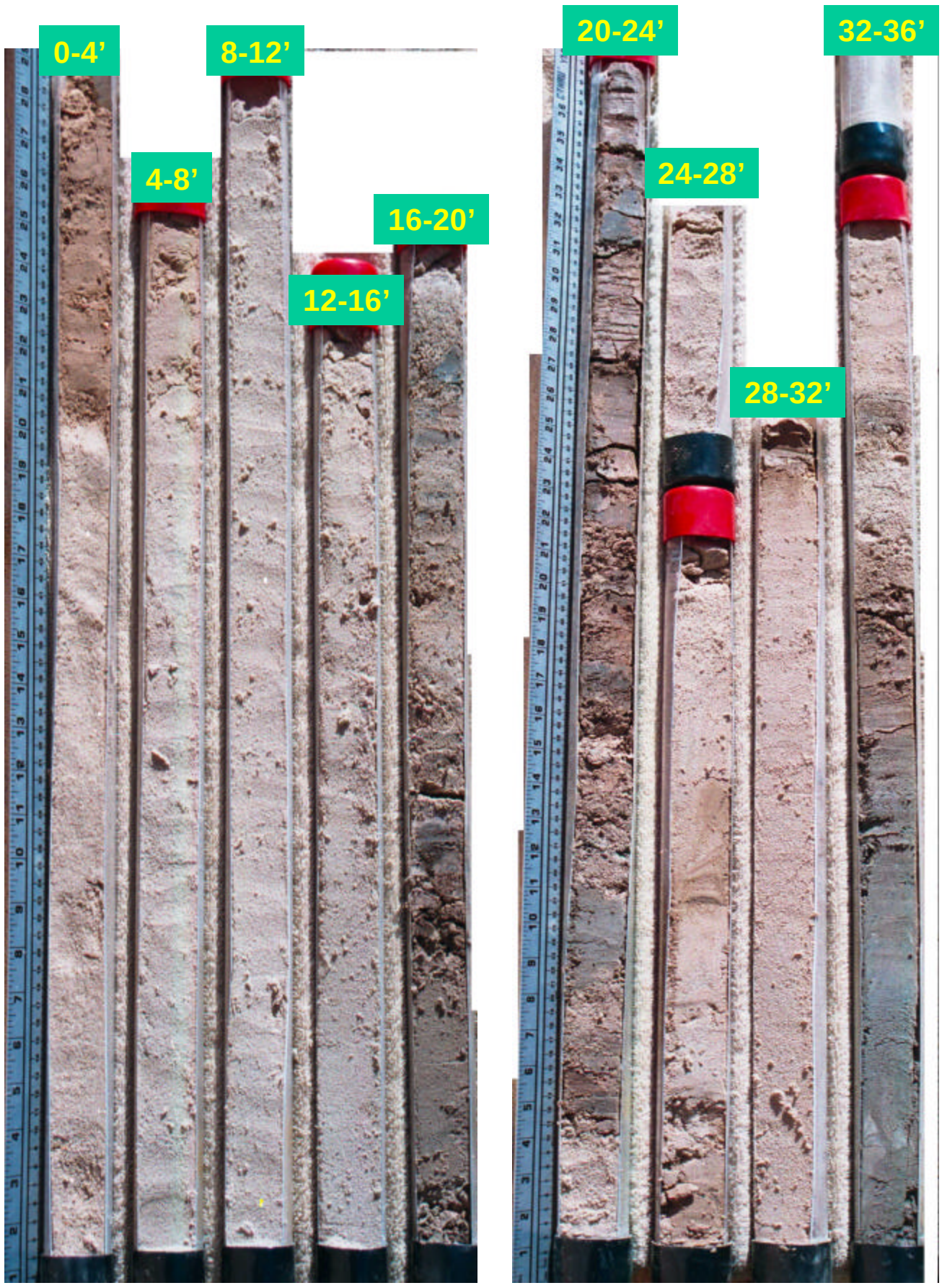

<u>Well #64</u> –
Canadian River Floodplain

<u>Well #73</u> – Canadian River Floodplain

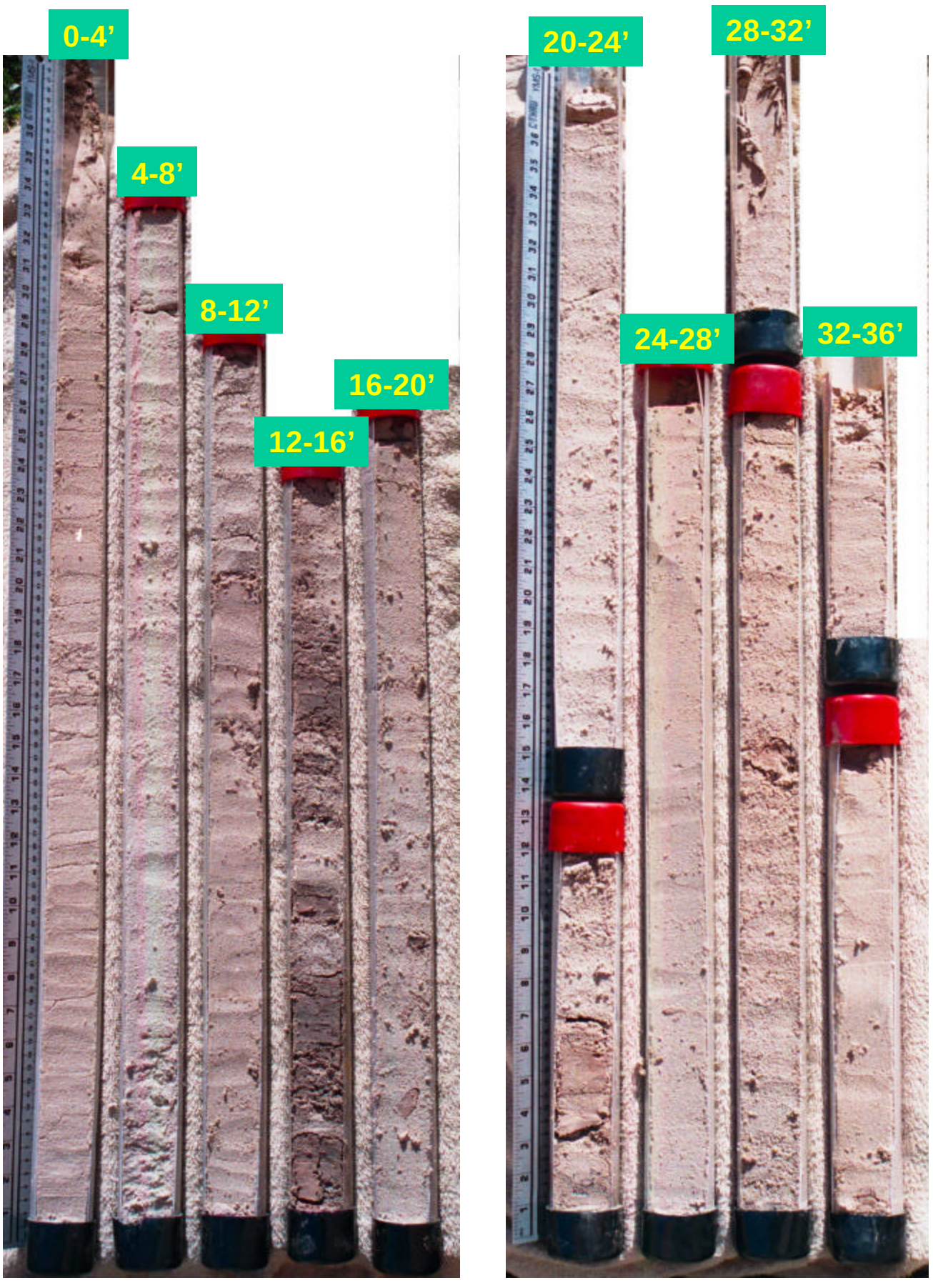

Well #73
Canadian River Floodplain

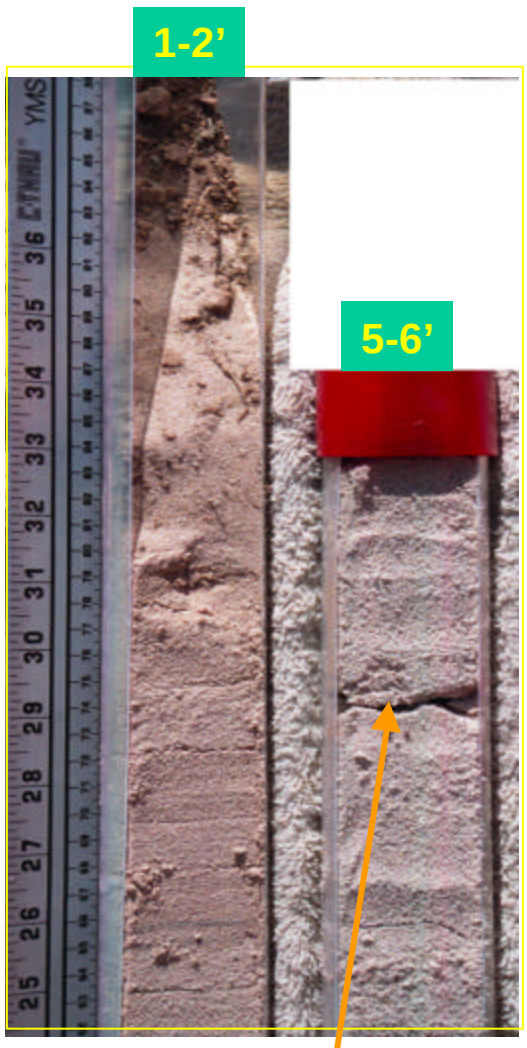

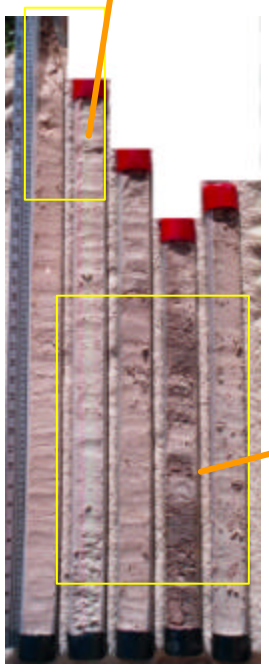

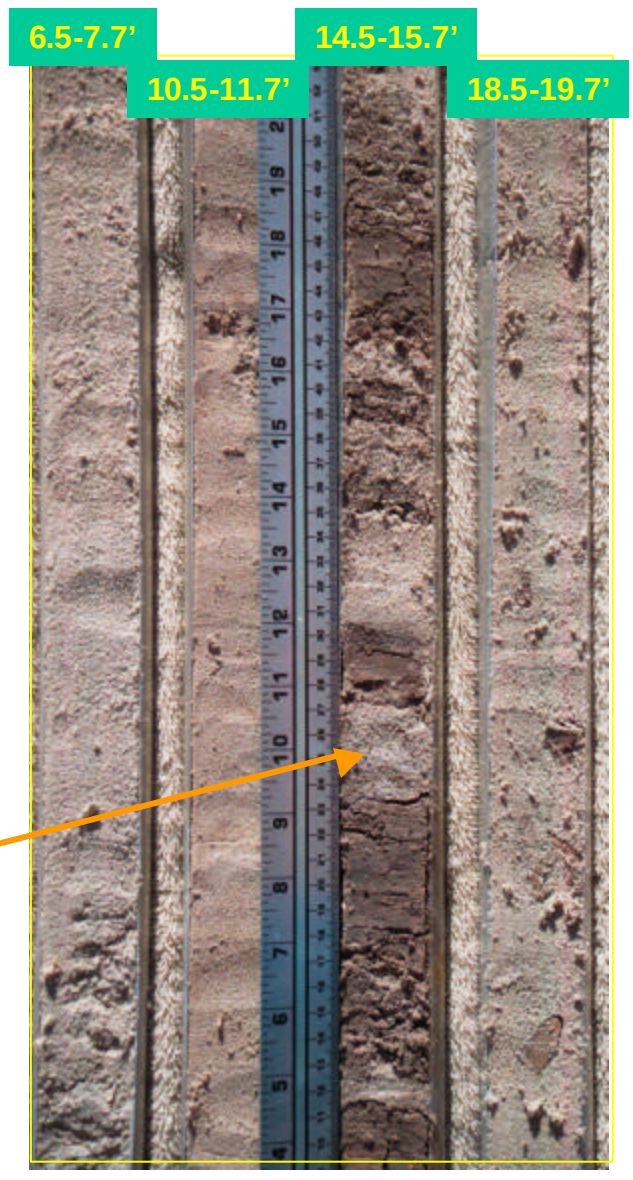

Well #73
Canadian River Floodplain

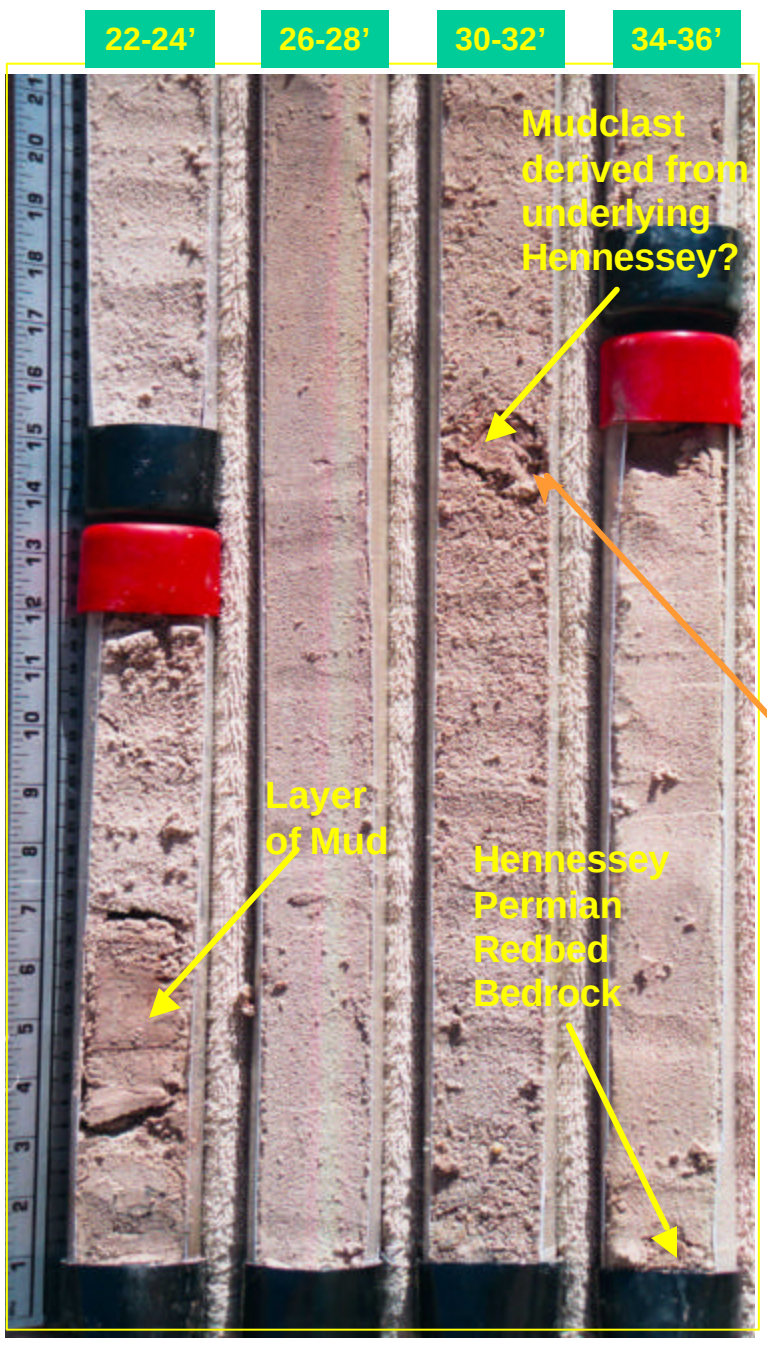

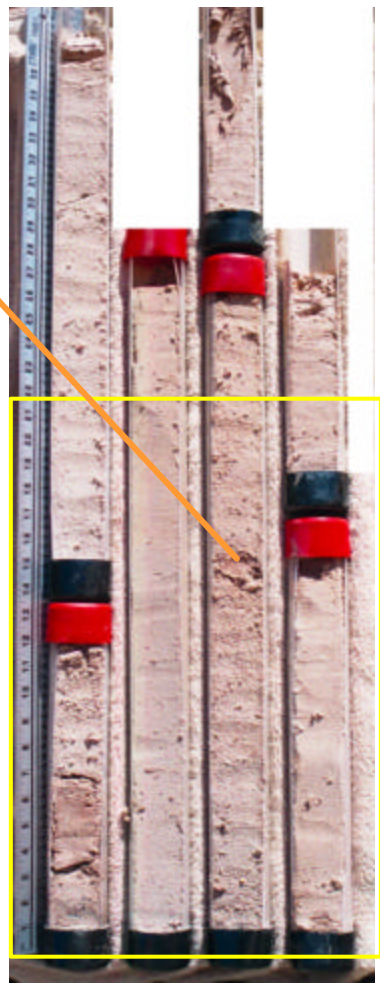

<u>Well #74</u> – Canadian River Floodplain

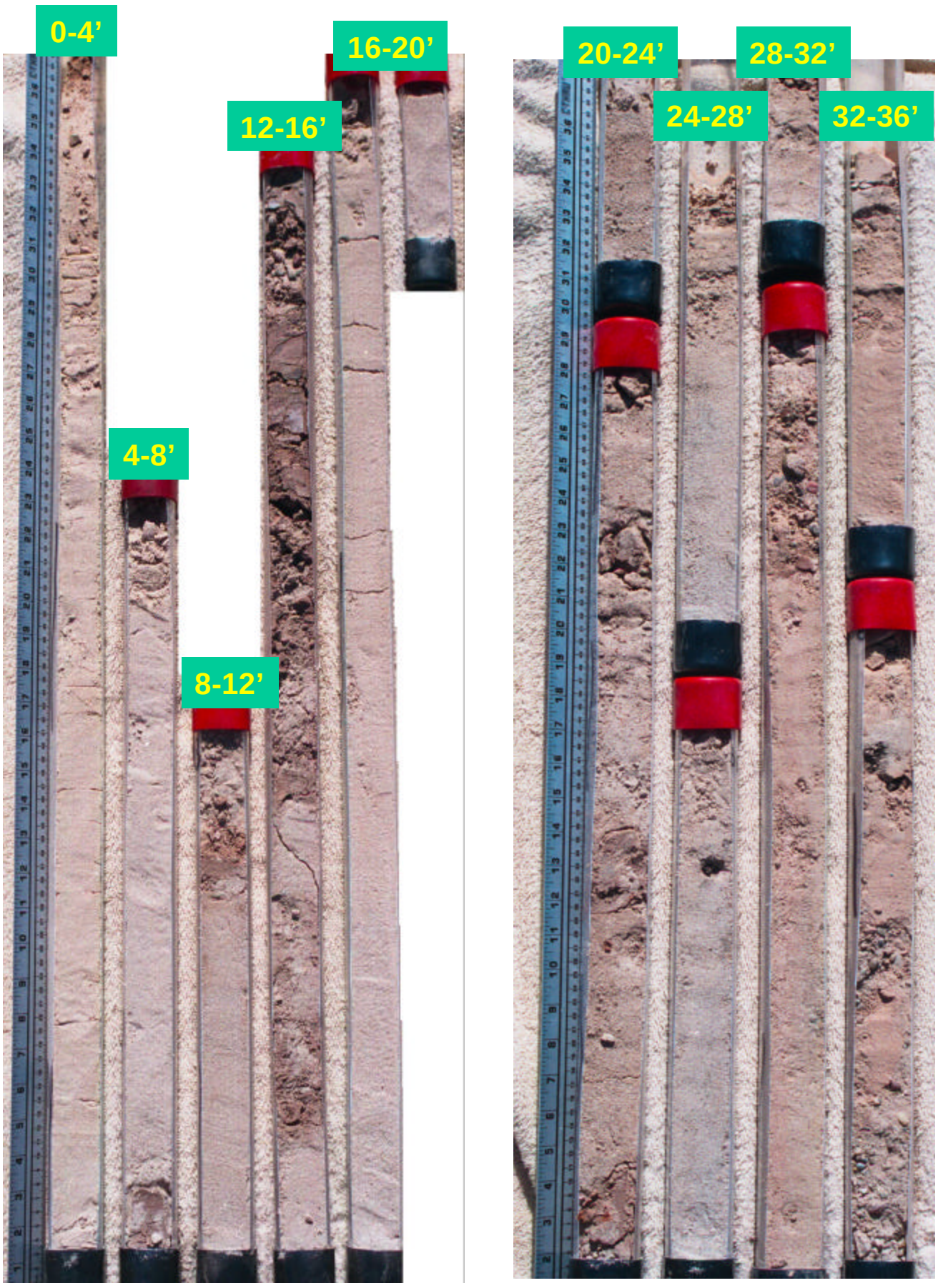

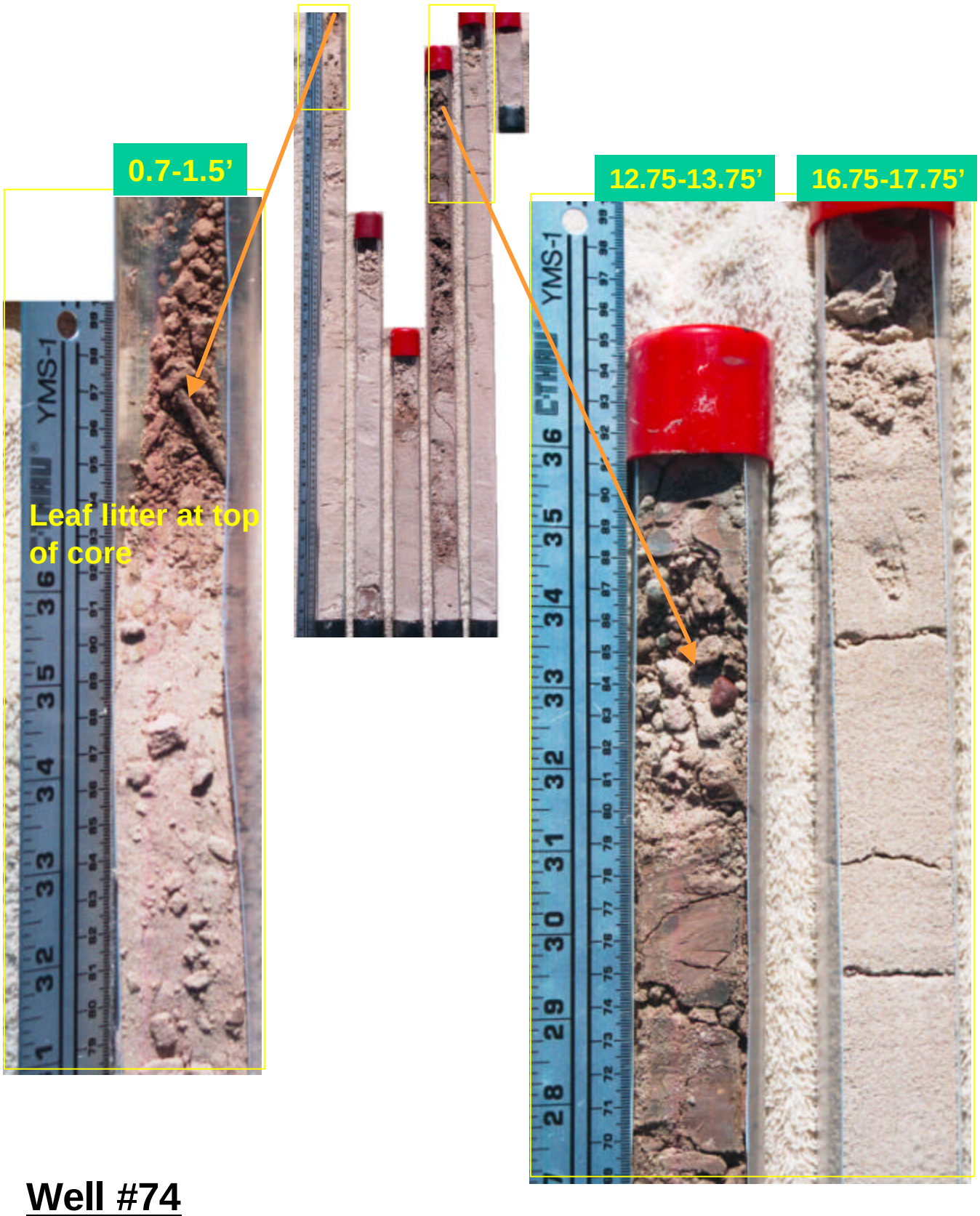

Well #74

Canadian River Floodplain

Well #74

Canadian River Floodplain

26.5-27.25’

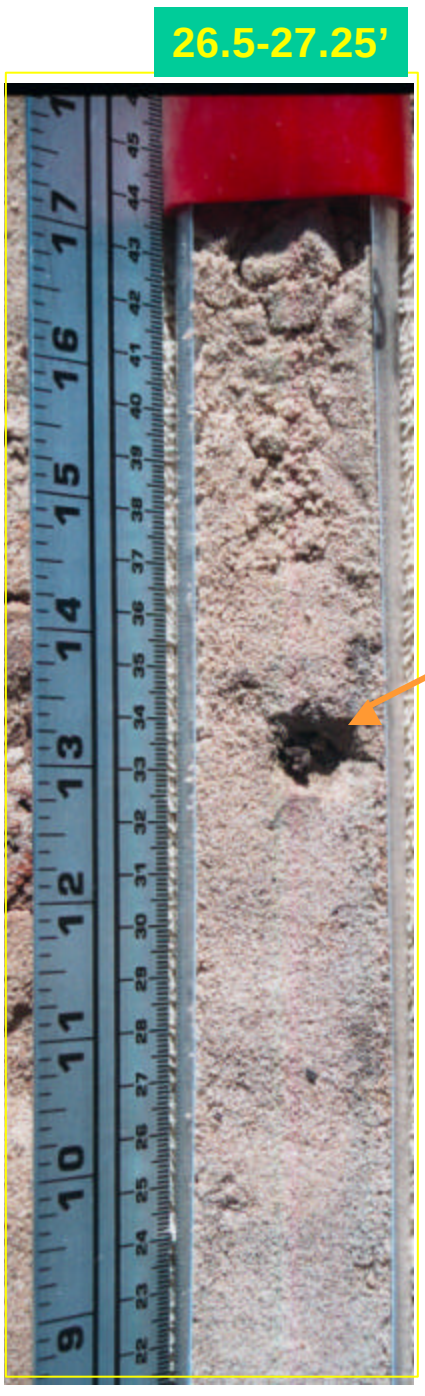

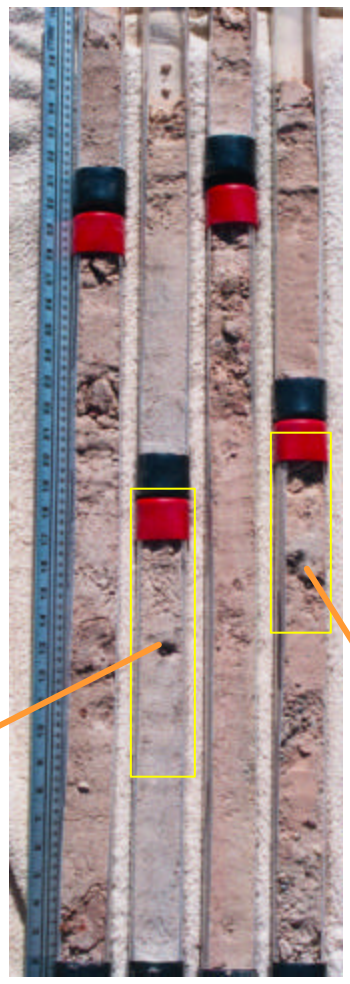

34.25-34.75’

<u>Well #74</u>

Canadian River Floodplain

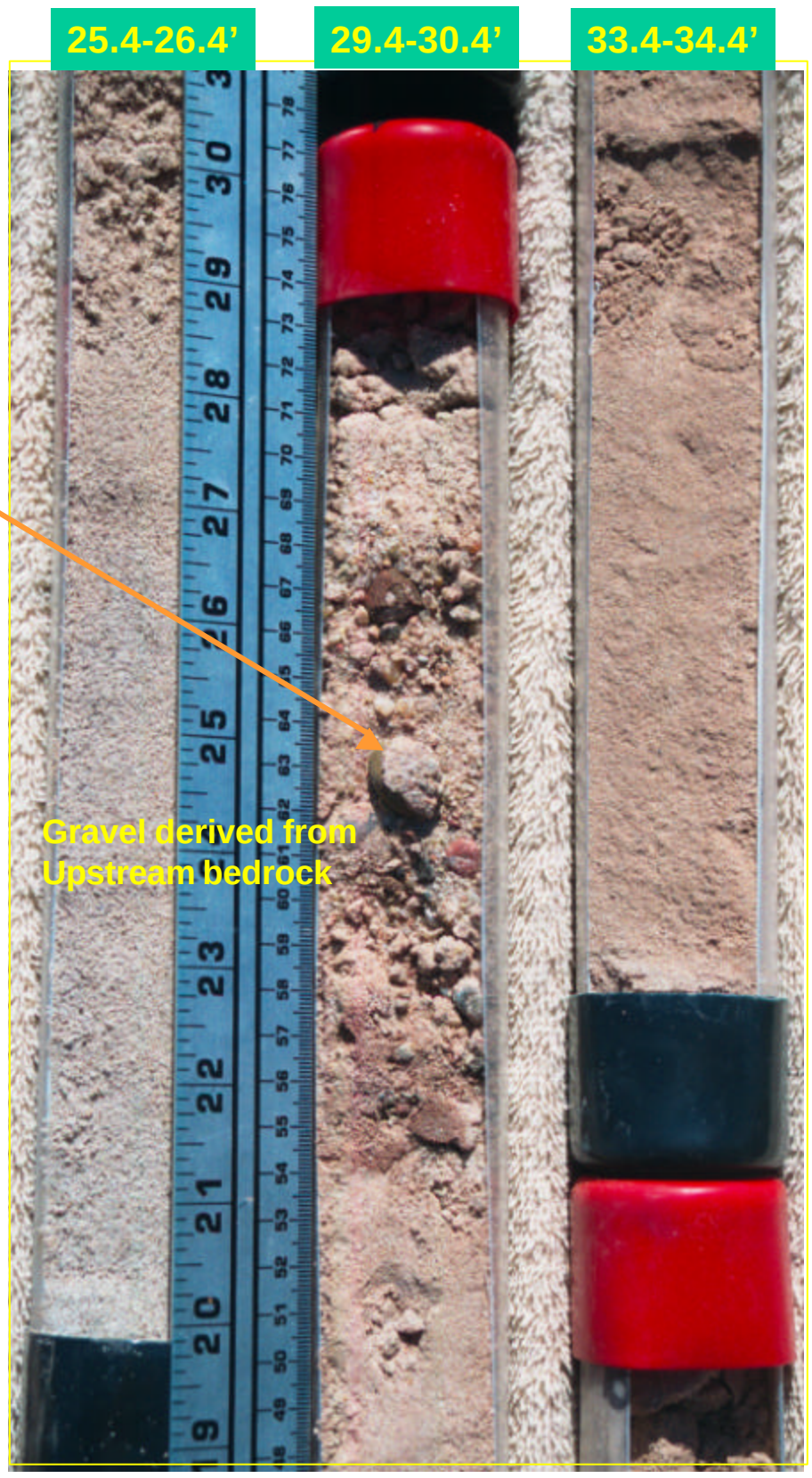

<u>Well #78</u> – Canadian River Floodplain

Well #78

Canadian River Floodplain

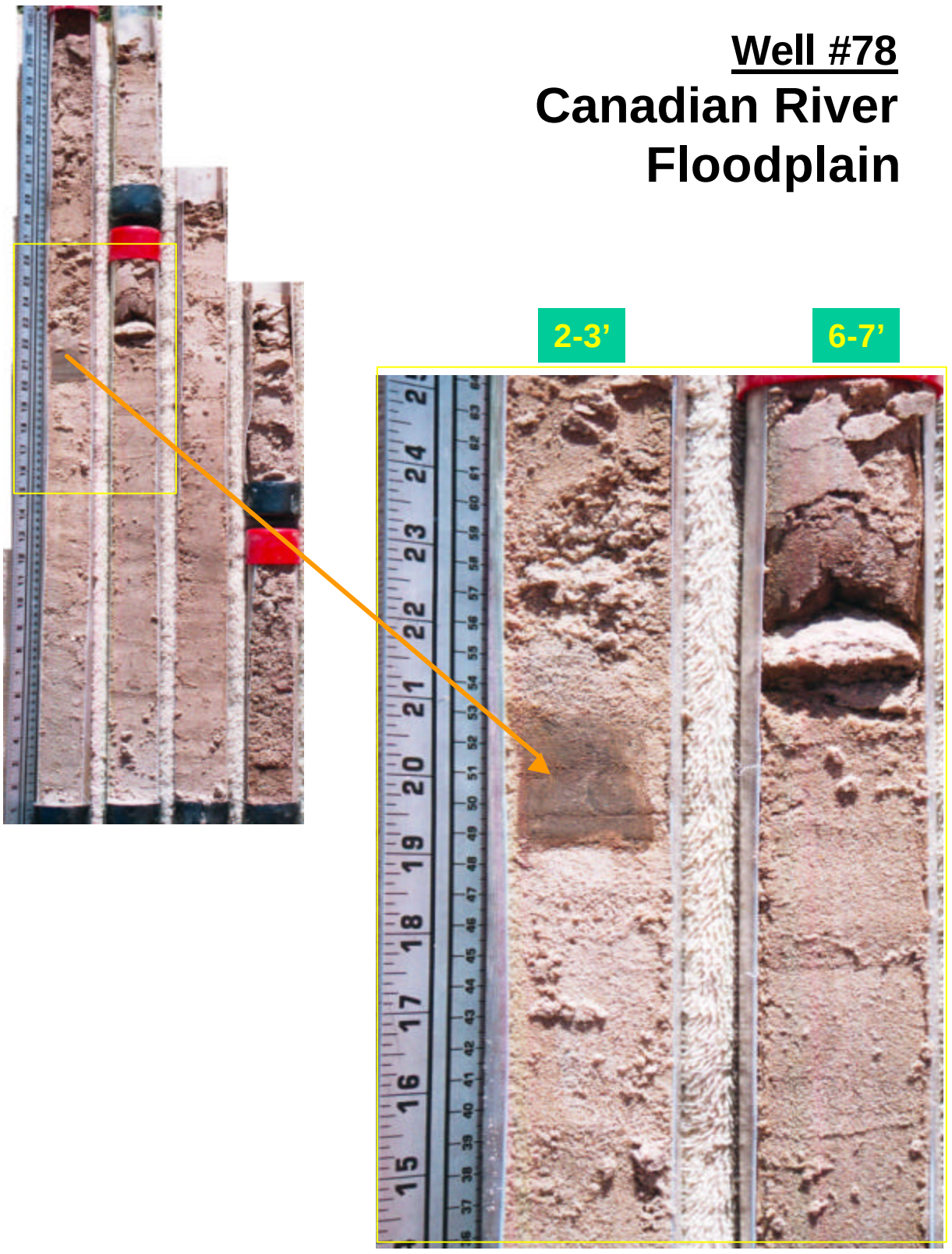

Well #78

Canadian River Floodplain

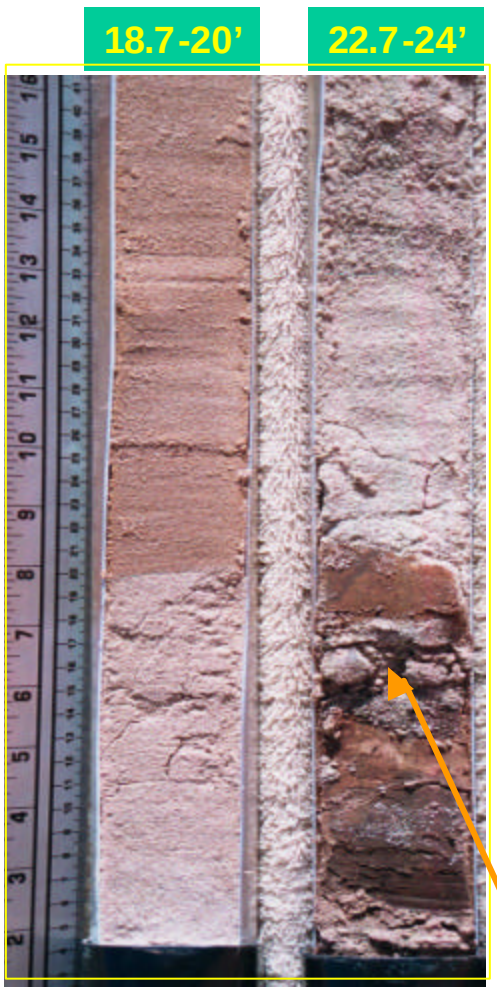

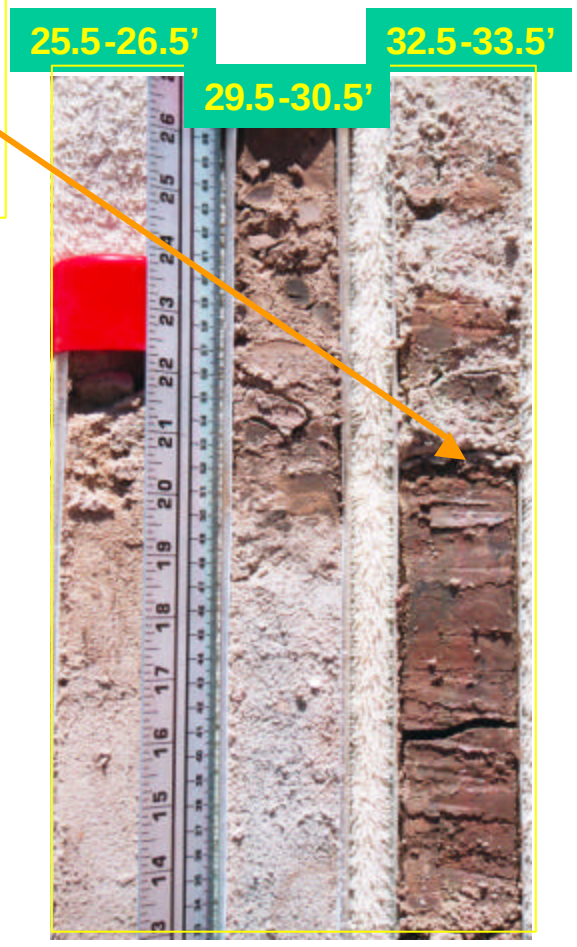

APPENDIX C

CUMULATIVE GRAIN SIZE CURVES

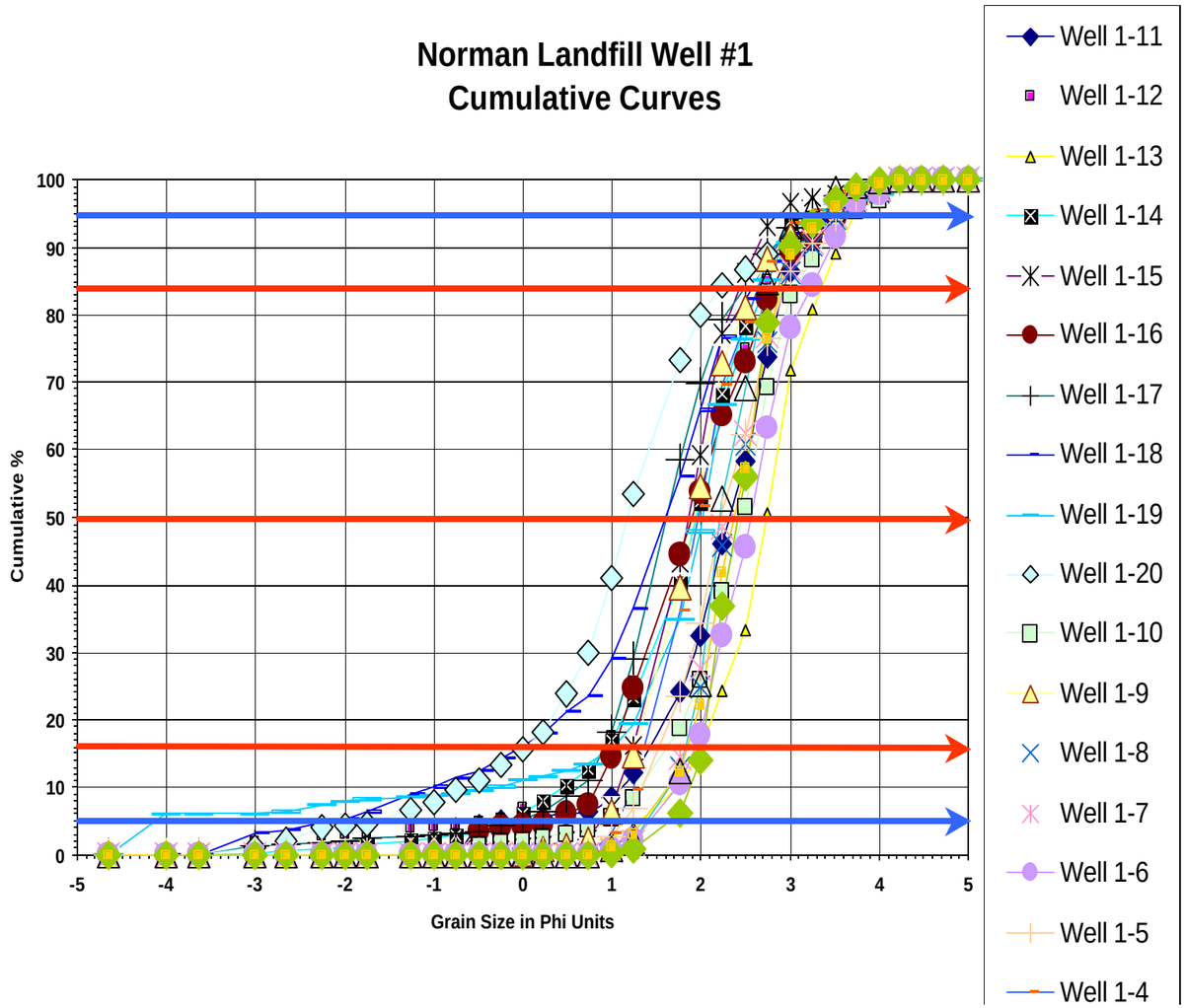
Norman Landfill Well #1
Cumulative Curves
Cumulative %
100
90
80
70
60
50
40
30
20
10
0
-5
-4
-3
-2
-1
0
1
2
3
4
5
Grain Size in Phi Units
Well 1-11
Well 1-12
Well 1-13
Well 1-14
Well 1-15
Well 1-16
Well 1-17
Well 1-18
Well 1-19
Well 1-20
Well 1-10
Well 1-9
Well 1-8
Well 1-7
Well 1-6
Well 1-5
Well 1-4

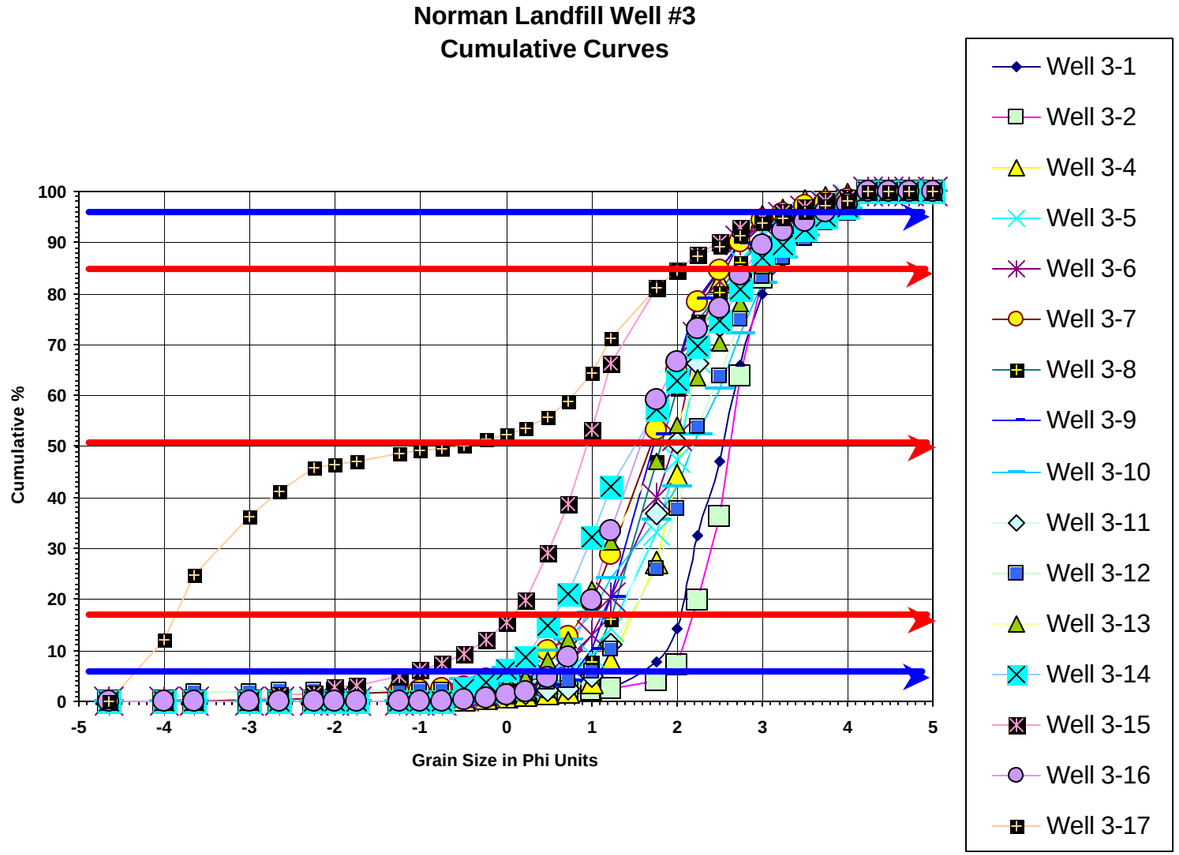
Norman Landfill Well #3
Cumulative Curves
Cumulative %
100
90
80
70
60
50
40
30
20
10
0
-5
-4
-3
-2
-1
0
1
2
3
4
5
Grain Size in Phi Units
Well 3-1
Well 3-2
Well 3-4
Well 3-5
Well 3-6
Well 3-7
Well 3-8
Well 3-9
Well 3-10
Well 3-11
Well 3-12
Well 3-13
Well 3-14
Well 3-15
Well 3-16
Well 3-17

Norman Landfill Well #7
Cumulative Curves

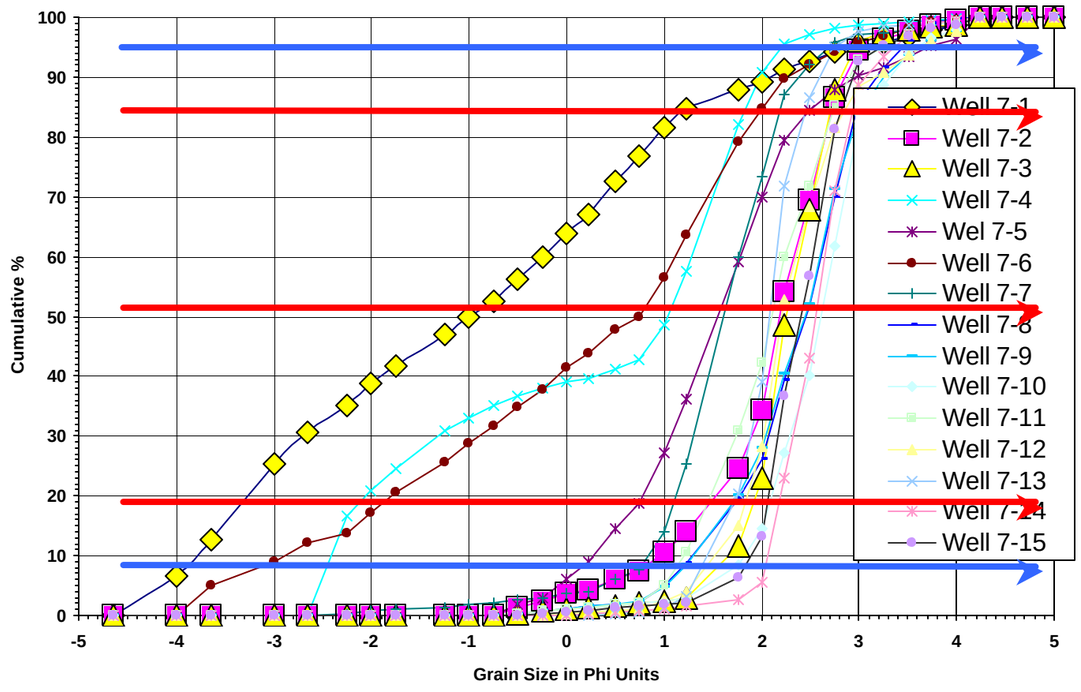

Norman Landfill Well #11
Cumulative Curves

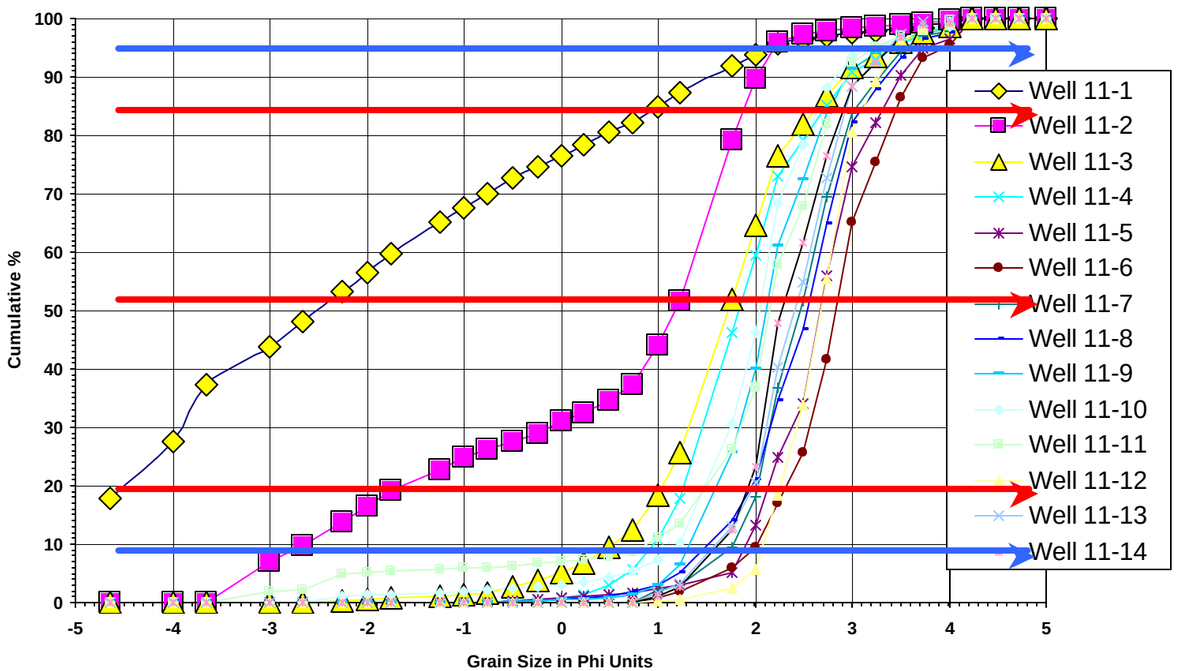

Norman Landfill Well #15
Cumulative Curves

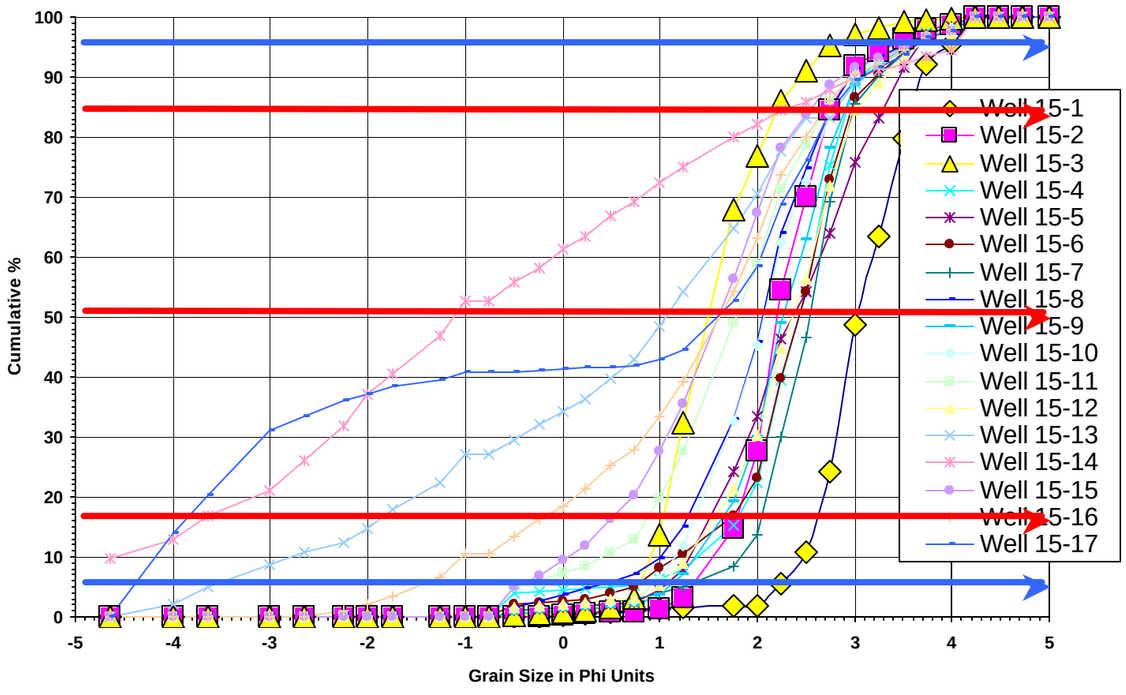

Norman Landfill Well #21
Cumulative Curves

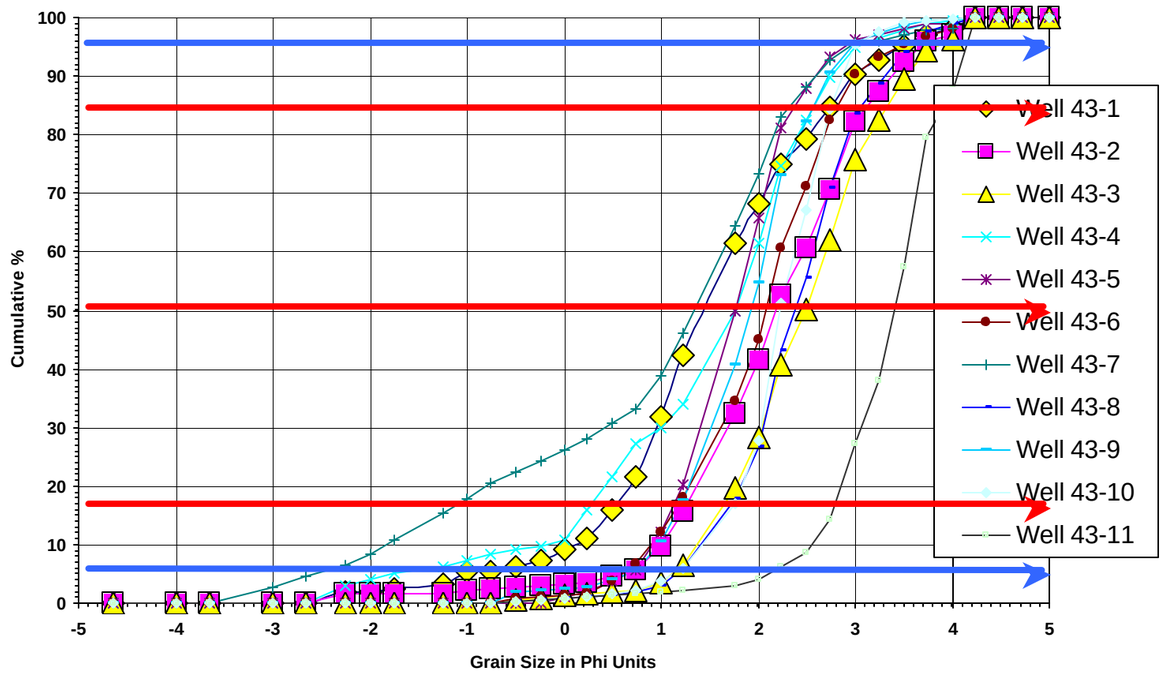

Norman Landfill Well #23
Cumulative Curves

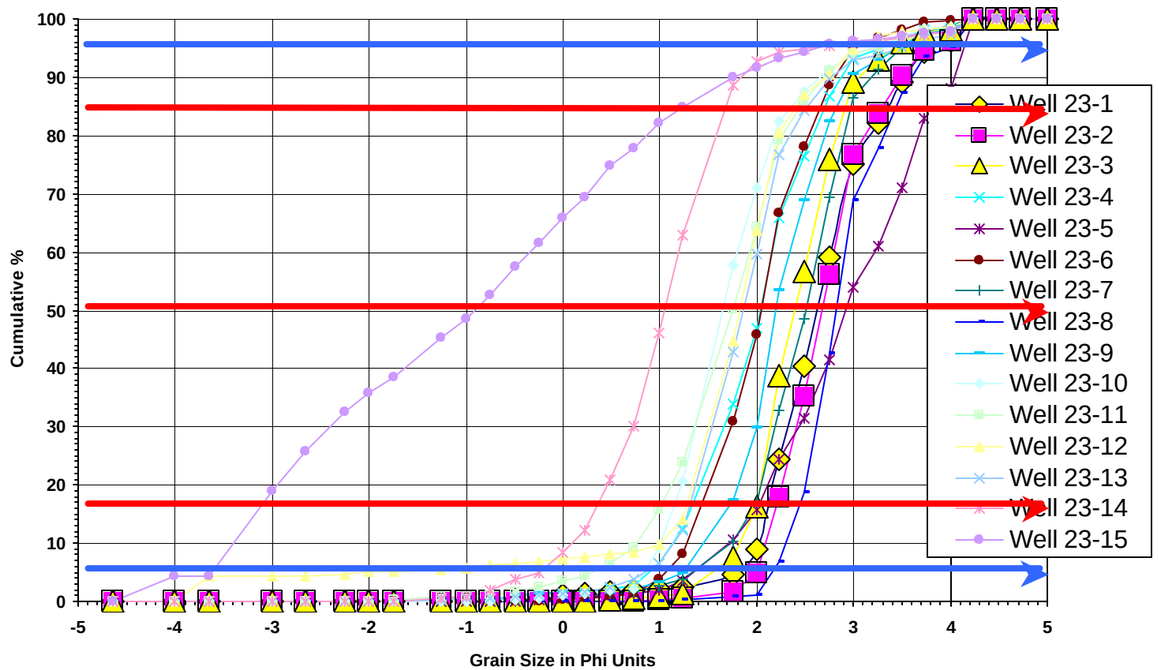

Norman Landfill Well #28
Cumulative Curves

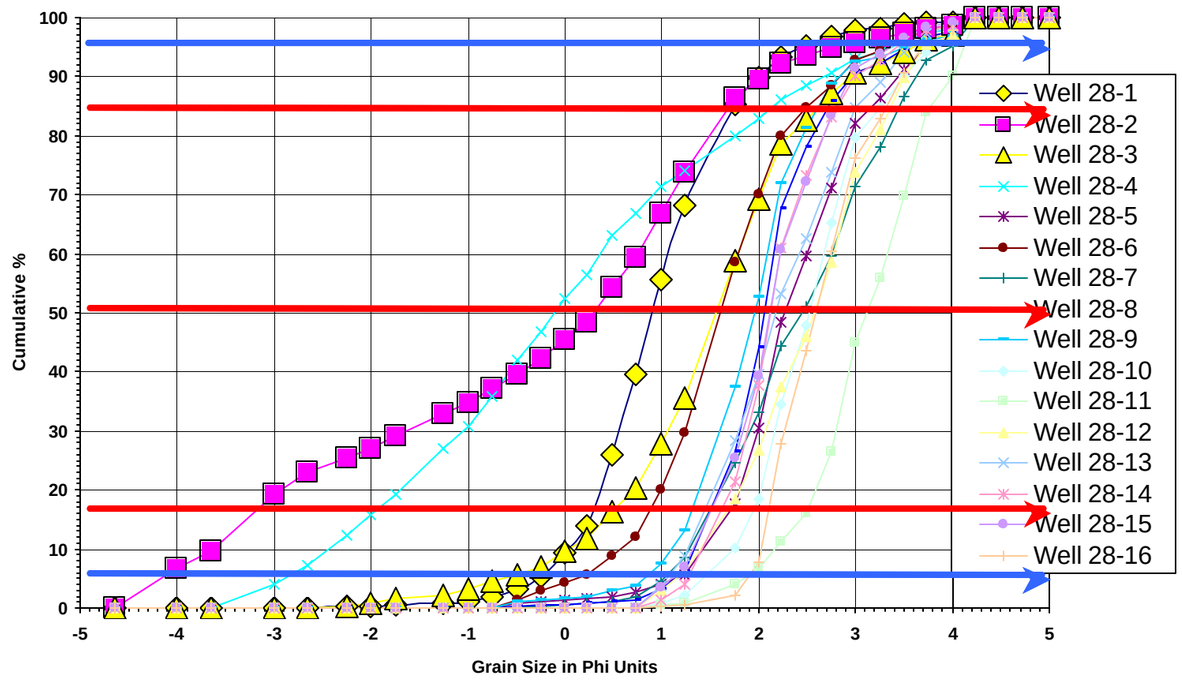

Norman Landfill Well #31
Cumulative Curves

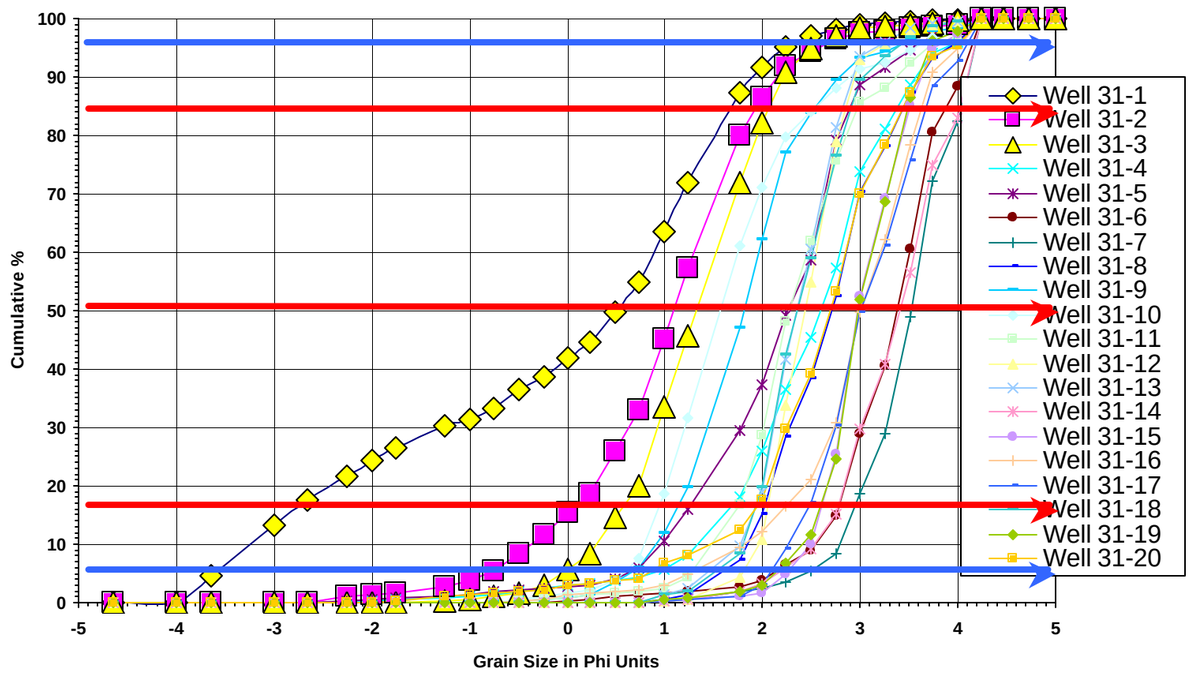

Norman Landfill Well #42
Cumulative Curves

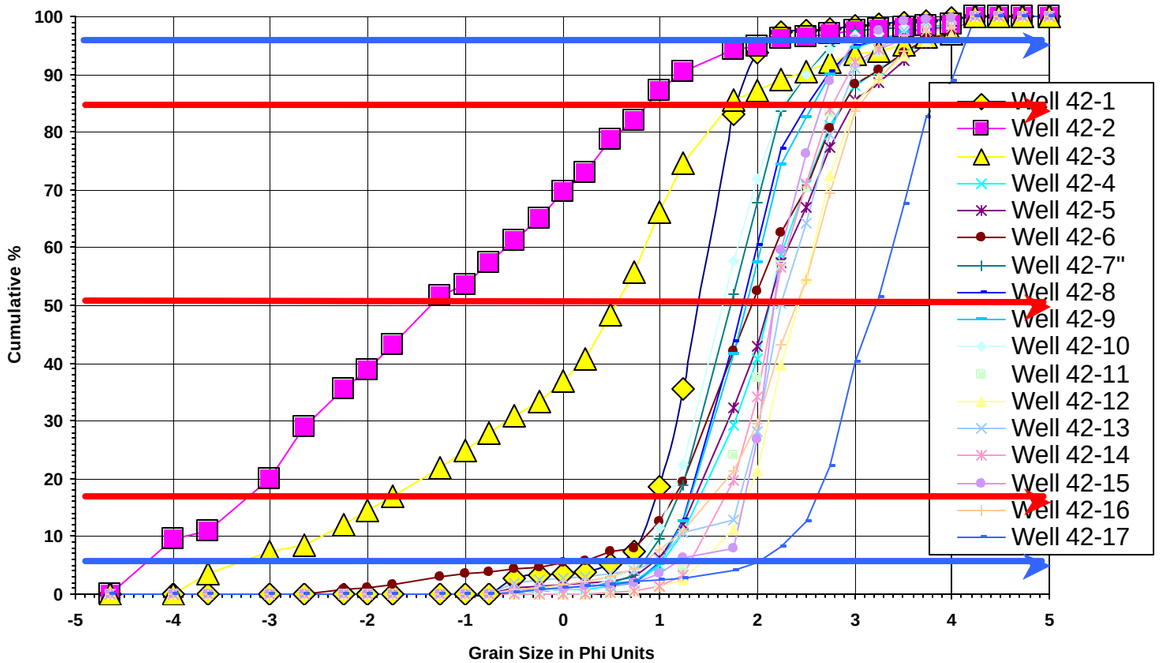

Norman Landfill Well #44
Cumulative Curves

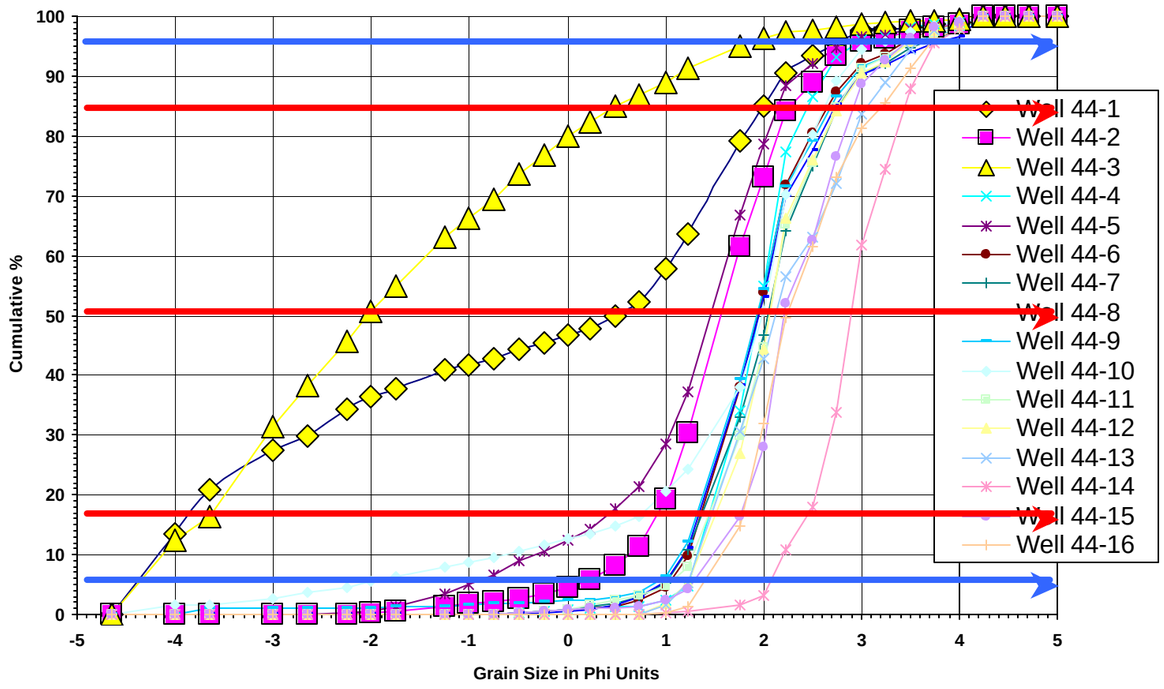

Norman Landfill Well #46
Cumulative Curves

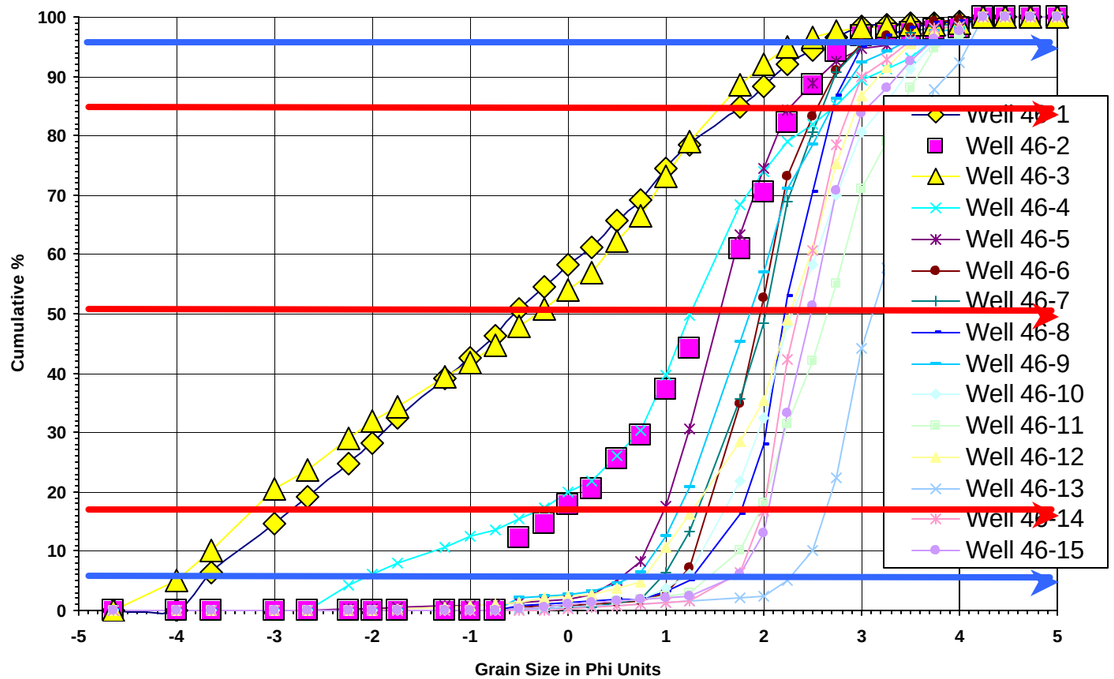

Norman Landfill Well #56
Cumulative Curves

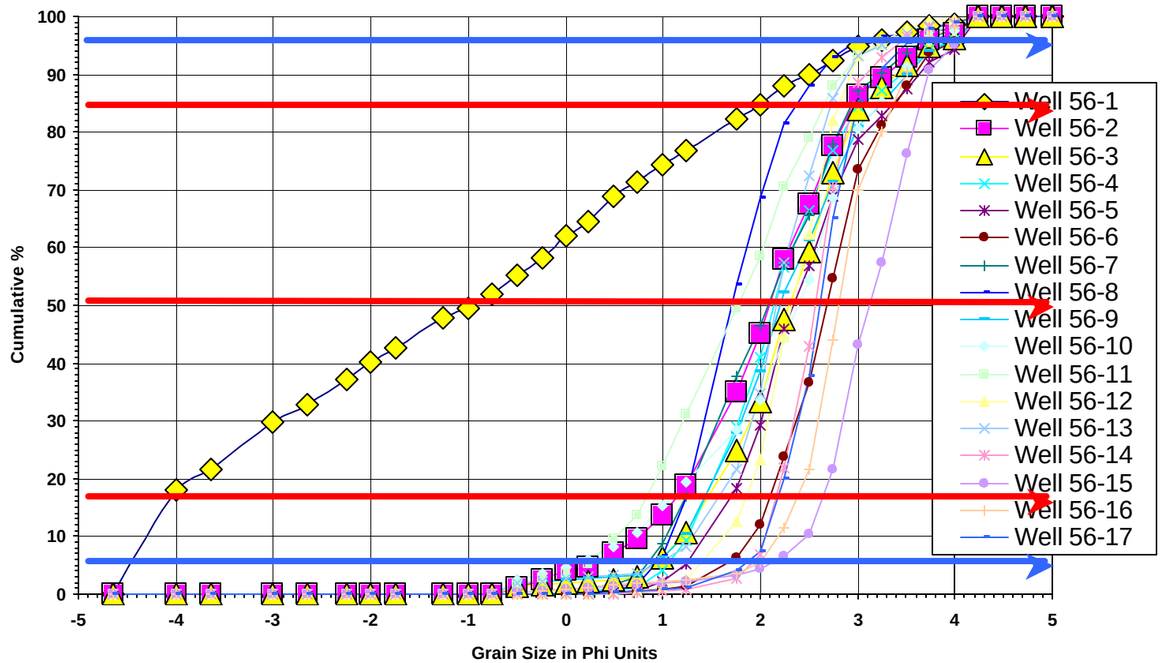

Norman Landfill Well #57
Cumulative Curves

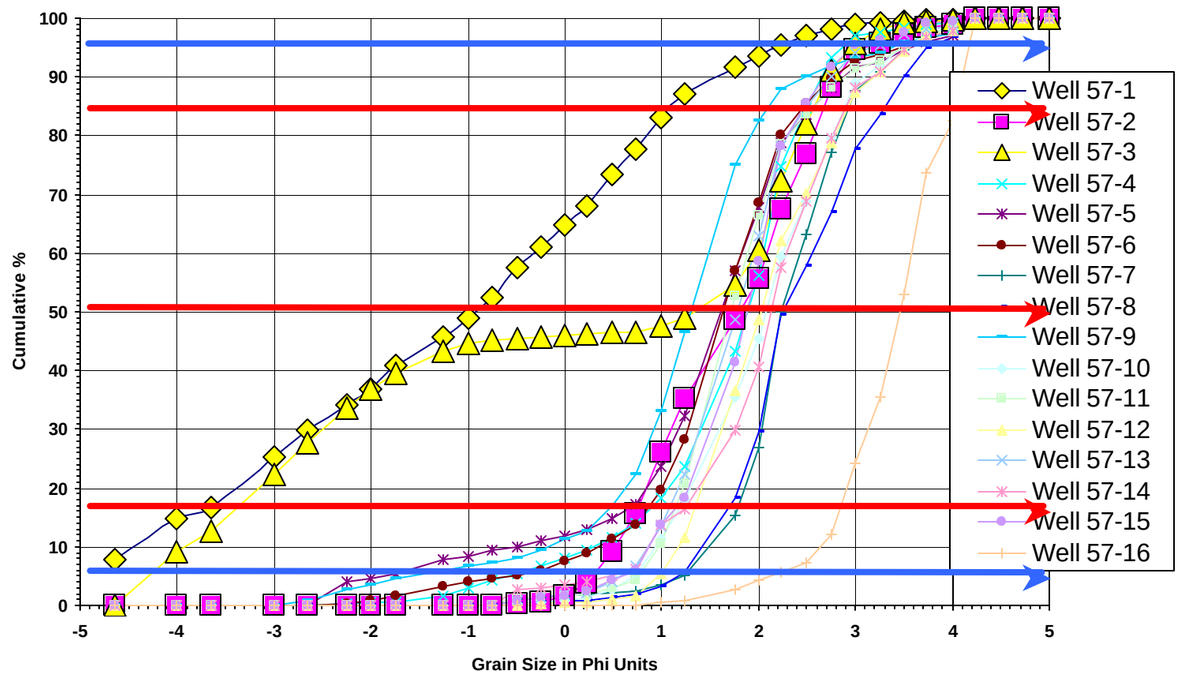

Norman Landfill Well #62
Cumulative Curves

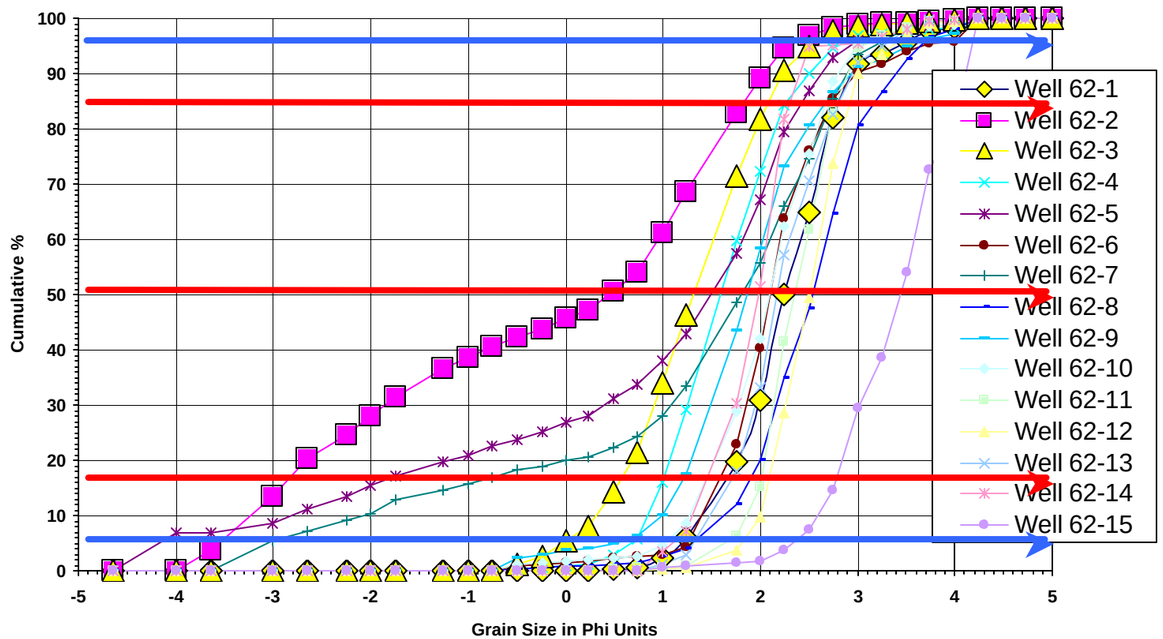

Norman landfill Well #64
Cumulative Curves

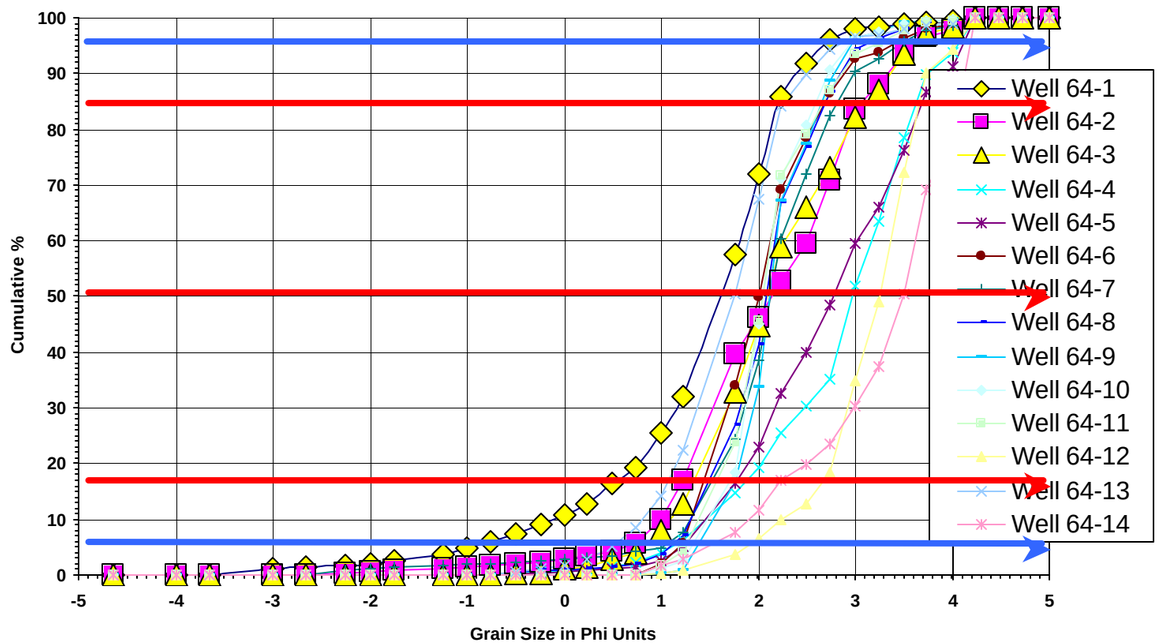

Norman Landfill Well #73
Cumulative Curves

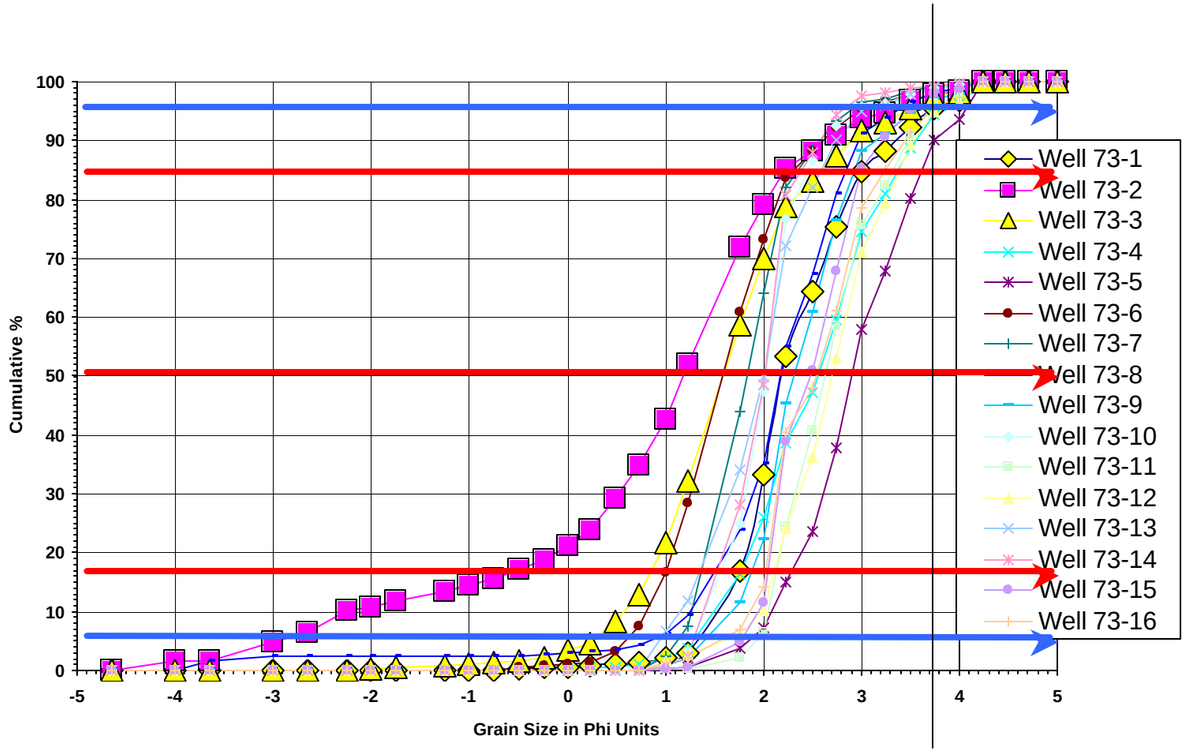

Norman Landfill Well #74
Cumulative Curves

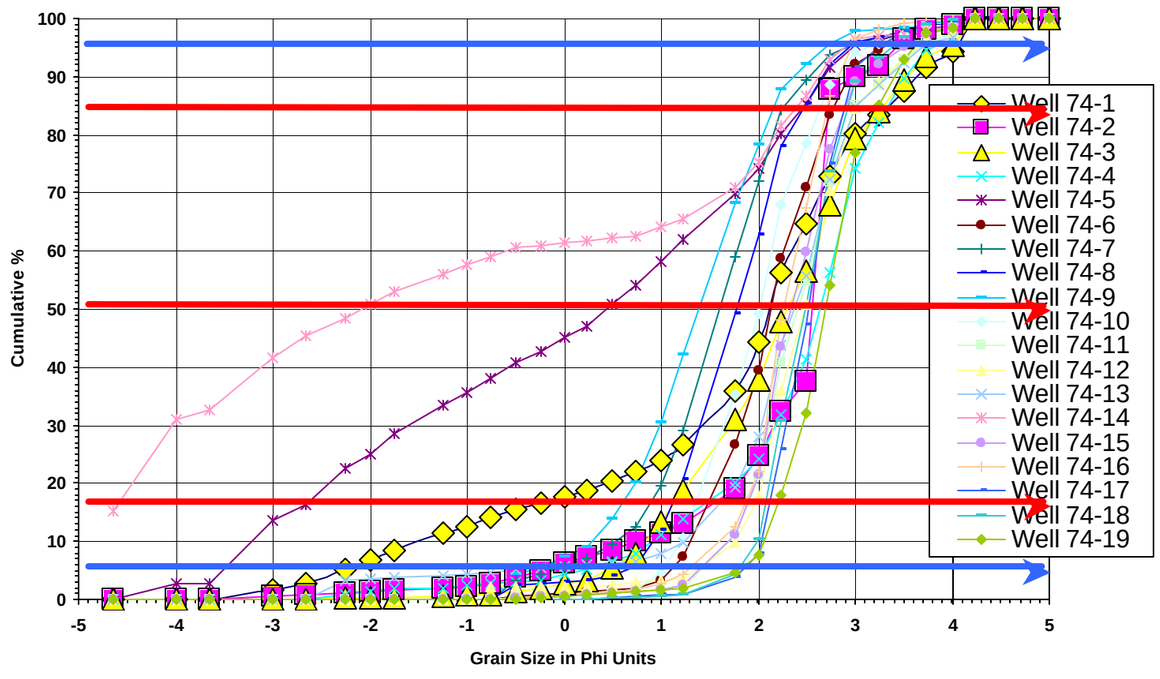

Norman Landfill Well #78
Cumulative Curves

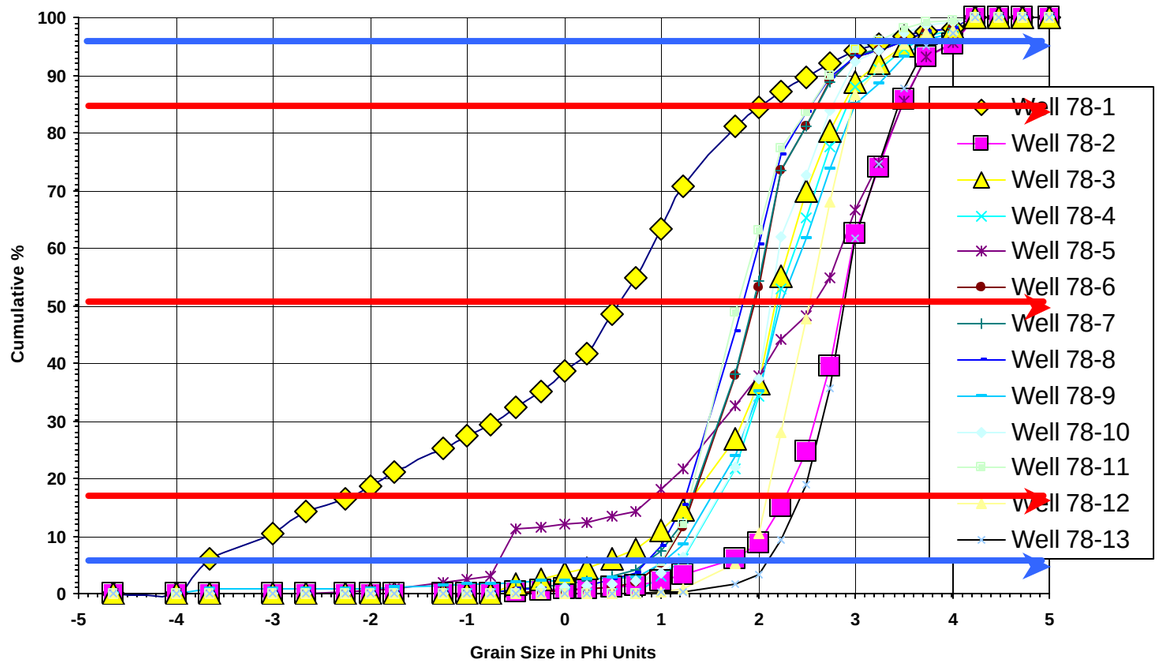

APPENDIX D

CROSS SECTIONS

Norman Landfill
Cross-Section A-A’

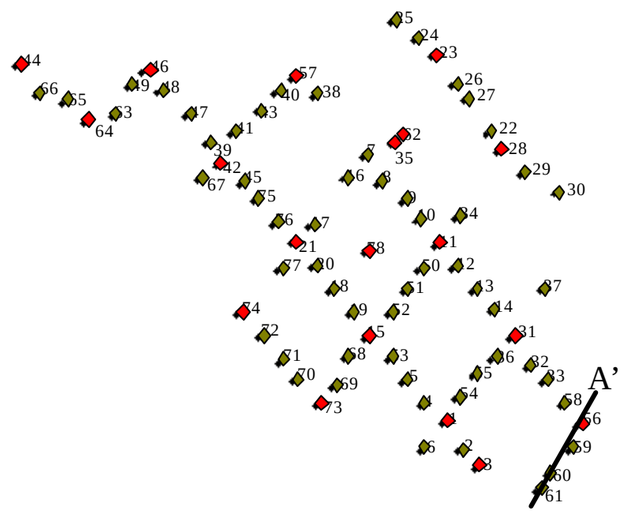

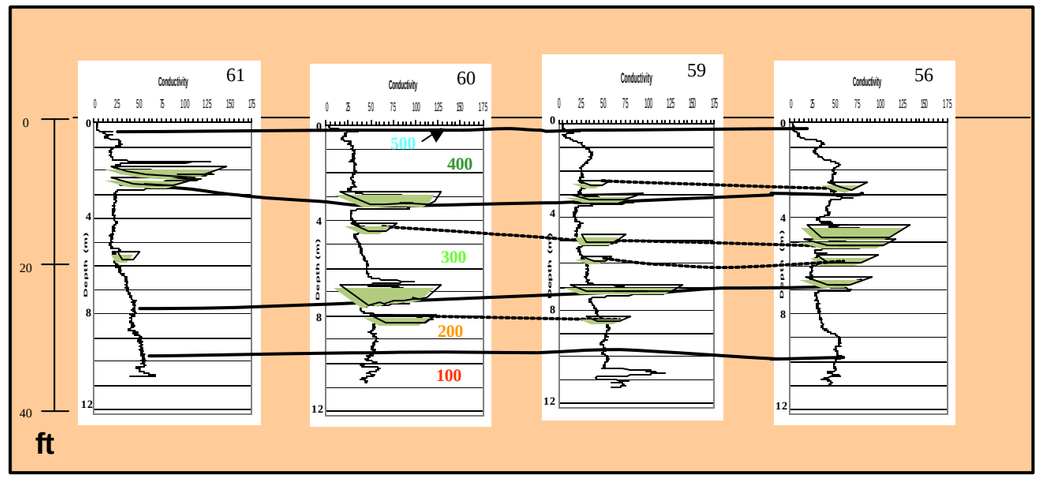

Norman Landfill
Cross-Section B-B’

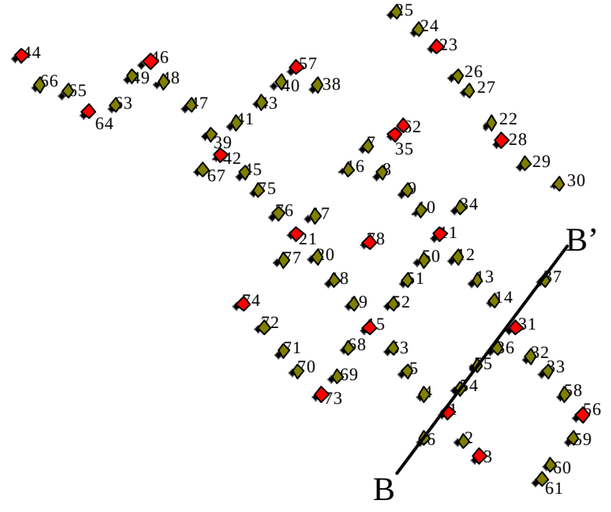

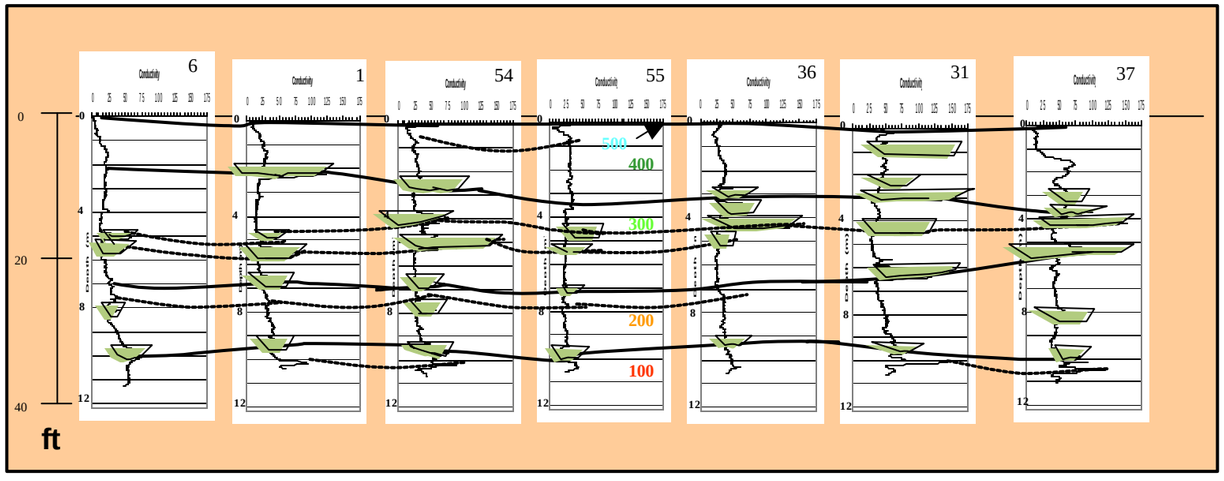

Norman Landfill
Cross-Section C-C’

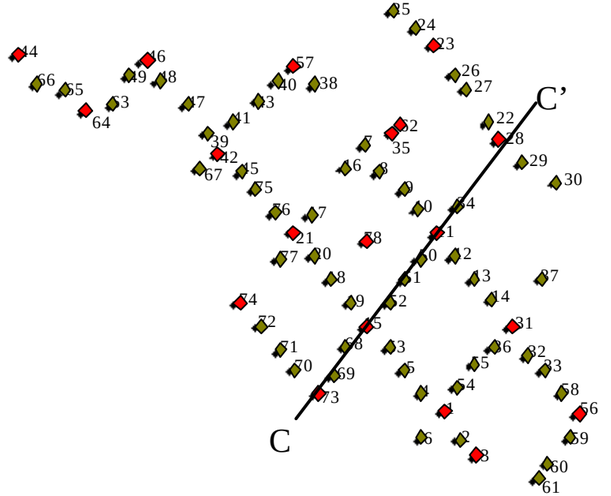

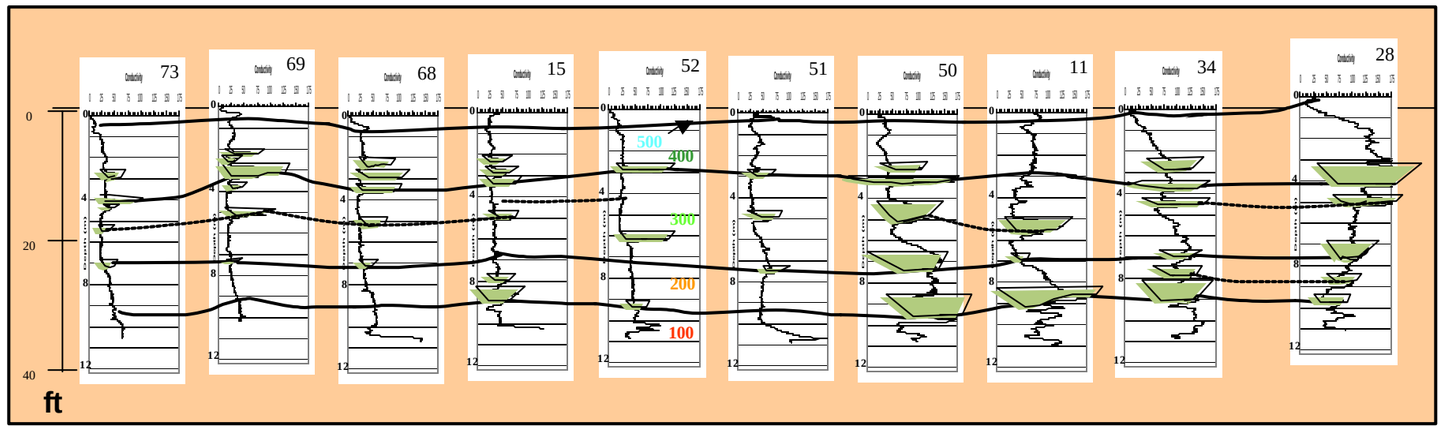

Norman Landfill
Cross-Section D-D’

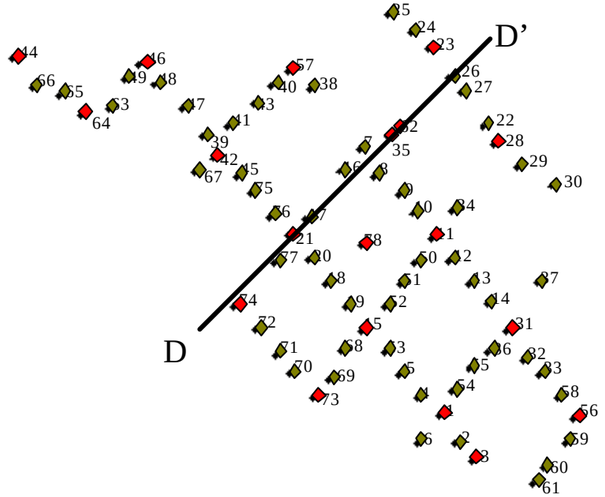

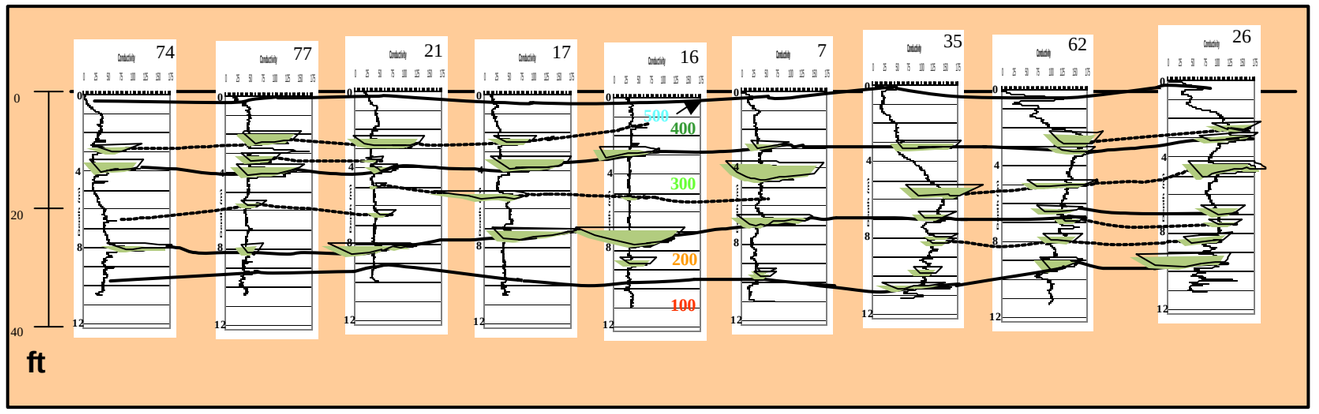

Fig. 18 – Example cross section running perpedicular to the point bar

Norman Landfill
Cross-Section E-E’

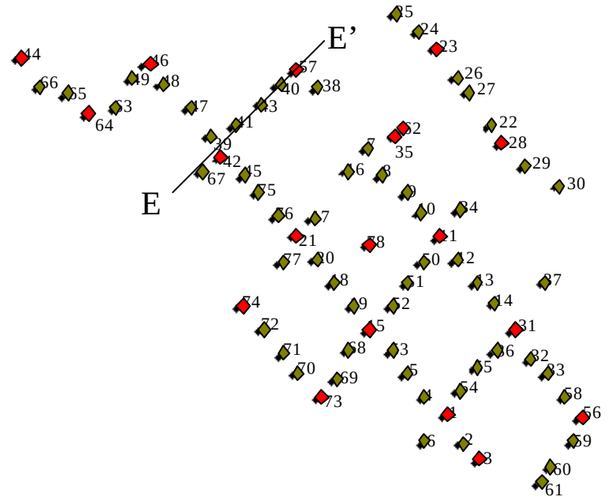

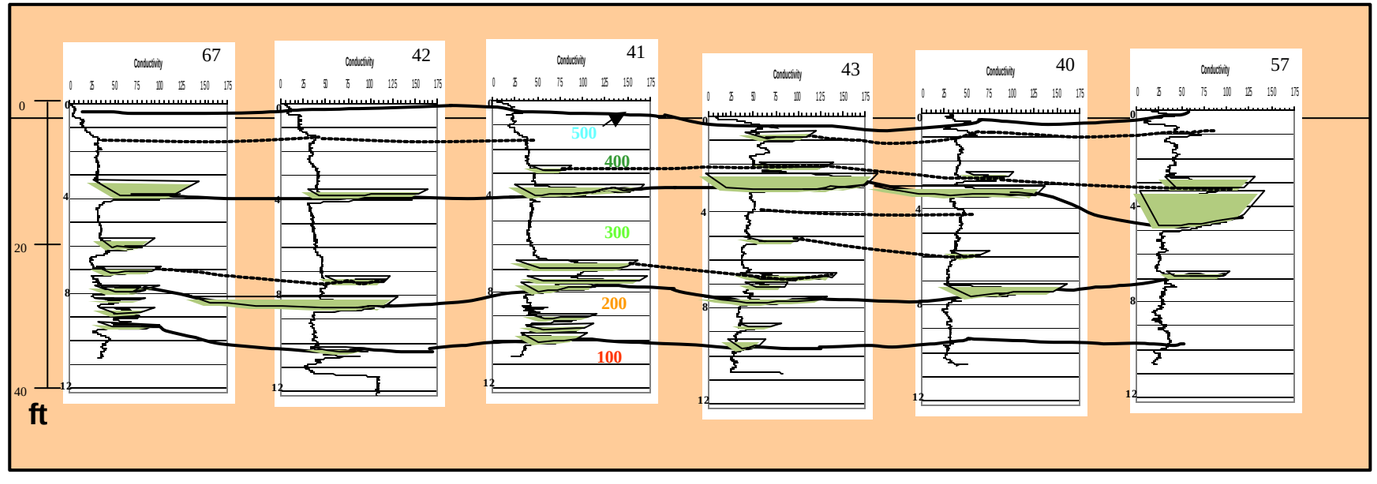

Norman Landfill
Cross-Section F-F’

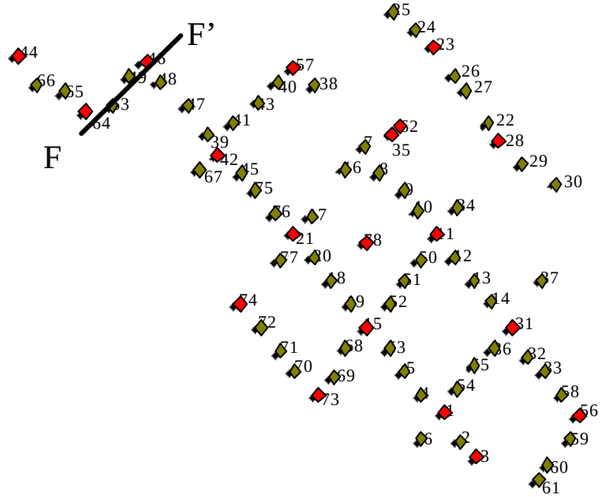

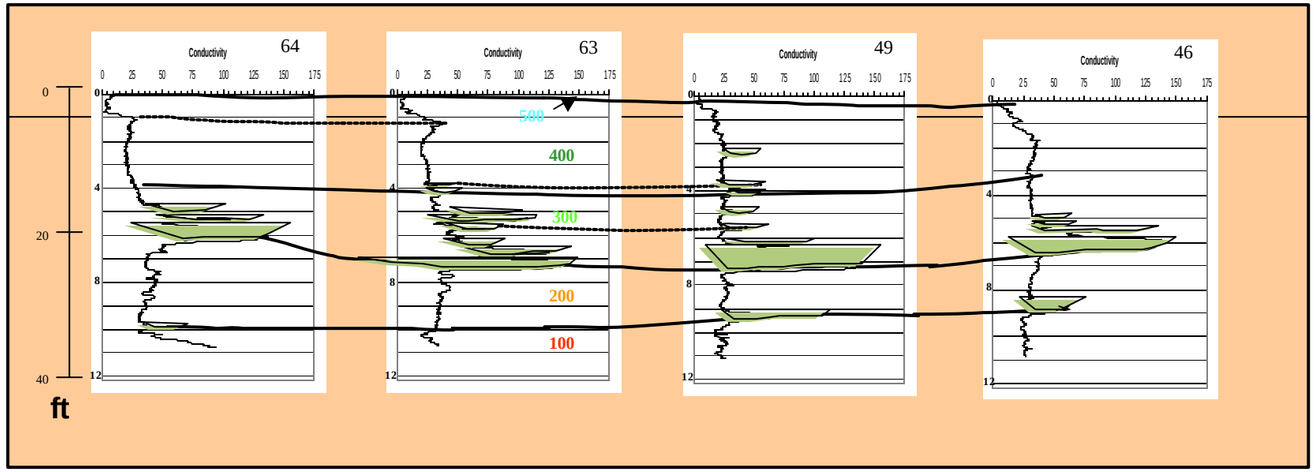

Norman Landfill
Cross-Section G-G’

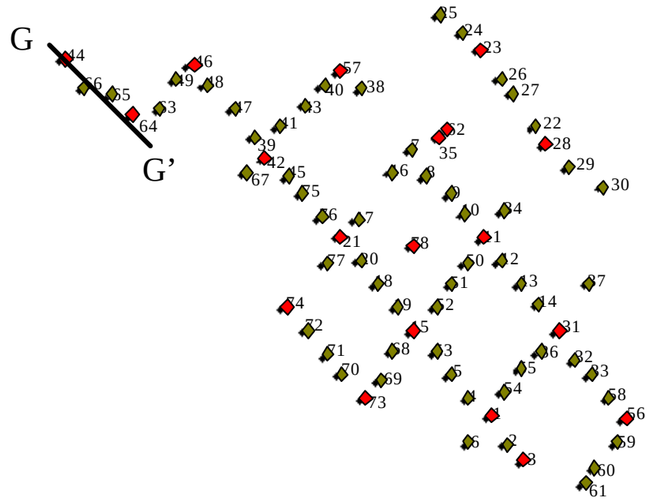

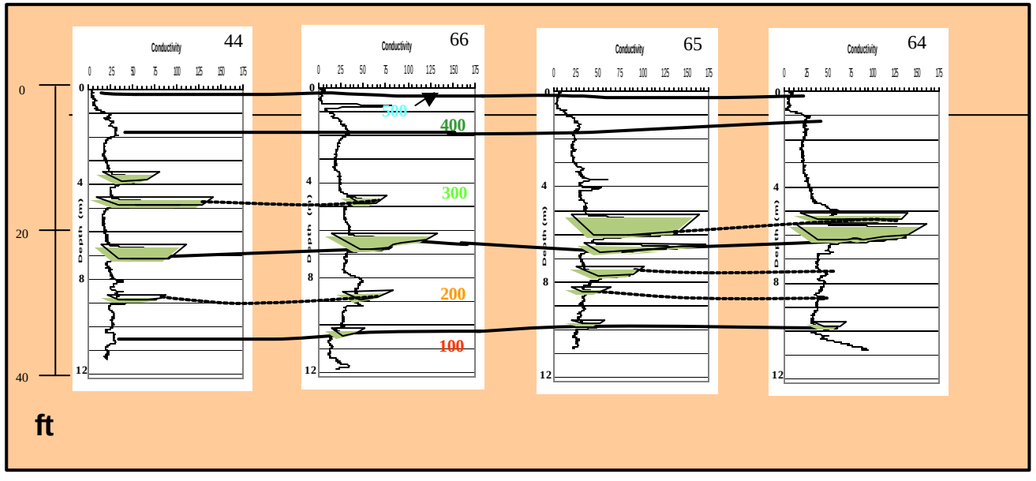

Normal Landfill
Cross-Section H-H’

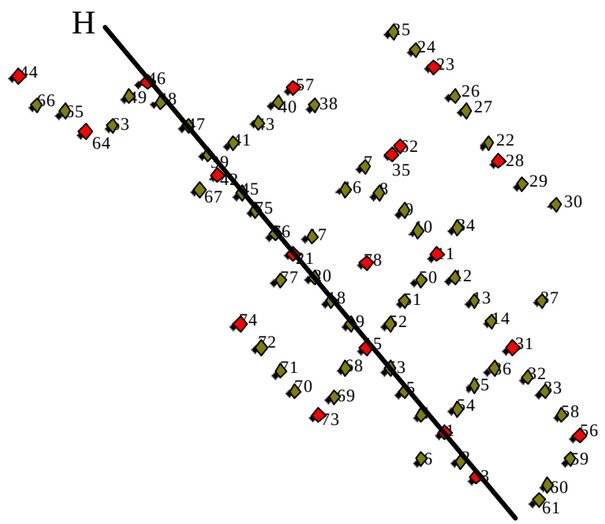

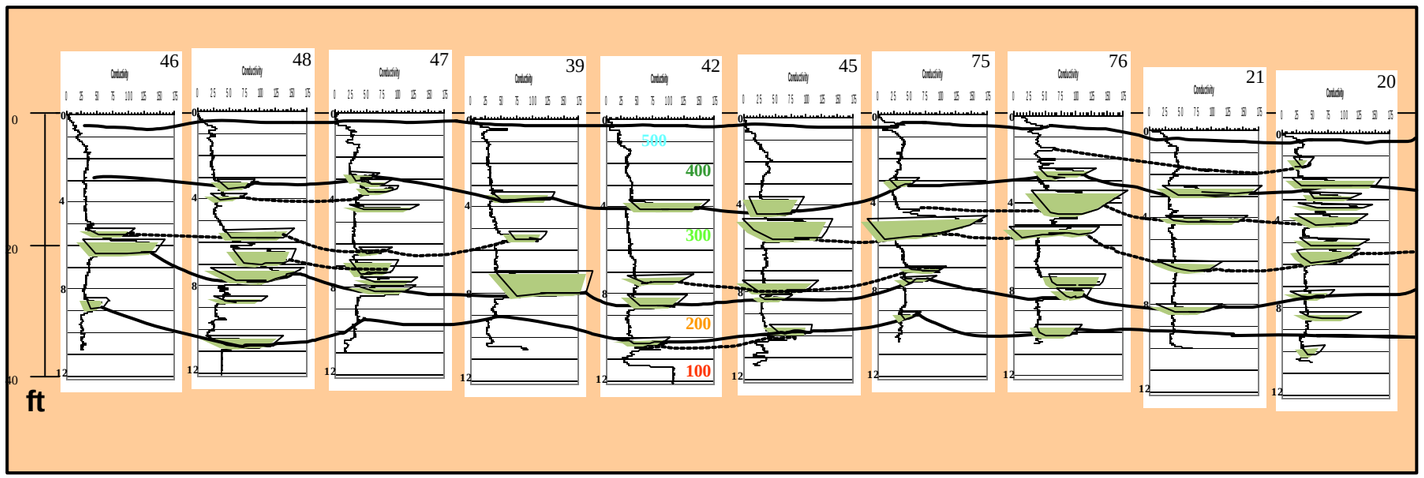

Norman Landfill
Cross-Section H-H’, cont.

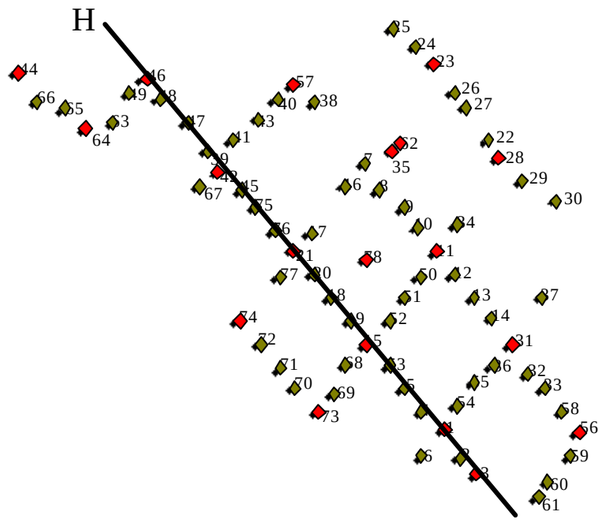

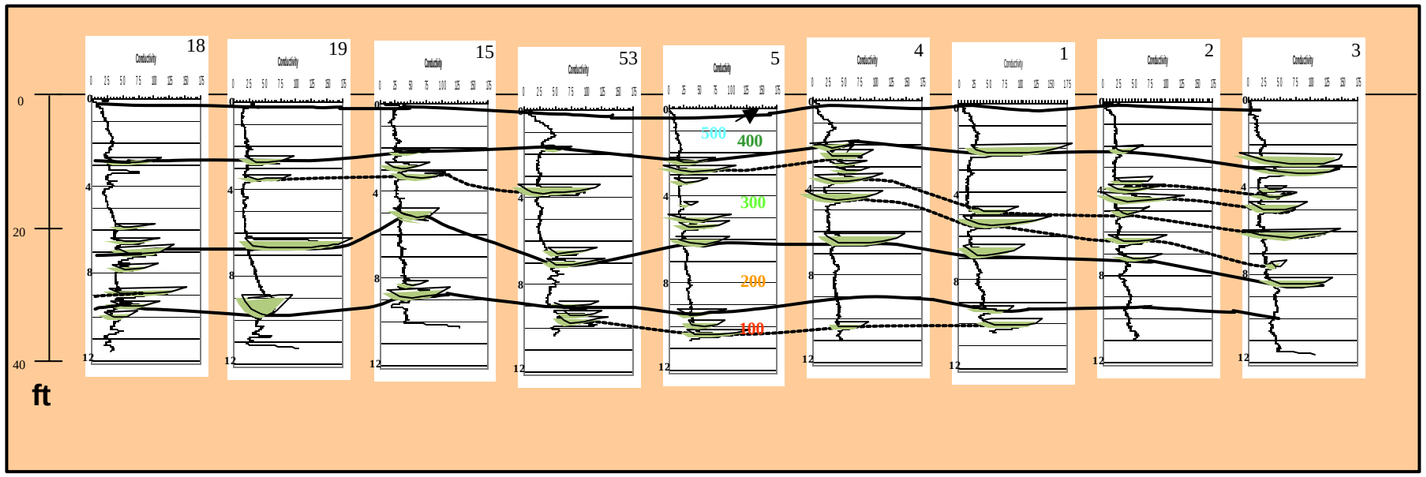

Norman Landfill
Cross-Section I-I’

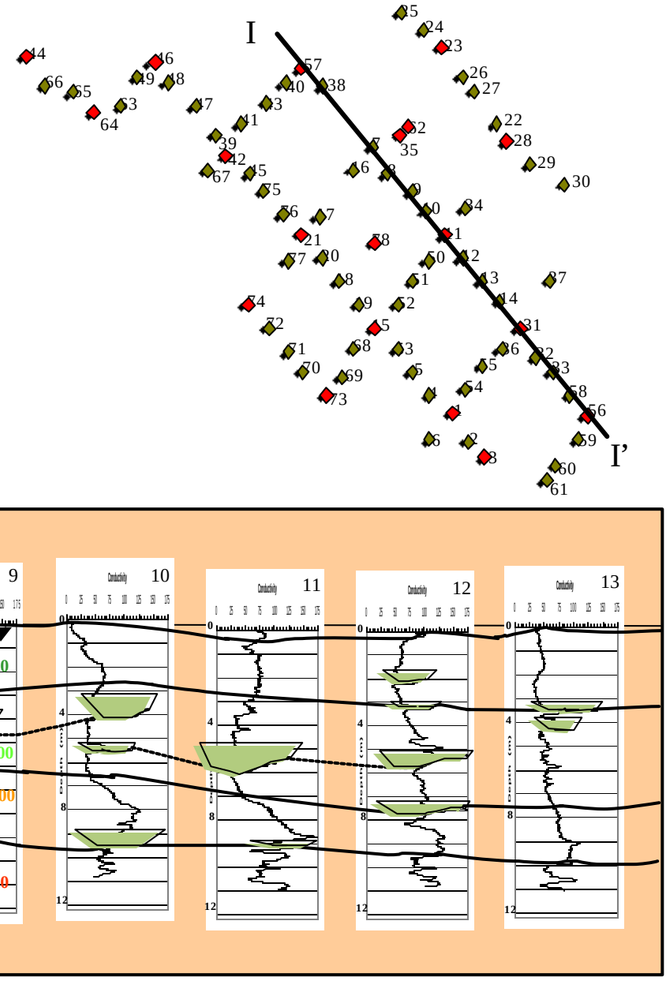

Fig. 19 – Example cross section running parallel to the point bar (complete cross-section is shown in Appendix D)

Norman Landfill
Cross-Section I-I', cont.

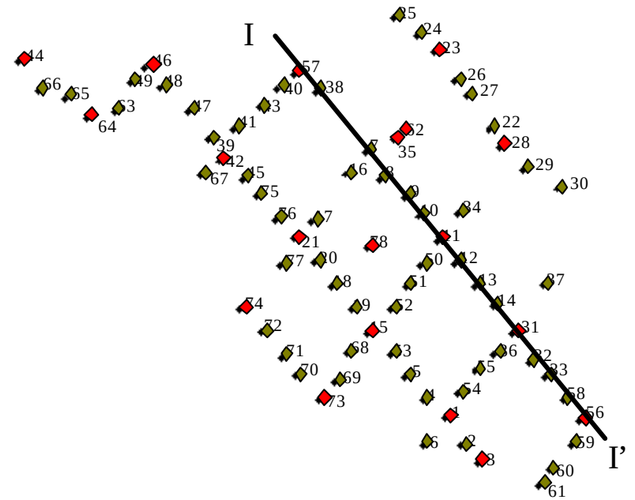

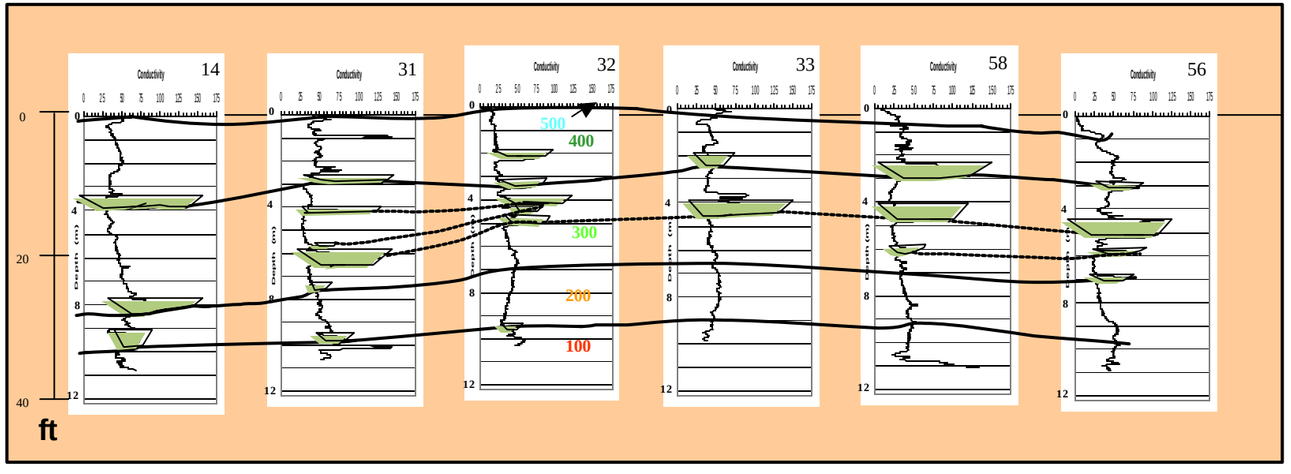

Norman Landfill
Cross-Section J-J’

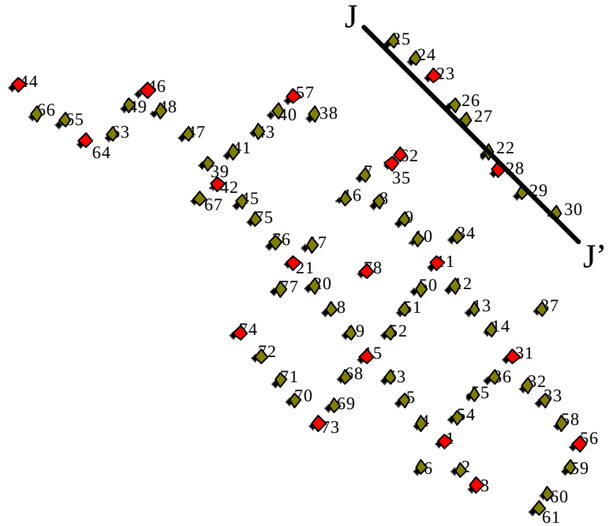

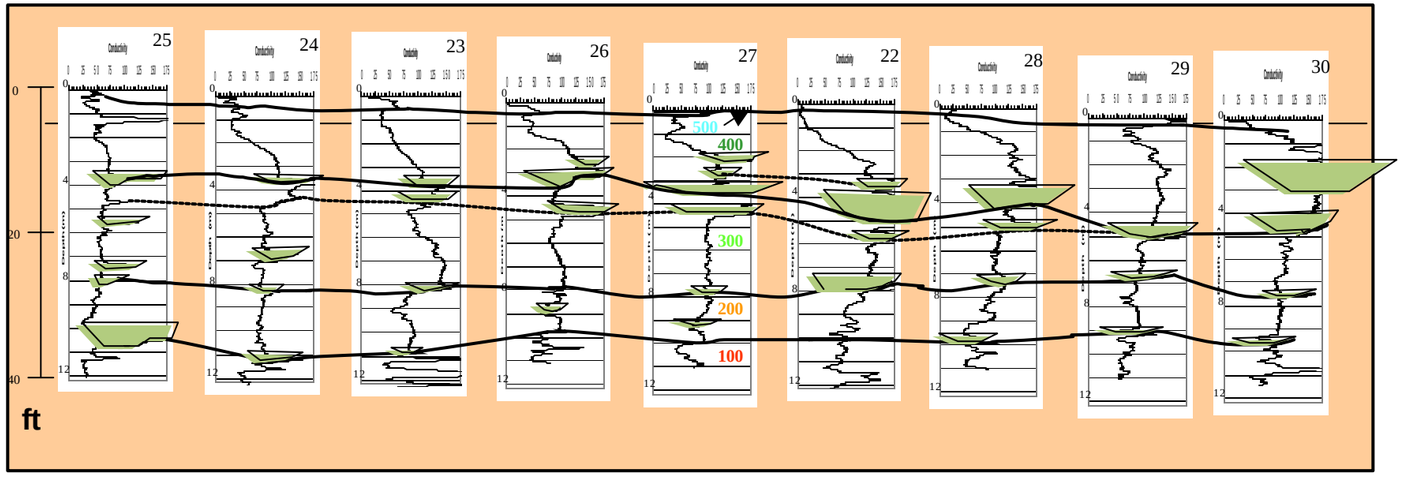

Norman Landfill
Cross-Section K-K’